

**TUTORIALS** *in*  
**CONTEMPORARY**  
**NONLINEAR METHODS**  
*for the* **BEHAVIORAL SCIENCES**

EDITED BY MICHAEL A. RILEY & GUY C. VAN ORDEN

**TUTORIALS** *in*  
**CONTEMPORARY**  
**NONLINEAR METHODS**  
*for the* **BEHAVIORAL SCIENCES**

A DIGITAL PUBLICATION AVAILABLE AT:  
[WWW.NSF.GOV/SBE/BCS/PAC/NMBS/NMBS.JSP](http://WWW.NSF.GOV/SBE/BCS/PAC/NMBS/NMBS.JSP)

EDITORS

MICHAEL A. RILEY  
UNIVERSITY OF CINCINNATI  
DEPARTMENT OF PSYCHOLOGY

&

GUY C. VAN ORDEN  
ARIZONA STATE UNIVERSITY  
DEPARTMENT OF PSYCHOLOGY

&

NATIONAL SCIENCE FOUNDATION  
PROGRAM IN PERCEPTION, ACTION, & COGNITION

The volume is intended to be freely distributed and reproduced for educational purposes. The volume may be posted, in its entirety, at world wide web or FTP locations other than the one listed above, provided that the Editors are notified in advance. Each chapter in this volume © 2005 the respective author(s).

## HOW TO CITE THIS WORK

Cite chapters from this digital volume just as you would cite chapters from a printed volume, with the exception that the typical information about the publisher is substituted with "Retrieved [date] from [URL of web site from which you downloaded the book]." For example,

Tuller, B. (2005). Categorization and learning in speech perception as dynamical processes. In M. A. Riley & G. C. Van Orden (Eds.), *Tutorials in contemporary nonlinear methods for the behavioral sciences* (pp. 353-400). Retrieved March 1, 2005, from <http://www.nsf.gov/sbe/bcs/pac/nmbs/nmbs.jsp>

Cite the entire book in a similar way:

Riley, M. A., & Van Orden, G. C. (2005). *Tutorials in contemporary nonlinear methods for the behavioral sciences*. Retrieved March 1, 2005, from <http://www.nsf.gov/sbe/bcs/pac/nmbs/nmbs.jsp>

## TABLE OF CONTENTS

<i>Preface</i>	M. A. Riley & G. C. Van Orden	iv
<i>Chapter 1.</i> Why nonlinear methods?	C. Carello & M. Moreno	1
<i>Chapter 2.</i> Recurrence quantification analysis of nonlinear dynamical systems	C. L. Webber, Jr., & J. P. Zbilut	26
<i>Chapter 3.</i> Application of recurrence quantification analysis: Influence of cognitive activity on postural fluctuations	G. L. Pellicchia & K. Shockley	95
<i>Chapter 4.</i> Cross recurrence quantification of interpersonal postural activity	K. Shockley	142
<i>Chapter 5.</i> Introduction to fractals	L. S. Liebovitch & L. A. Shehadeh	178
<i>Chapter 6.</i> Gauging the fractal dimension of cognitive performance	J. G. Holden	267
<i>Chapter 7.</i> $1/f$ dynamic in complex visual search: Evidence for self-organized criticality in human perception	D. J. Aks	319
<i>Chapter 8.</i> Categorization and learning in speech perception as dynamical processes	B. Tuller	353

## PREFACE

Chapters 2-8 in this volume were contributed by speakers at an October, 2003, workshop, "Nonlinear Methods in Psychology," held at George Mason University in Fairfax, VA, and sponsored by the National Science Foundation. The workshop served two specific purposes. The first was to provide the attendees (mostly graduate students) with tutorial lectures describing concepts and methods from nonlinear dynamics that have already shed light on problems in the behavioral sciences. The emphasis was on recurrence quantification analysis (Chapters 2, 3, 4) and fractals (Chapters 5, 6, 7), but the workshop included other, more established topics, such as applications of nonlinear dynamics to speech perception (Chapter 8), social group coordination, and human development. In addition to the authors of the chapters, we thank Stephen Guastello and Paul van Geert for their presentations at the workshop. The second purpose of the workshop was to provide the present authors with critical feedback. The chapters are intended to present these topics to a target audience of graduate students and other researchers who might lack specialized backgrounds often required to grasp the concepts and use the methods with real data. The students who attended the workshop also served as ad hoc reviewers of the chapters in this volume. They were instructed specifically to evaluate the chapters in terms of accessibility and usefulness for beginners. The reviewers and authors were thus charged with very difficult tasks that they enthusiastically embraced.

By design, this volume does not represent the full breadth of nonlinear methods that have been or are currently being used by researchers in the behavioral sciences. Instead, we focus on a narrow

subset of contemporary methods that are less well represented in other methods texts. The narrow focus allowed us to present formal, yet accessible, descriptions of methods and concepts along with detailed applications in the behavioral sciences. We hope to provide the reader with an in-depth, tutorial-style treatment—a detailed guide for the particular methods and a launching point for further studies. Thanks to the very hard work of the authors and the reviewers, we believe this volume achieves these goals.

This volume is somewhat unique also in the publication format and venue. Our aim was to balance availability and access with the utmost standards of academic rigor. We chose to publish the volume online (initially on the National Science Foundation's web site, linked from the web page of the Program in Perception, Action, and Cognition) so that it may be widely available and free of charge. By making the volume freely and easily available we may ensure that the methods and concepts described herein have a maximal impact. We chose a traditional format for the text (rather than a web-page format with hyperlinks) to maintain the feel of a typical, edited academic book. However, the electronic format also allowed us to post supplements to several of the chapters. Liebovitch and Shehadeh (Chapter 5) requested that their *PowerPoint* file be made available along with the chapter, so we have posted that file in addition to the PDF-formatted chapter. Pellicchia and Shockley (Chapter 3) made available the data set that they discuss in detail in their chapter. Aks (Chapter 7) plans to release a *Flash* demo of her eye movement model that we will also make available with this volume. We also provide links to pages from which free data analysis software can be obtained.

We are grateful to the authors and reviewers for their contributions to this project. We also acknowledge the support of the National Science Foundation, Social, Behavioral, & Economic Sciences Directorate, Division of Behavioral & Cognitive Sciences. Philip Rubin and Peg Barrat, Directors of the Division of Behavioral & Cognitive Sciences, supported this project from its inception to its completion. We especially thank Christy Contreras and Philip Johnson at NSF and Chris Kello, Debbie Kranz, and Daragh Sibley at George Mason University. Chris Kello arranged that we could meet at George Mason. Christy, Debbie, and Daragh handled the logistics of the workshop. Philip Johnson set the book up on the NSF website.

*The views expressed in this volume are the authors' and do not necessarily represent those of the National Science Foundation.*

Michael A. Riley  
University of Cincinnati  
Cincinnati, OH  
michael.riley@uc.edu

Guy C. Van Orden  
National Science Foundation  
Arlington, VA

Arizona State University  
Tempe, AZ  
guy.van.orden@asu.edu

## CHAPTER 1

# WHY NONLINEAR METHODS?

Claudia Carello

Center for the Ecological Study of Perception and Action  
University of Connecticut  
406 Babbidge Road  
Storrs, CT 06269-1020  
U. S. A.  
E-mail: [claudia.carello@uconn.edu](mailto:claudia.carello@uconn.edu)

Miguel A. Moreno

Haskins Laboratories  
300 George Street  
New Haven, CT 06511-6695  
U. S. A.  
E-mail: [miguel.moreno@uconn.edu](mailto:miguel.moreno@uconn.edu)

As behavioral scientists, we're in the business of understanding pieces of behavior. Everyone has his or her favorite types of behaviors, oftentimes things that simply derive from personal interest—we are fascinated by language or sport or animals and somehow contrive to make those into experimental topics. Apart from our idiosyncratic preferences we also bring our intellectual preferences, our assumptions about the kinds of explanations we expect to work. And although our theoretical positions are reasonably explicit, we also have metatheoretical positions that are typically somewhat hidden. Nonetheless, they sit implicitly behind what we do. Whether we are connectionists or computationalists or direct realists, the inherent philosophies of those positions dictate the kinds of problems we study and the kinds of variables by which we choose to define them. Our metatheories tell us what we think ought to be important.

But that's not the end of how we frame problems. In designing our studies, we still have a number of choices to make. Some of those choices are dictated by the requirements of the analyses that we'll use—repeated measures or factorial designs, randomized or blocked trials. Unlike our theoretical and metatheoretical positions, we tend to think of analyses as objective and benign with respect to intellectual assumptions. To be sure, all analyses assume criterial characteristics of the data that render the analysis in question legitimate. But we tend to think of those assumptions as mathematical. An important lesson of the chapters in this volume, however, is that our statistical analyses buy into intellectual assumptions as well. As you'll see, what we analyze and how we analyze it entails assumptions about the kinds of things that exist and assumptions about how those things can fit together. The

chapters show us how we might begin to change the way we understand the very nature of those pieces of behavior that interest us. At the very least, these chapters show that analyses that acknowledge the dynamical nature of certain behaviors reveal a good deal of rich structure that cannot be extracted with more familiar analyses.

Consider Figure 1.1, which illustrates a few of the many different kinds of patterns of data that behavioral scientists encounter. Panel A shows distributions of the kind that we assume are typical of our experiments. Some manipulation increased the likelihood of larger responses, although, in this case, with greater variability among the responses. Consequently, the means of the two distributions are numerically different but the variances are such that there is considerable overlap between the two distributions. Conventional analyses allow us to assess the extent to which the variability seems to be systematic (i.e., due to the manipulation) or random (e.g., due to the vagaries of individual differences among people) in order to determine whether those means are different enough to be reliable.

The remaining panels show data of the kind considered in these chapters. Whether they fit this conventional characterization is an issue. Panel B, for example, shows two distributions that appear to be of the same general sort as panel A. Distribution 2 is a little more variable than Distribution 1, but in this case their peaks are in the same location. A closer look, however, suggests a subtle difference. The mean of Distribution 2 is larger than the mean of Distribution 1, and by the same amount as in panel A. But this time the increase is not due to a straightforward, overall addition. There appears to be a stretching of the high end of the distribution so that more large values get included

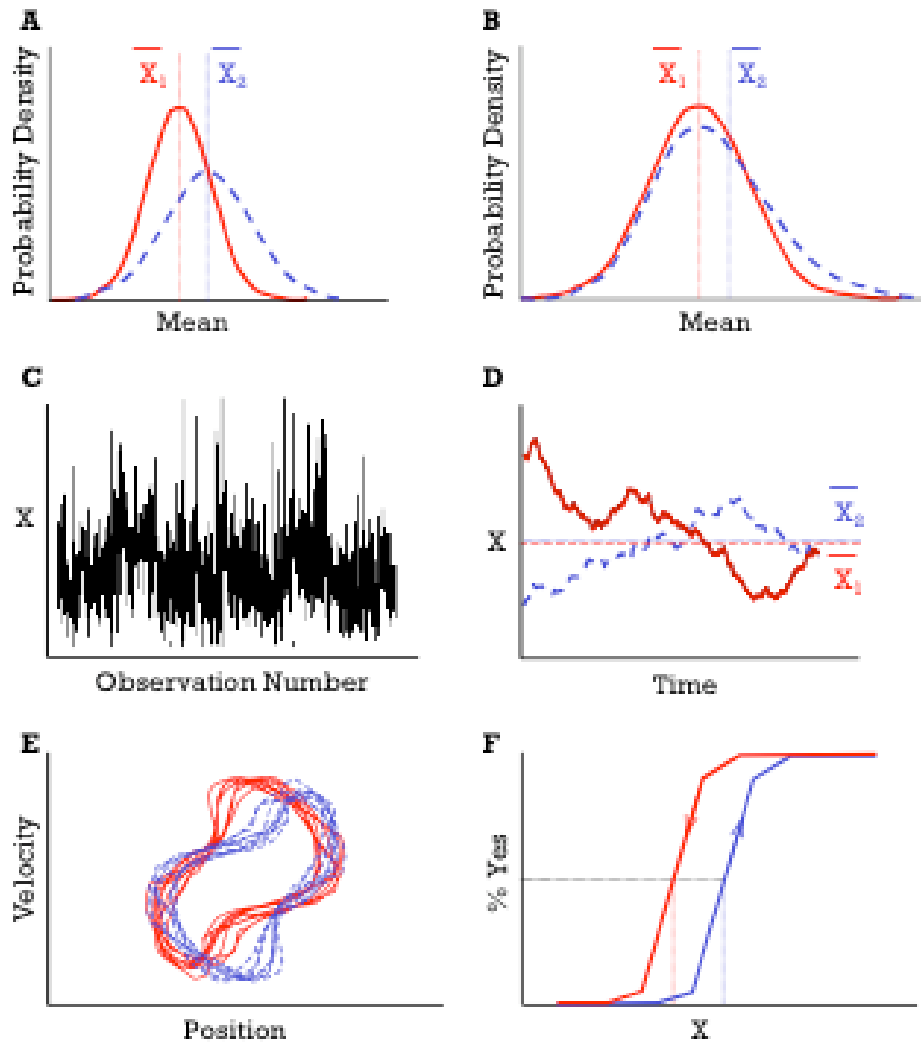


Figure 1.1. (A) Two normal distributions with different means and variances. (B) A normal distribution (solid line) and a distribution with a stretched “tail” (dashed line). (C) A time series. (D) Two time series with identical summary means. (E) Two time-ordered velocity  $\times$  position profiles. (F) Categorical responses with different orders of presentation (indicated by the arrows).

in the calculation of the mean (Moreno, 2001). Is it appropriate to say that the means of these two distributions differ? The central tendency is at the same value. Eliminating values of the dependent variable that are

larger than a certain cut-off might eliminate this tail but would that be an accurate depiction of the consequences of this particular experimental manipulation? Panels C-F show data for which the mean may be an even less appropriate measure. They are all time-series of one kind or another, depictions of individual responses being tracked over time or, at least, over order of presentation. In panel C you can see that the data are very noisy trial by trial. But there also appears to be some kind of large-scale wavy pattern overlaid on this noise. Summary statistics such as the mean and variance would be hard-pressed to capture this (see Chapter 6 by Holden). Panel D plots two time series together. The average position of the two series can be said to be the same if we simply add up the values and divide by the number of observations. But it is quite apparent that this single value is not an appropriate characterization of either time series or of the differences between them. Indeed, there is not really a single mean for either series; the mean of each changes over time, making it "illegal" to conduct conventional analyses. Panel E suggests that tracking the coincident changes in two variables might be informative. There is more to these data than a correlation could reveal. Whether small values of  $X_1$  go along with large or small values of  $X_2$  depends on when the observations occurred in the series. Finally, in panel F, two parallel functions are displaced from one another, not as a function of the  $X$  variable but as a function of whether that variable was encountered in an ascending series or a descending series (indicated by the arrows). There might be a temptation to average over the two presentation orders so as to identify "the" transition point, or to have ignored order altogether in a randomized presentation (but see Chapter 8 by Tuller).

In this opening chapter, we have two goals. First, we'll take one measure that is common in cognitive psychology research and use it to illustrate the kinds of intellectual assumptions that standard data analyses embrace. Second, we'll provide an overview of the issues that are treated in detail in the individual chapters.

## A BRIEF HISTORY OF DECOMPOSING PERFORMANCE INTO COMPONENTS

Reaction (or response) time is the workhorse for exploring the nature of cognitive systems. Traditional approaches have tried to understand responses as the sum of component effects. While such approaches allow that the intrinsic dynamics of components may be complex, they severely restrict the kinds of interactions that can occur between components. In particular, it is common to assume that interactions between components must be linear. Traditional approaches have gambled that the effect of each cognitive component combines additively with the effects of other components, which together define the shape of response time distributions. This brief history tracks the payoff, so far, of this gamble.

Linear interactions mean that the effect of an unobservable component can be recovered in an overall measure like response time because each component effect spans a sub-interval of response time. The overall finishing time of the same component doing the same job will vary from occasion to occasion, however. Thus, the overall time course of all components would appear, to an experimenter, as a distribution of finishing times (like one of those shown in Figure 1.1A).

The enterprise of decomposing response time performance into component processes is an old one. In 1868, Donders proposed a *subtractive method* for identifying stages of information processing. The subtractive method was based on the idea that a stage could be inserted into (or deleted from) a sequence of stages. Donders hypothesized that a new stage would be added to accompany specific modifications to an experimental task. Comparing response times from two tasks could estimate the duration of the added stage.

The subtractive method was the preferred procedure for revealing mental stages for decades (Wundt, 1874; Cattell, 1886; Jastrow, 1890). It fell out of favor for several reasons. One criticism was that task modifications are more likely to alter the entire sequence of stages than to insert or delete individual stages (Külpe, 1895). Devising an experimental manipulation that unambiguously introduced a new processing stage proved to be the downfall of the subtractive method.

A more contemporary effort to identify component processes adopted Donders' assumption of additive finishing times plus assumptions geared to the asymmetrical shape of response time distributions. Empirical response time distributions typically have a hyperbolic shape with an elongated, slow tail, much like the dashed-line distribution in Figure 1.1B. The slow tails of response time distributions resemble exponential distributions (Christie & Luce, 1956; McGill, 1963) and the fast tails resemble the left half of Gaussian distributions. Christie and Luce hypothesized that empirical response time distributions are the intertwining of an exponential distribution and a base distribution of an unspecified form.

Hohle (1965) suggested that the form of the base distribution was Gaussian and indeed the convolution of an exponential and a Gaussian distribution can approximate very closely the shape of empirical response time distributions (Luce, 1986). Based on this idea, response time distributions are the sum of numerous component distributions with similar variances plus an exponentially distributed component with a much greater variance.

Hohle's assumptions include Donders's core assumption of additivity, that the interactions between components are linear. Consequently the shape of response time distributions should reduce to three parameters. Two parameters,  $\mu$  and  $\Sigma$ , summarize the shape of an underlying Gaussian distribution.  $\mu$  describes the location of the Gaussian distribution along the time axis and  $\Sigma$  describes the extent of the distribution's spread. A single parameter,  $\tau$ , summarizes the location and spread of the exponential distribution.

Different component processes can be inferred if the parameter estimates systematically dissociate across experimental manipulations. Some manipulated factors should selectively influence one distribution (e.g., the exponential distribution) without affecting the other (e.g., the Gaussian distribution). This strategy for identifying component processes avoids one of the pitfalls of Donders' subtractive method, the requirement that two different tasks add (or delete) a stage of processing. Hohle's method requires that different conditions of the same task influence the exponential and Gaussian parameters independently.

As part of a model of response time performance, Hohle assumed that the exponential distribution is the effect of a response-

choice process and the Gaussian distribution is the sum of all other processes (see also, Christie & Luce, 1956). The mapping of parameters to component processes was merely intuitive, however. For example, McGill (1963) had opposite intuitions. He assigned response-choice and other decision processes to the Gaussian sum of processes and suggested that the exponential distribution represents motor processes.

Unfortunately these *ex-Gaussian* strategies (combining exponential and Gaussian distributions) fared no better than Donder's subtractive method (Sternberg, 1969). Different factor manipulations did not systematically discriminate among different component parameters across experiments (Hohle, 1967; Gholson & Hohle, 1968a, 1968b). This outcome presents a problem because the ex-Gaussian hypothesis combines so many assumptions. When results are inconclusive, it is difficult, or impossible, to decide which assumption is false. Another problem, pointed out by Sternberg, is that combinations of many other distributions also approximate response time distributions (see also Van Zandt & Ratcliff, 1995).

Sternberg (1969) realized that the core assumption that cognitive systems are composed of successive stages could be isolated from supplemental assumptions such as specifying the form of component distributions. Sternberg stripped the assumptions regarding the nature of cognitive systems down to their core and asked, "How do component processes interact?"—the recurring question in this brief history. Sternberg proposed that if the component processes interact linearly then there must exist some factors that when manipulated will selectively influence different component distributions. If components

interact linearly, then component distributions selectively influenced by separate factors will combine additively.

Sternberg's strategy of testing for linear interactions requires experimental manipulations of two or more factors. If the influence of one factor on overall performance is completely independent of the influence of another factor—a statistically additive interaction—then the two experimental factors relate to two different component processes. Alternatively, if the influence of one factor is modulated by another factor—a non-additive interaction—then both factors influence at least one common component process.

Assessments of additive interactions between component processes require estimates of component distributions that combine additively. Appropriate estimates of component finishing times, according to Sternberg (1969, p. 286), are arithmetic means. The mean of a sum of component distributions is the sum of component distribution means. Response time means, therefore, can be treated as the sum of component means.

Unfortunately, Sternberg's additive factors method has yet to identify any component process unequivocally. Additive interactions are the exception in cognitive studies. This situation could imply that the right set of factors has yet to be identified. The right set of factors could provide the necessary context to discover fundamental additive interactions. However, there is no guarantee that such a set of factors exists. Moreover, it may not be feasible to prove that such a set of factors does not exist. Sternberg provided an elegant and scientifically conservative test of the traditional assumption regarding the nature of

cognitive systems. Unfortunately, the results have yet to answer Sternberg's question, "how do components interact?"

Following Sternberg's lead, in some sense, the chapters in this volume focus on the question, "how do components interact?" Nonlinear dynamical systems provide another way to explore this question. Nonlinear dynamical systems do not exclude the possibility of linear interactions; linear interactions are special circumstances within the range of possibilities of a dynamical system. Thus, modeling response times, among other things, as a dynamical system is a very general and conservative approach. There are fewer a priori assumptions regarding the components of the system. Furthermore, there are fewer restrictions on how components may interact.

## THE CHAPTERS

The workshop focused on two types of analyses—recurrence quantification and fractals—that seem particularly fruitful for behavioral research. The general premises of these techniques are summarized in the chapters by Webber and Zbilut ("Recurrence Quantification Analysis of Nonlinear Dynamical Systems") and by Liebovitch and Shehadeh ("Introduction to Fractals") and each is followed by particular experimental implementations. Also included is an illustration of what can be gained by treating an established phenomenon dynamically from the start.

### *Recurrence Quantification Analysis*

Much of the behavior of living systems is complex and seemingly non-predictable. Nonetheless, aspects of this behavior can be counted on to repeat. The bits that repeat may do so over long stretches,

perhaps producing a pattern, or the recurrences can be quite short-lived. Consider an activity like a square dance. Much of a dancer's time is spent synchronized with the group in a large and obvious pattern, say, concentric circles alternately moving clockwise and counterclockwise. Only occasionally and briefly does one dancer get back together with his or her original partner. Both levels of recurrence—the circular patterns of the group and the momentary contact between partners—can be quantified and tell us something additional about the activity.

The levels of recurrence in the "RQA Dance"<sup>1</sup> as executed by other kinds of particles may not be as obvious, particularly the rare recurrences, but they are just as informative. And, it seems, the more complex the behavior the rarer and less obvious the recurrences, and the greater the need for ways to discover them. As noted by Webber and Zbilut, "the degree to which those systems exhibit recurrent patterns speaks volumes regarding their underlying dynamics." Even if we don't have a recurrent behavior as obvious as dancing partners holding hands, a system's underlying dynamics are accessible. Picking up on the theme that everything is connected to everything else, Takens (1981) introduced a theorem allowing a behavior space to be reconstructed from any measured variable. To be sure, a complex system is ultimately characterized by a number of participating variables. But these variables are necessarily coupled to one another and, therefore, each reflects the behavior of the system. In keeping

---

<sup>1</sup> The metaphor of RQA as describing a dance of particles was first illustrated by the duo of M. T. Turvey and Nobuhiro Furuyama during a typically staid Turvey lecture at the University of Tokyo in May, 2004.

with our intuitions that behavior evolves over time, Takens' reconstruction is accomplished through time-delayed copies of some nominated variable. That is, some variable  $x$  is chosen as a preliminary index of the system's behavior and we track what happens to  $x$  over time. But we also want to know how  $x$  behaves relative to itself at later points in time, say,  $t$  plus a delay of  $\delta$  or  $t$  plus a delay of  $2\delta$ . So the original variable  $x$  becomes a dimension of the system in question and each time-delayed copy becomes another dimension of the system. Trajectories are traced through this multi-dimensional space and recurrences are measured: Do the trajectories come together at a point, do they travel together for a sequence of points, and so on? Each of these becomes an objective indication of some aspect of the system's dynamics. An advantage here is that the analysis allows you to characterize the dynamics of the system from the measurement of any variable, not necessarily a variable that seems like it ought to be right (what standard analyses refer to as *face validity*).

This technique is illustrated in Shockley's chapter "Cross Recurrence Quantification of Interpersonal Postural Activity." He exploits RQA in a line of research aimed at quantifying the synchronization between two people who are engaged in a conversation. You can appreciate the challenge this behavior poses. What do you measure? The history of interpersonal synchrony is to treat it as a phenomenon of social coordination and to look for overt signs of that coordination. This means that the problem has been addressed fairly subjectively. For example, researchers might examine videotapes and look for signs of synchrony (e.g., similar gestures by a talker and a listener). As rigorously objective as researchers try to be,

they must still interject themselves into the process of identifying an occasion of synchrony. Shockley and his colleagues have instead chosen a behavior—the postural sway of the participants—that is not an overt part of the act of conversing and used RQA to sift through the trajectories and extract the recurrent patterns. This is unlikely to be a behavior that people are controlling consciously. It changes “for free,” pushed around by the fact that our heads are pretty massive sitting up on top of the relatively skinny sticks that are our bodies. So when we breathe and talk and gesture, those big heads move around, moving the body’s center of mass, CM, along with them. The trajectory of the CM is tracked over time, time-delayed copies of its trajectory can be generated, and you’re on your way to generating a behavior space. The subtle measures of RQA allow Shockley and colleagues to manipulate the constraints on just how coordinated the joint behavior is. They have people talk to each other or to someone else, at the same time or in the course of taking turns, using words that differ in their similarity, and so on—in order to uncover influences on the degree of coordination. This means that motor behavior, a level of behavior that some might like to relegate to the bin of basic behaviors that we can take for granted, can be used as an index of language, something we take to be one of our fanciest behaviors.

In the chapter on related work by Pellecchia and Shockley “Application of Recurrence Quantification Analysis: Influence of Cognitive Activity on Postural Fluctuations,” RQA is applied to a single postural trajectory. This time, your big head is moved around not by coordinating with another person but simply by standing while directing some of your attention to another task. Here the emphasis is

not so much on the objectivity to be gained—postural sway indexed by the excursions of the center of pressure (COP) is a common measure in some domains. But Pellecchia and Shockley point out that more traditional postural measures are summary measures, for example, of COP path magnitude and variability. But these summary measures turn out to be insufficiently sensitive to the varied ways in which cognitive attentional load can influence certain aspects of postural stability but not others. They “do not reflect the dynamical properties of postural control.” In particular, they miss the temporal structure of a COP time series. One challenge is that posture data are what is called *nonstationary*. No single summary measure adequately captures them because the mean changes over time and the variability changes over time (see Figure 1.1C). The notion of an average postural location doesn’t make sense. But this nonstationarity also makes posture data inappropriate for analyses that assume stationarity. RQA, in contrast, makes no such assumptions about the way the data are distributed.

Pellecchia and Shockley deal with some of the technical aspects of carrying out RQA. When you’re evaluating the RQA dance, what qualifies as an instance of the two original partners having come together? Do they actually have to touch hands or can they simply slap hands or wave in the vicinity of each other? When you’re generating your behavior space through time-delayed copies, what should the delay be? How many dimensions define your hyper-space? Pedagogically, our preference is to illustrate it with three because we can visualize three-space. But there are no such mundane constraints on RQA. Pellecchia and Shockley suggest a kind of exploratory strategy in which the RQA quantities are calculated for a range of parameter

values (numbers of dimensions, size of time-delay), and then settle on a value of the latter from a range that doesn't have dramatic consequences for the RQA measures. The upshot in the research they describe is that RQA promotes a different understanding of what attention does. In the particular experiment they described, for example, summary measures of COP were all affected in the same way by attentional demands, suggesting that attention causes a decrement in postural control. The RQA measures, in contrast, yielded differences that suggest a nuanced understanding of the ways in which postural components (e.g., the front to back vs. side to side movements) might be modulated by a stander in order to meet attentional demands. Variability is something to be harnessed by the system to achieve a goal.

### ***Fractal Analyses***

Most of the things that we need to measure tend to be irregular. This is no less true when the things we measure are behaviors rather than objects. Geometrically, this means that things are more like coastlines than rectangles. As Liebovitch and Shehadeh point out in "Introduction to Fractals," this not only makes them hard to measure, it makes the ruler that we use important. Quite surprisingly, the measured size of the coastline depends on the size of the ruler. Smaller rulers get into more of the nooks and crannies, thereby including more stretches of coastline than would be the case with a large ruler that is forced to bridge those gaps. So the level of resolution that we choose to achieve in our measurement affects the values we get. Consider one classic value that is typically used to characterize the behavior of a system, its mean. The mean is a measure derived from a collection of

property or performance values that all tend to distribute around this more or less central value. It is considered a value that typifies the thing being measured. But with irregular objects like coastlines, there really is no typical value. The mean depends on the resolution of the measurement and isn't all that meaningful.

Subjectivity in measurement is certainly a problem to be reckoned with. You can appreciate how standard assumptions about normal distributions (most notably, more samples should lead to more precision, not more stuff) will be inappropriate in such circumstances. But so-called fractal objects, which are defined, in part, by this dependency on measurement resolution, have an additional property that makes them especially interesting. Fractal objects are *self-similar*, that is, structure at the large scale (or the structure of behavior at the large scale) is duplicated at the small scale: "...the statistics of the small pieces are similar to the statistics of the large pieces." This is so whether we are talking about the structure at different scales of space or at different scales of time. What happens within a square centimeter mimics what happens within a square meter; what happens within a one second window mimics what happens within a one minute window. Self-similarity can reveal much about the dynamics of a system. Depending on how the variability relates to the size of the window—a relationship indexed by what is called the Hurst exponent—it tells you whether an increase in the value of a measure taken now is likely to be followed by an increase or a decrease in that measure taken later. In essence, continuous dynamical processes manifest a kind of memory without the logical attributions and storage metaphors we gravitate to in the behavioral sciences.

A respect for unfolding dynamics encourages the treatment of order effects as entities of interest in an experiment rather than as sources of contamination. This is illustrated by Holden in "Gauging the Fractal Dimension of Cognitive Performance." He uses a simple repetitive time-estimation task to demonstrate the options for analyzing a time series of response times. A participant attempted to produce a sequence of equal intervals to mimic a presented target interval. Here our interest is not so much in accuracy as in the kind of process that produced the performance that was obtained. The way in which the variability changes over time is the source of the insight. Holden provides a nice intuitive metaphor here. If the interval estimates did not vary, then a graph (of value over time) would yield a one-dimensional straight line. To the extent that the time series is messy, it more closely resembles a two-dimensional plane. The *fractal dimension* of the time series can be calculated from the time series, with a value of 1.5 indicating randomness and 1.2 indicating pink noise, a time-scale dependent variability. It is, of course, more complicated than this, since order matters. Shuffling the data yields white noise because you've destroyed the fractal structure, the pattern of variability at short time scales that is echoed at ever-longer time scales.

Holden's chapter also contains several caveats for conducting these kinds of nonlinear analyses. Caveats are necessary because there are options and we are sensitive to the fact that options often entail assumptions. Let's consider a few that routinely arise due to the practical finiteness of data collection. Ordinary statistics tell us that outliers are a problem and should be eliminated. Sympathy for dynamics burdens us with the knowledge that outliers are not

necessarily produced by an aberrant procedural hiccup. We have to assess the extent to which they would dominate the analysis. You also have to be careful that the analysis is not dominated by spurious trends (e.g., a stretch of linearity) in the finite data set that might be part of something else if the data collection had continued. So the longer the time series the better in order to see the cascading structure of varied time scales. But since our interest is in emergence over time, we cannot pretend that data collected over several days are the same as data collected in one sitting. Finally, with all of these options, you're bound to come up with varied characterizations depending on which choices you made. So you need to conduct more than one analysis type (e.g., spectral and dispersion analyses) as converging operations.

In her chapter "1/f Dynamic in Complex Visual Search: Evidence for Self-Organized Criticality in Human Perception" Aks applies this perspective to visual search behavior, the eye movements that people engage in when looking for a specific small detail amidst a clutter of distracting detail. These movements appear quite haphazard. Our eyes dart back and forth, up and around, in a mix of short jumps and long, often landing on the same places time and again. We do not follow a systematic path, say, from upper left to lower right that would seemingly guarantee that the target would be encountered. Our behavior doesn't show in any obvious way that we remember where we looked in vain before. Yet the repetitive, jerky movements are surprisingly effective—we find our friend in the crowd; we select the

perfect bolt from a stash of culch.<sup>2</sup> Indeed, the ordinary conditions under which visual search happens don't really favor the tidy, thorough search. We don't have all the time in the world; our targets or our goals are often on the move.

At issue in this research domain is what guides visual search. If eye movements truly were random, we would have to conclude that they were driven by something other than what the system had done before, that there was no real role for memory. But it is in the superficially random noisiness that a fractal analysis uncovers subtle structure. By quantifying how the noise changes over time we gain insight into the kind of system that has produced that noise. Presenting subjects with a difficult search task (looking for a target with a conjunction of features, not just one) reveals that a bout of scanning has its own internal history. What we do early in the bout does indeed influence what we do later in that same bout. But this dynamic history is quite different from more standard characterizations of memory that entail a certain degree of address-specific tagging. It implicates more subtle contingencies, indexed by what is called 1/f behavior.

The final chapter by Tuller does not incorporate either recurrence or fractal analyses. Instead, she illustrates the advantage of a general dynamical attitude in designing an experiment, with subsequent opportunities for new interpretations of seemingly well-understood results. The generality is especially apparent in that this is strictly a perception experiment. The relevant series is not of the *timing*

---

<sup>2</sup> In the New England vernacular, culch refers to items that may (or may not) come in handy someday.

of the responses but of their *content*—why should a speech token sound like one syllable versus another? Tuller tackles the classic phenomenon of categorical perception. Syllables are synthesized to vary incrementally on some acoustic property. Even though each syllable token is defined by a different value taken from a wide range of the acoustic property, each is heard as either one syllable or the other; they belong to one syllable category or the other. Categorical perception has historically been treated statically: You hear a token and it maps better onto one representation than another. But Tuller shows that thinking of the process as dynamical—with stable, attractive states that change abruptly—focuses the experimenter on finding what encourages those nonlinear shifts from one stability to another.

Tuller's major caveat is that some standard methodological choices, most notably, randomizing the order in which stimuli are presented, obscure the dynamics of a system. In a now-familiar refrain for this volume, she notes that far from being a nuisance that has to be controlled, order effects allow a system's dynamical signature to emerge. A dynamical perspective requires that the stimuli be presented in order, for example, alternating increasing and decreasing levels of the acoustic property. This allows an interpretation of the acoustic property as a *control parameter* rather than as a cue. Now the categorical shift can be mined. Does it happen at the same value of the control parameter in one order as the other (see Figure 1.1F)? Does the syllable you first hear persist? Or do you switch to the other syllable at a low level on the way up but a high level on the way down? Tuller notes that all three of these patterns have been observed and one or the other can be encouraged. Most notably, the abrupt change from one

syllable to another, from one stable state to another, comes about during situations of instability. What had been unanimity of responses becomes somewhat mixed. Such instability links this perceptual phenomenon to the general phenomenon of self-organized pattern formation. This linkage allows one to write the differential equations that "define systems with attractor properties that fit the observed experimental data." That is to say, the linkage is far from metaphorical. A perception system is modeled in the same way, with the same ontological status, as an action system, clearly a different direction from the traditional treatment of categorical perception.

## CONCLUSIONS

Behavioral scientists study the actions of humans and animals. Some of these actions make sense at the level of the individual and some emerge only in a social setting. As we noted at the outset, we make a number of choices in conducting our studies. The practical issue of what kind of equipment we have, how many participants are available, and so on, are supplemented by the kinds of analyses we know how to do and the kinds of data we collected to put into those analyses. We have suggested that such choices are not necessarily as benign and objective as we would like to believe. Do we try to avoid data like those shown in panels B-F of Figure 1.1 because they are messy? Or do we try to contrive our manipulations to produce those kinds of data because they allow the richness of dynamical systems to be seen? The following chapters are of a mind that we should not be afraid of variability. It may well be the driving force of nature.

#### AUTHOR NOTE

Preparation of this work was supported by grants from the National Science Foundation (SBR 00-04097) and the National Institutes of Health (HD-01994).

#### REFERENCES

Cattell, J. McK. (1886). The time taken up by the cerebral operations. *Mind*, *11*, 220-242.

Christie, L S., & Luce, R. D. (1956). Decision structure and time relations in simple choice behavior. *Bulletin of Mathematical Biophysics*, *18*, 89-112.

Cramer, H. (1946). *Mathematical methods of statistics*. Princeton: Princeton University Press.

Donders, F. C. (1868). Over de snelheid van psychische processen. Onderzoekingen gedaan in het Physiologisch Laboratorium der Utrechtsche Hoogenschool, 1868-1869, Tweede reeks, II, 92-120. Transl. By W. G. Koster, *Acta Psychologica*, *30*, 412-431.

Gholson, B., & Hohle, R. H. (1968a). Verbal reaction time in hues and hue names and forms vs. form names. *Perception & Psychophysics*, *3*, 191-196.

Gholson, B., & Hohle, R. H. (1968b). Choice reaction time to hues printed in conflicting hue names and nonsense words. *Journal of Experimental Psychology*, *76*, 413-418.

Carello and Moreno

Hohle, R. H. (1965). Inferred components of reaction time as functions of foreperiod duration. *Journal of Experimental Psychology*, *69*, 382-386.

Hohle, R. H. (1967). Component process latencies in reaction times of children and adults. In L.P. Lipsitt & C.C. Spiker (Eds.), *Advances in child development and behavior, Vol III*. New York: Academic Press.

Jastrow, J. (1890). *The time-relations of mental phenomena*. New York: N.D.C. Hodges.

Külpe, O. (1895). *Outlines of psychology*. New York: MacMillan, Secs. 69, 70.

Luce, R. D. (1986). *Response times: Their role in inferring elementary mental organization*. New York: Oxford University Press.

McGill, W. J. (1963). Stochastic latency mechanisms. In R. D. Luce, R. R. Bush, & E. Galanter (Eds.), *Handbook of mathematical psychology, Vol I*. New York: Wiley.

Moreno, M. A. (2001) A nonlinear dynamical systems perspective on response time distributions. Unpublished doctoral dissertation, Arizona State University, Tempe, AZ.

Sternberg, S. (1969). The discovery of processing stages: Extensions of Donders' method. *Acta Psychologica*, *30*, 276-315.

Van Zandt, T., & Radcliff, R. (1995). Statistical mimicking of reaction time data: Single-process models, parameter variability, and mixtures. *Psychonomic Bulletin & Review*, *2*, 20-54.

Why nonlinear methods?

Wundt, W. (1874). *Grundzuge der Physiologischen Psychologie*. Leipzig:  
Engelmann.

## CHAPTER 2

# Recurrence Quantification Analysis of Nonlinear Dynamical Systems

Charles L. Webber, Jr.

Department of Physiology  
Loyola University Medical Center  
Maywood, Illinois 60153-3304  
U. S. A.  
E-mail: [cwebber@lumc.edu](mailto:cwebber@lumc.edu)

Joseph P. Zbilut

Department of Molecular Biophysics and Physiology  
Rush University Medical Center  
Chicago, IL 60612-3839  
U. S. A.  
E-mail: [jzbilut@rush.edu](mailto:jzbilut@rush.edu)

## RECURRENCES IN NATURE

Comprehension of the physical world depends upon observation, measurement, analysis, and, if possible, prediction of patterns expressed ubiquitously in nature. Linear or near-linear systems possess a regularity and simplicity that are readily amenable to scientific investigations. Yet numerous other systems, especially those in the animate realm, possess complexities that are at best non-linear and non-predictable. Common ground between living and non-living systems resides in their shared property of recurrence. That is, within the dynamical signals expressed by living and non-living signals are stretches, short or long, of repeating patterns. Actually, recurrence properties are taken advantage of in signal compression techniques (Wyner, Ziv, & Wyner, 1998)—one billion sine waves at a constant frequency will perfectly collapse to a fraction of one sine cycle with loss of no information. As signals grow in complexity, however, recurrences become rarer, and efficient compressibility is resisted. For so-called random systems such as radioactive decay, recurrences occur theoretically by chance alone. But the lesson is clear: Insofar as natural patterns are found in all dynamical systems, the degree to which those systems exhibit recurrent patterns speaks volumes regarding their underlying dynamics. And, on reflection, it should be appreciated that the entire scientific enterprise is based upon the concept of recurrence: To be accepted as valid, experimental results must be repeatable in the hands of the primary investigator and verifiable by independent laboratories.

Patterns of recurrence in nature necessarily have mathematical underpinnings (Eckmann, Kamphorst, & Ruelle, 1987) which will

readily become apparent in the sections that follow. Although recurrence quantification analysis (RQA) is scantily a decade old (Zbilut & Webber, 1992; Webber & Zbilut, 1994), the concept of recurrence in mathematics has a much longer history (Feller, 1950; Kac, 1959). However, any appreciation of nonlinear dynamics and associated terms the reader brings to the table (fractals, attractors, non-stationarity, singularities, etc.) will greatly facilitate the comprehension of recurrence analysis (see Glass & Mackey, 1988; Bassingthwaite, Liebovitch, & West, 1994; Kaplan & Glass, 1995). Indeed, our primary goal in this chapter is to provide clear details regarding the proper implementation of one nonlinear technique, RQA, in the assessment or diagnosis of complex dynamical systems. Using carefully selected examples pertinent to the field of psychology and parallel disciplines, we will build a case for the fundamentals of RQA, its derivation, and its utility. Patience is required of the learner, for there are no short cuts to RQA strategies; proper implementations are application-specific. A mathematical framework is constructed to give quantitative legitimacy to RQA, but for those unfamiliar with mathematical notation, an Appendix is provided with discrete numerical examples (Webber, 2004).

The up and down motions of sea waves originally inspired Joseph Fourier to characterize signals in terms of their frequency-domain features (e.g., cycles per sec); that technique now bears his name (Grafakos, 2003). Likewise, for our recurrence purposes, consider a system of literal waves on the sea as measured from buoy instrumentation and plotted in Figure 2.1A. During the 9.4 days of 226 hourly measurements the wave heights rise and fall in a nonlinear,

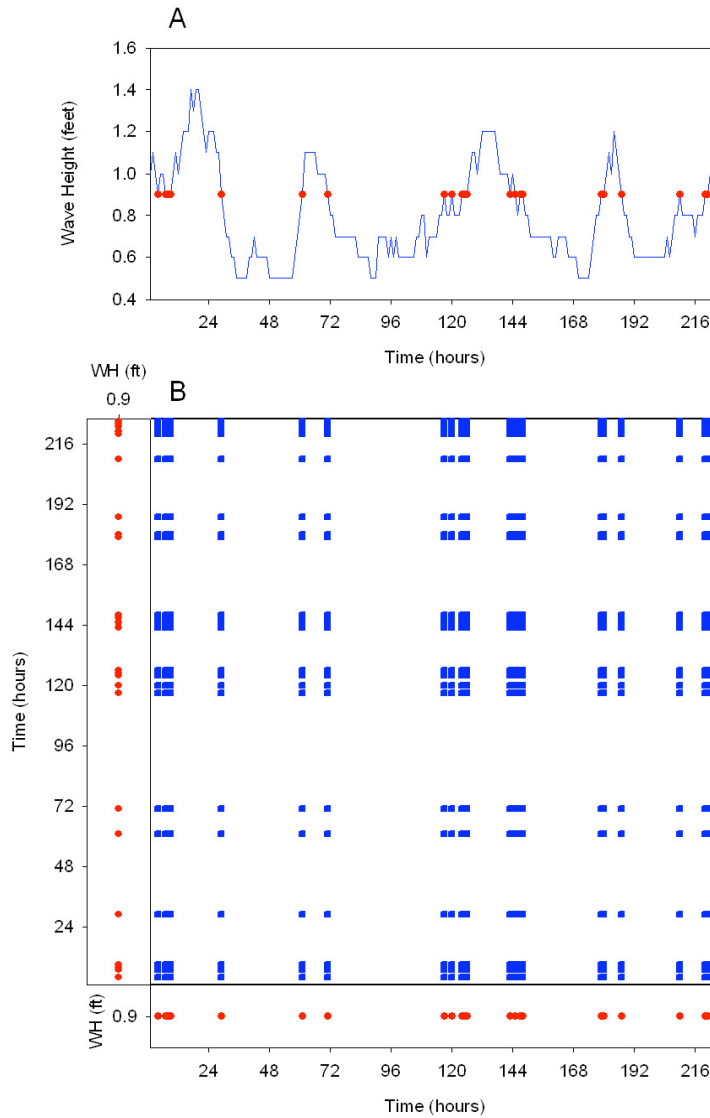


Figure 2.1. (A) Wave height measurements recorded hourly for 226 hours from buoy instrumentation located 33 nautical miles south of Islip, LI, NY (National Data Buoy Center Station 44025). Wave heights are expressed in feet to the nearest 0.1 ft from hour 14, July 10 through hour 23, July 19, 2002. Dots are placed on all waves having identical heights of exactly 0.9 ft that occur at 25 aperiodic points in time (hours: 4, 7-9, 29, 61, 71, 117, 120, 124-126, 143, 145, 147-148, 179-180, 187, 210, 220-221, 223-225). These wave data are owned by the NSW Department of Land and Water Conservation (DLWC) as collected and provided by the Manly Hydraulic Laboratory (MHL), Sydney, Australia. Time series data from data file *BOUY* ( $n=226$  points). (B) Matrix plot of identical wave heights at 0.9 ft. The same time series of 25 aperiodic time points is aligned along both horizontal and vertical time axes, and intersecting pixels are darkened to map out recurrence matches at 0.9 ft wave heights only. All other wave heights are excluded from the matrix. Recurrence data computed from data file *BOUY9* using program *RQD.EXE*. ROA parameters:  $P_1-P_{last} = 1-226$ ;  $RANDSEQ = n$ ;  $NORM = \text{max norm}$ ;  $DELAY = 1$ ;  $EMBED = 1$ ;  $RESCALE = \text{absolute}$ ;  $RADUS = 0$ ;  $COLORBND = 1$ ;  $LINE = 2$ .

aperiodic fashion over different time scales (long-periods, large amplitudes; short-periods, small amplitudes). To capture the fundamental notion of recurrence, a dot is placed on every wave of the time series that is exactly 0.9 ft in height. As illustrated, this forms an imaginary line of horizontal dots cutting through the waves at 25 specific time points. That is, each of these waves is exactly recurrent (same height) with one another at certain instances in time that are non-periodic. To graphically represent the recurrent structuring of the data matrix at 0.9 ft height only, the time-positions of these waves are plotted against each other in Figure 2.1B. All other wave heights are excluded.

To get a more accurate picture, however, it is necessary to include waves of all possible heights. Because the waves range in height from 0.5 to 1.4 ft with a measurement resolution of 0.1 ft, there are necessarily 10 different possible wave heights. The recurrence plot of Figure 2.2A shows the distribution of recurrent points (darkened pixels) for all waves of exactly the same height, including low-, medium-, and high-amplitude waves. For the sea wave data it can be seen that the recurrence plot forms a delicate, lace-like pattern of recurrent points. By necessity, there is a long diagonal line (wave heights always self-match), the plot is symmetrical across that diagonal (if height of wave  $i$  matches height of wave  $j$ , then the height of wave  $j$  matches height of wave  $i$ ), and the recurrence plot is 2-dimensional.

What happens if we relax the constraint that wave heights must be exactly the same before registering them as recurrent? For example, if we let sea waves within 0.2 ft of each other be considered recurrent, a 1.0 ft wave would recur with other waves ranging in height

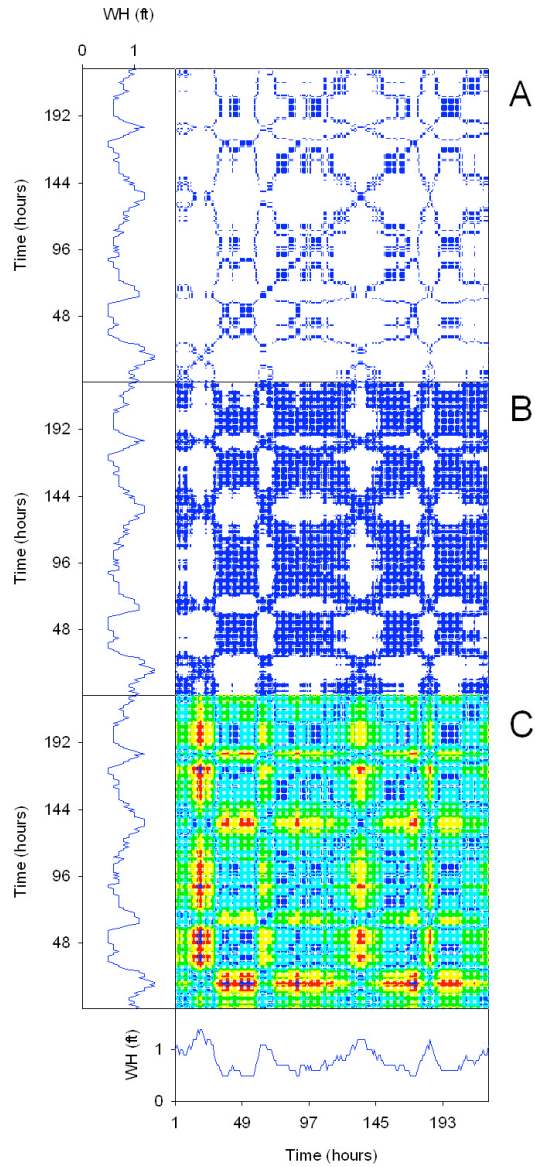


Figure 2.2. Recurrence plots of wave height data for different radius (RADIUS) settings and computed recurrence densities (%REC). (A) Exact recurrences (RADIUS = 0.0 ft; %REC = 13.479%). (B) Approximate recurrences (RADIUS = 0.2 ft; %REC = 54.938%). (C) Saturated recurrences (RADIUS = 0.9 ft, %REC = 100.000%). Like color-contour maps, the recurrence plot in C is color-coded in 0.2 ft increments of RADIUS: blue (0.0-0.2 ft); cyan (0.2-0.4 ft); green (0.4-0.6 ft); yellow (0.6-0.8 ft); red (0.8-0.9 ft). Time series of wave height data (WH, feet versus hours) align along the horizontal and vertical axes of each recurrence plot (time calibration of hour 1 through hour 226). Recurrence data computed from file *BUOY* using program *RQD.EXE*. RQA parameters:  $P_1$ - $P_{last}$  = 1-226; RANDSEQ = n; NORM = max norm; DELAY = 1; EMBED = 1; RESCALE = absolute; RADIUS = 0.0 (A), 0.2 (B) or 1.0 (C); COLORBND = 1 (A and B) or 0.2 (C); LINE = 2.

from 0.8 to 1.2 ft. Therefore, applying this rule to all points in the time series should result in the recruitment of more recurrent points. Indeed this is the case, as demonstrated in the recurrence plot of Figure 2.2B. The density of recurrences is decidedly higher, and the lace-like quality of the former plot is replaced by broader areas of approximate recurrences. Carrying this relaxation rule to its limit, what would the recurrence plot look like if all waves were recurrent with one another? This is easily done for the present example by defining two time-points recurrent if they are within 0.9 ft in height. The 0.9 ft limit comes from the difference between the largest wave (1.4 ft) and the smallest wave (0.4 ft). In this case, we would correctly expect every pixel in the recurrence plot to be selected, creating one huge dark square with loss of all subtle details (not shown). Discriminating details of distances can be retrieved, however, by color-coding the differences in wave heights according to a simple coloring scheme as illustrated in Figure 2.2C. All we need to do is change the assigned color in 0.2 ft increments, constructing a color-contour map of wave heights. Actually, this type of coloring is not unlike any contour mapping using different colors to designate various elevations above or below sea level. It is very instructive to make mental correlations between the wave height data (time series along horizontal and vertical axes) and the attendant recurrence plots.

### RECURRENCE PLOTS

With this simple introduction to recurrence plots, it is now necessary to become more mathematical. Published numerical examples (Webber, 2004) are reiterated in the Appendix to assist in the

learning of these important details. As will be carefully shown, the recurrence plot is nothing more (or less) than the visualization of a square recurrence matrix (RM) of distance elements within a cutoff limit. We will work up to the definition of seven recurrence parameters (user-adjustable constants) which control the distances within the matrix, their rescaling, and recurrence plot texture. To do this, we will introduce the straightforward ECG signal recorded from a human volunteer as plotted in Figure 2.3A. We could easily generate a recurrence plot of this signal like was done for the sea wave data, identifying as recurrent those time points with identical or similar voltages. But to do so would only be the first-dimensional approach to the problem (represented in a 2-dimensional recurrence plot); as we describe in the following paragraphs, such a 1-dimensional approach may not suffice.

Consider the ECG signal in its one-dimensional representation of voltage as a function of time (Figure 2.3A). Does not this signal actually “live” in higher dimensions? Of course it does. Since the ECG derives from summed cardiac potentials that move simultaneously in three dimensions (frontal, saggital, and horizontal orthogonal planes), the 1- and 2-dimensional representations are mere projections of the signal to lower dimensions. To accurately represent the ECG in three dimensions it would be necessary to simultaneously record electrical potentials in three orthogonal planes from the subject. But here is where things get very interesting. About a quarter century ago Takens (1981), elaborating upon key conceptual ideas of Ruelle, introduced his theorem of higher-dimensional reconstruction by the method of time delays. What this theorem states is that the topological features of any

## Recurrence Quantification Analysis

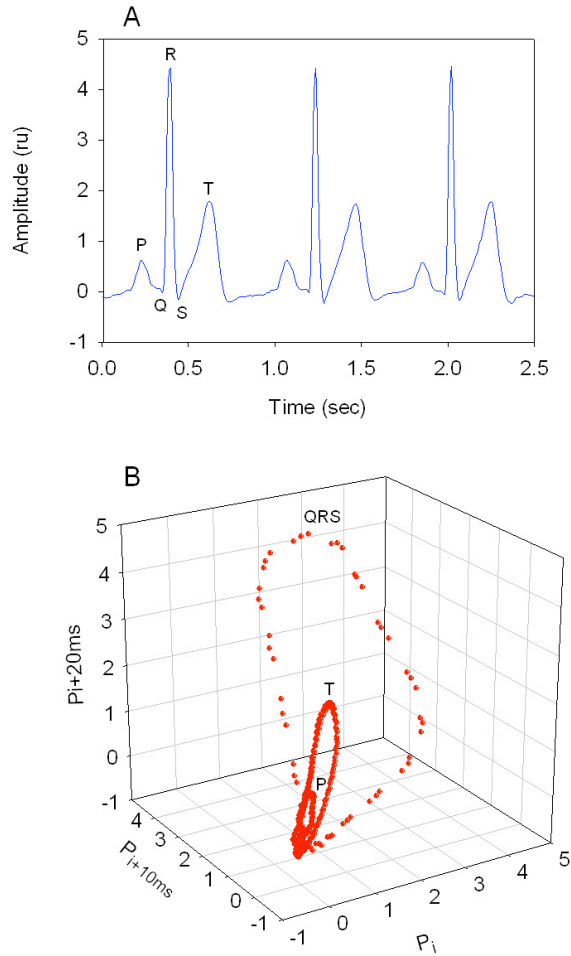


Figure 2.3. (A) Time series of a one-dimensional, lead II electrocardiogram recorded from a normal human volunteer and digitized at a rate of 200 Hz. Displayed are the first three cardiac cycles with characteristic P waves (atrial depolarization), QRS complexes (ventricular depolarization) and T waves (ventricular repolarization). (B) Three-dimensional reconstruction of the ECG signal in phase space by the method of time delays ( $\tau = 10$  ms). Each ECG wave (P, QRS, T) forms its own unique loop (three times), returning to isopotential (0,0,0 amplitude units) between waves (T-P interval). Time series data from file ECG (A) with 5 ms per point. Phase-space data from file ECG with DELAY = 2 points (10 ms) or 4 points (20 ms).

higher-dimensional system consisting of multiple coupled variables can be reconstructed from but a single measured variable of that system. That is, the actual dimension of the system ( $D$ ) is set by a

number of participant variables, but we may only need to measure one of those variables to learn interesting features of the system's underlying dynamics. The reconstruction is performed by defining time-delayed vectors ( $V_i$ ) of  $M$  points ( $P_i$ ) that are delayed or offset in time ( $\tau$ ). Thus, each point represents a single amplitude (scalar) at a specific instance in time.

$$\text{D-dimensional vector, } V_i = P_i + P_{i+\tau} + P_{i+2\tau} + \dots + P_{i+(D-1)\tau} \quad [2.1]$$

Think of what this means graphically for our single-lead ECG signal. If the 1-dimensional data (ECG vector) are plotted against itself twice delayed ( $\tau$  and  $2\tau$ ) on a three-axis plot, the signal is promoted into 3-dimensional space as shown in Figure 2.3B. As seen, the morphology of this normal electrocardiogram forms three loops in phase space corresponding to the P, QRS and T waves of the ECG time series. Topologically, these loops are identical to the simultaneous plotting of three orthogonal leads, had they been recorded. That is, the one measured variable (ECG lead II) becomes a surrogate for the two unmeasured variables (ECG leads I & III).

Careful examination of Equation 2.1 explicitly introduces two of the seven recurrence parameters mentioned previously. First we need to know into what dimension the dynamic should be projected, the embedding dimension ( $M$ ), where  $M \geq D$ . And second, for  $M > 1$ , we need to pick an appropriate delay ( $\tau$ ) between sequential time points in the 1-dimensional signal. It must be appreciated that the selections of embedding dimension and delay are not trivial, but are based on

nonlinear dynamical theory. Moreover, the presence of noise complicates the situation, as will be discussed later.

*Embedding dimension* (M or EMBED), the first recurrence parameter, can in principle be estimated by the nearest-neighbor methodology of Kennel, Brown, and Abarbanel (1992). Parameter M is increased in integer steps until the recruitment of nearest neighbors of the dynamic under scrutiny becomes unchanging. At this particular value of M, the information of the system has been maximized (and, technically speaking, the attractor has been completely unfolded). Thus, there is no need to explore higher dimensions since no new information would be recruited anyway. This methodology works well on stable and low-noise systems, which are most notably found in mathematical examples such as the Lorenz attractor (Lorenz, 1963). But when it comes to real-world data, noise inflates the dimension (D) (Parker & Chua, 1989), and non-stationarities (transients, drifts) in the system modulate the critical M. Thus, in practice,  $M > D$ . Because of these practical limitations, we typically use embedding dimensions of 10 to 20 on biological systems, but no higher. It is a curious fact that when the embedding dimension is set to too high, even random/stochastic systems (which in theory exhibit recurrence only by chance) display strong, yet artifactual, patterns of recurrence.

*Delay* ( $\tau$  or DELAY), the second recurrence parameter, should be selected so as to minimize the interaction between points of the measured time series. This, in effect, opens up the attractor (assuming one exists), by presenting its largest profile. An analogy would be the construction of a circle by plotting a sine wave against itself delayed by 90 degrees (whereas delaying by a mere 1 degree would yield a very

thin, slightly bowed line profile). Two common ways of selecting a proper delay include finding the first minimum in either the (linear) autocorrelation function or (nonlinear) mutual information function (Frazer & Swinney, 1986) of the continuous time series. For discontinuous signals (maps as opposed to flows), such as R-R intervals extracted from the continuous ECG signals, the delay is best set to 1 (no points in the time series are skipped). In special cases, parameter  $\tau$  can also be set to 1 for continuous flows if the goal is to perform waveform matching (recurrence matching of similar waveforms, point-for-sequential-point). As a corollary to this discussion, Grassberger, Schreiber, and Schaffrath (1991) demonstrated that the delay is a non-critical critical parameter, provided the attractor is sufficiently opened up. When any parameter is non-critical it simply means that the quantitative features of the system are robust and stable against changes in the named parameter. This comes as good news for physiological systems in which we need not over concern ourselves with finding the optimal delay (which anyway is non-existent for transient states), since many delays will suffice for the same system.

The third recurrence parameter is the *range*, defined by the selected starting point ( $P_{\text{start}}$ ) and ending point ( $P_{\text{end}}$ ) in the time series to be analyzed. For an embedded time series ( $M > 1$ ) of  $N$  points, it becomes obvious that  $M - 1$  embedded points must extend beyond  $P_{\text{end}}$ . Thus  $P_{\text{end}}$  can extend no further than  $N - M + 1$  points into the available data. In effect, the range defines a window ( $W = P_{\text{end}} - P_{\text{start}} + 1$ ) on the dynamic under investigation. As will be stressed, short windows focus on small-scale recurrences, whereas long windows focus on large-scale recurrences (see Figure 2.8).

The fourth recurrence parameter is the *norm*, of which there are three selections possible: Minimum norm, maximum norm, and Euclidean norm. As implied by its name, the norm function geometrically defines the size (and shape) of the neighborhood surrounding each reference point. The recurrence area is largest for the max norm, smallest for the min norm, and intermediate for the Euclidean norm (see Marwan, 2003a). (Since a vector must have at least two points, each norm is unique if and only if  $M > 1$ , else all norms are exactly equivalent for  $M = 1$ .) But before we can get explicit about norms, it is necessary to be absolutely clear as to how vectors are defined from the 1-dimensional time series. Think of it this way. Take a vector time series (T) of N scalar points (P) and double label the time series as follows:

$$T_i = T_j = P_1, P_2, P_3, P_4, \dots, P_N. \quad [2.2]$$

The dual subscripts ( $i \neq j$ ) refer to different points ( $P_i$  and  $P_j$ ) in  $T_i$  and  $T_j$  when  $M = 1$ , but to different vectors ( $V_i$  and  $V_j$ ) in  $T_i$  and  $T_j$  when  $M > 1$ . Each vector is constructed by starting with an initial point and taking  $M - 1$  subsequent points offset by  $\tau$  (see Equations 2.3 and 2.4 and compare with Equation 2.1). The distances between all possible combinations of  $i$ -vectors ( $V_i$ ) and  $j$ -vectors ( $V_j$ ) are computed according to the norming function selected. The minimum or maximum norm at point  $P_i, P_j$  is defined, respectively, by the smallest or largest difference between paired points in vector- $i$  and vector- $j$  ( $V_i - V_j$ ). The Euclidean norm is defined by the Euclidean distance between paired vectors (Equation 2.5).

$$V_i = P_i + P_{i+\tau} + P_{i+2\tau} + \dots + P_{i+(M-1)\tau} \quad [2.3]$$

$$V_j = P_j + P_{j+\tau} + P_{j+2\tau} + \dots + P_{j+(M-1)\tau} \quad [2.4]$$

$$\text{Euclidean distance} = \sqrt{\sum (V_i - V_j)^2} \quad [2.5]$$

Computed distance values are distributed within a distance matrix  $DM[j, i]$  which aligns vertically with  $T_j$  and horizontally with  $T_i$  ( $i = 1$  to  $W$ ;  $j = 1$  to  $W$ ; where maximum  $W = N - M + 1$ ). The distance matrix has  $W^2$  elements with a long central diagonal of  $W$  distances all equal to 0.0. This ubiquitous diagonal feature arises because individual vectors are always identical matches with themselves ( $V_i = V_j$  whenever  $i = j$ ). The matrix is also symmetrical across the diagonal (if vector  $V_i$  is close to vector  $V_j$  then by necessity vector  $V_j$  is close to vector  $V_i$ ).

The fifth recurrence parameter is the *rescaling* option. The distance matrix can be rescaled by dividing down each element in the distance matrix (DM) by either the mean distance or maximum distance of the entire matrix. In general, DM rescaling allows systems operating on different scales to be statistically compared. Mean distance rescaling is useful in smoothing out any matrix possessing an outlier maximum distance. But maximum distance rescaling is the most commonly used (and recommended) rescaling option, which redefines the DM over the unit interval (0.0 to 1.0 or 0.0% to 100.0%). It is also possible to leave the DM unaltered by not rescaling. In such special cases, DM distances are expressed in absolute units identical to the amplitude units of the input time series (volts, mm Hg, angstroms, seconds, etc.).

The sixth recurrence parameter is the *radius* (RADIUS), which is always expressed in units relative to the elements in the distance matrix, whether or not those elements have been rescaled. In the sea wave example, the radius was actually set to three different values: RADIUS = 0.0, 0.2, and 0.9 ft (Figures 2.2A, B, and C, respectively). In that case we can speak in absolute distances because the distance matrix was never rescaled. In effect, the radius parameter implements a cut-off limit (Heavyside function) that transforms the distance matrix (DM) into the recurrence matrix (RM). That is, all (i, j) elements in DM with distances at or below the RADIUS cutoff are included in the recurrence matrix (element value = 1), but all other elements are excluded from RM (element value = 0). Note carefully that the RM derives from the DM, but the two matrices are not identical. As seen for the wave data (Figure 2.2), as the radius increases, the number of recurrent points increases. Only when RADIUS equals or exceeds the maximum distance is each cell of the matrix filled with values of 1 (the recurrence matrix is saturated). The “shotgun plot” of Figure 2.4 provides a conceptual framework for understanding why an increasing RADIUS captures more and more recurrent points in phase space. Thus, if one becomes too liberal with RADIUS, points ( $M = 1$ ) or vectors ( $M > 1$ ) that are actually quite distant from one another will nonetheless be counted as recurrent (the recurrence matrix is too inclusive). Proper procedures for selecting the optimal RADIUS parameter will be described below.

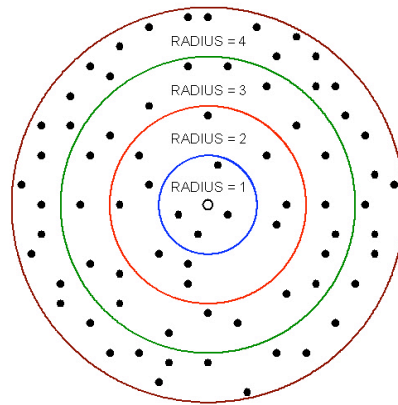


Figure 2.4. Representation of a hypothetical system in higher-dimensional phase space with a splay of points (closed dots) surrounding a single reference point (open dot). The points falling within the smallest circle (RADIUS = 1 distance units) are the nearest neighbors of the reference point. That is, those points are recurrent with the reference point. The second concentric circle (RADIUS = 2 distance units) includes a few more neighbors, increasing the number of recurrences from 4 to 14. Increasing the radius further (RADIUS = 3 or 4 distance units) becomes too inclusive, capturing an additional 20 or 60 distant points as nearest neighbors when, in fact, they are not.

The seventh and last parameter is termed the *line* parameter (LINE). This parameter is important when extracting quantitative features from recurrence plots (see next section), but exerts no effect on the recurrence matrix itself. If the length of a recurrence feature is shorter than the line parameter, that feature is rejected during the quantitative analyses. Typically, the line parameter is set equal to 2 because it takes a minimum of two points to define any line. But it is possible to increase the line parameter (in integer steps) and thereby implement a quantitative filter function on feature extractions, but this is not necessarily recommended.

## RECURRENCE QUANTIFICATION

Simply put, recurrence plots, especially colored versions expressing recurrence distances as contour maps, are beautiful to look at (e.g., Figure 2.2C). With little debate, global recurrence plots of time series and signals extant in nature captivate one's attention. Admittedly, such curious and intriguing graphical displays tend more to evoke artistic than scientific appreciation, and rightfully so. Recalling the brief history of recurrence analysis, recurrence plots were originally posited as qualitative tools to detect hidden rhythms graphically (Eckmann et al., 1987). From the outset, color was not the key; rather the specific patterns of multi-dimensional recurrences gave hints regarding the underlying dynamic. Early on it was understood how important it was to hold the radius parameter to small values so as to keep the recurrence matrix sparse. In so doing, emphasis was placed on local recurrences that formed delicate, lacy patterns. All of this is well and good, but the next logical step was to promote recurrence analysis to quantitative status (Zbilut & Webber, 1992; Webber and Zbilut, 1994). Instead of trusting one's eye to "see" recurrence patterns, specific rules had to be devised whereby certain recurrence features could be automatically extracted from recurrence plots. In so doing, problems relating to individual biases of multiple observers and subjective interpretations of recurrence plots were categorically precluded.

We will highlight the fundamental rules of recurrence quantification analysis (RQA) by employing the classic strange attractor of Hénon (1976). This chaotic attractor is a geometrical structure (system) that derives its form (dynamic) from the nonlinear coupling of

two variables. Note in Equation 2.6 that the next data point,  $X_{i+1}$ , is a nonlinear function of the previous  $X_i$  and  $Y_i$  terms (the  $X_i^2$  term provides the nonlinear interaction), whereas in Equation 2.7 the next  $Y_{i+1}$  is a linear function of the previous  $X_i$  term.

$$X_{i+1} = Y_i + 1.0 - (1.4X_i^2) \quad [2.6]$$

$$Y_{i+1} = 0.3X_i \quad [2.7]$$

We seeded the coupled Hénon variables with initial zero values (e.g.,  $X_0 = Y_0 = 0.0$ ) and iterated the system 2000 times to create a sample time series. To make sure the dynamic settled down on its attractor, the first 1000 iterations were rejected as transients. The next 200 iterations of the system are plotted in Figure 2.5 (cycles 1001 through 1200), which shows the complex dynamics of the coupled variables. Plotting  $Y_i$  as a function of  $X_i$  generates the Hénon strange attractor (Figure 2.6A). It is called an attractor because dynamical points are “attracted” to certain positions on the map and “repelled” from other positions (the white space). Note that the points remain confined within tight limits ( $\pm 1.3$  for  $X$  and  $\pm 0.4$  for  $Y$ ) without flying off to infinity. The dimension of the Hénon attractor is estimated to be around 1.26 (Girault, 1991), which is a fractal or non-integer dimension. Fractal dimensions relate more to the mathematical concept of scaling than real-world dimensions, which must be integers (see Liebovitch & Shehadeh, Chapter 5). Recalling the method of time delays as discussed for the ECG example (Figure 2.3), plotting  $X_i$  (current value) as a function of  $X_{i+1}$  (next value) topologically reproduces the Hénon

attractor (Figure 2.6B). So does plotting  $Y_i$  as a function of  $Y_{i+1}$  (Figure 2.6C). These relationships underscore the remarkable power of surrogate variables to adequately substitute for unmeasured variables by using the method of time delays (Takens, 1981).

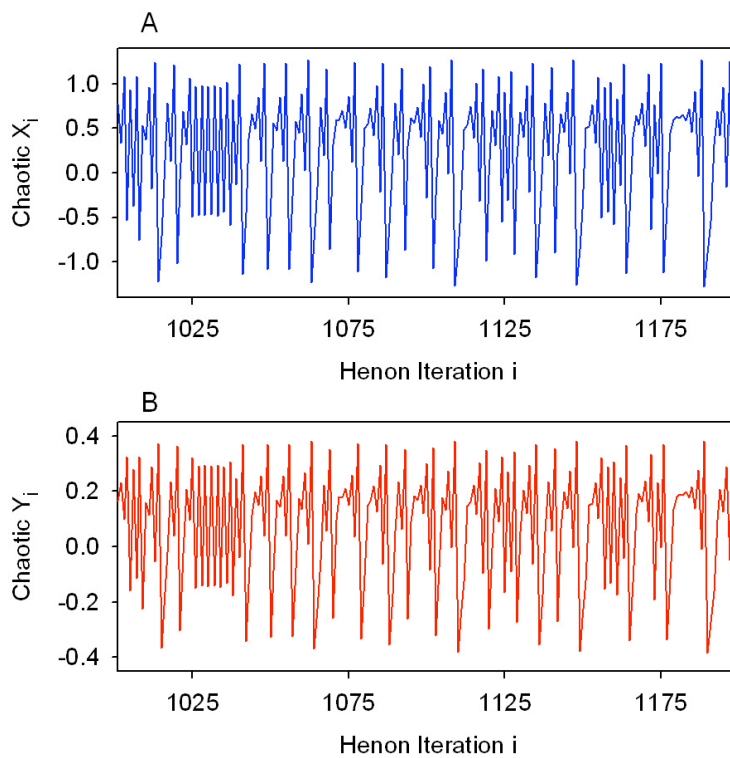


Figure 2.5. Fluctuations of the  $X_i$  and  $Y_i$  variables comprising the Hénon system in its chaotic mode (Equations 2.6 and 2.7). The first 1000 iterations are rejected before plotting the next 200 iterations (cycles 1001-1200). The dynamic behaviors of both variables are complex, but bounded to the Hénon attractor (see Figure 2.6). The dynamics are also fully deterministic, yet noisy, depending upon the round-off routines implemented by the digital computer that generated the data. Iterated data from files *HENCX* and *HENCY*.

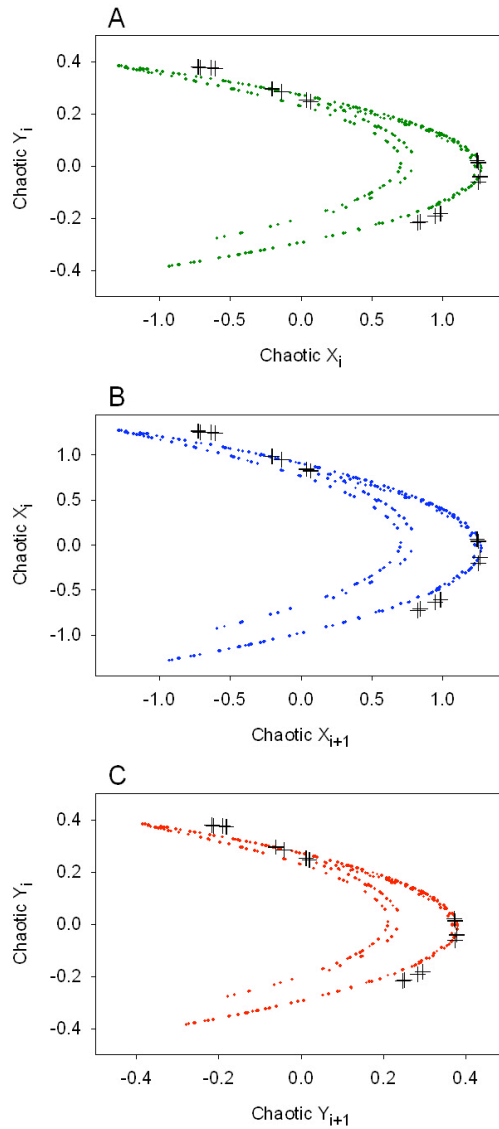


Figure 2.6. Reconstruction of the Hénon strange attractor in phase space by three separate methods. (A) Plotting  $Y_i$  versus  $X_i$  generates the familiar Hénon strange attractor (dots; Equations 2.6 and 2.7) or 16-point Hénon periodic attractor (crosshairs; Equations 2.18 and 2.19). (B) Plotting  $X_i$  versus  $X_{i+1}$  reconstructs the topological features of the original Hénon strange attractor by the method of time delays. (C) Plotting  $Y_i$  versus  $Y_{i+1}$  also reconstructs the attractor. Plots generated from data files *HENCX*, *HENCY*, *HENPX*, *HENPY* (with DELAY = 1 for B and C).

Let us select the Hénon X variable (Figure 2.5A) and generate a recurrence plot of this single variable, as shown in Figure 2.7. The window size ( $W$ ) is 200 points (e.g., cycles 1001-1200). This is an auto-recurrence plot since the Hénon X variable is being compared with itself (points  $X_i =$  points  $X_j$ , 3 points at a time since  $M = 3$ ). Qualitative examination of the symmetrical recurrence plot reveals short line segments parallel to the central diagonal, a cluster of points correspondent to a brief period-2 structure in the dynamic (cycles 1025-1036), and a few isolated points representing chance recurrences. We will focus on the diagonal and vertical structures since from those stem the seven recurrence (dependent) variables or quantifications. Because the recurrence plot is symmetrical across the central diagonal, all quantitative feature extractions take place within the upper triangle, excluding the long diagonal (which provides no unique information) and lower triangle (which provides only redundant information).

The first recurrence variable is **%recurrence** (%REC). %REC quantifies the percentage of recurrent points falling within the specified radius. This variable can range from 0% (no recurrent points) to 100% (all points recurrent). For a given window size  $W$ , Equation 2.8 holds true. For the Hénon attractor (Figure 2.7), %REC = 1.201% confirming that the recurrence matrix is sparse (as is desired).

$$\%REC = 100 (\# \text{recurrent points in triangle}) / (W(W - 1) / 2) \quad [2.8]$$

The second recurrence variable is **%determinism** (%DET). %DET measures the proportion of recurrent points forming diagonal line structures. Diagonal line segments must have a minimum length

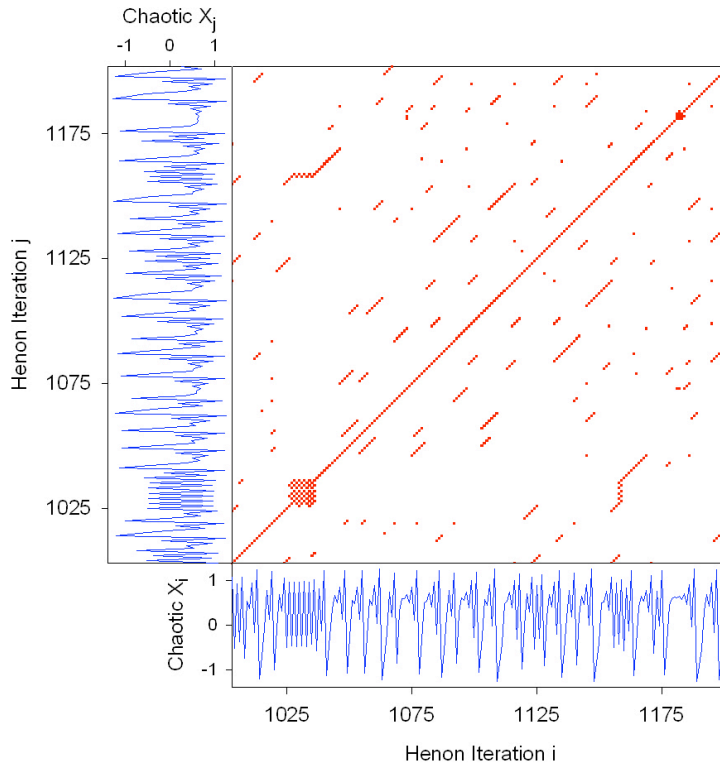


Figure 2.7. Recurrence plot of the Hénon chaotic  $X$  variable. The same variable is plotted on the horizontal (chaotic  $X_i$ ) and vertical axes (chaotic  $X_j$ ) from iterations of coupled Equations 2.6 and 2.7. When vectors of 3 points (e.g.,  $M = 3$ ) match, recurrent points are plotted at the corresponding  $(i, j)$  intersections. The most striking feature of this plot is the short diagonal line structures parallel to the main diagonal. Recurrence data computed from file *HENCX* using program *RQD.EXE*. RQA parameters:  $P_1$ - $P_{last} = 1001$ -1200; RANDSEQ = n; NORM = Euclid; DELAY = 1; EMBED = 3; RESCALE = max dist; RADUS = 3; COLORBND = 1; LINE = 2. RQA variables: %REC = 1.201; %DET = 88.703; LMAX = 12; ENT = 2.557; TND = -4.505; %LAM = 2.510; TT = 2.000.

defined by the line parameter, lest they be excluded. The name determinism comes from repeating or deterministic patterns in the dynamic. Periodic signals (e.g. sine waves) will give very long diagonal lines, chaotic signals (e.g. Hénon attractor) will give very short diagonal lines, and stochastic signals (e.g. random numbers) will

give no diagonal lines at all (unless parameter RADIUS is set too high). For the Hénon attractor (Figure 2.7), %DET = 88.703% showing that most of the recurrent points present are found in deterministic structures.

$$\%DET = 100 (\#points \text{ in diagonal lines}) / (\#recurrent \text{ points}) \quad [2.9]$$

The third recurrence variable is *linemax* (LMAX), which is simply the length of the longest diagonal line segment in the plot, excluding the main diagonal line of identity ( $i = j$ ). This is a very important recurrence variable because it inversely scales with the most positive Lyapunov exponent (Eckmann et al., 1987; Trulla et al., 1996). Positive Lyapunov exponents gauge the rate at which trajectories diverge, and are the hallmark for dynamic chaos. Thus, the shorter the linemax, the more chaotic (less stable) the signal. For the Hénon attractor (Figure 2.7), LMAX = 12 points.

$$LMAX = \text{length of longest diagonal line in recurrence plot} \quad [2.10]$$

The fourth recurrence variable is *entropy* (ENT), which is the Shannon information entropy (Shannon, 1948) of all diagonal line lengths distributed over integer bins in a histogram. ENT is a measure of signal complexity and is calibrated in units of bits/bin. Individual histogram bin probabilities ( $P_{bin}$ ) are computed for each non-zero bin and then summed according to Shannon's equation. For the Hénon attractor (Figure 2.7), ENT = 2.557 bits/bin due to a wide distribution of diagonal line lengths. For simple periodic systems in which all diagonal lines are of equal length, the entropy would be expected to be

0.0 bins/bin (but see Figure 2.12). The units of bits per bin come from taking the base-2 logarithm. For further discussion of ENT see Pellechia and Shockley (Chapter 3).

$$\text{ENT} = -\#(P_{\text{bin}})\log_2(P_{\text{bin}}) \quad [2.11]$$

The fifth recurrence variable is *trend* (TND), which quantifies the degree of system stationarity. If recurrent points are homogeneously distributed across the recurrence plot, TND values will hover near zero units. If recurrent points are heterogeneously distributed across the recurrence plot, TND values will deviate from zero units. TND is computed as the slope of the least squares regression of %local recurrence as a function of the orthogonal displacement from the central diagonal. Multiplying by 1000 increases the gain of the TND variable. For the Hénon attractor (Figure 2.7), TND = -4.505 units, which is within the  $\pm 5$  units, confirming system stationarity (Webber et al., 1995) as achieved by rejecting the first 1000 points.

$$\text{TND} = 1000(\text{slope of \%local recurrence vs. displacement}) \quad [2.12]$$

The sixth and seventh recurrence variables, *%laminarity* (%LAM) and *trapping time* (TT), were introduced by Marwan, Wessel, Meyerfeldt, Schirdewan, and Kurths (2002). %LAM is analogous to %DET except that it measures the percentage of recurrent points comprising vertical line structures rather than diagonal line structures. The line parameter still governs the minimum length of vertical lines to be included. TT, on the other hand, is simply the average length of

vertical line structures. For the Hénon attractor (Figure 2.7), %LAM = 2.510% and TT = 2.000, showing that vertical line structures are not common for this system.

$$\%LAM = 100(\#points\ in\ vertical\ lines)/(\#recurrent\ points) \quad [2.13]$$

$$TT = \text{average length of vertical lines} \times \text{parameter line} \quad [2.14]$$

Recurrence plots and recurrence quantifications are strongly dependent on the sequential organization of the time series or data string. By contrast, standard statistical measures such as mean and standard deviation are sequence independent. Random shuffling of the original sequence destroys the small-scale structuring of line segments (diagonal as well as vertical) and alters the computed recurrence variables, but does not change the mean and standard deviation. A good analogy would be that of Morse code. Random shuffling of the dots and dashes would not change the percentage of dots and dashes in the code, but it would certainly alter/destroy the encoded message! This important idea will be expanded upon when we discuss linguistic texts and protein codes.

## RECURRENCE EPOCHS

So far we have demonstrated that time series data (linear vectors of sequential scalar measurements of length N) can be embedded into higher dimensional space by the method of time delays (Takens, 1981). Distances between all possible vectors are computed and registered in a distance matrix, specific distance values being based on the selected

norm parameter. A recurrence matrix (RM) is derived from the distance matrix (DM) by selecting an inclusive radius parameter such that only a small percentage of points with small distances are counted as recurrent (yielding a sparse RM). The recurrence plot (RP), of course, is just the graphical representations of RM elements at or below the radius threshold. Seven features (recurrence variables) are extracted from the recurrence plot within each window ( $W$ ) of observation on the time series. The question before us now is how can these recurrence variables be useful in the diagnosis of dynamical systems?

Whenever any dynamic is sampled, we are taking a "slice of life," as it were. The dynamic was "alive" before we sampled it, and probably remained "alive" after our sampling. Consider, for example, the EMG signal recorded from the biceps muscle of a normal human volunteer and its attendant recurrence plot in Figure 2.8 (Webber, Schmidt, & Walsh, 1995). The focus is on the first 1972 points of the time series digitized at 1000 Hz (displayed from 37 ms to 1828 ms). But how might these digitized data be processed in terms of recurrence analysis? It would certainly be feasible to perform recurrence quantifications within the entire window ( $W_{\text{large}} = 1972$  points) as represented by the single, large, outer RM square. On the other hand, the data can be windowed into four smaller segments ( $W_{\text{small}} = 1024$  points) as represented by the four smaller and overlapping RM squares. In the latter case the window offset of 256 points means the sliding window jogs over 256 points (256 ms) between windows. Two effects are at play here. First, larger windows focus on global dynamics (longer time frame) whereas smaller windows focus on local dynamics

## Recurrence Quantification Analysis

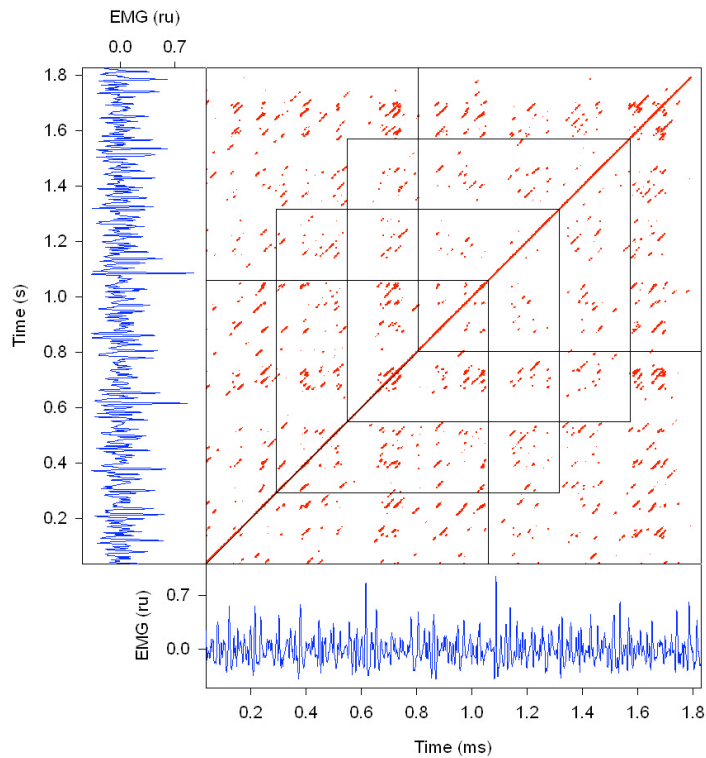


Figure 2.8. Windowed recurrence analysis of resting biceps brachii EMG signal. The large outer square displays the large scale recurrence plot ( $W = 1792 = N$  points). The four small inner squares (epochs) block off the small scale recurrence plots ( $W = 1024 < N$ ) with an offset of 256 points between windows. Recurrence data computed from file *EMG* using program *RQD.EXE*. RQA parameters:  $P_1$ - $P_{last} = 1$ -1972 (for large square) or 1-1024, 257-1280, 513-1536, 769-1792 (for small squares);  $RANDSEQ = n$ ;  $NORM = \text{Euclid}$ ;  $DELAY = 4$ ;  $EMBED = 10$ ;  $RESCALE = \text{max dist}$ ;  $RADUS = 15$ ;  $COLORBND = 1$ ;  $LINE = 2$ . RQA variables (for large square): %REC = 0.335; %DET = 60.905; LMAX = 118; ENT = 1.711; TND = -0.129; %LAM = 55.660; TT = 2.501. RQA variables (for small squares, respectively): %REC = 0.471, 0.407, 0.331, 0.311; %DET = 68.560, 65.603, 66.474, 68.140; LMAX = 118, 118, 118, 59; ENT = 1.753, 1.778, 1.751, 1.572; TND = -0.488, -0.663, -0.644, -0.464; %LAM = 59.635, 54.435, 45.759, 44.506; TT = 2.454, 2.500, 2.396, 2.425.

(shorter time frame). Second, larger window offsets yield lower time-resolution RQA variables, whereas smaller window offsets yield higher time-resolution variables. Remember, seven RQA variables are computed (extracted) from each RM (or RP). By implementing a sliding window design, each of those variables is computed multiple times,

creating seven new derivative dynamical systems expressed in terms of %REC, %DET, LMAX, ENT, TND, %LAM, and TT. Alignment of those variables (outputs) with the original time series (input) (adjusting for the embedding dimension,  $M$ ) might reveal details not obvious in the 1-dimensional input data.

Here are the important details of this the muscle fatigue experiment performed by Webber et al. (1995) which illustrate these fundamental rules of sliding windows (termed *epochs*). While seated comfortably, normal human volunteers were instrumented for the recording of surface EMG signals from the biceps brachii as shown in Figure 2.9A. Subjects were asked to hold their forearm parallel to the floor and their elbow at  $90^\circ$ . A 1.4 kg weight was placed in the open palm and a control EMG recording was digitized at 1000 Hz. After 60 seconds of recording, the weight load was increased to 5.1 kg, which led to total muscle fatigue in 1 to 6 minutes (or 2.8 minutes for the example subject in Figure 2.9), depending upon the biceps muscle mass of the subject. The experiment was designed to compare the performance of nonlinear RQA and linear spectral analysis on identical EMG signals. Might the two techniques have differential sensitivities?

The recorded time series ( $N = 227,957$  points) was partitioned in shorter windows ( $W = 1024$ ) or epochs, each 1.024 seconds long. Adjacent windows were offset by 256 points (75% overlap), fixing the time resolution to 256 ms. Spectral features and recurrence quantifications were then computed for each of the 887 sliding windows. As shown in Figure 2.9B and 2.9C, respectively, the spectral center frequency ( $F_c$ ) and recurrence %DET were stable during the 60 second, low-weight control period. For statistical purposes, 95%

## Recurrence Quantification Analysis

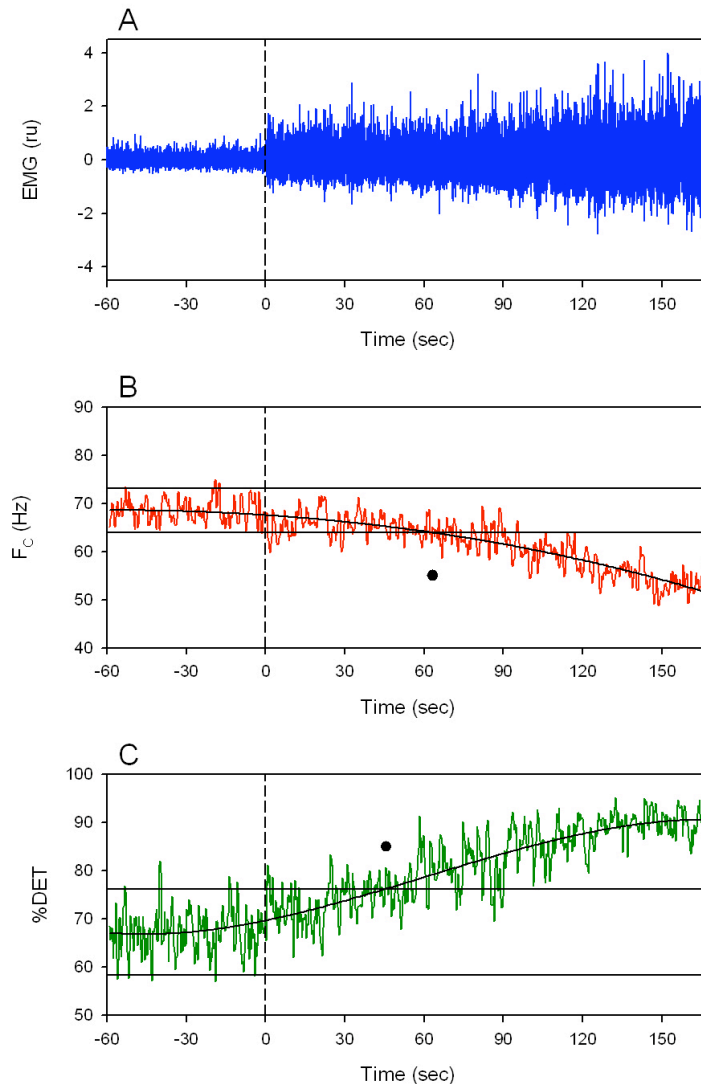


Figure 2.9. Muscle fatigue experiment in a human volunteer, designed to force the system through a series of state changes until task failure occurs. (A) Bipolar surface EMG recording from the biceps brachii muscle during light-weight loading (1.4 kg) before time zero, and heavy-weight loading (5.1 kg) starting at time zero. After 60 sec of control (steady-state dynamics), the subject was forced onto a trajectory (transient dynamic) ending in task failure over the next 167 sec. (B) Spectral center frequency ( $F_c$ ) remains constant during the light-weight loading, but slowly decreases during the heavy-weight loading. The first spectral detection of fatigue occurs at 63.3 sec when the 3<sup>rd</sup> degree polynomial breaks out of the control 95% confidence limits (dot). (C) Recurrence variable %DET also remains constant during the light-weight loading, but increases during the heavy-weight loading. Fatigue is detected by %DET after only 45.6 sec (dot) or 28% sooner than  $F_c$ . EMG digitized at a rate of 1000 Hz. Recurrence data computed from data file *EMG* using program *RQE.EXE*. RQA parameters:  $P_1$ - $P_{last}$  (first epoch) = 1-1024; SHIFT = 256; #EPOCHS = 887; RANDSEQ = n; NORM = Euclid; DELAY = 4; EMBED = 10; RESCALE = max dist; RADUS = 15; LINE = 2.

confidence limits were drawn for each control trace, and a 3<sup>rd</sup> degree polynomial was constructed through each data set. Increasing the load, however, perturbed the steady-state dynamics and set the biceps' contractile machinery on a transition trajectory toward muscle fatigue and ultimate task failure. Examination of the output data shows that during the fatiguing process,  $F_C$  decreased whereas %DET increased. Both variables can be interpreted as indicators of larger motor unit recruitment and synchronization, but that is not the point being made here. What is significant is the fact that the %DET broke out of its 95% confidence limit before  $F_C$  broke out of its 95% confidence limit (e.g. at 45.6 sec versus 63.3 sec after the heavy loading, respectively, or 28% sooner). It can be concluded that whereas both spectral and recurrence strategies are responsive to dynamical changes in physiological systems such as fatiguing muscle, recurrence quantification is substantially more sensitive. In other words, subtle dynamical departures from "steady state" occurring in time series data might be delayed or even missed by spectral tools, but detected sooner and/or more accurately by recurrence tools.

This EMG example illustrates the power of sliding recurrence windows, but we glanced over the determination of the several important recurrence parameters. As mentioned, each window consisted of 1024 points (range). But we also selected the Euclidean norm, maximum distance rescaling, and a line of 2 (all typical choices). But what about the delay, radius, and embedding dimension parameters—how were they selected? First, to estimate an ideal delay time, the control EMG data (58 windows of non-overlapping, adjacent windows, 1.024 sec each) were subjected to autocorrelation analysis.

The average delay, based on the first zero crossing of the autocorrelation function (a zero value indicates no correlation), was found to be 4 digitized points or 4 ms. Second, to estimate the proper radius threshold, the beginning control EMG data (1 window or epoch or 1024 points) were subjected to recurrence scaling analysis. In this case, recurrence variables were recomputed for a family of radius values from 0% to 100% in steps of 1% (of the maximum distance in the distance matrix). Figure 2.10 depicts the results with respect to %REC and %DET. With increasing RADIUS values, %REC increased smoothly to its maximum, following either a sigmoidal curve with linear scaling (Figure 2.10A) or a more linear curve with double logarithmic scaling (Figure 2.10B). On the other hand, %DET exhibited a hitch or shelf with a first local minimum at a radius of 17%. This oddity is due to the faster recruitment of isolated recurrent points than points contributing to diagonal line structures as RADIUS is incremented (Figure 2.10C; see Equation 2.9).

There are three guidelines for selecting the proper radius (in order of preference): (1) RADIUS must fall with the linear scaling region of the double logarithmic plot; (2) %REC must be kept low (e.g., 0.1 to 2.0%); and (3) RADIUS may or may not coincide with the first minimum hitch in %DET. Weighing all three factors together, a radius of 15% was selected for the example EMG data (vertical dashed lines in Figure 2.10), which fits all three criteria. Because there are mathematical scaling rules linking  $\log(\%REC)$  with  $\log(RADIUS)$ , as will be discussed below, the first guideline for RADIUS selection is preferred. In contrast, since there are no known rules describing the hitch region in %DET, this latter method must be applied with caution—user beware.

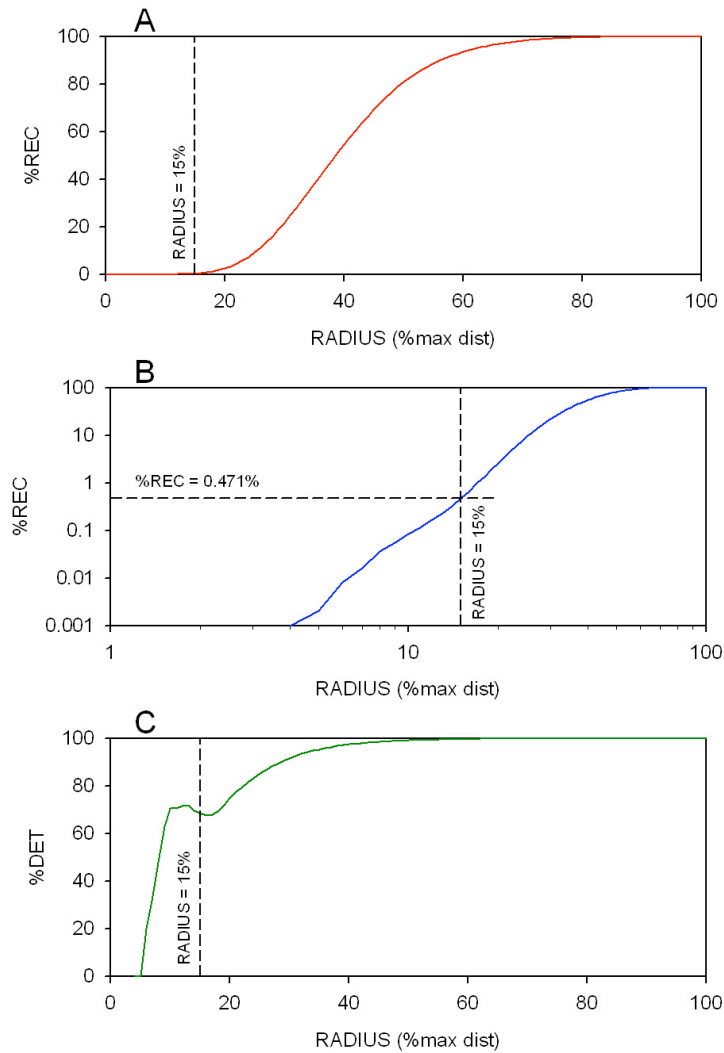


Figure 2.10. Methods for selecting the proper radius parameter for recurrence analysis of the control EMG recording. (A) With step increases in RADIUS, the density of recurrence points (%REC) increases along a sigmoid curve ( $M = 10$ ). (B) Double-logarithmic plot of %REC as a function of RADIUS defines a linear scaling region from RADIUS = 8% to 15%. RADIUS is selected at 15% where %REC is 0.471% (sparse recurrence matrix). (C) Linear plot of %DET as a function of RADIUS showing a short plateau and small trough near RADIUS = 15% which may or may not be coincidental. Recurrence data computed from file *EMG* using program *RQS.EXE*. ROA parameters:  $P_1$ - $P_{last} = 1$ -1024; RANDSEQ =  $n$ ; NORM = Euclid; DATA MIN = DATA MAX = 4; EMBED MIN = EMBED MAX = 10; RESCALE = max dist; RADIUS MIN = 0; RADIUS MAX = 100; RADIUS STEP = 1; LINE = 2.

The third parameter requiring explanation is the embedding dimension. Why did we set  $M = 10$ ? The mathematics underlying the distance matrix are equivalent to the correlation integral implemented by Grassberger and Procaccia (1983) for dimensional analysis of dynamical systems. Theoretically, the Grassberger-Procaccia dimension (GPD) is a measure of the number of independent variables participating in the system at any given instant. Thus, GPD is another measure of complexity, since the greater the number of participant variables, the more complex the system. Practically, the G-P dimension can be estimated by observing how the number of recurrences (#REC) scales with increases in absolute radius (R), as shown by Equation 2.15. The exponential form of this equation is easily converted to its linear form by taking the logarithm of both sides, yielding Equation 2.16. Then, substitution into this equation of %recurrence (%REC) for #REC and relative radius (RADIUS) for absolute radius (R), respectively, gives Equation 2.17.

$$\#REC = R^{GPD} \quad [2.15]$$

$$\log(\#REC) = \log(R)GPD \quad [2.16]$$

$$\log(\%REC) = \log(RADIUS)GPD \quad [2.17]$$

The G-P Dimension is easily computed by taking the ratio (or slope) of %log(%REC) to %log(RADIUS) over a linear scaling region, as discussed by Mayer-Kress and Holzfuss (1987). Such a double-logarithmic plot is illustrated in Figure 2.11A for embedding

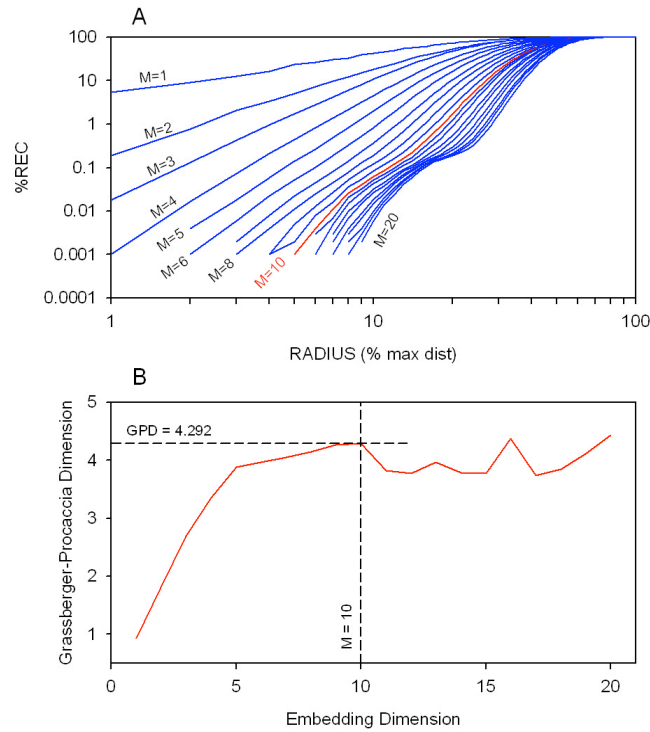


Figure 2.11. Relationship between  $\log(\%REC)$  and  $\log(RADIUS)$  over a range of embedding dimensions ( $M = 1$  to  $20$ ) for the control EMG recording. (A) Each curve in the family of curves has a linear scaling region that is used to estimate the Grassberger-Procaccia dimension (**GPD**) when the slope becomes unchanging with increases in  $M$ . The dashed line refers to the same line plotted in Figure 2.10B at  $M = 10$ . (B) **GPD** plotted as a function of embedding dimension saturates at  $GPD = 4.292$  when  $M = 10$ , the proper embedding for this dynamic. Recurrence data computed from file *EMG* using program *RQS.EXE*. RQA parameters:  $P_1$ - $P_{last} = 1$ -1024;  $RANDSEQ = n$ ;  $NORM = Euclid$ ;  $DATA\ MIN = DATA\ MAX = 4$ ;  $EMBED\ MIN = 1$ ;  $EMBED\ MAX = 20$ ;  $RESCALE = max\ dist$ ;  $RADUS\ MIN = 0$ ;  $RADIUS\ MAX = 100$ ;  $RADIUS\ STEP = 1$ ;  $LINE = 2$ .

dimensions ranging from 1 to 20. As shown in Figure 2.11B, as the embedding dimension ( $M$ ) increases, the slope increases to a “plateau” of  $GPD = 4.292$  (a fractal dimension) starting at  $M = 10$ . Further embeddings do not result in any further increases in GPD. This is the reason why we selected  $M = 10$ . As is most often the case for real data, it should be recognized that  $M > GPD$ . The reason for this is that noise artificially inflates the dimension. Parka and Chua (1989) stated

that for noisy systems, the embedding dimension maximizes at  $M = 2 \times \text{GPD} + 1$ . An  $M$  of 10 for our EMG signal is very close to this theoretical limit ( $M = 2 \times 4.292 + 1 = 9.6$ ). There are numerous practical problems associated with the estimation of  $M$ , including non-stationary dynamics, high-dimensional attractors, and the presence of noise. For example, inspection of the log-log plots (Figure 2.11B) shows a worsening “double hump” of unknown origin in the curves for  $M > 10$ . Therefore, we typically bypass any G-P analysis or nearest-neighbor strategy, and usually set parameter  $M$  to 10, but never higher than 20, for real data.

## RECURRENCE INTERVALS

Recurrence intervals (or recurrence times) quantify the periodicities expressed by dynamical systems. By way of one mundane example, it is proper to say that the recurrence interval (or recurrence time) for the earth’s sun is 24 hours, day in and day out. But for heuristic purposes, let us revisit the coupled Hénon equations discussed above (Equations 2.6 and 2.7) in which the constant multiplier of the nonlinear term  $X_i^2$  is changed from 1.4 to 1.054 as follows:

$$X_{i+1} = Y_i + 1.0 - (1.054X_i^2), \quad [2.18]$$

$$Y_{i+1} = 0.3X_i. \quad [2.19]$$

Such minor tweaking of the equation converts the Hénon chaotic attractor into the Hénon 16-point periodic attractor in phase space (see 16 crosshairs in Figures 2.6A, B, & C). Expressing this periodic

attractor in recurrence space, however, produces a series of parallel lines spanning from border to border as shown in Figure 2.12. Recurrence interval analysis verifies that the vertical spacing between recurrent points throughout the entire plot (including recurrent points in the upper and lower triangles, as well as the central diagonal) is a perfect 16 points, as expected. Since the border effectively truncates diagonal lines to different lengths, an artifactual  $ENT > 0.0$  bit/bin is observed.

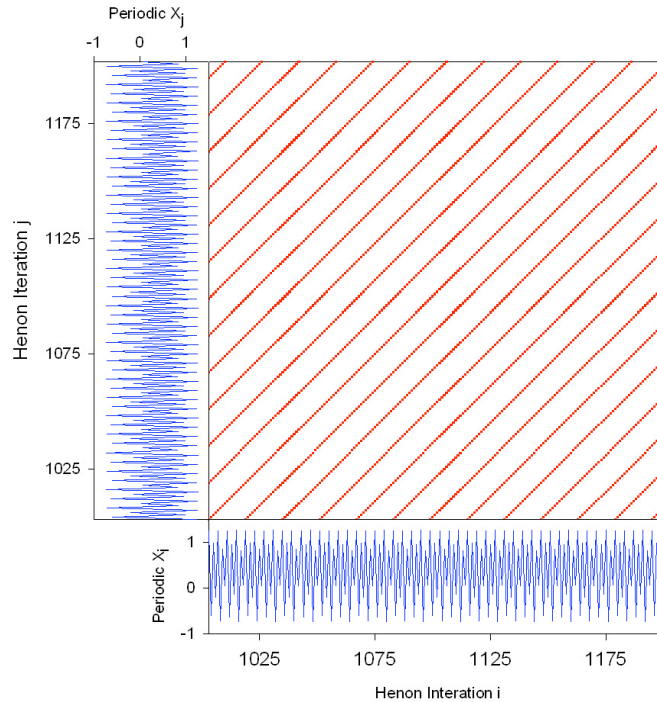


Figure 2.12. Recurrence plot of the 16-point Hénon periodic  $X$  variable. The same variable is plotted on the horizontal (periodic  $X_i$ ) and vertical axes (periodic  $X_j$ ) from iterations of coupled Equations 2.18 and 2.19. When vectors of 3 points (e.g.  $M = 3$ ) match, recurrent points are plotted at the corresponding  $(i, j)$  intersections. The most striking feature of this plot is the long diagonal line structures parallel to the main diagonal and offset by exactly 16 points. Recurrence data computed from file *HENPX* using program *RQD.EXE*. RQA parameters:  $P_1$ - $P_{last} = 1001$ -1200; RANDSEQ = n; NORM = Euclid; DELAY = 1; EMBED = 3; RESCALE = max dist; RADUS = 0.5; COLORBND = 1; LINE = 2. RQA variables: %REC = 5.789; %DET = 100.000; LMAX = 184; ENT = 3.585 (line truncation effect); TND = 12.449; %LAM = 0.000; TT = undefined.

Moving from theoretical mathematics to practical physiology, it is important to demonstrate the power and utility of recurrence interval analysis on revealing subtle features in human electroencephalographic (EEG) signals. To illustrate this, EEG data from a normal quiescent subject were obtained from a local clinical electrophysiology laboratory. The subject was instrumented with 21 active unipolar electrodes referenced to the nose according to the standard 10-20 EEG recording system (electrodes spaced at intervals 10%-20% of head circumference) (Misulis & Head, 2003). The signals were digitized at 500 Hz and bandpass filtered (0.15 Hz - 70.0 Hz). However, instead of selecting just one of the active electrode sites for analysis, Euclidean distances (ED) were computed for each instance in time (every 2 ms) across all 21 electrodes ( $E_n$ ) according to Equation 2.20. In effect, an  $[N,21]$  matrix of 21 parallel vectors was collapsed into a single  $[N]$  vector time series with  $N$  points.

$$ED_i = \sqrt{(E_{1i}^2 + E_{2i}^2 + E_{3i}^2 + \dots + E_{20i}^2 + E_{21i}^2)} \quad [2.20]$$

Recurrence analysis was conducted on 2000 points (4.0 s) of the composite EEG signal (Euclidean vector), which is plotted horizontally and vertically in Figure 2.13. Because the signal was already projected into higher dimensional space ( $D=21$ ), it was inappropriate to set the embedding dimension to anything other than one ( $M = 1$ ). The minimum norm was chosen and the delay parameter was set equal to one ( $\tau = 1$ ), but neither parameter was critical since with an embedding dimension of one, no points were time delayed. The radius was set to 0.2% of the maximum distance rescaling, insuring that %REC < 1%.

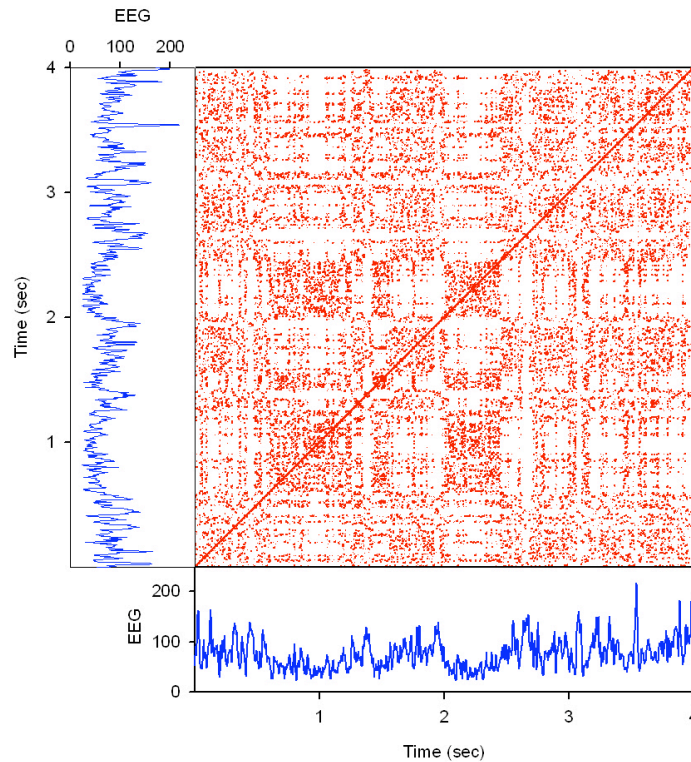


Figure 2.13. Recurrence interval analysis of a normal human electroencephalogram (EEG) digitized at 500 Hz. The time series data are derived from computing the Euclid distances across 21 simultaneously recorded leads of the 10-20 system of electrodes positioned around the skull. Voltages were updated at each instant in time (2 msec) for 40 sec (2000 data points) for recurrence analysis. The recurrence plot has both fine-scale and large-scale features that were captured by measuring the vertical time interval between all recurrent points (see Figure 2.14). Recurrence data computed from file *EEG* using program *RQD.EXE*. RQA parameters:  $P_1$ - $P_{last} = 1$ -2000; RANDSEQ = n; NORM = min norm; DELAY = 1; EMBED = 1; RESCALE = max dist; RADIUS = 0.2; COLORBND = 1; LINE = 2. RQA variables: %REC = 0.804; %DET = 7.318; LMAX = 5; ENT = 0.445; TND = -0.102; %LAM = 11.207; TT = 2.087. These EEG data were kindly provided by Lukasz Konopka, Ph.D., Director of Biological Psychiatry, Hines V.A., Hines, IL 60141.

The recurrence plot for this system (Figure 2.13) reveals a much more complex structuring than that observed with the Hénon 16-point periodic system (Figure 2.12). In fact, the seven recurrence variables were quantified for this EEG signal as follows: %REC = 0.804%; %DET = 7.318%; LMAX = 5; ENT = 0.445; TND = -0.102; %LAM = 11.207%; TT

= 2.087. The homogeneous distribution of recurrent points is quantified by the near zero TND value, indicating the stationary state of the EEG signal in this individual. The %DET value indicates that the signal has deterministic features arising from repeated (recurrent) EEG waves at various frequencies. Likewise, the %LAM value reveals significant laminate structuring of recurring dynamical features in the vertical plane (strings of multiple j-points recurring with single i-points). However, it is the vertical spacing between recurrent points (recurrence intervals) that is of interest to us.

Recurrence quantification interval (RQI) analysis was conducted on this example EEG signal using the exact same parameter settings as indicated above. The distribution of recurrence intervals is plotted in a double logarithmic histogram in Figure 2.14. Of the 32,142 intervals counted, 2,075 (6.46%) recurrence intervals are located in the first bin at 2 ms. These points are usually excluded as noise since they come from adjacent points forming vertical line structures (whence see %LAM). Recurrence intervals spanning 4 to 398 ms were distributed rather uniformly, but over the range from 400 through 1,600 msec the recurrence counts scaled with recurrence time. The remainder of intervals from 1,602 to 3,398 ms contained mostly single-digit counts and comprised the noise floor beyond the scaling region. Within the scaling regions, however, slope (S) defines the scaling relationship between the number of intervals (#INT) and interval length (L).

$$\#INT = L^S \quad [2.21]$$

$$\log(\#INT) = \log(L)S \quad [2.22]$$

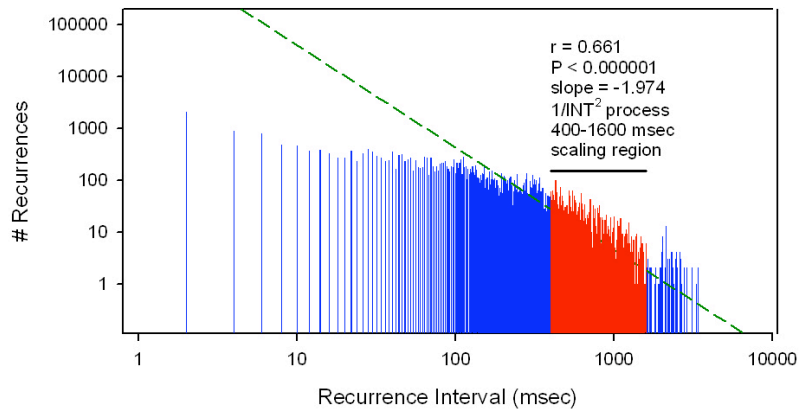


Figure 2.14. Double-logarithmic scaling relation between number of recurrence intervals (tally counts) and duration of recurrence intervals (ms) computed from a normal EEG signal (Figure 2.13). A scaling relation spans the range 400 to 1600 ms and has a significant negative slope ( $p < 0.0000001$ ) of  $-1.974$  (dashed line) indicative of a  $1/INT^2$  process. Recurrence data computed from file *EEG* using program *RQI.EXE*. RQA parameters:  $P_1$ - $P_{last} = 1$ -2000;  $RANDSEQ = n$ ;  $NORM = \text{max norm}$ ;  $DELAY = 1$ ;  $EMBED = 1$ ;  $RESCALE = \text{max dist}$ ;  $RADIUS = 0.2$ .

The linear scaling region (Figure 2.14) has a negative slope  $S = -1.974$ , which is consistent with a  $1/INT^2$  process (where  $INT$  is the recurrence interval) and is highly significant ( $p < 0.000001$ ) for the 380 points defining the scaling region. These data indicate that there are scaling rules in place for the lowest EEG frequency (delta  $< 4$  Hz), but not the higher frequencies (beta  $> 13$  Hz; alpha  $> 8$  Hz; theta  $> 4$  Hz) (Misulis & Head, 2003). This type of RQI analysis is analogous to uncovering  $1/f$  scaling rules, but in the latter case the lower frequencies (longer intervals) carry most of the power (Bassingthwaight et al., 1994; see also Aks, Chapter 7, and Liebovitch & Shehadeh, Chapter 5).

Thomasson, Heoppner, Webber, and Zbilut (2001) and Thomasson, Webber, and Zbilut (2002) performed RQI analysis on

human EEG signals and were able to demonstrate different scaling regions for control EEGs versus pre-ictal EEGs. That is, just prior to seizure activity, the scaling relation became more correlated (steeper negative slope), consistent with a self-organizing process leading to synchronized and focal brain activity. These studies provide evidence that subtle recurrence changes in the electrical dynamic may forecast seizure states in the brain.

### CROSS RECURRENCE

So far we have been speaking of recurrence quantitative analysis from the single signal perspective. That is, in RQA recurrence patterns are sought within individual signals in the spirit of autocorrelation. However, in the spirit of cross correlation, it is possible to detect recurrence patterns shared by paired signals by cross recurrence analysis (KRQA) (Zbilut, Giuliani, & Webber, 1998a; Marwan et al., 2002; Marwan 2003a; see also Shockley, Chapter 4). The mathematics of cross recurrence, as well as the parameters and variables of cross recurrence, all are the same as explained for auto-recurrence. There are two principle differences, however. First, in KRQA distances are computed between two different signals. It is assumed that the two signals arose from coupled systems, were sampled simultaneously at the same digitization rate (which prohibits the drifting of one signal with respect to the other), and are on the same amplitude scale (which permits low distances between signals to be computed). The last requirement can be achieved by rescaling the input data over the unit interval (minimum:maximum mapped to 0.0:1.0), provided that neither of the paired input data streams possess strong nonstationarity (upward

or downward drifts). Second, in KRQA the shared symmetry between the upper and lower triangles of the auto-recurrence plot is lost. In fact the entire central line of identity vanishes. Because of these expected differences from auto-RQA, quantitative cross-recurrence quantifications must be made across the entire matrix (plot), not just the upper half (upper triangle).

Shockley, Butwill, Zbilut, and Webber (2002) performed a very simple experiment on mechanically coupled oscillators. A tray (which served as a driver), filled with fluids of differing viscosities (oil, syrup, or honey), was set into reciprocal, sine-wave motion by a strong sinusoidal motor. A rotor blade (the follower—what was driven by the driver) was positioned within the viscous fluid and was set into independent motion by a pulley system and falling weight (gravity activated). The position of the tray and rotor were monitored by separate motion-tracking sensors and digitized at 60 Hz. Four experimental runs were performed at each of three viscosities. Transients due to acceleration were rejected and 600 points of steady state data (10 s) were collected for each trial. KRQA was performed using the driver-tray as the *i*-signal (*i*-vector,  $V_i$ ) and the follower-rotor as the *j*-signal (*j*-vector,  $V_j$ ). The cross recurrence plot for one of the trials at a medium coupling viscosity is presented in Figure 2.15 ( $M = 5$ ; DELAY = 1; RADIUS = 2.0%). The long diagonal, always present for auto-recurrence plots (e.g., Figures 2.2, 2.7, 2.8, 2.12, and 2.13), is noticeably absent. But short diagonals appear in the plot wherever waveform coupling occurs between the driver (independent and constant frequency) and rotor (dependent and variable frequency).

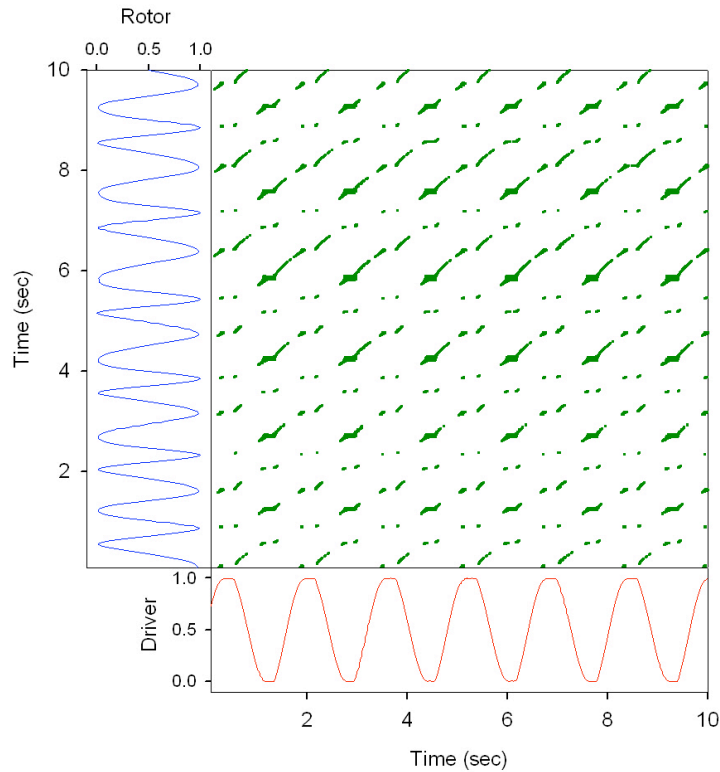


Figure 2.15. Cross recurrence plot of coupled oscillators in a low-viscosity coupling. The positions of the different oscillators are plotted along the horizontal axis (driver oscillator) or vertical axis (rotor oscillator). When vectors of 5 points each match (e.g.  $M = 5$ ), recurrent points are plotted at the corresponding  $i, j$  intersections. The most striking feature of this plot is the unusual distribution of recurrent points reflective of various phasic couplings between the two oscillators. Recurrence data computed from files *DRIVER* and *ROTOR* using program *KRQD.EXE*. RQA parameters:  $P_1 - P_{last} = 1 - 596$ ;  $RANDSEQ = n$ ;  $NORM = Euclid$ ;  $DELAY = 1$ ;  $EMBED = 5$ ;  $RESCALE = \max \text{ dist}$ ;  $RADUS = 2$ ;  $COLORBND = 1$ ;  $LINE = 2$ . RQA variables:  $\%REC = 1.480$ ;  $\%DET = 94.103$ ;  $LMAX = 24$ ;  $ENT = 3.041$ ;  $TND = -0.813$ ;  $\%LAM = 74.834$ ;  $TT = 3.300$ .

Cross recurrence interval analysis (KRQI) on the coupled oscillators results in the frequency spectrum plotted in Figure 2.16. To accomplish this, recurrence intervals were transformed to the frequency domain by taking their reciprocals. For spectral comparison, the Fast Fourier transform (FFT) spectrum is computed on

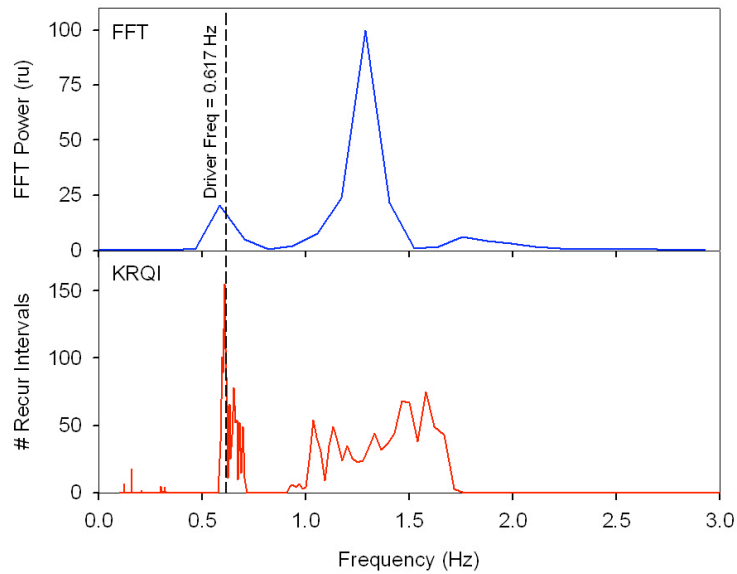


Figure 2.16. Frequency characteristics of the low-viscosity coupled driver-rotor system from linear (FFT) and non-linear (KRQI) perspectives. Spectral analysis (FFT) of the rotor dynamic shows a dominant (uncoupled) frequency faster than the driver frequency at low resolution. Cross recurrence analysis (1/KRQI) reveals similar features but with greater details at high resolution. For example, the high frequency peak is splayed out over a wider frequency band due to subtle nonlinear interactions not detected by FFT. Recurrence data computed from coupled files *DRIVER* and *ROTOR* using program *KRQI.EXE*. RQA parameters:  $P_1$ - $P_{last} = 1$ -596; RANDSEQ = n; NORM = Euclid; DELAY = 1; EMBED = 5; RESCALE = max dist; RADUS = 2; LINE = 2.

the rotor data only. The linear FFT spectrum reports two peaks, a low amplitude peak near the driver frequency (dashed line), and a high amplitude peak at a higher frequency (non-harmonic). The nonlinear KRQI spectrum provides much more details on the partially coupled system. More spectral power is found at the higher, uncoupled frequency, but the frequency band is splayed out due to nonlinear interactions between the rotor and driver. At the lower, coupled frequency (dashed line), the KRQI resolution is superior to the FFT resolution. More importantly, subtle changes in relative viscosity from

0.693 to 0.711 units (1.00 units for high viscosity coupling) gave significant changes in KRQA variables %REC, %DET, and LMAX (not shown). This example illustrates the ease with which cross-recurrence analysis handles non-linearities in short data sets, and at a higher resolution than the FFT to boot.

There is still much work to be done with respect to cross-recurrence analysis, but it is posited that KRQA may be a formidable tool in the examination of coupled oscillators. This may be particularly true for coupled biological oscillators where subtle, short scale changes in coupling may indicate (forecast) altered dynamics that may or may not be healthful for the examined system in part or even the entire organism as a whole. Shockley (Chapter 4) presents a psychological application of KRQA.

#### RECURRENCE PATTERNS OF SPEECH

Recurrence analysis, auto-recurrence or cross-recurrence, is fully amenable to linguistic systems or symbolic dynamics. Actually, one of the easiest explanations of recurrence can be purchased at the price of the simple children's book authored by Dr. Seuss (Geisel, 1960), *Green Eggs and Ham*. Webber and Zbilut (1996, 1998) have repeatedly used this example for instructive purposes. The reasoning goes as follows. Ask a child this riddle, "How can Dr. Seuss write a book with 812 words if he has a limited vocabulary of only 50 words?" The obvious answer is that words must be reused—that is, words recur. While we are at it, why not ask the child, "How can books with thousands of words be written in English, if there are only 26 alphabet letters available?" In this case, letters must be reused. So at the word

level or orthographic (spelling) level, symbols are simply reused in any combination desired by the author, as long as they correspond to allowable words in the language of choice. Common experience informs us that letters in words or words in sentences do not, and need not, appear at periodic intervals. Rather, actual linguistic sequences are at once highly nonlinear and highly meaningful as well. In this context, Orsucci, Walter, Giuliani, Webber, and Zbilut (1999) implemented RQA to study the linguistic structuring of American poems, Swedish poems, and Italian translations of the Swedish poems. They found invariance among the various language exemplars, suggesting hidden structuring at the orthographic level.

It is intriguing to consider the potential ability of recurrence strategies in the analysis of written text or spoken words as first explored by Orsucci et al. (1999) using American and Italian speech samples. Do different authors or various speakers have specific recurrence signatures that betray their individual identities? We might proceed at the orthographic level, rendering any speech text numeric by arbitrarily substituting integers for letters: A=1; B=2; C=3;...; X=24; y=25; Z=26; and for numbers: 0=27; 1=28; 2=29 ...; 7=34; 8=35; 9=36. We can keep things simple by ignoring cases of letters, all punctuation marks, spaces, carriage returns, and linefeeds. But how should the recurrence parameters be set? Well, since the encoding scheme is entirely arbitrary (we could have used: Z=1; Y=2; X=3; ...; etc.), the most important constraint is that the radius must be set to 0 distance units. This will insure that only identical letters (unique integers) will recur with each other. The embedding dimension can be set to one or higher, but for  $M > 1$  the delay should be set to one so as not to skip any

letters in the string. The length of the text sets the maximum size of the window, but smaller windows can parcel the text into a series of epochs. It makes no difference whether the distance matrix is rescaled or not, because the only allowable radius is 0 units. The line parameter should be set to 2, lest one wants to exclude short words longer than two characters each (but that is not advised). With these preliminaries complete, what might diagonal line structures in the recurrence plot signify? If only identical letters count as recurrent points, a string of diagonal recurrences must indicate that the identical string of characters appears at different positions in the text. Actually, lines of varying length must represent words of varying length. Very loosely speaking, we might (correctly) envisage words as vectors of letters! In any case, recurrence quantifications can be captured in the seven recurrence variables we have discussed at length with respect to other dynamical systems.

But let us leave the letter level, and focus rather on words. We now face a new problem, one that involves choosing a scheme for encoding words. Unlike English letters that are limited to 26 characters and 10 digits, English words can number in the hundreds of thousands. For example, The Oxford English Dictionary Online (2003) has some 290,000 entries and 616,500 different English word forms. To encode words, we can assign ascending integer values to each new word, but whenever a former word recurs, its old integer value must be reused. To keep it simple, we can treat all punctuation marks as spaces. After the full text is encoded, the total number of integers in the derived file must equal the total number of words in the text. The number of

different words in the text (vocabulary size) will be represented by the numerical value of the largest integer.

It has long been known that the psychiatric illness of schizophrenia is characterized by disordered speech (Kasanin & Lewis, 1944). So to provide a practical example of quantitative textual analysis using RQA strategies, let us examine the speech patterns of a schizophrenic patient and “normal” academic as quoted by Wróbel (1990). Each quote consists of exactly 165 words. First quoted is the schizophrenic (Wróbel, 1990, p. 77), the context of which reveals this patient’s altered sense of reality. To get the gist of how the 165 words were encoded, here are the codes for the first 26 words (“pre-started” counts as 2 words due to replacement of the dash with a space): 1-2-3-4-5-6-7-8-9-10-11-12-13-*14-15-16*-17-18-*14-15-16*-3-19-18-14-20 (note the repeat pattern of *14-15-16*: “before me and”):

In Wroclaw I pre-started to pray, you know, the psychiatrist Kobohen came before me and he stood before me and I also stood before him, because he came to the ward on a visit, you know, he came before and he says: oh, that's the new one—he says—he arrived today—he says and he made a sign of the cross, you know, like this before me. I felt in the presence of that such terrible desires to pray because of that cross, that I began praying incredibly, I prostrated myself, I prayed on my knees, prostrate, I so implored the Lord God as much as possible, you know, and I felt myself a ruler, you know, I thought I was the supreme ruler on this earth, that over the whole world I was the supreme ruler, I began praying so incredibly with various crosses, yes I prayed so incredibly with crosses, with perfection and in different ways. He was dismissed from there, ...

Second quoted is a normal academic (Wróbel, 1990, p. 99) who speaks logically and with intent purpose. The first 26 words (of 165 words) were encoded as follows: 1-2-3-4-5-6-7-8-9-10-11-9-10-12-13-14-15-6-16-17-18-19-20-21-22-23 (note the repeat pattern of 9-10: "of the").

Newtonian mechanics, for example, imposes a unified form of the description of the world. Let us imagine a white surface with irregular black spots on it. We then say that whatever kind of picture these make, I shall be able to approximate as closely as I wish to the description of it by covering the surface with a sufficiently fine square mesh, and saying of every square whether it is black or white. In this way I shall have imposed a unified form on the description of surface. The form is optional, since I could have achieved the same result by using a net with a triangular or hexagonal mesh. Possibly the use of a triangular mesh would have made the description simpler: that is to say, it might be that we could describe the surface more accurately with a coarse triangular mesh than with a fine square mesh (or conversely), and so on. The different nets correspond to different systems for describing the world.

Recurrence plots were constructed for the 165 words of text comprising each subject's speech as shown in Figure 2.17. Here,  $M = 1$ ,  $DELAY = 1$ , and  $RADIUS = 0$ . The "time series" beside each recurrence plot present as "saw-tooth" patterns due to the reusing (recurrence) of words. Recurrent points are plotted only when exact word matches are found. Recurrence quantifications are reported in Table 2.1 for these two subjects, both at the orthographic and word levels, before and after random shuffling. The 742-character normal text was truncated to 670 characters to match the number of characters

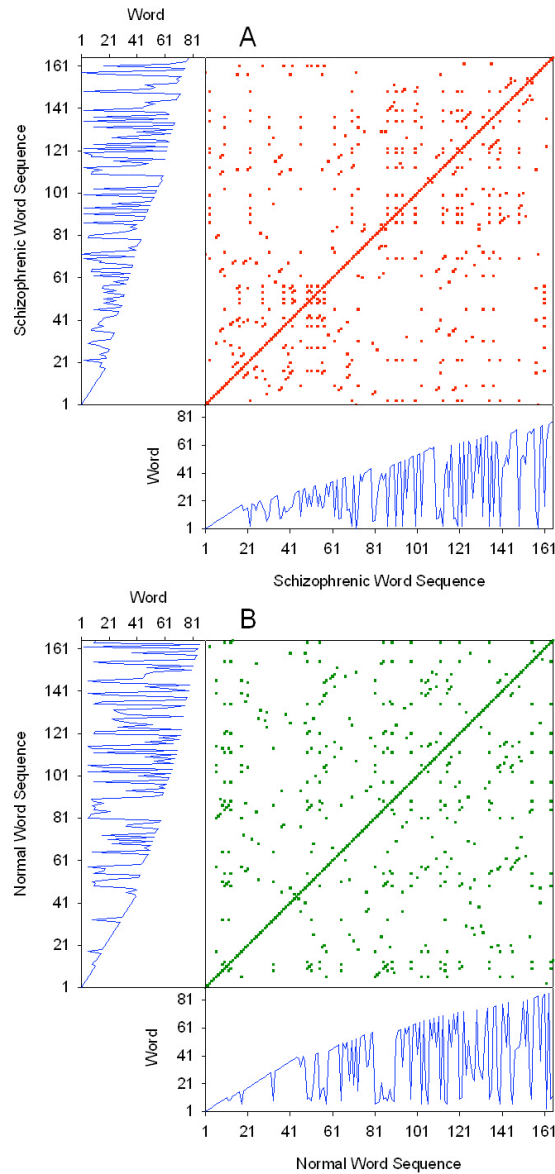


Figure 2.17. Recurrence analysis of human speech patterns at the word level. (A) Schizophrenic speech. (B) Normal speech. Recurrences occur only for exact word matches. Recurrence data computed from individual files *SCHIZWRD* and *NORMWRD* using program *RQD.EXE*. RQA parameters:  $P_1$ - $P_{last}$  = 1-165; RANDSEQ = n; NORM = Euclid; DELAY = 1; EMBED = 1; RESCALE = absolute; RADUS = 0; COLORBND = 1; LINE = 2. RQA variables for schizophrenic speech (A): %REC = 1.870; %DET = 26.087; LMAX = 5; ENT = 0.675; TND = -8.361; %LAM = 0.000; TT = undefined. RQA variables for normal speech (B): %REC = 1.567; %DET = 23.113; LMAX = 3; ENT = 0.773; TND = -1.898; %LAM = 0.000; TT = undefined. See also Table 1.

in the schizophrenic text. cursory review of the data reveal more differences at the word level than orthographic level. Shuffling decidedly distorts the deterministic structures. Admittedly, these examples are only anecdotal exercises without statistical merit. But what is being emphasized is the potential for nonlinear recurrence methodology to be employed on different speech patterns from many subjects, with careful attention being paid to proper experimental design.

Table 2.1. *Recurrence quantification analysis of human speech patterns. Data were computed from native sequences (and shuffled sequences) of letters (data files SCHIZLET and NORMLET) and words (data files SCHIZWRD and NORMWRD) using program RQD.EXE.*

RQA Variable	Schizophrenic Letters (N = 670)	Normal Letters (N = 670)	Schizophrenic Words (N = 165)	Normal Words (N = 165)
%REC	6.511% (6.511%)	6.312% (6.312%)	1.870% (1.870%)	1.567% (1.567%)
%DET	22.257% (12.019%)	22.280% (11.600%)	26.087% (3.953%)	23.113% (0.943%)
LMAX	19 (4)	16 (4)	5 (2)	3 (2)
ENT	0.995 (0.317)	0.986 (0.359)	0.675 (0.000)	0.773 (0.773)
TND	0.104 (0.029)	0.251 (0.240)	-8.361 (2.108)	-1.898 (-1.898)
%LAM	4.495% (12.636%)	1.484% (18.576%)	0.000% (11.067%)	0.000% (0.943%)
TT	2.000 (2.185)	2.000 (2.104)	2.000 (undefined)	undefined (2.000)

## RECURRENCE PATTERNS OF PROTEINS

It is a simple matter to move from recurrence analysis of English texts to amino acid patterns of proteins. The amino acid alphabet is a 20-letter code of naturally occurring amino acids found in eukaryotic proteins. Protein function depends upon protein shape in 3-dimensional space (tertiary and quaternary structures), and protein shape depends upon the specific 1-dimensional amino acid sequence. Thus, recurrence analysis of amino acid sequences may yield interesting differences among the various classes of proteins. One approach would be to encode amino acids with unique integers from 1 to 20 and perform RQA computations using  $M = 1$ ,  $DELAY = 1$ , and  $RADIUS = 0$ . When this is done, however, it has been shown that amino acid sequences are only slightly different from shuffled sequences (Webber & Zbilut, 1998). That is, naturally occurring sequences are almost random sequences, at least in terms of arbitrary amino acid names (residues). But even at this lowly name level, cross recurrence plots may prove useful in identifying stretches of identical residue patches (e.g., between protein isoforms) which would graphically plot as long diagonal lines (identical matches) with intervening gaps (mismatches).

A change in perspective is in order. Thinking through the problem, it becomes clear that what imparts a 3-dimensional shape to proteins is the physical properties of their 1-dimensional string of amino acids. Specific sequences of amino acids twist and fold on themselves, forming protein globules with specific features. Two of the strongest physical properties that amino possess are their hydrophobicity and net charge. By merely substituting the name of

each amino acid by one of its physical properties, it is possible to generate new sequence amenable for recurrence analysis in higher dimensions.

To illustrate, consider human hemoglobin, a quaternary protein with two alpha-chains (141 amino acids each) and two beta-chains (146 amino acids each) of amino acids. Recurrence quantifications were performed on the alpha chain, first at the orthographic level ( $M = 1$ ;  $DELAY = 1$ ;  $RADIUS = 0\%$  maximum distance), and second following hydrophobic substitutions using the hydrophobicity scale of Miyazawa and Jernigan (1996) ( $M = 3$ ;  $DELAY = 1$ ;  $RADIUS = 5\%$  maximum distance). Recurrence plots for both representations of the same system are shown in Figure 2.18. Recurrences seem denser for the hemoglobin residue names (orthographic level) than for their hydrophobic substitutions. Conversely, the diagonal line structuring seems to be more common in hydrophobic space. But we cannot trust our eyes, which always see things from our own biased perspective. Nevertheless, these first impressions are confirmed in the data of Table 2.2, which lists the results of RQA performed on native residue sequences as well as their randomly shuffled versions. Thus the hydrophobic representation of hemoglobin has a lower %REC but higher %DET than at the residue name (“spelling”) level. The hydrophobic signal is also more complex (higher ENT value), a reflection of its greater non-stationarity (higher absolute TND value). The bottom line is that by transforming single-letter amino acid residues into hydrophobic signals, the amino-acid sequence can be

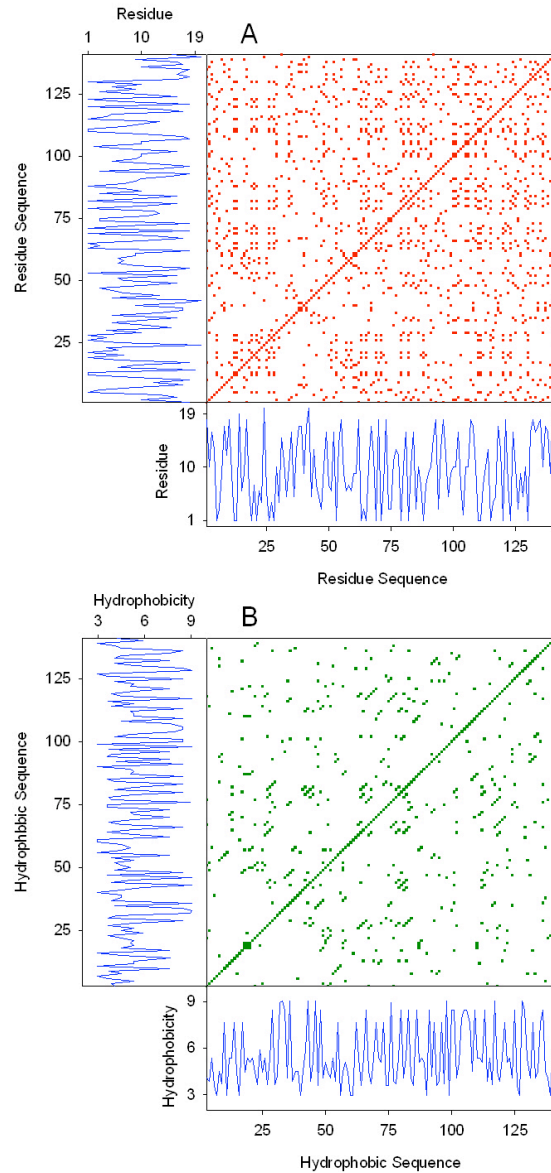


Figure 2.18. Recurrence analysis of human hemoglobin protein (alpha chain) at two levels. (A) Residue name level. Recurrences occur only for identical residue matches. Recurrence data computed from file *HEMOALET* using program *RQD.EXE*. RQA parameters:  $P_1$ - $P_{last}$  = 1-139; RANDSEQ = n; NORM = Euclid; DELAY = 1; EMBED = 1; RESCALE = absolute; RADUS = 0; COLORBND = 1; LINE = 2. RQA variables: %REC = 7.518; %DET = 15.633; LMAX = 3; ENT = 0.219; TND = -2.002; %LAM = 12.129; TT = 2.000. (B) Residue hydrophobicity level. Recurrences occur for similar hydrophobic patches. Recurrence data computed from file *HEMOAHYD* using program *RQD.EXE*. RQA parameters:  $P_1$ - $P_{last}$  = 1-139; RANDSEQ = n; NORM = Euclid; DELAY = 1; EMBED = 3; RESCALE = max dist; RADUS = 10; COLORBND = 1; LINE = 2. RQA variables: %REC = 2.669; %DET = 46.875; LMAX = 5; ENT = 1.113; TND = -6.289; %LAM = 0.781; TT = 2.000. See also Table 2.

## Recurrence Quantification Analysis

projected into higher dimensional space ( $M > 1$ ) where approximate recurrences become legitimate ( $RADIUS > 0$ ). For these and other reasons RQA is making significant headway into the problem of protein folding (Zbilut, Sirabella, Giuliani, Manetti, Colosimo, & Webber, 2002; Giuliani, Benigni, Zbilut, Webber, & Sirabella, 2002).

Table 2.2. *Recurrence quantification analysis of human hemoglobin protein. Data were computed from native sequences (and shuffled sequences) of protein letters (data file HEMOALET) and protein hydrophobicities (data file HEMOAHYD) using program RQD.EXE.*

RQA Variable	Hemoglobin-A Residue Names (N = 141)	Hemoglobin-A Hydrophobicity (N = 141)
%REC	7.518% (7.518%)	2.669% (2.627%)
%DET	15.633% (10.377%)	46.875% (41.667%)
LMAX	3 (3)	5 (4)
ENT	0.219 (0.176)	1.113 (0.957)
TND	-2.002 (-8.333)	-6.289 (-5.814)
%LAM	12.129% (11.860%)	0.781% (8.730%)
TT	2.000 (2.000)	2.000 (2.000)

## SUMMARY

The focus on this chapter has been on the proper implementation strategies of RQA. We have not emphasized the large and growing recurrence literature amassed over the last decade. Most of this literature, exceeding 170 references, is accessible from the website of Marwan (2003b). But it is appropriate here to just list several of the fields impacted by nonlinear recurrence analysis over the last decade: Chaos science (Trulla, Giuliani, Zbilut, & Webber, 1996), respiration (Webber, 1991), heartbeat dynamics (Giuliani, Piccirillo, Marigliano, & Colosimo, 1998), blood pressure (Mestivier, Dabire, Safar, & Chau, 1998), otoacoustic emissions (Zimatore, Hatzopoulos, Giuliani, Martini, & Colosimo, 2002), muscle fatigue (Farina, Fattorini, Felici, & Filligoi, 2002), postural control (Riley, Balasubramaniam, & Turvey, 1999), genomics (Bultrini, Pizzi, Del Giudice, & Frontali, 2003), proteomics (Zbilut et al., 2002), molecular dynamics (Manetti, Ceruso, Giuliani, Webber, & Zbilut, 1999), and even finance (Antonioniou & Vorlow, 2000). In fact, any time series (or spatial series, for that matter) is amenable to RQA. If it wiggles in time (physiology) or space (anatomy) RQA can quantify the dynamic.

For parting thoughts, the mere fact that ants can lift 50 times their body weight whereas humans cannot is one lowly illustration of non-linearity in our shared world with insects. As we have seen, many of the dynamical, real-world systems common to man are notoriously non-linear, non-stationary, and noisy. To successfully analyze such systems it seems best to use non-linear tools that are independent of prescribed statistical distributions of the data (e.g., Gaussian), can deal with short data sets (e.g., polypeptides), are not stymied by actual signal

transients and outliers (e.g., observations beyond a few standard deviations of the mean), and can project the input signal into higher-dimensional space (e.g., embedding capabilities). So far, recurrence analysis seems to fit the bill in all of these important aspects. But the recurrence approach is not a stand-alone technique, some kind of end-all, be-all of extant nonlinear dynamical tools. For instance, significant advances are also being made by combining recurrence quantification analysis (RQA) with principle component analysis (PCA). By this means the complex relationship among the several recurrence variables can be objectively compared and processed as an ensemble (Zbilut, Giuliani, & Webber, 1998b; Giuliani, Colafranceschi, Webber, & Zbilut, 2001).

RQA functions like a microscope, snooping out higher-dimensional subtleties in the dynamics that are not obvious its first-dimensional representation. Returning to the animal world, one analogy would be with farmers who can best forecast weather patterns by observing altered behaviors of their barnyard livestock. Evidently, these domesticated animals can sense actual physical phenomena beyond the human sensory range. Indeed, Marino and Frilot (2003) used RQA strategies to convincingly demonstrate the sensitivity of rabbits to magnetic fields. In addition, Mohr, Langbein, and Nürnberg (2002) applied RQA to assess stress levels in calves and cows. But whatever the case, whether it be forecasting dynamical events in the medical field, geophysics, or meteorology, the future of recurrence analysis looks bright and promising.

## SOFTWARE

Some investigators are writing their own programs to perform recurrence quantifications. But for those wishing to download recurrence software from the World Wide Web, at least three sites are available as shown below: *Visual Recurrence Analysis (VRA)* from Eugene Kononov; *Cross Recurrence Plots-Toolbox (CRP)* from Norbert Marwan; *RQA (Recurrence Quantification Analysis)* from Charles Webber.

*VRA 4.6*: <http://home.netcom.com/~eugenek/download.html>

*CRP 4.5*: <http://www.agnld.uni-potsdam.de/~marwan/intro.html>

*RQA 8.1*: <http://homepages.luc.edu/~cwebber>

REFERENCES

Antoniou, A., & Vorlow, C. (2000). Recurrence plots and financial time series analysis. *Neural Network World*, *10*, 131-145.

Bassingthwaite, J. B., Liebovitch, L. S., & West, B. J. (1994). *Fractal physiology*. New York: Oxford University Press.

Bultrini, E., Pizzi, E., Del Giudice, P., & Frontali, C. (2003). Pentamer vocabularies characterizing introns and intron-like intergenic tracts from *Caenorhabditis elegans* and *Drosophila melanogaster*. *Gene*, *304*, 183-192.

Eckmann, J.-P., Kamphorst, S. O., & Ruelle, D. (1987). Recurrence plots of dynamical systems. *Europhysics Letters*, *4*, 973-977.

Farina, D., Fattorini, L., Felici, F., & Filligoi G. (2002). Nonlinear surface EMG analysis to detect changes of motor unit conduction velocity and synchronization. *Journal of Applied Physiology*, *93*, 1753-1763.

Feller, W. (1950). *An introduction to probability theory and its applications, Vol. 1*. New York: John Wiley & Sons.

Fraser, A. M., & Swiney, H. L. (1986). Independent coordinates for strange attractors from mutual information. *Physical Review A*, *33*, 1134-1140.

Webber & Zbilut

Geisel, T.S. (Dr. Seuss, pseudonym) (1960). *Green eggs and ham*. New York: Random House, Inc.

Girault, P. (1991). Attractors and dimensions. In G. Cherbit (Ed.), *Fractals: Non-Integral Dimensions and Applications* (pp. 60-82). Chinchester: John Wiley & Sons.

Giuliani, A., Benigni, R., Zbilut, J. P., Webber, C. L., Jr., Sirabella, P., & Colosimo, A. (2002). Nonlinear signal analysis methods in the elucidation of protein sequence-structure relationships. *Chemical Reviews*, *102*, 1471-1491.

Giuliani, A., Colafranceschi, M., Webber, C. L., Jr., & Zbilut, J. P. (2001). A complexity score derived from principal components analysis of nonlinear order measures. *Physica A*, *301*, 567-588.

Giuliani, A., Piccirillo, G., Marigliano, V., & Colosimo, A. (1998). A nonlinear explanation of aging-induced changes in heartbeat dynamics. *American Journal of Physiology*, *275*, H1455-H1461.

Glass, L., & Mackey, M.C. (1988). *From clocks to chaos: The rhythms of life*. Princeton: Princeton University Press.

Grafakos, L. (2003). *Classical and modern Fourier analysis*. Upper Saddle River: Prentice Hall.

Grassberger, P., & Procaccia, I. (1983). Measuring the strangeness of strange attractors. *Physica D*, *9*, 189-208.

Grassberger, P., Schreiber, T., & Schaffrath, C. (1991). Non-linear time series analysis. *International Journal of Bifurcation and Chaos*, *1*, 521-547.

Hénon, M. (1976). A two-dimensional mapping with a strange attractor. *Communications in Mathematical Physics*, *50*, 69-77.

Kac, M. (1959). *Probability and related topics in physical sciences*. New York: Interscience Publishers.

Kaplan, D., & Glass, L. (1995). *Understanding nonlinear dynamics*. New York: Springer Verlag.

Kasanin, J. S., & Lewis, N. D. C. (1944). *Language and thought in schizophrenia: Collected papers*. Berkeley: University of California Press.

Kennel, M. B., Brown, B., & Abarbanel, H. D. I. (1992). Determining embedding dimension for phase-space reconstruction using a geometrical construction. *Physical Review A*, *45*, 3403-3411.

Lorenz, E. N. (1963). Deterministic non-periodic flows. *Journal of Atmospheric Sciences*, *20*, 130-141.

Webber & Zbilut

Manetti, C., Ceruso, M.-A., Giuliani, A., Webber, C. L., Jr., & Zbilut, J. P. (1999). Recurrence quantification analysis as a tool for the characterization of molecular dynamics simulations. *Physical Review E*, *59*, 992-998.

Marino, A. A., & Frilot, C. (2003). Localization of electroreceptive function in rabbits. *Physiology and Behavior*, *79*, 803-810.

Marwan, N. (2003a). *Encounters with neighbors: Current developments of concepts based on recurrence plots and their application*. Unpublished doctoral dissertation, Institute for Physics, University of Potsdam.

Marwan, N. (2003b). Cross recurrence plots toolbox.  
<http://www.agnld.uni-potsdam.de/~marwan/intro.html>

Marwan, N., Wessel, N., Meyerfeldt, U., Schirdewan, A., & Kurths, J. (2002). Recurrence-plot-based measures of complexity and their application to heart rate variability data. *Physical Review E*, *66*, 026702.1-026702.8.

Mayer-Kress, G., & Holzfuss, J. (1987). Analysis of the human electroencephalogram with methods from nonlinear dynamics. In L. Rensing, U. van der Heiden, & M. C. Mackey (Eds.), *Temporal Disorder in Human Oscillatory Systems* (pp. 57-68). Berlin: Springer-Verlag.

Mestivier, D., Dabire, H., Safar, M., & Chau, N. P. (1998). Use of nonlinear methods to assess effects of clonidine on blood pressure in spontaneously hypertensive rats. *Journal of Applied Physiology*, *84*, 1795-1800.

Misulis, K. E., & Head, T. C. (2003). *Essentials of clinical neurophysiology* (3<sup>rd</sup> edition). Burlington: Butterworth-Heinemann.

Miyazawa, S., & Jernigan, R. L. (1996). Residue-residue potentials with a favorable contact pair term and an unfavorable high packing density term, for simulation and threading. *Journal of Molecular Biology*, *256*, 623-644.

Mohr, E., Langbein, J., & Nürnberg, G. (2002). A noninvasive approach to measure stress in calves and cows. *Physiology and Behavior*, *75*, 251-259.

Orsucci, F., Walter, K., Giuliani, A., Webber, C. L., Jr., & Zbilut, J. P. (1999). Orthographic structuring of human speech and texts: Linguistic application of recurrence quantification analysis. *International Journal of Chaos Theory Applications*, *4*, 21-28.

*The Oxford English Dictionary Online*, (2003). <http://www.oed.com>  
Oxford: Oxford University Press.

Parker, T. S., & Chua, L. O. (1989). *Practical numerical algorithms for chaotic systems*. New York: Springer-Verlag.

Webber & Zbilut

Riley, M. A., Balasubramaniam, R., & Turvey, M. T. (1999). Recurrence quantification analysis of postural fluctuations. *Gait and Posture, 9*, 65-78.

Shannon, C. E. (1948). A mathematical theory of communication. *Bell Systems Technical Journal, 27*, 379-423 & 623-656.

Shockley, K., Buttwill, M., Zbilut, J. P., & Webber, C. L., Jr. (2002). Cross recurrence quantification of coupled oscillators. *Physics Letters A, 305*, 59-69.

Takens, F. (1981). Detecting strange attractors in turbulence. In D. Rand, & L.-S. Young (Eds.), *Lecture Notes in Mathematics, Vol. 898, Dynamical Systems and Turbulence, Warwick 1980* (pp. 366-381). Berlin: Springer-Verlag.

Thomasson, N., Hoepfner, T. J., Webber, C. L., Jr., & Zbilut, J. P. (2001). Recurrence quantification in epileptic EEGs. *Physics Letters A, 279*, 94-101.

Thomasson, N., Webber, C. L., Jr., & Zbilut, J. P. (2002). Application of recurrence quantification analysis to EEG signals. *International Journal of Computer Applications, 9*, 1-6.

Trulla, L. L., Giuliani, A., Zbilut, J. P., & Webber, C. L., Jr. (1996). Recurrence quantification analysis of the logistic equation with transients. *Physics Letters A, 223*, 255-260.

Webber, C. L., Jr. (1991). Rhythmogenesis of deterministic breathing patterns. In H. Haken & H. P. Koepchen (Eds.), *Rhythms in Physiological Systems* (pp. 177-191). Berlin, Heidelberg, New York: Springer-Verlag.

Webber, C. L., Jr. (2004). Introduction to recurrence quantification analysis. *RQA version 8.1 README.TXT*:  
<http://homepages.luc.edu/~cwebber/>

Webber, C. L., Jr., Schmidt, M. A., & Walsh, J. M. (1995). Influence of isometric loading on biceps EMG dynamics as assessed by linear and nonlinear tools. *Journal of Applied Physiology*, *78*, 814-822.

Webber, C. L., Jr., & Zbilut, J. P. (1994). Dynamical assessment of physiological systems and states using recurrence plot strategies. *Journal of Applied Physiology*, *76*, 965-973.

Webber, C. L., Jr., & Zbilut, J. P. (1996). Assessing deterministic structures in physiological systems using recurrence plot strategies. In M. C. K. Khoo (Ed.), *Bioengineering Approaches to Pulmonary Physiology and Medicine* (pp. 137-148). New York: Plenum Press.

Webber, C. L., Jr., & Zbilut, J. P. (1998). Recurrent structuring of dynamical and spatial systems. In A. Colosimo (Ed.) *Complexity in the Living: A Modelistic Approach* (pp. 101-133). Proceedings of an International Meeting, February 1997, University of Rome "La Sapienza."

Webber & Zbilut

Wróbel, J. (1990). *Language and schizophrenia*. Amsterdam: John Benjamins Publishing Company.

Wyner, A. D., Ziv, J., & Wyner, A. J (1998). On the role of pattern matching in information theory. *IEEE Transactions on Information Theory*, *44*, 2045-2056.

Zbilut, J. P., Giuliani, A., & Webber, C. L., Jr. (1998a). Detecting deterministic signals in exceptionally noisy environments using cross-recurrence quantification. *Physics Letters A*, *246*, 122-128.

Zbilut, J. P., Giuliani, A., & Webber, C. L., Jr. (1998b). Recurrence quantification analysis and principle components in the detection of short complex signals. *Physics Letters A*, *237*, 131-135.

Zbilut, J. P., Sirabella, P., Giuliani, A., Manetti, C., Colosimo, A., & Webber, C. L., Jr. (2002). Review of nonlinear analysis of proteins through recurrence quantification. *Cell Biochemistry and Biophysics*, *36*, 67-87.

Zbilut, J. P., & Webber, C. L., Jr. (1992). Embeddings and delays as derived from quantification of recurrence plots. *Physics Letters A*, *171*, 199-203.

Zimatore, G., Hatzopoulos, S., Giuliani, A., Martini, A., & Colosimo, A. (2002). Comparison of transient otoacoustic emission responses from neonatal and adult ears. *Journal of Applied Physiology*, *92*, 2521-2528.

## APPENDIX: Mathematical Construction of the Recurrence Matrix

(Webber, 2004)

RQA employs the method of time delays to embed experimental data into higher dimensions. Explicit examples of how distance matrices (DM) and recurrence matrices (RM) are constructed for Euclidean, maximum, and minimum norms are detailed below for a contrived time-series vector (TS) with 29 elements.

$$TS = [3.7, 9.2, 2.1, -5.4, 0.0, -10.9, 9.2, 3.1, 1.7, 1.8, -0.3, -4.9, 2.7, 3.5, 7.5, -9.9, -9.9, -4.7, 1.3, 2.7, 7.6, 3.9, 7.3, 8.0, 0.3, -1.9, 5.1, 8.8, 8.2]$$

For DELAY=8, EMBED=4, FIRST=1 and LAST=5, the following 5 time-delay vectors are constructed:

$$\begin{aligned} V1 &= [+3.7, +1.7, -9.9, +0.3] \\ V2 &= [+9.2, +1.8, -4.7, -1.9] \\ V3 &= [+2.1, -0.3, +1.3, +5.1] \\ V4 &= [-5.4, -4.9, +2.7, +8.8] \\ V5 &= [+0.0, +2.7, +7.6, +8.2]. \end{aligned}$$

Comparison of the 5 vectors constructs a single  $5 \times 5$  recurrence matrix of distances for each of the 3 norm types. For example, the Euclidean distance between vectors V4 and V5 is calculated as follows:

$$DM(\text{Euclid norm at } i=4, j=5) = \text{SQRT} (\text{SQR}(-5.4 - 0.0) + (\text{SQR}(-4.9 - 2.7) + \text{SQR}(2.7 - 7.6) + \text{SQR}(8.8 - 8.2))) = 10.549.$$

To compute the maximum and minimum distances between vectors V4 and V5, the vectors are compared element by element.

$$\begin{aligned} \text{ABS}(-5.4 - 0.0) &= 5.4 \\ \text{ABS}(-4.9 - 2.7) &= 7.6 \text{ (largest difference)} \\ \text{ABS}(2.7 - 7.6) &= 4.9 \\ \text{ABS}(8.8 - 8.2) &= 0.6 \text{ (smallest difference)} \end{aligned}$$

By definition, maximum and minimum distances are simply the maximum and minimum differences, respectfully.

$$\begin{aligned} DM(\text{max norm at } i=4, j=5) &= 7.6 \\ DM(\text{min norm at } i=4, j=5) &= 0.6 \end{aligned}$$

This procedure is repeated for each cell, giving the following results for DM(i,j). Only the distances in the upper triangle are shown since the lower half is perfectly symmetrical. Note that the central diagonal is designated by 0.00 distances (vector identity matches).

DM(Euclid norm) =

[1,5]=19.58; [2,5]=18.41; [3,5]=7.92; [4,5]=10.55; [5,5]=0.00  
 [1,4]=18.90; [2,4]=20.67; [3,4]=9.65; [4,4]=0.00  
 [1,3]=12.45; [2,3]=11.83; [3,3]=0.00  
 [1,2]=7.88; [2,2]=0.00  
 [1,1]=0.00

DM(max norm) =

[1,5]=17.50; [2,5]=12.30; [3,5]=6.30; [4,5]=7.60; [5,5]=0.00  
 [1,4]=12.60; [2,4]=14.60; [3,4]=7.50; [4,4]=0.00  
 [1,3]=11.20; [2,3]=7.10; [3,3]=0.00  
 [1,2]=5.50; [2,2]=0.00  
 [1,1]=0.00

DM(min norm) =

[1,5]=1.00; [2,5]=0.90; [3,5]=2.10; [4,5]=0.60; [5,5]=0.00  
 [1,4]=6.60; [2,4]=6.70; [3,4]=1.40; [4,4]=0.00  
 [1,3]=1.60; [2,3]=2.10; [3,3]=0.00  
 [1,2]=0.10; [2,2]=0.00  
 [1,1]=0.00

These distances are all expressed in absolute units and can be retained as such by selecting rescaling option 1.

By selecting rescaling option 2, RM distances are normalized to the mean distance of the RM by dividing each cell by the absolute mean distance and multiplying by 100. All central diagonal values of zero are excluded from the calculation of mean distance.

DM mean distance (Euclid norm) = 13.783 = 100.0%

DM mean distance (max norm) = 10.220 = 100.0%

DM mean distance (min norm) = 2.310 = 100.0%

## Recurrence Quantification Analysis

By selecting rescaling option 3, DM distances are normalized to the maximum distance of the DM by dividing each cell by the absolute maximum distance and multiplying by 100. Be careful not to confuse max distance and max norm, which are different.

DM max distance (Euclid norm) = 20.671 = 100.0%

DM max distance (max norm) = 17.500 = 100.0%

DM max distance (min norm) = 6.700 = 100.0%

Recurrence matrices are derived from distance matrices by setting a RADIUS threshold. As shown below, the Heavyside function assigns values of 0 or 1 to array elements. The RADIUS parameter is always relative to the reported MAXDIST, whether it be expressed in absolute units or relative units. Only those distances in RM[I,J] equal to or less than the RADIUS are defined as recurrent points at coordinates I, J.

RM (Euclid norm with RADIUS of 8.0) =

[1,5]=0; [2,5]=0; [3,5]=1; [4,5]=0; [5,5]=1

[1,4]=0; [2,4]=0; [3,4]=0; [4,4]=1

[1,3]=0; [2,3]=0; [3,3]=1

[1,2]=1; [2,2]=1

[1,1]=1

RM (max norm with RADIUS of 12.3) =

[1,5]=0; [2,5]=1; [3,5]=1; [4,5]=1; [5,5]=1

[1,4]=0; [2,4]=0; [3,4]=1; [4,4]=1

[1,3]=1; [2,3]=1; [3,3]=1

[1,2]=1; [2,2]=1

[1,1]=1

RM (min norm with RADIUS of 1.2) =

[1,5]=1; [2,5]=1; [3,5]=0; [4,5]=1; [5,5]=1

[1,4]=0; [2,4]=0; [3,4]=0; [4,4]=1

[1,3]=0; [2,3]=0; [3,3]=1

[1,2]=1; [2,2]=1

[1,1]=1

RQA looks for patterns among these recurrent points, and this need not/must not be done manually (too subjective). Objective pattern recognition algorithms are written into the many recurrence programs to define the RQA variables %REC, %DET, ENT, LMAX, TND, %LAM, and TT.

## CHAPTER 3

# Application of Recurrence Quantification Analysis: Influence of Cognitive Activity on Postural Fluctuations

Geraldine L. Pellecchia

Department of Physical Therapy  
School of Allied Health  
University of Connecticut  
358 Mansfield Rd., Unit 2101  
Storrs, CT 06269-2101  
U. S. A.  
E-mail: [geraldine.pellecchia@uconn.edu](mailto:geraldine.pellecchia@uconn.edu)

Kevin Shockley

Department of Psychology  
University of Cincinnati  
ML 0376, 429 Dyer Hall  
Cincinnati, OH 45221-0376  
U. S. A.  
E-mail: [kevin.shockley@.edu](mailto:kevin.shockley@.edu)

Control of a stable standing posture is requisite to many everyday actions. During upright standing, the body undergoes continuous, low-amplitude sway. These spontaneous postural fluctuations are often indexed by the center of pressure (COP). The COP is the location of the net vertical ground reaction force and is calculable from the forces and moments measured by a device called a force platform. During upright standing with equal weight bearing on each foot, the COP is located midway between the feet. The path traversed by the COP over time reflects the dynamic nature of postural control. Figure 3.1 depicts a typical COP path during 30 s of upright standing on a compliant surface. The ease with which COP measures can be obtained with a force platform provides a means to explore factors that may influence postural control.

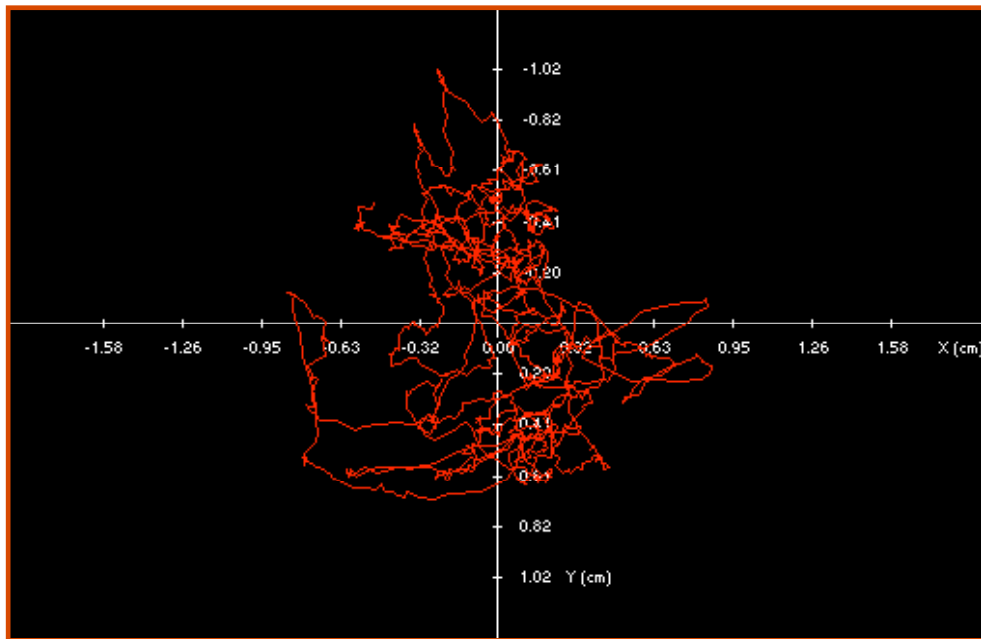


Figure 3.1. A sample 30 s center of pressure (COP) profile. COP path is shown for an individual standing upright with feet together on a compliant surface.

An important aspect of many routine activities of daily living is the ability to concurrently maintain an upright posture and perform an unrelated cognitive task. For example, we often walk while talking. Despite that such scenarios are commonplace, executing cognitive and postural tasks concurrently is not without consequence. Numerous studies have demonstrated changes in performance on either the cognitive, postural, or both tasks when carried out simultaneously compared to when the same tasks are performed separately (e.g., Dault, Geurts, Mulder, & Duysens, 2001; Kerr, Condon, & McDonald, 1985; Lajoie, Teasdale, Bard, & Fleury, 1993; Maylor, Allison, & Wing, 2001; Maylor & Wing, 1996; Stelmach, Zelaznik, & Lowe, 1990).

In a recent paper, Pellecchia (2003) examined the effect of attentional demand on postural sway. COP was recorded as participants stood on a force platform and performed cognitive tasks that varied in attentional requirements. Attentional demand was quantified using information reduction tasks modeled after those described by Posner (1964; Posner & Rossman, 1965). An information reduction task is one in which the required cognitive operation results in a reduction of information from stimulus to response. The size of that transformation is quantified by the difference in the amount of information contained in the stimulus and the response. Posner asserted that the attentional requirements of a cognitive task could be manipulated by varying the processing demands of the task. For a set of numeric tasks, Posner demonstrated a direct relation between task difficulty and the magnitude of information reduced in carrying out a task. Information reduction tasks have been an effective means of

manipulating the attentional requirements of cognitive activity (for an example, see Pellecchia & Turvey, 2001).

To examine the influence of attentional demand on postural sway, Pellecchia (2003) adopted a conventional approach to data analysis. Specifically, the mean magnitude and variability of the COP path during upright standing were compared across a set of information reduction tasks. This traditional method has been used extensively in previous studies examining effects of various experimental manipulations on postural control (for examples, see Derave, De Clercq, Bouckaert, & Pannier, 1998; Gravelle et al., 2002; Guerraz, Thilo, Bronstein, & Gresty, 2001; Polonyova & Hlavacka, 2001; Vuillerme, Forestier, & Nougier, 2002; Vuillerme, Nougier, & Teasdale, 2000). Although well established, this approach to the analysis of COP data is of limited usefulness. Summary measures of COP path magnitude and variability do not reflect the dynamical properties of postural control (Newell, 1998). In contrast, recurrence quantification analysis (RQA), a relatively new analytical method, examines the time evolution of data series (see Webber & Zbilut, Chapter 2). In recent years, investigators have begun using RQA to explore the dynamics of postural control. For example, Riley and Clark (2003) employed RQA to investigate how changes in sensory information influenced the temporal structure of spontaneous postural sway, and thereby to gain insight into the adaptive nature of postural control. RQA is a useful tool for identifying structure that is inherent in postural fluctuations but not evident when using conventional methods of analyzing COP data. The purpose of this chapter is to demonstrate the application of RQA to the study of postural fluctuations during standing as a function of varying

attentional demands of an unrelated, concurrent, cognitive task. Following a description of the experimental method, we review the results of the traditional analysis of COP data as previously reported by Pellecchia (2003). Next, we employ the methods of RQA to examine the dynamical properties of COP time series.

### COGNITIVE ACTIVITY & POSTURAL CONTROL: THE EXPERIMENT

An AMTI Accusway System for Balance and Postural Sway Measurement (Advanced Mechanical Technology, Inc., Watertown, Massachusetts) was used to collect data. The Accusway System consists of a portable force platform and *SWAYWIN* software for data acquisition and analysis. The force platform produces six signals—three force measures,  $F_x$ ,  $F_y$ , and  $F_z$ , and three moment measures,  $M_x$ ,  $M_y$ , and  $M_z$ , where the subscripts  $x$ ,  $y$ , and  $z$  denote medio-lateral (ML; side-to-side), anterior-posterior (AP; front-to-back), and vertical directions, respectively. *SWAYWIN* software uses the forces and moments to calculate  $x$  and  $y$  coordinates of the position of the COP. The Accusway System samples at a rate of 50 Hz. Therefore, a 30 s trial period yielded 1500 data points for the ML COP (position of the center of pressure in the ML direction) time series and 1500 data points for the AP COP (position of the center of pressure in the AP direction) time series.

The postural task consisted of standing on a 10 cm thick foam pad that had been placed on top of the force platform, as shown in Figure 3.2. The foam pad created a compliant surface, thereby altering the somatosensory information available for postural control and making the postural task more challenging than simply standing on a firm, flat surface.



Figure 3.2. The experimental set-up used in the present experiment. Participants stood with feet together, arms by side, and looking straight ahead at a blank wall. A foam pad was placed on the force platform to create a compliant surface.

Three information reduction tasks—digit reversal, digit classification, and counting backward by 3s—were used to vary the attentional demands of the concurrent cognitive task. The amount of information reduced in performing each task was determined using the method described by Posner (1964; Posner & Rossman, 1965; see also Note 1 in Pellecchia & Turvey, 2001). In digit reversal, the task was to reverse the order of a pair of digits. For example, on hearing the

stimulus **4, 7**, a correct response would be **7, 4**. The input contained 6.5 bits of information, and the output contained 6.5 bits of information. Therefore, digit reversal was a 0-bit reduction task. In digit classification, the task was to combine a pair of single digits into a double-digit number and to classify that number as high (if > 50) or low (if < 50), and odd or even. For example, the single digits **4, 7**, combine to form the double-digit number **47**; correct classification would be **low, odd**. The input contained 6.5 bits of information; the output contained 2 bits of information. Therefore, digit classification required 4.5 bits of information reduction. In the counting back by 3s task, participants were given a 3 digit number from which to start counting. Participants were instructed to first recite the starting number, and then count backward by 3s from that number. Correct responses to the stimulus **365** would be **365, 362, 359, 356**, and so on. We determined that counting back by 3s from a randomly chosen three-digit number required approximately 5.9 bits of information reduction.

A pre-recorded audiotape provided stimuli for the digit reversal and digit classification tasks. The audiotape consisted of pairs of random single digits presented at a rate of 2 digits/s with a 2 s pause between pairs. For the counting backward by 3s task, a different starting number was selected for each trial. Starting numbers ranging between 200 and 999 were chosen from a random number table. Prior to data collection, participants practiced the three information reduction tasks for a minimum of 15 s each while seated in a chair.

During the experiment, participants stood in stocking feet on the foam pad that rested on the force platform. The force platform was positioned approximately 2 m from a blank wall. Participants were

instructed to stand with the feet together, the arms by the sides, and with the eyes open and looking straight ahead. COP data were collected under four cognitive task conditions: Quiet standing (i.e., performing no cognitive task), standing combined with digit reversal, standing combined with digit classification, and standing combined with counting backward by 3s. Participants performed two 30 s trials of each condition, for a total of eight trials. The order of the four experimental conditions was randomized. Data collection for each participant's first trial began 30-60 s after the participant assumed the proper position on the force platform. For those trials in which standing was combined with a cognitive task, force platform data collection began after the participant voiced their first response. There was a 30-60 s break between trials, during which time the participant remained standing on the platform. Participants' verbal responses to the cognitive tasks were audiotape-recorded for subsequent analysis. Practice and data collection together lasted approximately 30 min.

## TRADITIONAL APPROACH TO ANALYSIS OF COP DATA

### *Data Analysis*

**SWAYWIN** software was used to calculate five dependent measures: Total COP path length (LCOP), antero-posterior (AP) and medio-lateral (ML) COP range, and AP and ML COP variability. LCOP is the total distance traveled by the COP over the 30 s trial period (see Figure 3.1 for a visual display of LCOP). AP COP range and ML COP range are the differences between the two extreme position values in the respective directions. AP and ML COP variability are the standard deviations of the COP in the respective directions. Means of those

quantities were calculated for the two trials in each experimental condition, and the means were used in all subsequent analyses. Separate repeated-measures analyses of variance (ANOVA) were used to determine the effect of cognitive task condition on each COP measure. Pearson product-moment correlations examined the relation between bits of information reduced and each dependent variable.

To examine performance on the cognitive tasks, the number of errors was determined for each trial by listening to the audiotape recording of participants' responses. Error rate was calculated as the number of errors divided by the total number of responses for each 30 s trial. Error rates were averaged for each participant's two trials in each experimental condition. The mean error scores were used in subsequent repeated measures ANOVAs to examine cognitive task performance. Post-hoc analyses were conducted using least significant difference pair-wise multiple comparison tests.

### ***Results of Traditional Analyses***

The effects of attentional requirements on postural sway and cognitive task performance were previously reported (Pellecchia, 2003) and are summarized in Figure 3.3. Repeated-measures ANOVAs revealed a main effect of cognitive task condition on LCOP,  $F(3, 57) = 8.09$ ,  $p < .001$ , as shown in Figure 3.3a. Figures 3.3b-e depict similar results for the other four COP measures. Separate ANOVAs revealed a main effect of cognitive task condition on AP range  $F(3, 57) = 9.84$ ,  $p < .001$ , ML range  $F(3, 57) = 3.03$ ,  $p < .05$ , and AP variability,  $F(3, 57) = 5.70$ ,  $p < .01$ . Post-hoc tests showed sway measures of LCOP, AP range, ML range, and AP variability were greater for the counting back by 3s

## RQA of Postural Fluctuations

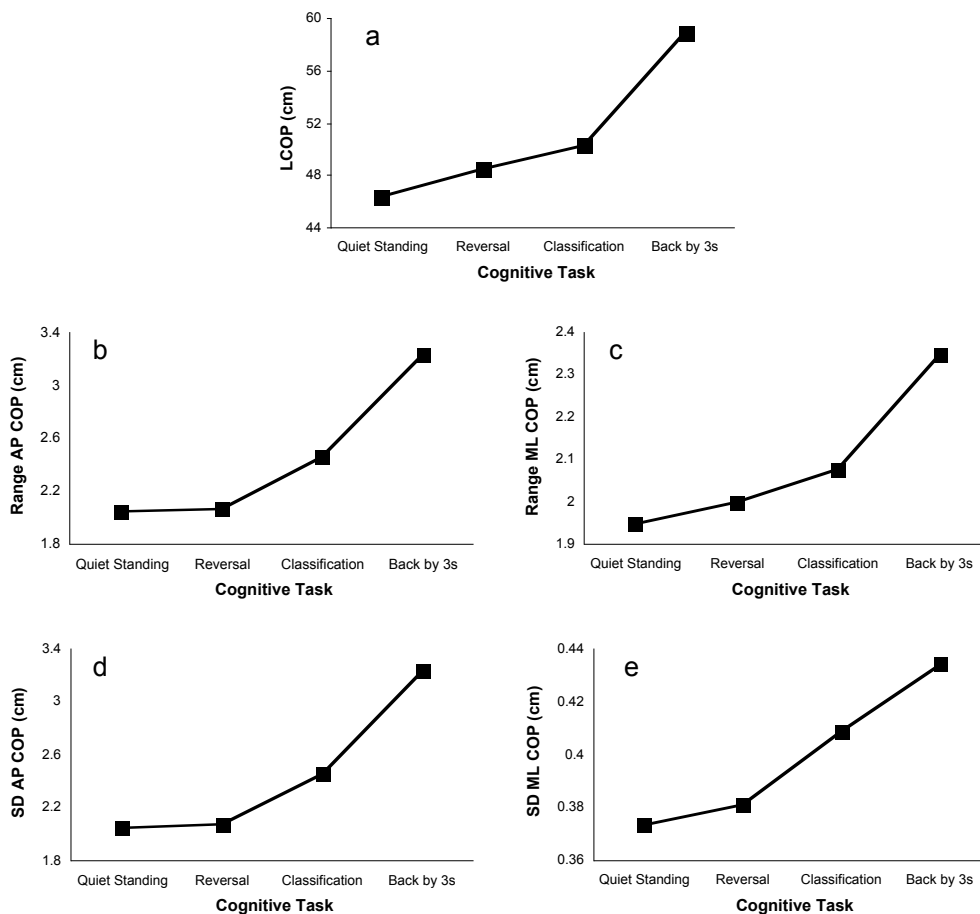


Figure 3.3. Five summary measures of the center of pressure (COP) as a function of cognitive task condition. (a) Total length of the path of the center of pressure (LCOP); (b) Range of COP motion in the anterior-posterior (AP) direction; (c) Range of COP motion in the medio-lateral (ML) direction; (d) standard deviation (SD) of AP COP motion; and (e) SD of ML COP motion.

task than for the other three cognitive task conditions. In addition, AP sway range was greater for digit classification than for quiet standing. For ML variability, the main effect of cognitive task condition approached statistical significance,  $F(3, 57) = 2.35$ ,  $p = .08$ . Pair-wise

comparisons suggested greater ML variability for the counting back by 3s task than for digit reversal ( $p < .05$ ) and quiet standing ( $p = .06$ ).

As noted previously, digit reversal, digit classification, and counting back by 3s required 0, 4.5, and 5.9 bits of information reduction, respectively. Inspection of Figures 3.3a-e suggests that postural sway was directly related to the magnitude of information reduced for the cognitive tasks. Separate correlation analyses confirmed this relation between bits of information reduced and each COP measure. Specifically, Pearson correlation coefficients for LCOP, AP range, ML range, AP variability, and ML variability were .79, .89, .82, .89, and .97, respectively.

In the evaluation of cognitive task performance, repeated measures ANOVA revealed a main effect of cognitive task on error rate,  $F(2, 36) = 7.58$ ,  $p < .01$ . The error rate for counting back by 3s ( $M = 0.113$ ) was greater than error rates for digit classification ( $M = 0.026$ ) and digit reversal ( $M = 0.003$ ).

To summarize, the traditional approach to analysis of COP data revealed greater magnitude and variability of COP motion with higher attentional demands of a concurrent, unrelated, cognitive task. Upon further inspection of Figures 3.3a-e, the various COP measures appear to provide redundant information. In fact, these measures are highly correlated. Pearson correlation coefficients examining the relation among mean values of the five COP measures ranged from .96 to .99.

#### ***Discussion of Results of Traditional Analysis***

Considering the results of the traditional analysis of COP data, one might assume that only a single measure of the COP need be considered. That is, each summary measure of the COP suggested a

similar conclusion about the influence of attentional requirements on postural sway. More specifically, performing a concurrent cognitive task was associated with increases in all five measures. Furthermore, there were no apparent differential effects of attentional demands on AP or ML COP motion.

A conventional viewpoint holds that the degree of postural sway reflects performance of the postural control system. In individuals free of neuromuscular or balance disorders, small amplitude and variability of COP excursions is considered to indicate *good* balance, whereas large amplitude and variability of COP motion is considered to indicate *poor* balance. From this perspective, the observed increases in sway magnitude and variability in the present experiment suggest that carrying out a concurrent cognitive task compromises postural stability. Consistent with this view and the traditional notion of attention as limited capacity or limited processing resources, one might conclude that counting backward by 3s while standing upright exceeds an individual's attentional capacity, and brings about a decline in performance of the postural control system (Woollacott & Shumway-Cook, 2002). This interpretation is intuitively appealing and broadly held. On second blush, however, the notion that concurrent performance of a fundamental motor task such as maintaining an upright posture and a relatively simple arithmetic task could exceed human attentional resources is somewhat suspect.

The traditional approach to the analysis of COP data provides limited information about the postural control system's response to concurrent performance of an unrelated cognitive task. In particular, summary measures of COP magnitude and variability do not inform

about the temporal structure of the COP time series. Consider Figure 3.4, which depicts the AP COP and ML COP time series for the COP profile shown in Figure 3.1. Using the methods of RQA, we can explore the temporal structure of these postural fluctuations, and perhaps gain further insight into changes brought about in the postural control system by varying the attentional requirements of cognitive activity.

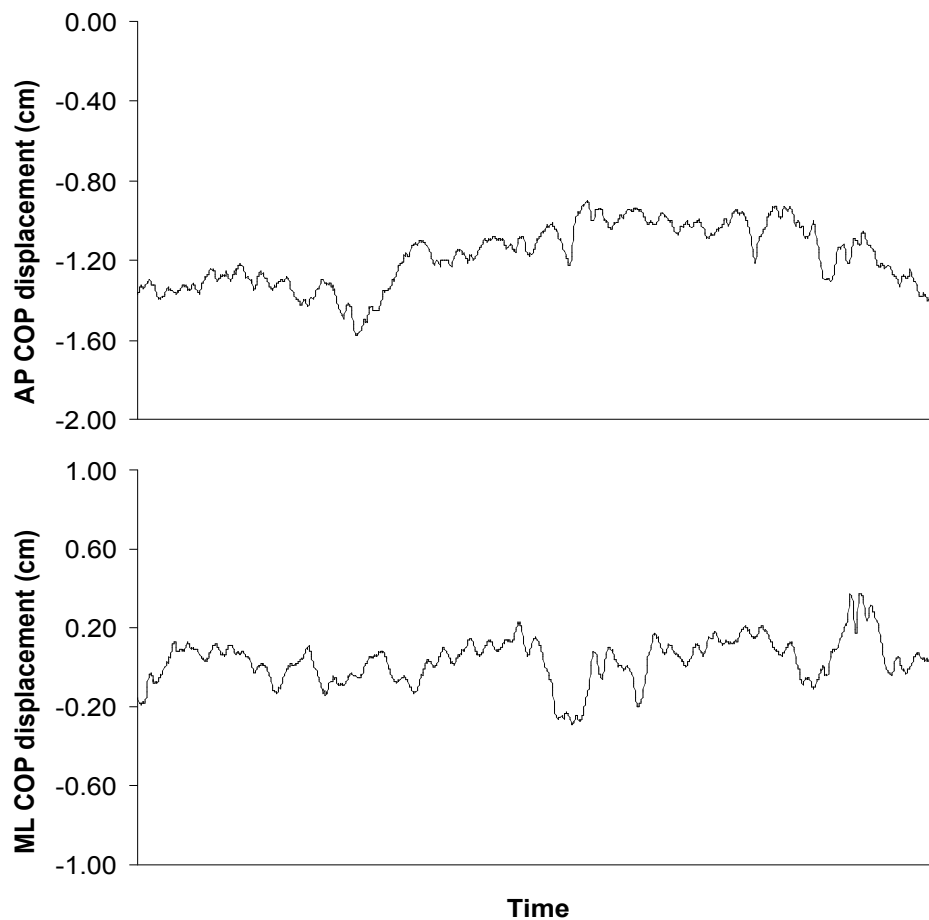


Figure 3.4. AP COP (top) and ML COP (bottom) times series for the COP profile shown in Figure 3.1.

## RECURRENCE QUANTIFICATION ANALYSIS

RQA, a relatively new tool for the analysis of nonlinear dynamical systems, can be used to identify subtle patterns of recurrence in a data series (Webber & Zbilut, 1994, 1996; Zbilut & Webber, 1992; for a detailed tutorial, see Webber & Zbilut, Chapter 2). Time-delayed copies of a single scalar time series are used as surrogate variables to reconstruct a higher dimensional phase space. Through examination of the reconstructed phase space, RQA is able to detect system dynamics that are intrinsic to, though not readily apparent in, the one-dimensional time series. In the reconstructed phase space, the distances between all possible vectors are determined and used to create a distance matrix. Next, a recurrence matrix of recurrent points is generated from the distance matrix. Recurrent points are those points in the distance matrix that fall within a specified distance of one another.

A recurrence plot is simply a graphical depiction of the recurrence matrix. The recurrence plot is an autocorrelation plot of  $\mathbf{x}(t)$  with  $\mathbf{x}(i)$  along the abscissa and  $\mathbf{x}(j)$  along the ordinate. Only those points that satisfy  $\mathbf{x}(i) = \mathbf{x}(j)$ , defined as values of  $i$  and  $j$  that fall within a specified radius or distance of one another, are plotted. Visual inspection of recurrence plots may reveal patterns in the data not evident from examination of the time series. RQA uses pattern recognition algorithms (see discussion of quantification of qualitative features below) to quantify the recurrence features depicted in recurrence plots, and, therefore, is more objective than visual inspection of recurrence plots.

In the present chapter, we apply RQA to the COP data generated by the experiment described above to examine the effects of cognitive activity on postural fluctuations. An important characteristic of RQA is that, unlike other analytic techniques, it does not assume data stationarity. This is of particular relevance in the analysis of COP time series, which have been shown to be nonstationary—drift in the first (mean) and second (standard deviation) moments over time (Newell, 1998; Newell, Slobounov, Slobounova, & Molenaar, 1997; Schumann, Redfern, Furman, El-Jaroudi, & Chaparro, 1995). In addition, RQA requires no assumptions about data set size or distribution of the data.

RQA of the COP data from the present experiment was performed using recurrence software available free of charge from <http://homepages.luc.edu/~cwebber/>. *Recurrence Quantification Analysis* version 6.2 was used to conduct the present analyses, but a more recent version of the software is now available. The software includes 20 programs for examining recurrence in a single time series and cross-recurrence in two time series. All programs run in *MSDOS*, requiring the user to have a basic knowledge of how to work in a DOS environment. The *README.TXT* file is a valuable resource and should be read by all first-time users of the software. Toward the beginning of that file, programs are listed by purpose for which they are used. This provides a useful guide for selecting an appropriate program. For example, when the aim is to generate a recurrence plot, the user can look under the heading “2 programs display recurrence plots” and select from *RQD.EXE*, which is used to generate recurrence quantification plots for a single time series, and *KRQD.EXE*, which is used to generate cross-recurrence plots from two different files. Later

in the *README.TXT* file descriptions of each program detail program usage, input parameters that must be defined, and output that will be generated. The section of the *README.TXT* file titled “Mathematical Construction of the Recurrence Matrix” (see also Webber & Zbilut, Chapter 2) is a particularly helpful tool for understanding the process of RQA. In addition, near the end of the file, the creators of the software discuss several important points to consider in conducting RQA.

We used program *RQD.EXE* (Recurrence Quantification Display) to create recurrence plots. Figure 3.5 depicts recurrence plots for the AP COP and ML COP time series shown in Figure 3.4. The data used to generate these recurrence plots are available for download for the reader who wishes to reproduce these plots. As noted above, points plotted in the recurrence plot are those points determined to be “neighbors” in the reconstructed phase space, that is, COP values that are within a specified distance of one another. The basic features of recurrence plots and our choices of parameter values used to generate the plots with program *RQD.EXE* are explained below in the subsections entitled *Quantification of Qualitative Features of Recurrence Plots* and *Parameter Selection*. Additional information about the qualitative features of recurrence plots can be found in Riley, Balasubramaniam, and Turvey (1999).

Our plan was to use program *RQE.EXE* (Recurrence Quantification Epochs) to examine effects of cognitive task condition on five recurrence variables: *%recurrence* (%REC), *%determinism* (%DET), *maxline* (MAXL), *entropy* (ENT), and *trend* (TND).

In contrast to the program *RQD.EXE*, which we used to generate the recurrence plots, the output of *RQE.EXE* is entirely quantitative.

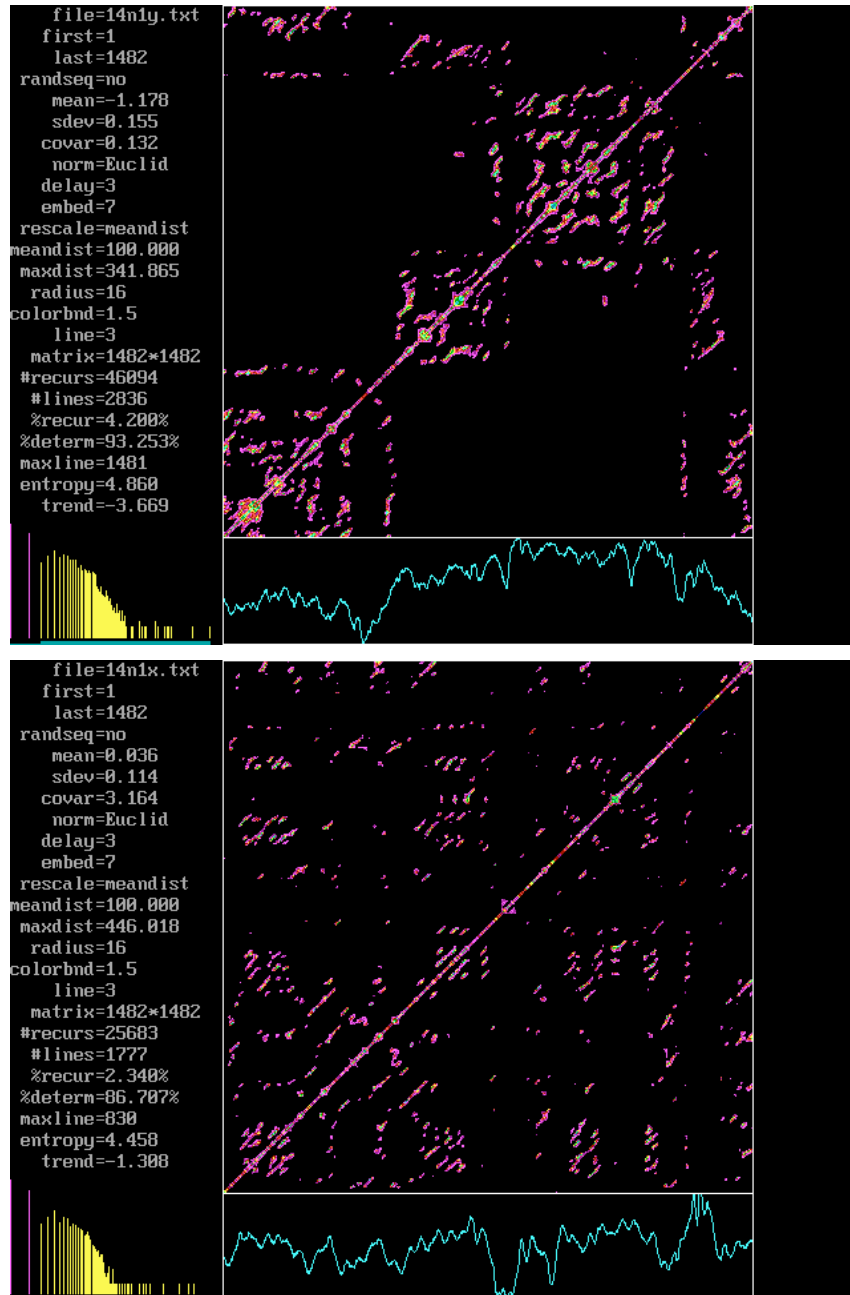


Figure 3.5. Recurrence plots for the AP COP (top) and ML COP (bottom) time series shown in Figure 3.4. The time series are plotted at the bottom of the figure. Recurrence parameters and recurrence output are listed to the left of the plot. Distribution of line lengths is graphed at the bottom left.

Recurrence variables are calculated from the upper triangular area of the recurrence plot, excluding the central diagonal, because the plot is symmetrical about the main diagonal. %REC is the percentage of data points that are recurrent, defined as those points falling within a distance specified by a selected radius value (see below). %DET, an index of degree of determinism, is the percentage of recurrent points that form diagonal lines in a recurrence plot (parallel to the central diagonal). In other words, %DET refers to the percentage of consecutive recurring points. The number of consecutive points needed to constitute a line is determined by the value selected for the line length parameter. MAXL is the length of the longest diagonal line, excluding the main diagonal. MAXL is inversely proportional to the largest positive Lyapunov exponent, and thereby provides a measure of the dynamical stability of the system. According to Webber and Zbilut (Chapter 2), "the shorter the [MAXL], the more chaotic (less stable) the signal." ENT is calculated as the Shannon information entropy of a histogram of diagonal line lengths, and is an index of the complexity of the deterministic structure of the time series. TND provides a measure of the degree of system stationarity, with values of TND at or near zero reflecting stationarity and values deviating from zero indicating drift in the system.

#### ***Quantification of Qualitative Features of Recurrence Plots***

Visual inspection of recurrence plots may be useful for a qualitative understanding of the quantitative recurrence measures described above. To this end, we have generated several recurrence plots for time series with known structure. In particular, we show recurrence plots for a simple sinusoid (Figure 3.6), the same sinusoid

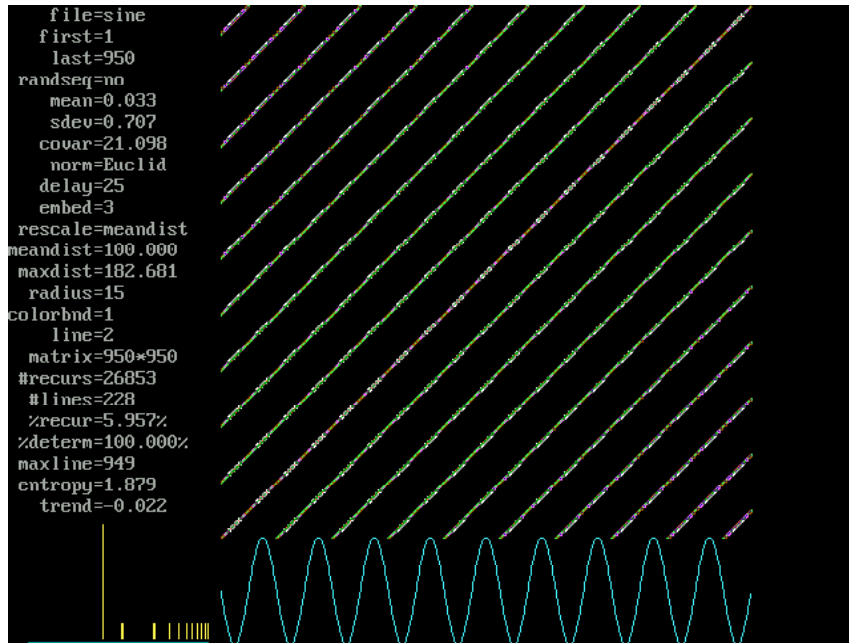


Figure 3.6. Recurrence plot for a simple sinusoid.

with superimposed white noise (Figure 3.7), the same sinusoid with a linear drift (Figure 3.8), a sample time series from a known complex mathematical system—the Lorenz attractor (Figure 3.9), and time series from two regimes of another mathematical system, the Hénon attractor (Figure 3.10). Comparison of the recurrence plots will help to illustrate what the quantitative recurrence measures actually mean.

**%REC & %DET.** Consider the simple sinusoid, which is an entirely deterministic signal, depicted in the bottom of Figure 3.6. By entirely deterministic, we mean that each value in the time series recurs and is part of a string of consecutive recurring values. This aspect of the time series is illustrated by every illuminated pixel in the recurrence plot corresponding to part of a diagonal line. This means

## RQA of Postural Fluctuations

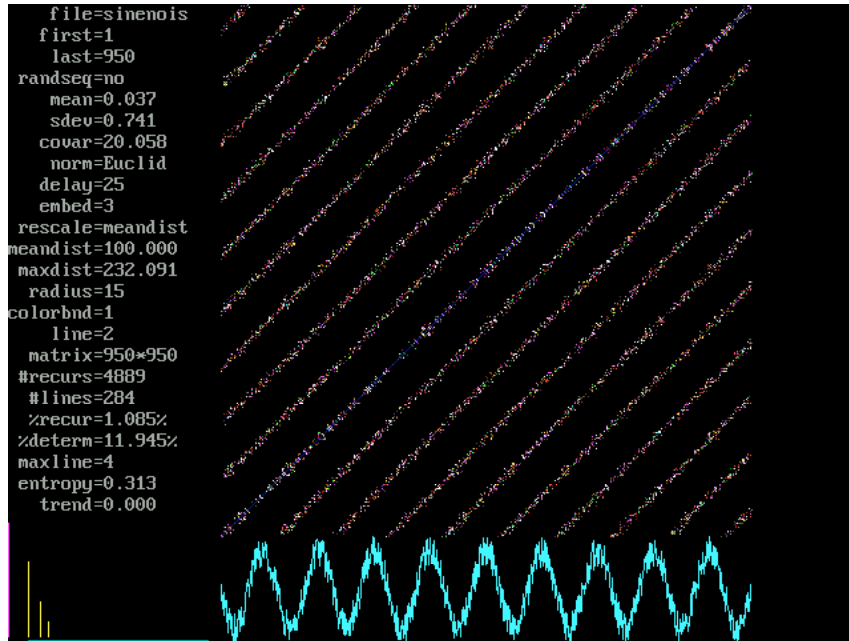


Figure 3.7. Recurrence plot for a sinusoid with superimposed white noise.

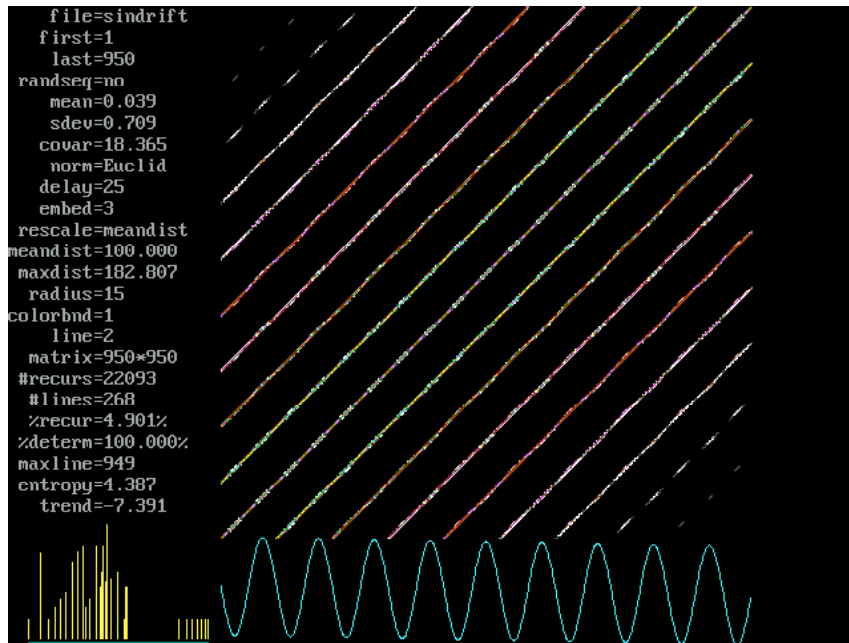


Figure 3.8. Recurrence plot for a sinusoid with linear drift.

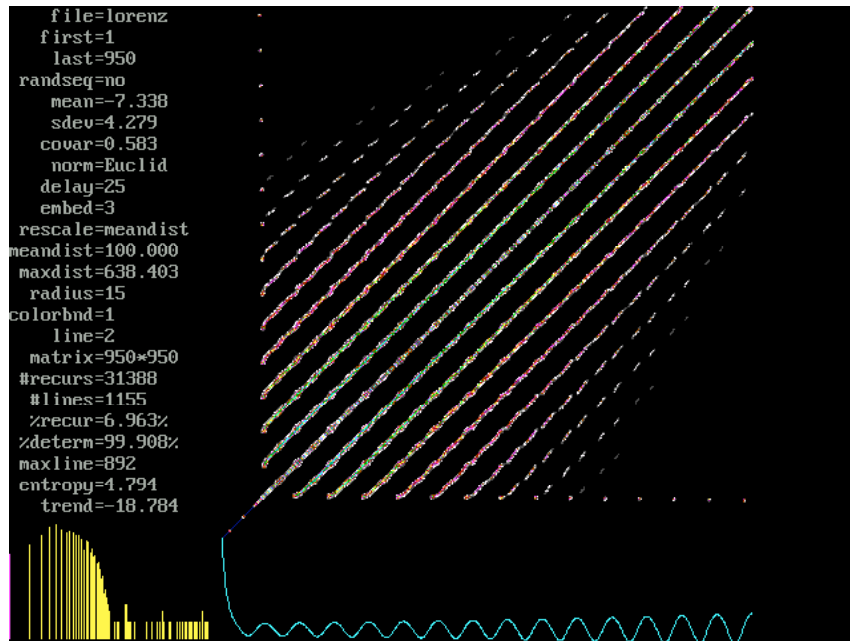


Figure 3.9. Recurrence plot for a time series from the Lorenz attractor.

that the proportion of recurring points that are part of a diagonal line is 100% (i.e., %DET = 100%). Note that just because every value in the time series recurs does not mean that every possible point in the recurrence plot is recurrent. In this particular example, of all of the possible locations that could be recurrent in a time series of a length of 950 data points ( $950 \times 950 / 2 = 451,250$ ), 26,853 were recurrent (~6%) (the total number of possible recurrent points [ $950 \times 950$ ] is divided by 2 because only one of the triangular regions is used to calculate recurrence, since the plot is symmetrical about the main diagonal).

For the time series depicted in Figure 3.7, we no longer have an entirely deterministic signal, given that we have added a random component (white noise). Each value in the time series no longer recurs and each value that does recur is no longer necessarily part of a

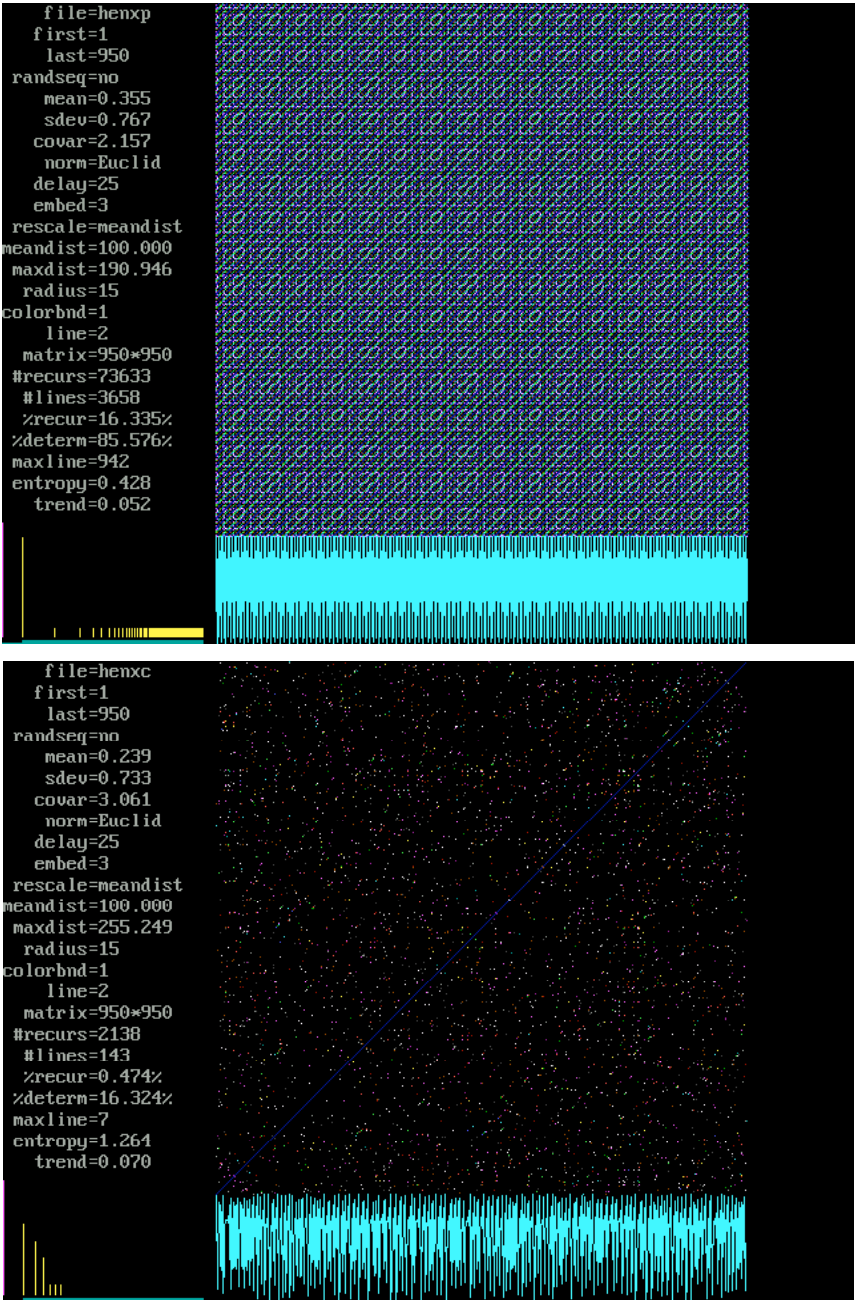


Figure 3.10. Recurrence plot for a times series from a periodic regime (top) and a chaotic regime (bottom) of the Hénon attractor.

diagonal line. The fact that each value in the time series no longer recurs is illustrated by fewer illuminated pixels in the plot (4,889 as compared to 26,853 in Figure 3.6) and a lower proportion of values recurring (~1%). The fact that the noisy signal in Figure 3.7 is no longer entirely deterministic is illustrated by the fact that fewer of the illuminated pixels form diagonal lines, which results in a lower value of %DET (~ 12%) than the signal in Figure 3.6.

*TND*. The time series depicted in Figure 3.8 is nonstationary—the mean state drifts (becomes lower in this case) over time. This was achieved simply by adding a monotonic decrease (a negatively sloped straight line) to the time series depicted in Figure 3.6. Note that we only have a modest change in %REC (~5%), and no change in %DET (100%) as compared to the time series in Figure 3.6 (~6% and 100%, respectively). However, one can see a qualitative difference between the recurrence plots depicted in Figures 3.6 and 3.8.

Recall that the central diagonal corresponds to sameness in time. This location in the recurrence plot is ubiquitously recurrent because it represents comparison of a value to itself. But note that as one moves perpendicularly away from the central diagonal, this represents deviation in time. For example, as one moves upward and left away from the diagonal, this means that one is comparing a point early in the time series (indicated by a value on the x-axis near the origin) to a point later in the time series (indicated by a value on the y-axis near the extreme). As one moves perpendicularly away from the central diagonal in Figure 3.8, the pixel density decreases. This occurs because over time there is a drift in the mean state of the time series. The average value of the first 100 points in the time series is

approximately 0.09, while the average of the last 100 points is approximately -0.09. The color density does not change, however, in the recurrence plot depicted in Figure 3.6. This qualitative aspect of the recurrence plot is quantified by the measure of trend (TND)—the slope of %REC as a function of distance away from the diagonal. Note that TND for Figure 3.8 is considerably different than zero (-7) while the value of TRD for Figure 3.6 is approximately equal to zero.

*ENT.* The time series depicted in Figure 3.9 is a sample of data generated from the Lorenz model. The Lorenz system is a nonlinear, chaotic system that would be considered a complex system by most. The equations representing the Lorenz system and the true and reconstructed phase spaces of the system may be seen in Shockley (Chapter 4). We have selected sample data from this system to illustrate how recurrence analysis may be used to quantify the complexity of a time series. Note that in the time series depicted in the bottom of Figure 3.9 the system appears to be somewhat periodic, as indicated by the peaks and valleys occurring at similar periods. However, the amplitude of the signal changes over time and abrupt shifts in the value of the system occur at irregular intervals (compare the first part of the time series to the later parts). Note that most of the illuminated pixels form diagonal lines (as indicated by %DET = 99%) and that we see a similar proportion of recurrent points as in Figure 3.6 (~7%). However, the recurrence plot in Figure 3.9 looks different than the recurrence plot in Figure 3.6. This distinction between the plots can be captured most readily by the frequency distribution of line lengths shown in the lower left of each figure. The distribution of line lengths for the Lorenz system (Figure 3.9) has a richer variety than that for the

simple sinusoid (Figure 3.6). This variety of structure is what is meant by complexity in recurrence analysis. This aspect of the time series is quantified by the Shannon entropy (*ENT*; the negative sum of the normalized  $\log_2$  probabilities [*P*] of lines corresponding to given line lengths) of the line length distributions in question (see Equation 2.11 in Webber & Zbilut, Chapter 2). Note that the entropy for the Lorenz system ( $ENT = \sim 5$ ) is greater than the entropy for a simple sinusoid ( $ENT = \sim 2$ ), indicating that the Lorenz system is more complex than a simple sinusoid.

*MAXL.* To illustrate the meaning of the recurrence measure maxline (MAXL), we have selected data sets generated from the Hénon system. The Hénon system is a model of the dynamics of stars moving within galaxies. It is governed by the following two equations of motion:

$$\dot{x} = y + 1 - ax^2 \quad [3.1]$$

$$\dot{y} = bx \quad [3.2]$$

where *x* and *y* correspond to the dimensions of change,  $\dot{x}$  and  $\dot{y}$  with overdots correspond to rate of change along those dimensions, and *a* and *b* are parameters.

One of the interesting features of the Hénon system is that depending on the values of the parameters (*a* and *b*) the Hénon system may exhibit behavior that is highly predictable (periodic) or chaotic behavior that is only predictable in the very short term. Figure 3.10 shows recurrence plots of a periodic regime (oscillation among 16 values; e.g., *a* = 1.055, *b* = 0.3) and a chaotic regime of the Hénon

system (e.g.,  $a = 1.4$ ,  $b = 0.3$ ) (the data sets used in the present example are provided with the RQA software at <http://homepages.luc.edu/~cwebber/>). By definition, the chaotic regime is less stable than the periodic regime. By stability we mean that two trajectories that are initially nearby one another stay nearby one another longer in a more stable system than in a less stable system. MAXL has been shown to be sensitive to the stability of the system in question (Eckmann, Kamphorst, & Ruelle, 1987).<sup>1</sup> The larger MAXL, the more stable the system—nearby trajectories diverge less quickly than for a system with a smaller MAXL. For the chaotic regime of the Hénon attractor the longest diagonal line is quite short (MAXL = 7) as compared to the longest diagonal line for the periodic regime (MAXL = 942). While it is the case that MAXL will change considerably depending on the system under scrutiny (as can be seen by comparison of MAXL values for Figures 3.6-3.10), what is of interest is how MAXL changes within the same system (in this case the Hénon system) under different conditions.

### ***Parameter Selection***

Prerequisite to generating plots and calculating recurrence variables is the selection of appropriate settings for seven parameters:

---

<sup>1</sup> Lyapunov exponents quantify the exponential rate of divergence of nearby trajectories along a given dimension in the system. A negative Lyapunov exponent quantifies the average rate of convergence of trajectories over time, while positive Lyapunov exponents characterize the average rate of divergence over time. For a highly stable system (e.g., periodic systems), two trajectories that are initially nearby one another will continue to be nearby one another at any given later point in time. This means that the Lyapunov exponent would be at or near zero (i.e., no divergence over time). One hallmark of chaotic systems, however, is that they have at least one positive Lyapunov exponent (meaning that along at least one dimension, two trajectories that are initially nearby one another will diverge exponentially over time). Chaotic systems that exhibit bounded regions in which trajectories unfold (e.g., the Lorenz attractor or the Hénon attractor for certain parameter ranges) also have at least one negative Lyapunov exponent. MAXL has been shown to be inversely proportional to the largest positive Lyapunov exponent (larger MAXL smaller value of Lyapunov exponent; see Eckmann, Kamphorst, & Ruelle, 1987).

Embedding dimension, delay, range, norm, rescaling, radius, and line length (see Webber & Zbilut, Chapter 2). Selection of these parameter values is challenging. Although some guidelines are available, there are as of yet no absolute standards for identifying the most appropriate parameter values. A summary of the decision making that was involved in our choice of parameters follows.

Selection of some parameters is more difficult than others. Choosing a proper embedding dimension, delay, and radius are among the most challenging decisions that must be made. We followed the approach described by Zbilut and Webber (1992) and used by Riley et al. (1999) to select values for those three parameters. The general strategy is to calculate RQA measures for a range of parameter values, and select a value from a range in which small changes in parameter settings result in small, continuous changes in the RQA measures. To follow that strategy, we enlisted program *RQS.EXE* (Recurrence Quantification Scale), which "...scales recurrence quantifications for a single epoch of data by incrementing parameter values over specified ranges" (Webber, 2004, p. 6). In the following paragraphs, we describe first the decision making involved in selecting a range of parameters for embedding dimension, delay, and radius for use in *RQS.EXE*, and next the choice of a single setting for each parameter.

***Embedding Dimension.*** Embedding dimension specifies the n-dimensions of the reconstructed phase space, that is, the dimension into which the dynamic of the system under study will be projected (see discussion of delay below). Selecting an embedding dimension that is too high can amplify the effects of noise. Choosing an

embedding dimension that is too low will result in underdetermination, that is, the dynamics of the system will not be fully revealed. Webber (2004) suggested, for physiological data, starting with embedding dimensions between 10 and 20 and working downward. Investigators applying RQA to the study of COP data have reported embedding dimension 8 (Schmit et al., submitted), 9 (Riley & Clark, 2003) and 10 (Balasubramaniam, Riley, & Turvey, 2000; Riley et al., 1999). Based on Webber's suggestion and previous papers, we decided to examine RQA output for embedding dimensions 7 through 10.

*Delay.* As mentioned previously, time-delayed copies of the data series are used as surrogate variables to project the data into higher-dimensional space. The delay parameter specifies the time lag to use in reconstructing that phase space. For example, imagine a time series for which we selected a delay ( $\tau$ ) of 10 and embedding dimension of 3. Our first embedding dimension  $[\mathbf{x}(t)]$  in the reconstructed phase space would start at data point 1 of the original time series ( $\mathbf{x}$ ), the second embedding dimension  $[\mathbf{x}(t + \tau)]$  would start at data point 11, and the third embedding dimension  $[\mathbf{x}(t + 2\tau)]$  would start at data point 21. A two-dimensional phase space could be constructed the same way that one plots a two-dimensional scatterplot to evaluate the relationship between two variables in correlation or regression, the two variables in this case being  $\mathbf{x}(t)$  and  $\mathbf{x}(t + \tau)$ . One could add a third (or higher) dimension to the phase space in the same fashion (see Figure 4.4 in Shockley, Chapter 4). Previous studies in which COP data were sampled at 100 Hz used time delays ranging between 0.04 s and 0.09 s. Considering the sampling rate of the force plate used in the present study (50 Hz), delays of 2 to 5 data points corresponded to time delays

of 0.04 to 0.10 seconds. We decided to examine RQA output for delays ranging between 2 and 10 data points.

**Radius.** The radius parameter defines the Euclidean distance within which points are considered neighbors in the reconstructed phase space. Said differently, the radius sets the threshold for recurrence. The larger the radius, the more points will be considered recurrent. As a general guideline, a radius should be selected such that %REC remains low (see Webber & Zbilut, Chapter 2). We wanted a radius that was small enough to yield relatively low %REC (no larger than 5%), but not so small as to produce a floor effect with values of %REC near or at 0.0%. Other investigators have used a radius of 10 or 11 in the analysis of COP data (Balasubramaniam et al., 2000; Riley et al., 1999; Riley & Clark, 2003). We decided to examine RQA output for radius settings ranging between 10 and 26.

**Norm.** The norm parameter determines the method used for computing distances between vectors in the reconstructed phase space. We selected Euclidean normalization, which is consistent with previous studies using RQA to examine COP data (see Riley et al., 1999; Riley & Clark, 2003).

**Rescale.** The rescale parameter determines the method used to rescale the distance matrix. Although rescaling to maximum distance is a typical choice, we decided to rescale relative to mean distance. Mean distance rescaling minimizes the influence of an outlier, which can be a problem when rescaling to maximum distance. An assumption of rescaling to mean distance, however, is that the distribution of the distances is Gaussian.

**Range.** The range of data points included in the recurrence analysis is specified by setting the first point,  $P_{\text{start}}$  (the data point in the time series at which the analysis will start), and the last point,  $P_{\text{end}}$  (the data point in the time series at which the analysis will end). We wanted to include as many of the data points in the time series as possible in our recurrence analysis. For that reason, we input the first point as 1 and the last point as 1410, thereby selecting the largest range possible, given constraints due to the number of data points in the time series ( $N = 1500$ ), maximum embedding dimension ( $M = 10$ ), and maximum delay ( $\tau = 10$ ). The last data point was determined by  $P_{\text{end}} = N - (M - 1) \times \tau$ . This guarantees the use of the maximal number of data points and the same number of data points within each surrogate dimension in the phase space. When using *RQS.EXE*, however, we did not actually have to compute  $P_{\text{end}}$ , because when the program prompts the user to input LAST ( $P_{\text{end}}$ ), it specifies the last possible point in the time series that could be used. We simply input that last possible point, 1410, as our value for  $P_{\text{end}}$ .

**Line Length.** Line length specifies the number of consecutive recurrent points required to define a line segment. Often, line length is set at two points. Specifying a line length of more than two points yields increasingly conservative estimates of the deterministic structure in the system. In the present study, line length was set to three points.

Having determined a range of parameter settings for embedding dimension, delay, and radius, and selected settings for norming method, rescaling method, range, and line length, our next step was to choose (at random) a few trials from each experimental condition and use program *RQS.EXE* to compute recurrence measures for the selected

parameter ranges. To reiterate, our purpose in running *RQS.EXE* on a sample of experimental trials was to generate recurrence measures for a range of embedding dimensions, delays, and radius values. As noted above, we set minimum embedding dimension at 7, maximum embedding dimension at 10; minimum delay at 2 samples, maximum delay at 10 samples; and minimum radius at 10, maximum radius at 26. Table 3.1 lists each of the parameter settings we selected in running *RQS.EXE*.

We inspected the recurrence measures that were generated by *RQS.EXE* for our sample of trials to decide on specific settings for embedding dimension, delay, and radius to be used in carrying out the RQA of all experimental trials. To recap, we were looking for small changes in parameter settings yielding smooth changes in output measures, %REC values ranging between 1% and 5%, and absence of ceiling or floor effects on %DET. We created in *Matlab* (Mathworks, Inc., Natick, MA) a series of surface plots to visualize changes in %REC as a function of embedding dimension, delay, and radius. A separate plot was created for each of the four embedding dimensions under examination (see Figure 3.11), with radius on the x-axis, delay on the y-axis, and the dependent variable %REC on the z-axis. The surface plots in Figure 3.11 illustrate well that in spite of the fact that increasing values of radius yielded higher %REC, each of the plots looks qualitatively similar. That is, there are no qualitative differences in the patterns of %REC (i.e., the shape of each surface) for this range of parameter settings. The fact that incremental changes in parameter values yield smooth (not abrupt) changes in %REC (e.g., steady increases in %REC with increases in radius or steady decreases in

## ROA of Postural Fluctuations

Table 3.1. *Parameter settings selected when prompted by program RQS.EXE. MIN = minimum; MAX = maximum; RANDSEQ = randomize data sequence. See README.TXT file accompanying software for further explanation of parameters listed above (Webber, 2004). NORM value of 3 corresponds to Euclidean normalization. Selection of RANDSEQ n is a “no” response to the option of randomly sequencing points in the data set, thereby retaining the original order of points in the time series. Rescale value of 2 instructs the program to rescale the matrix to mean distance.*

Parameter	Setting
DELAY MIN	2
DELAY MAX	10
EMBED MIN	7
EMBED MAX	10
NORM	3
FIRST	1
LAST	1410
RANDSEQ	n
RESCALE	2
RADIUS MIN	10
RADIUS MAX	26
RADIUS STEP	1
LINE	3

%REC with increases of embedding dimension) suggests that using a set of parameters within the selected range will not yield notable changes in %REC that are artifacts of parameter selection. For additional information about surface plots, see Shockley’s (Chapter 4)

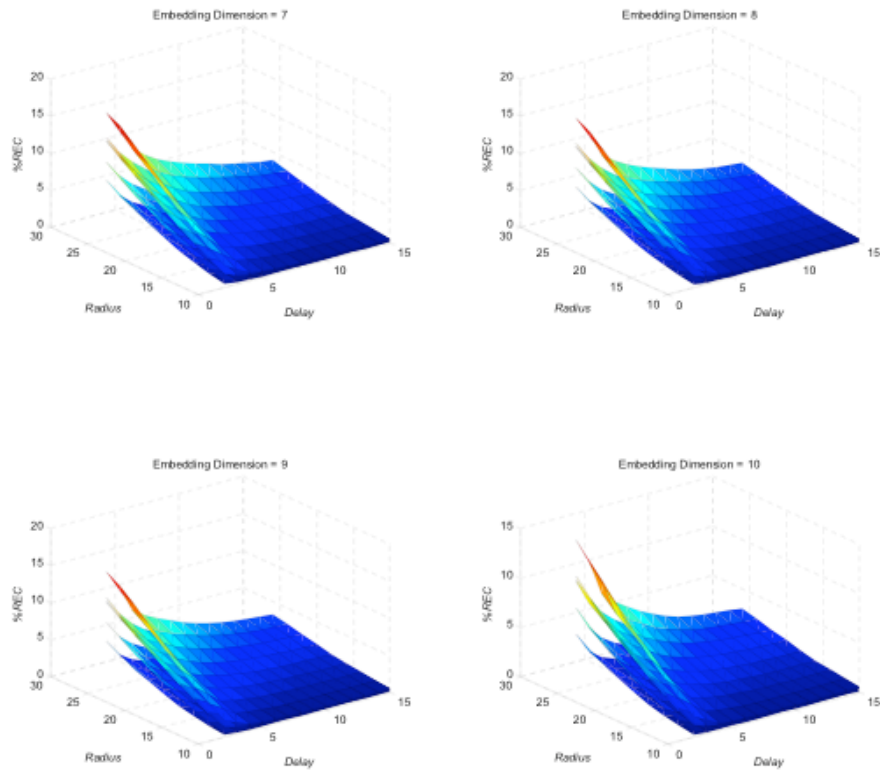


Figure 3.11. Surface plots for embedding dimensions 7-10, showing steady increase in percentage of recurrent points (%REC) with increasing values of radius, but no apparent difference in the pattern of %REC across the four plots.

application of cross-recurrence analysis. Based on our inspection of the surface plots and the numerical recurrence output generated by program *RQS.EXE*, we selected the following parameter settings: Embedding dimension of 7, time delay of 3 samples (corresponding to a 0.06 s lag), and radius of 16. Our decision to set the radius parameter at 16 means that points falling within 16% of the mean Euclidean distance of each other would be considered recurrent. As can be seen in the surface plots, this radius ensures that our %REC values will be in

our target range of 1-5%. It is important to note that had we selected slightly different parameters, we would still have seen the same basic pattern in the results, although the particular magnitudes of recurrence measures would have scaled up or down.

Our next step was to run the RQA with the selected parameter settings on the entire set of experimental trials. Program *RQE.EXE* was used to compute the five recurrence variables of interest, %REC, %DET, MAXL, ENT, and TND. As a practical note, recurrence analysis can take a long time (hours) to run, depending on file size, number of trials, and processor speed. An advantage of using *RQE.EXE* as opposed to *RQD.EXE*, for example, is that the former allows multiple analyses to be executed in batch mode, rather than waiting for each file to be analyzed and typing the next command for the next file to be analyzed. Computations were performed using the following parameter settings: Delay = 3, embedding dimension = 7, range = 1-1482, norm = Euclidean, rescaling = mean distance, radius = 16, and line length = 3. The program *RQEP.EXE* was used to generate a parameter file, to be called by the batch file commands, containing those parameter selections. An ASCII (text), tab-delimited batch file (*filename.bat*) was set up such that each row corresponded to the *MSDOS* command for analyzing one file using *RQE.EXE*. The number of rows corresponded to the number of files to be analyzed (see *README.TXT* file for complete instructions). Program run time for the present data was approximately four hours. Mean values for the recurrence measures were calculated for the two trials in each condition. Separate ANOVAs were conducted on each recurrence measure for AP COP and ML COP time series.

After the RQA was complete for all of the experimental trials, we reran the RQA for six randomly chosen trials using the same parameter settings, but selecting the option to randomize the order of the data points. Comparing the RQA findings of the randomly shuffled data and the normally sequenced data provides the means to confirm our choice of parameter settings as appropriate for revealing the deterministic structure present in the original time series (see Webber & Zbilut, Chapter 2).

Figure 3.12 depicts the recurrence plots generated with random shuffling of data from the time series in Figure 3.4. Although the values in the time series of Figure 3.12 (just below the recurrence plot) are exactly the same as those for the time series in Figure 3.5, because they are randomly shuffled, nearness in time no longer necessarily means nearness in value. For example, in a typical time series, the value for the 10<sup>th</sup> data point will be reasonably close to the value for the 11<sup>th</sup> data point, simply because a person cannot instantaneously move the body across large distances. However, when the values are randomly shuffled, the 100<sup>th</sup> data point from the original time series could end up next to the 10<sup>th</sup> data point of the original time series. When the data points from the new, randomly shuffled time series are connected by a line for plotting, the time series now looks extremely densely packed as compared to the original, in spite of the fact that none of the values have changed. This, however, is simply an artifact of “connecting the dots,” as it were.

What is more important than comparing the time series of Figures 3.5 and 3.12 is comparing the recurrence plots. Recall that only recurring points are plotted in a recurrence plot. Visual comparison of

## RQA of Postural Fluctuations

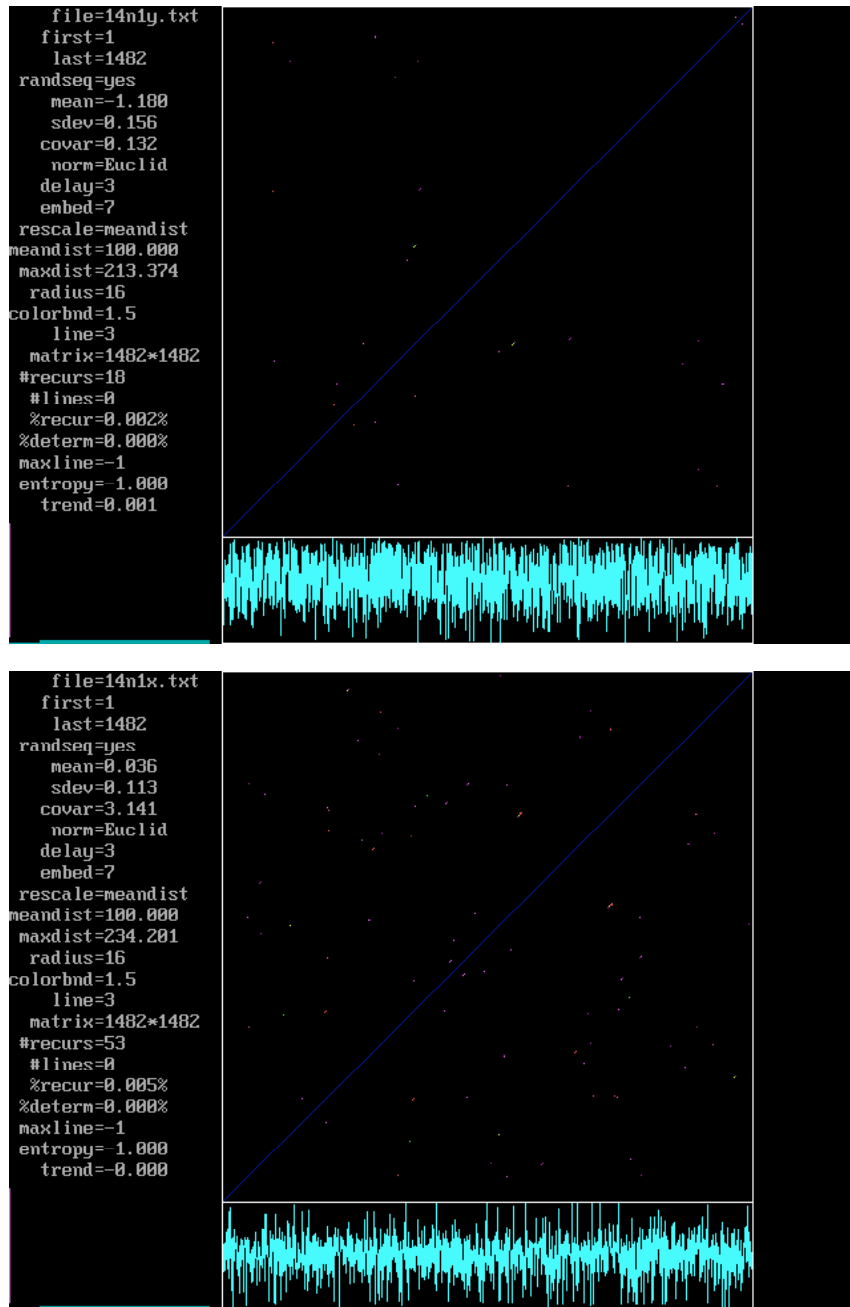


Figure 3.12. Recurrence plots for the AP COP (top) and ML COP (bottom) data sets shown in Figure 3.4, but randomly shuffled. The data series (following random shuffling) are shown at the bottom of the figure; recurrence parameters and recurrence output are listed to the left of the plot. Note that the same recurrence parameters were used to generate recurrence plots for the original times series (see Figure 3.5) and the randomly shuffled data sets.

the recurrence plots in Figures 3.5 and 3.12 shows that fewer points are recurrent for the randomly shuffled data and that almost none of those recurrent points form diagonal lines. This qualitative change is reflected quantitatively by the fact that, for the randomly shuffled data, %REC < 0.01% and %DET < 0.001%. Randomizing the data reduced the number of recurrent points, but, perhaps more importantly, it eliminated the deterministic structure of the original time series. The interested reader can reproduce the plots shown in Figure 3.12 by using the data that accompany this chapter and running program *RQD.EXE* with the parameter settings listed previously (and depicted at the left side of the plots in Figure 3.12) and selecting 'y' for the *randomize data sequences* option.

#### ***Results of RQA***

For AP COP, ANOVA revealed a main effect of cognitive task condition on %DET,  $F(3, 57) = 3.52$ ,  $p < .05$ , which is shown in Figure 3.13a. %DET was greater for counting back by 3s ( $M = 88.70$ ) than quiet standing ( $M = 85.65$ ) and digit reversal ( $M = 83.61$ ). This finding suggests that the temporal structure of AP postural fluctuations became more regular as the attentional demands of the cognitive task increased. Recalling the results of the traditional analysis of AP COP data (Figures 3.3b and 3.3d) in view of the observed changes in %DET for the AP COP time series, we see that although the amplitude and variability of postural sway increased with greater attentional demands of the concurrent cognitive task, the postural fluctuations became more deterministic (regular). ANOVAs on %REC, MAXL, ENT, and TND did not reveal any other effects of cognitive task condition for the AP COP time series.

### RQA of Postural Fluctuations

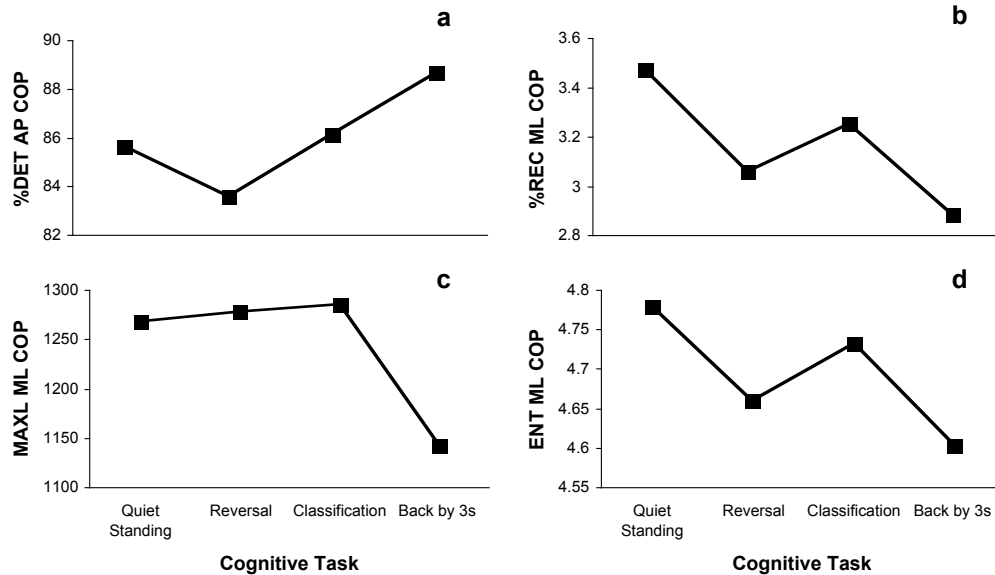


Figure 3.13. Results of RQA for all experimental trials. (a) Percent determinism (%DET) for AP COP as a function of cognitive task condition. For ML COP, (b) Percentage of recurrent points (%REC), (c) maxline (MAXL), and (d) entropy (ENT) as a function of cognitive task condition.

For ML COP, ANOVA on %REC showed that the effect of cognitive task condition approached significance,  $F(3, 57) = 2.64$ ,  $p < .06$  (see Figure 3.13b). Pair-wise comparisons revealed a lower percentage of recurrent points ( $p < .05$ ) for the counting back by 3s cognitive task ( $M = 2.89$ ) than for digit classification ( $M = 3.25$ ) and quiet standing ( $M = 3.47$ ). Generally, ML COP fluctuations were less recurrent when performing concurrent cognitive and postural tasks than when simply standing.

ANOVA on MAXL of the ML COP time series revealed a main effect of cognitive task condition,  $F(3, 57) = 2.83$ ,  $p < .05$ . MAXL was shorter for counting back by 3s ( $M = 1142.9$ ) than for digit classification ( $M = 1286.8$ ) and digit reversal ( $M = 1278.3$ ). This finding, depicted in

Figure 3.13c, suggests that the temporal structure of the ML COP was less mathematically stable when the cognitive task required higher attentional demands.

Figure 3.13d shows the significant main effect of cognitive task condition on ENT of the ML COP data,  $F(3, 57) = 4.25, p < .01$ . ENT was lower for counting back by 3s ( $M = 4.60$ ) than for digit classification ( $M = 4.73$ ) and quiet standing ( $M = 4.78$ ). This finding suggests the deterministic structure of the ML COP was less complex for the cognitive task of highest attentional demand.

ANOVAs for the ML COP data did not indicate an effect of cognitive task condition on the recurrence measures of %DET and TND.

## GENERAL DISCUSSION

The present research highlights the utility of RQA for the study of postural fluctuations. Using a traditional approach to the analysis of COP data, we found that total COP excursion, as well as the range and variability of AP and ML COP motion, were impacted by attentional demands in a similar manner. Results of the traditional analyses showed that performing a concurrent cognitive task increased the magnitude and variability of postural sway. These findings could lead one to conclude that carrying out an unrelated but concurrent cognitive task compromises postural stability.

The RQA results suggest an alternative interpretation. Attentional demands impacted postural sway, but not necessarily in the form of a decline in the effectiveness of the postural control system. Examination of the temporal structure of postural fluctuations revealed that attentional demands influenced AP COP and ML COP in different ways.

Whereas with higher attentional demands fluctuations in ML COP became less recurrent, less stable, and less complex, AP COP fluctuations became more deterministic. What might explain these observed differences in recurrence patterns in the two COP component directions? One possibility is that the RQA findings reflect a strategy being used by the central nervous system (CNS) to optimize postural control. Recall the stance position maintained by study participants, which is shown in Figure 3.2. In keeping with instructions to stand with feet together, participants adopted a narrow base of support during testing. Thus, it is likely that the perceived limit of stability (PLOS—the distance an individual can sway without losing balance or taking a protective step) was smaller for ML motion than for AP motion. Increases in ML COP motion may have presented a greater threat to postural stability than AP COP motion, since increased ML motion would bring the ML COP closer to the PLOS. The changes in recurrence patterns of ML COP data series may follow from the increased COP motion in that direction. Of note, spontaneous ML postural sway, rather than AP sway, has been shown to be predictive of fall risk in older adults (Lord, Rogers, Howland, & Fitzpatrick, 1999; Maki, Holliday, & Topper, 1994).

Why wouldn't the CNS simply reduce sway range and variability as a way of promoting postural stability under conditions of greater attentional demand? The observed increase in the deterministic structure of AP COP may be a more efficient and more effective means of optimizing postural control. Sway range and variability are important aspects of exploratory postural behavior—sway is “exploratory” because it generates stimulation regarding the current state of postural

stability. The regularization of AP motion could be a strategy that simplifies the problem of postural control without sacrificing the pick-up of perceptual information made available through spontaneous postural sway. In short, rendering AP COP motion more deterministic may be one approach by which the postural system adjusts to the attentional demands of a concurrent cognitive task.

To summarize, it is difficult to interpret the results of the traditional analysis of COP data in terms other than a classical dual-task effect, in which concurrent performance of a cognitive task brings about a decrement in the ability of the CNS to control posture. Results of RQA, however, suggest adaptation of the postural system (perhaps proactively as well as reactively) to changing task demands. Although a full understanding of the findings reported here must await further research, a few points are clear. The results of the RQA brought to light dynamical processes inherent in postural control that are not evident in summary measures of COP path magnitude and variability. In addition, our findings offer further evidence that AP and ML COP motion can be affected differentially in response to varying task requirements (Balasubramaniam et al., 2000). Most importantly, the present study supports the notion that the response of the postural control system to dual-task requirements is one of adaptation not deterioration.

## CONCLUSION

A conventional approach to the analysis of COP data revealed increases in measures of COP path magnitude and variability during performance of a concurrent cognitive task. Those findings are consistent with the notion that dual-tasking compromises postural

control. Also of note, AP COP and ML COP summary measures were impacted in a similar manner. In a second stage of data analysis, RQA revealed changes in the dynamical properties of postural sway brought about by concurrent performance of cognitive and postural tasks. Among the observed changes were differential effects on the AP and ML components of postural fluctuations. The results of RQA suggest that the postural control system adapts, rather than deteriorates, in response to changing attentional requirements. The analytic tools available through RQA promise insight into the mechanisms and processes underlying postural control not accessible with a conventional approach to the study of postural sway.

#### AUTHOR NOTE

This work was supported in part by a Patrick and Catherine Weldon Donaghue Medical Research Foundation grant awarded to G. L. Pellechia. The authors thank Michael Riley for many helpful discussions about RQA parameter settings for COP data.

#### REFERENCES

Balasubramaniam, R., Riley, M. A., & Turvey, M. T. (2000). Specificity of postural sway to the demands of a precision task. *Gait and Posture, 11*, 12-24.

Dault, M. C., Geurts, A. C. H., Mulder, T. W., Duysens, J. (2001). Postural control and cognitive task performance in healthy participants while balancing on different support-surface configurations. *Gait and Posture, 14*, 248-255.

Derave, W., De Clercq, D., Bouckaert, J., & Pannier, J. L. (1998). The influence of exercise and dehydration on postural stability. *Ergonomics, 41*, 782-789.

Eckmann, J. P., Kamphorst, S. O., Ruelle, D. (1987). Recurrence plots of dynamical systems. *Europhysics Letters, 5*, 973-977.

Gravelle, D. C., Laughton, C. A., Dhruv, N. T., Katdare, K. D., Niemi, J. B., Lipsitz, L. A., & Collins, J. J. (2002). Noise-enhanced balance control in older adults. *Neuroreport, 13*, 1853-1856.

Guerraz, M., Thilo, K., V., Bronstein, A. M., & Gresty, M. A. (2001). Influence of action and expectation on visual control of posture. *Cognitive Brain Research, 11*, 259-266.

Kerr, B., Condon, S. M., & McDonald, L. A. (1985). Cognitive spatial processing and the regulation of posture. *Journal of Experimental Psychology: Human Perception and Performance, 11*, 617-622.

Lajoie, Y., Teasdale, N., Bard, C., & Fleury, M. (1993). Attentional demands for static and dynamic equilibrium. *Experimental Brain Research, 97*, 139-144.

Lord, S. R., Rogers, M. W., Howland, A., & Fitzpatrick, R. (1999). Lateral stability, sensorimotor function and falls in older people. *Journal of the American Geriatrics Society, 47*, 1077-1081.

Maki, B. E., Holliday, P. J., & Topper, A. K. (1994). A prospective study of postural balance and risk of falling in an ambulatory and independent elderly population. *Journals of Gerontology: Medical Science, 49*, M72-M84.

Maylor, E. A., Allison, S., & Wing, A. M. (2001). Effects of spatial and nonspatial cognitive activity on postural stability. *British Journal of Psychology, 92*, 319-338.

Maylor, E. A., & Wing, A. M. (1996). Age differences in postural stability are increased by additional cognitive demands. *Journals of Gerontology: Series B, Psychological Sciences and Social Sciences*, *51B*, P143-P154.

Newell, K. M. (1998). Degrees of freedom and the development of postural center of pressure profiles. In K. M. Newell & P. C. M. Molenaar (Eds.), *Applications of Nonlinear Dynamics to Developmental Process Modeling* (pp. 63-84). Mahwah, NJ: Erlbaum.

Newell, K. M., Slobounov, S. M., Slobounova, B. S., & Molenaar, P. C. M. (1997). Short-term non-stationarity and the development of postural control. *Gait and Posture*, *6*, 56-62.

Pellecchia, G. L., & Turvey, M. T. (2001). Cognitive activity shifts the attractors of bimanual rhythmic coordination. *Journal of Motor Behavior*, *33*, 9-15.

Pellecchia, G. L. (2003). Postural sway increases with attentional demands of concurrent cognitive task. *Gait and Posture*, *18*, 29-34.

Polonyova, A., & Hlavacka, F. (2001). Human postural responses to different frequency vibrations of lower leg muscles. *Physiological Research*, *50*, 405-410.

Posner, M. I. (1964). Information reduction in the analysis of sequential tasks. *Psychological Review*, *71*, 491-504.

Posner, M. I., & Rossman, E. (1965). Effect of size and location of information transforms upon short-term retention. *Journal of Experimental Psychology*, *70*, 496-505.

Riley, M. A., Balasubramaniam, R., & Turvey, M. T. (1999). Recurrence quantification analysis of postural fluctuations. *Gait and Posture*, *9*, 65-78.

Riley, M. A., & Clark, S. (2003). Recurrence analysis of human postural sway during the sensory organization test. *Neuroscience Letters*, *342*, 45-48.

Schmit, J. M. , Riley, M. A., Dalvi, A. , Sahay, A., Shear, P. K., Shockley, K. D., & Pun, R. Y.-K. (submitted). Recurrence quantification analysis of postural sway in Parkinson's disease.

Schumann, T., Redfern, M. S., Furman, J. M., El-Jaroudi, A., & Chaparro, L. F. (1995). Time-frequency analysis of postural sway. *Journal of Biomechanics*, *27*, 603-607.

Stelmach, G. E., Zelaznik, H. N., & Lowe, D. (1990). The influence of aging and attentional demands on recovery from postural instability. *Aging*, *2*, 155-161.

Vuillerme, N., Forestier, N., & Nougier, V. (2002). Attentional demands and postural sway: the effect of the calf muscles fatigue. *Medicine and Science in Sports and Exercise*, *34*, 1907-1912.

Vuillerme, N., Nougier, V., & Teasdale, N. (2000). Effects of a reaction time task on postural control in humans. *Neuroscience Letters*, *291*, 77-80.

Webber, C. L., Jr. (2004). Introduction to recurrence quantification analysis. *RQA version 8.1 README.TXT*. Retrieved February 13, 2004, from <http://homepages.luc.edu/~cwebber/>

Webber, C. L., Jr., & Zbilut, J. P. (1994). Dynamical assessment of physiological systems and states using recurrence plot strategies. *Journal of Applied Physiology*, *76*, 965-973.

Webber, C. L., Jr., & Zbilut, J. P. (1996). Assessing deterministic structures in physiological systems using recurrence plot strategies. In M. C. K. Khoo (Ed.), *Bioengineering Approaches to Pulmonary Physiology and Medicine* (pp. 137-148). New York: Plenum Press.

Woollacott, M., & Shumway-Cook, A. (2002). Attention and the control of posture and gait: A review of an emerging area of research. *Gait and Posture*, *16*, 1-14.

Zbilut, J. P., & Webber, C. L., Jr. (1992). Embeddings and delays as derived from quantification of recurrence plots. *Physics Letters A*, *171*, 199-203.

## CHAPTER 4

# Cross Recurrence Quantification of Interpersonal Postural Activity

Kevin Shockley

Department of Psychology  
University of Cincinnati  
Cincinnati, OH 45221-0376  
U. S. A.  
E-mail: [kevin.shockley@uc.edu](mailto:kevin.shockley@uc.edu)

Measuring interpersonal coordination in the context of conversation has been a challenging problem in psychology for at least three decades. This is an interesting problem because observations of interpersonal coordination in the context of cooperative conversation appear to index the coordination that is required to complete the goals of a particular interaction (Clark, 1996). This type of coordination has been indexed in a number of ways, including the convergence of speaking rate (Street, 1984), vocal intensity (Natale, 1975), pausing frequency (Cappella & Planalp, 1981), and even in the convergence of conversational partners' dialects (Giles, Coupland, & Coupland, 1991). Conversational partners have also been observed to mirror or mimic each others' postures (LaFrance, 1982). Until very recently, however, such indices of coordination have been based on fairly subjective observation procedures. For example, Condon and Ogston (1971) assessed interpersonal coordination by hand scoring video-taped interactions to evaluate the timing of listeners' movements with reference to the rhythmic properties of a speaker.

More recent techniques of quantifying interpersonal coordination have made the visual scoring approach somewhat more systematic by sketching joint angles from video tapes and quantifying the number of joint angle changes (Newtson, 1994; Newtson, Enquist, & Bois, 1977; Newtson, Hairfield, Bloomingdale, & Cutino, 1987). Spectral profiles of periodicity of joint angle changes were then compared across conversers. This strategy has revealed apparent coupling of the *behavioral waves* of conversers. While the Newtson et al. approach is certainly an improvement over previous methods, problems with distortions from scoring 2-dimensional video tapes of 3-dimensional

Shockley

movements cannot be avoided. The magnitude of angle changes of joints based on visual estimates of a 2-D video is dependent upon the angle of the video-taped person relative to the 2-D viewing plane of the video screen. Thus, visual estimates of angle changes from video will be distorted unless the movements are always aligned with the viewing plane. An additional drawback is that the degree of joint angle change is not measured—all that is measured is that joint angles changed.

Shockley, Santana, and Fowler (2003) introduced a strategy for evaluating the degree of interpersonal coordination that involves submitting measurements of postural sway to cross recurrence quantification (CRQ) analysis. The advantage of CRQ over conventional linear methods is that it requires no assumptions about the nature of the data in question, and it offers an objective method for studying interpersonal coordination. The purpose of this chapter is to provide a tutorial for how to apply this recently developed analysis to postural data using the method and data of Shockley et al. (2003). Before discussing the CRQ technique and its theoretical foundations, however, some understanding of postural sway is necessary to make it clear why such an approach is warranted.

## POSTURAL SWAY

Although standing upright seems straightforward and effortless to most of us, it is actually quite challenging to explain how we are able to accomplish this task. Consideration of the underlying anatomical constraints and surrounding physiological processes reveals that the apparently simple act of standing upright is quite complex and yields a correspondingly complex behavior that is not straightforward to

quantify. The fact that postural activity is complex motivates the need for measures that are not restricted by the assumptions of linear methods.

Operationally, upright stance is best understood as the maintenance of the horizontal position of the center of mass of the body within the boundaries of the base of support of the body. Imagine a line drawn straight down to the ground along the direction of gravity from the center of mass of the body (generally in the region of the abdomen). In order to avoid falling down, the projected line from the center of mass must remain within the base of support of the body (usually the anterior-posterior and lateral extents of the feet).

The simplest image of this control requirement is to keep an inverted pendulum upright. To build your intuitions, try to balance an inverted broomstick on one finger. Note that in order to keep the inverted broomstick upright, quick adjustments to the position of the supporting finger are required as the broomstick begins to fall in one direction or another. This is a useful image, but the inverted pendulum image is certainly not an adequate model of postural control, however, given that most animals are of the multi-segmental variety. The consequence of this fact is that the center of mass must effectively be balanced over the base of support across many joints.

One may imagine that simply freezing all joints in a particular position would achieve the desired goal of standing upright. The physiological activity surrounding all of our actions, however, must also be considered. For example, instability in the position of the center of mass is introduced by physiological processes such as the inherent tremor of muscular tensile states, heart compressions, and the

Shockley

expansion and compression of the chest cavity involved in breathing. These inherent perturbations result in instability of the position of the center of mass over time; this is generally referred to as postural sway (see Figure 4.1).

Postural sway occurs even during so-called *quiet stance* (standing without engaging in other activities; Collins & De Luca, 1994; Newell, Slobounov, Slbounova, & Molenaar, 1997), but occurs especially when supra-postural tasks (e.g., reading, talking, pointing, reaching) are added to the demands of maintaining upright stance (Balasubramaniam, Riley, & Turvey, 1997; Belen'kii, Gurfinkel', & Pal'tsev, 1967; Fel'dman, 1966; Riccio & Stoffregen, 1988; Riley, Mitra, Stoffregen, & Turvey, 1997; Stoffregen, Pagulayan, Bardy, & Hettinger, 2000). For example, the seemingly benign act of raising one's arm compromises postural stability and requires concurrent (and often prior) compensation of the muscles of the thighs, hips, and trunk to keep the center of mass within the base of support (Belen'kii, Gurfinkel', & Pal'tsev, 1967; Pal'tsev & Elnor, 1967). Speaking and gesturing are ubiquitous in conversation and, accordingly, add to the instability of the location of the body's center of mass.

## CAPTURING THE DYNAMICS OF UNKNOWN NONLINEAR SYSTEMS

The inherent instability of postural activity described above has made the quantification of postural sway quite challenging. The most direct methods for measuring postural sway involve the measurement of the center of pressure of the body using a force platform or the measurement of displacement of the center of mass using a motion

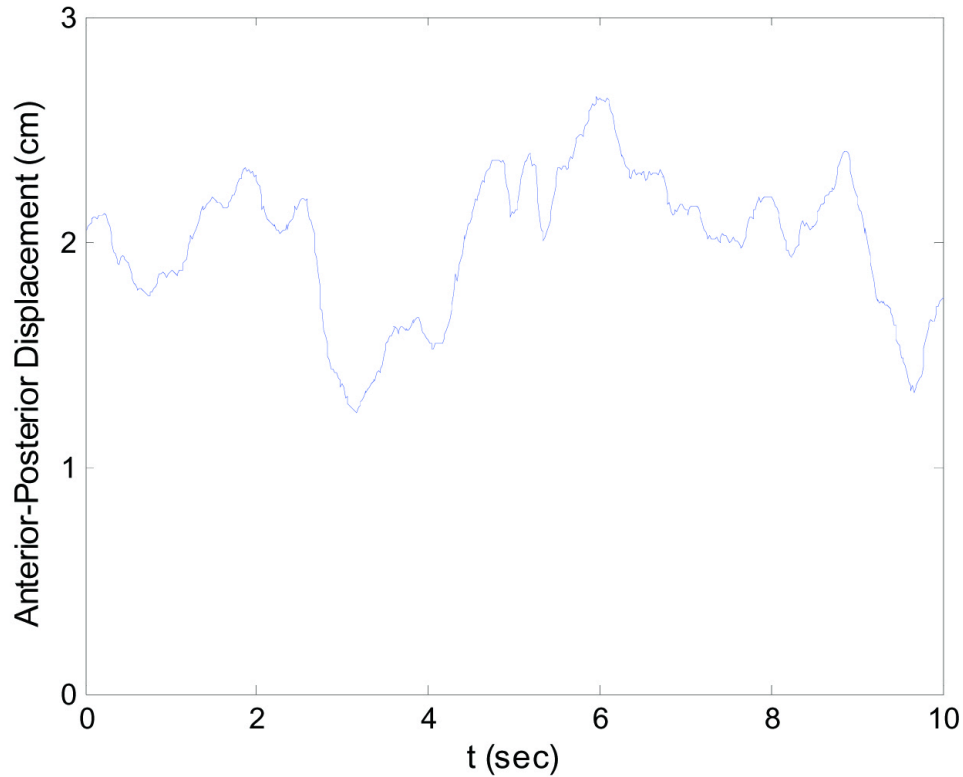


Figure 4.1. Sample postural sway time series during quiet stance. The abscissa corresponds to time (sec) while the ordinate corresponds to anterior-posterior displacement (cm).

tracking system.<sup>1</sup> These measures yield time series that are typically irregular, non-stationary (i.e., there is drift in the mean and/or standard deviation of the time series over time), and non-periodic (Carroll & Freedman, 1993; Collins & De Luca, 1993). Thus, conventional (linear) analyses that assume normal distributions and stationarity, such as correlational or spectral methods, are not appropriate for postural sway

<sup>1</sup> The center of pressure corresponds to the point of application of the sum of forces acting between the feet and the surface of support (see Pellecchia & Shockley, Chapter 3).

Shockley

data (see Riley, Balasubramaniam, & Turvey, 1999; see also Pellecchia & Shockley, Chapter 2, for a comparison of linear and nonlinear methods of analyzing postural sway).

### ***Linearity vs. Nonlinearity***

By definition, linear time series analysis methods assume independence and additivity of the multiple degrees of freedom that contribute to a given observable. Nonlinear systems have degrees of freedom that interact multiplicatively. Relatively recent investigations into nonlinear systems have inspired the development of analysis methods that capitalize on the interactive nature of nonlinear systems (see Abarbanel, 1996). In some cases, the variables that contribute to the dynamics of some nonlinear systems are known and can be indexed. Most often, however, the variables that contribute to the dynamics of a system under investigation are not known. The advantage of a nonlinear system, however, is that the dynamical variables interact. Thus, the influence of unknown (or perhaps unmeasurable) variables can be indexed by variables that *are* readily measurable. To illustrate this peculiar feature of nonlinear systems, I will show how the measurement of a single variable from a system with known dimensions can be used to capture the dynamics of the whole system.

### ***The Lorenz Attractor: A Nonlinear System With Known Dynamics***

The Lorenz (1963) system is a model of convection (i.e., heat transfer) in the atmosphere. The dynamics (i.e., changes in states) of the Lorenz model can be characterized with three first order differential equations,

$$\dot{X} = a(Y - X) \quad [4.1]$$

$$\dot{Y} = X(b - Z) - Y \quad [4.2]$$

$$\dot{Z} = XY - cZ \quad [4.3]$$

where  $X$ ,  $Y$ , and  $Z$  correspond to the three dynamical variables (corresponding to two temperature measures and a velocity measure), the over-dot corresponds to the rate of change (i.e., derivative) of the variable in question, and  $a$ ,  $b$ , and  $c$  are constant parameters. What makes the Lorenz system a complex, nonlinear system is the interaction of the three dynamical variables. As can be seen in Equations 4.1-4.3, changes in  $X$  are dependent not only upon the value of  $X$ , but also upon the values of  $Y$  and  $Z$ . Therefore, the influences of the variables  $X$ ,  $Y$ , and  $Z$  on the current state of the system are not independent and additive, but are instead mutually dependent and multiplicative. The interactive nature of dimensions along which a system may change embodies the complexity of nonlinear systems and is also the key to quantifying systems with unknown or unmeasured dynamical variables.

#### ***Phase Space Reconstruction and the Embedding Theorem***

Often, the interplay of dynamical variables is best characterized using a phase space (see Figure 4.2). A phase space is essentially a multidimensional scatterplot of each dynamical variable with respect to the other dynamical variables. As is often the case, however, the particular variables that comprise a given nonlinear system may not be known and perhaps may not even be knowable, *a priori*. Fortunately, lack of identification of the dynamical variables does not preclude one

Shockley

from gaining access to the underlying dynamics of the system in question.

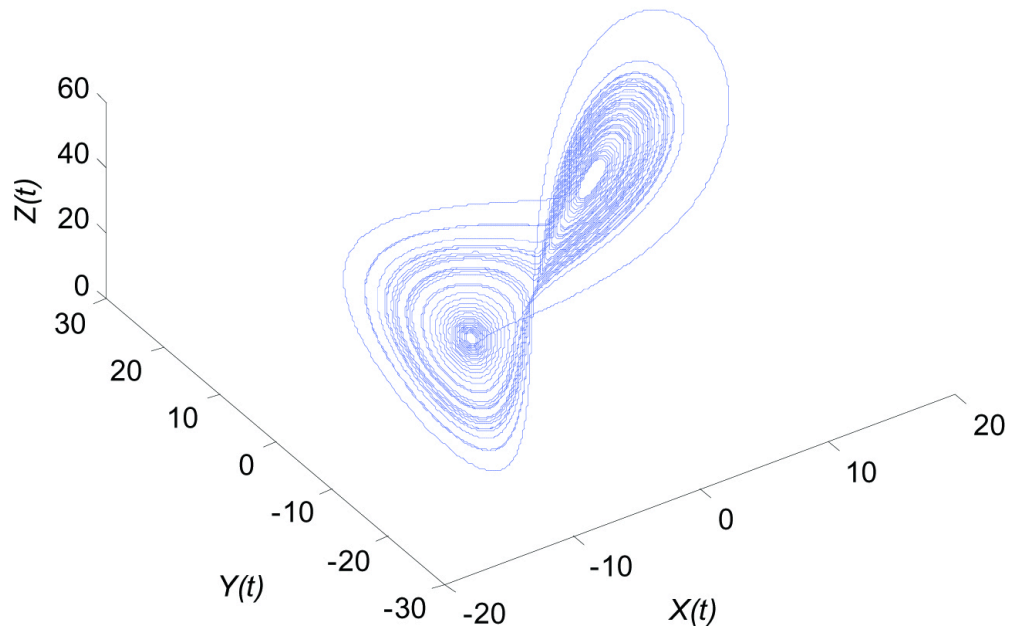


Figure 4.2. A three-dimensional plot (phase space) of the time evolution of the three dynamical variables ( $X$ ,  $Y$ , &  $Z$ ) of the Lorenz system (Equations 4.1-4.3).

Takens (1981) introduced the *embedding theorem*, which revealed that the preferred relations of the dynamical variables in a nonlinear system (its attractors) may be discovered by reconstructing a phase space for the system in question using time-delayed copies of a single, observable dynamical variable of the system. That is, the time series of a single dynamical variable can be used to reveal the underlying dynamics of the entire system by using time-delayed copies

of the measured time series. This is possible because (as described previously) in nonlinear systems the multiple dynamical variables interact with one another. The interactive nature of the dynamical variables comprising the nonlinear system generally yields quite messy and unpredictable time series of the variables in question. However, the interactive nature of the degrees of freedom of a nonlinear system dictate that the activity of a single variable will be influenced by the activity of all other dynamical variables. Access to one of the variables of a dynamical system can, accordingly, allow the dynamics of the entire system to be evaluated by unfolding the time series into the appropriate number of dimensions to reveal the underlying dynamics. In the next section I will illustrate how the dynamics of the Lorenz system may be unfolded using time-delayed copies of a single variable.

#### *Distortions Due to Projection*

Consider the time series of  $X$  in Figure 4.3. The evolution of this variable does not resemble the clearly defined attractor in Figure 4.2. This is because the time series of the observed variable is represented by only one dimension ( $X$ ), whereas the Lorenz system requires three dimensions to reveal the influence of the three dynamical variables. While the time series depicted in Figure 4.3 does *embody* the dynamics of the entire system, one cannot see the dynamics unfold properly because the dynamics of the 3-dimensional system are 'projected' onto a single dimension. Such a distortion can be illustrated using a less abstract example.

Imagine positioning your two hands such that both hands are between a light source and a wall. Both hands are some distance apart

Shockley

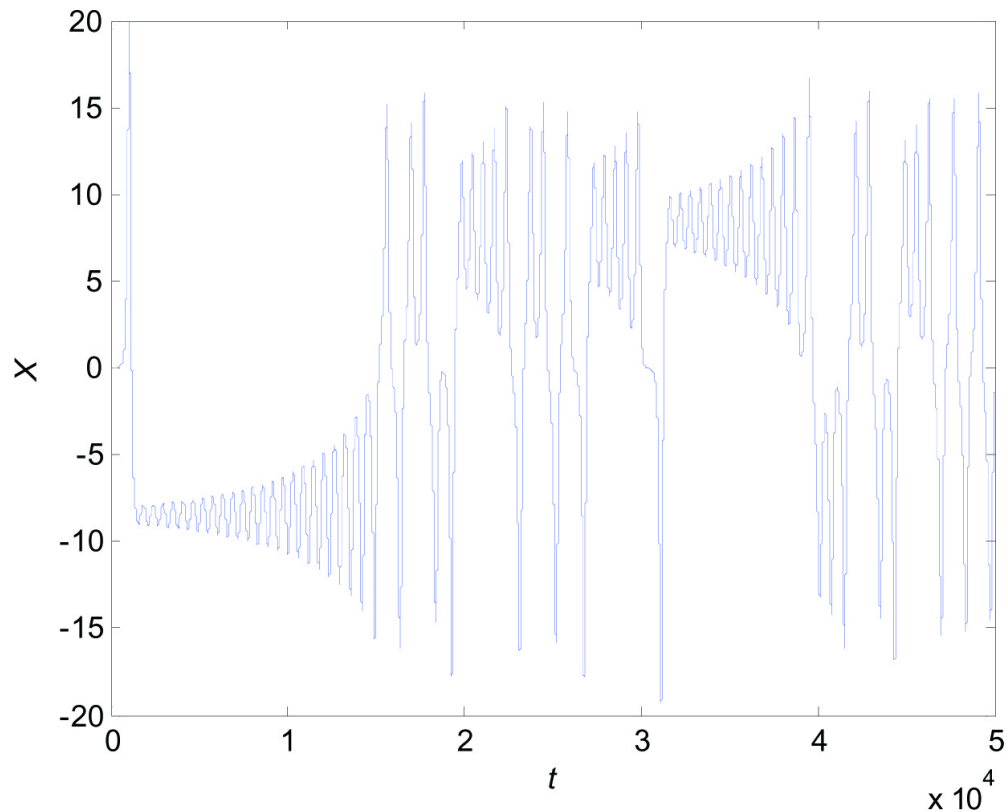


Figure 4.3. The time series  $X(t)$  generated from Equations 4.1-4.3. Given that the data are simulated, time ( $t$ ) corresponds to data points with no particular time units.

along the dimension separating the light source and the wall, but the two hands occupy the same position along the horizontal and vertical dimensions of the wall. In this configuration, the projected shadows of the two hands on the wall will appear to occupy the same space. This shadow example illustrates a distorted, two-dimensional projection of three-dimensional space.

### ***Unfolding the Time Series***

The lesson to be learned from Takens' theorem is that the dynamics of a nonlinear system of multiple degrees of freedom (e.g.,

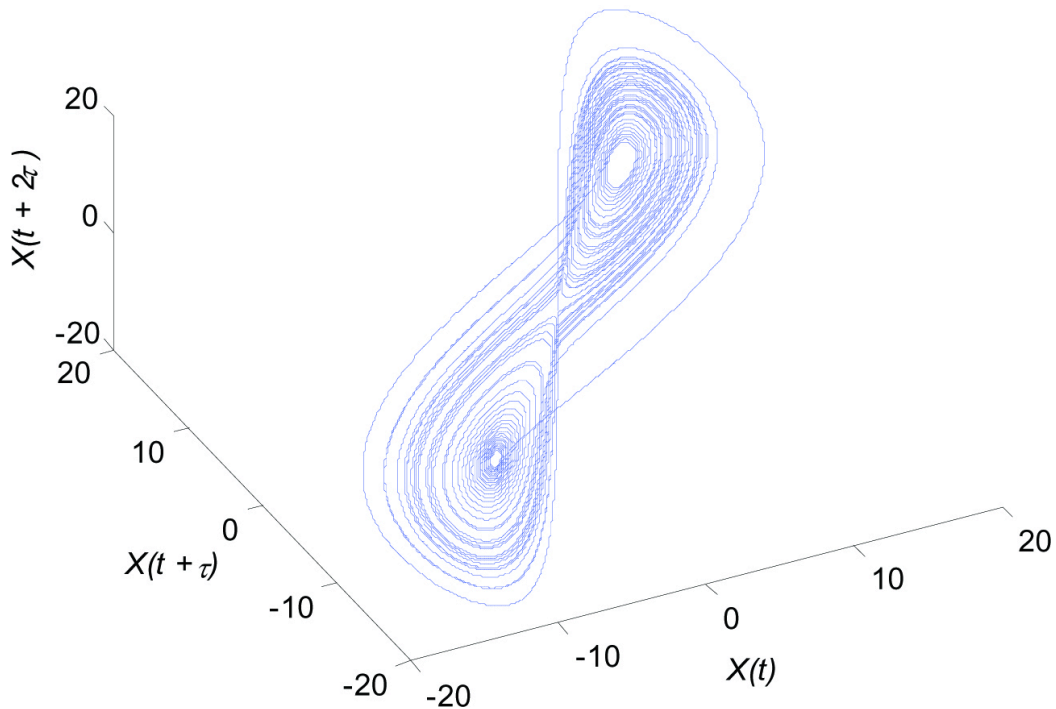


Figure 4.4. A reconstructed phase space of the Lorenz attractor using  $X(t)$  to create time-delayed copies to serve as surrogate dimensions. The delay ( $\tau$ ) used was 55 data points.

the Lorenz system) may be seen properly by unfolding the system into the appropriate number of dimensions using time-delayed copies of one measured dimension as surrogate dimensions in reconstructed phase space. This can be accomplished by using the original time series,  $X(t)$ , as the first dimension,  $X(t + \tau)$  as the second dimension, and  $X(t + 2\tau)$  as the third dimension, and so on for four and higher dimensions. In this example, I used a delay of 55 data points. So, the first dimension,  $X(t)$ , begins at data point 1 of the original time series. The second dimension,  $X(t + 55)$ , begins at data point 56 of the original time series. The third dimension begins at data point 111 of the original

Shockley

time series. What Takens demonstrated is that the reconstructed phase space is isomorphic to the true phase space of the system and, accordingly, allows the system in question to be evaluated in the appropriate number of dimensions (compare Figures 4.2 and 4.4). The purpose of the Lorenz example is to show that a phase space of a system can be reconstructed even with access to only one of the many possible dimensions of change.

## QUANTIFICATION OF POSTURAL SWAY

How can one take advantage of the technique of phase space reconstruction to quantify what appears to be terribly complex postural activity? Recent efforts have made headway in this regard and have demonstrated that nonlinear methods of quantification are useful in differentiating among postural sway time series that correspond to subtly different activities of the person standing (see Riley et al., 1999; Riley & Clark, 2003). For example, Riley et al. (1999) detected deterministic structure in postural sway time series that cannot reliably be differentiated from stochastic noise using conventional methods. The method they used was recurrence quantification analysis (RQA; Webber & Zbilut, Chapter 2), which capitalizes on Takens' embedding theorem.

### *Recurrence Analysis*

Webber and Zbilut (1994) introduced the basic RQA strategy, which involves reconstructing a phase space for a given time series, in the manner described above for the Lorenz system, and then tallying the number of instances that an unfolded time series visits each location in reconstructed phase space (i.e., how often a value recurs). The

degree of deterministic structure in the system may be assessed by quantifying how many sequences of recurrent points are repeated (i.e., repeating patterns of recurrent points). The variety of differing lengths of these sequences of recurrent points (number of data points forming a recurring sequence) may be used to determine the complexity of the signal by computing the Shannon entropy (see below) of the distribution of the lengths. The stability of the system may be measured by the longest of these sequences of recurrent points (maxline) (Eckmann, Kamphorst, and Ruelle, 1987). Finally, the degree of stationarity of the system may be assessed by determining the slope of the density of recurrent points as the points become more separated in time (trend). This procedure is known as auto-recurrence since a time series is compared to itself. See chapters in this volume by Webber and Zbilut (Chapter 2) and Pellecchia and Shockley (Chapter 3) for more extensive discussion and illustration of RQA measures.

## CROSS RECURRENCE QUANTIFICATION AS A MEASURE OF COUPLING

Cross Recurrence Quantification (CRQ) was introduced by Zbilut, Giuliani, and Webber (1998) as an extension to RQA (see also Webber & Zbilut, Chapter 2). This extension involves effectively embedding two synchronous time series in a reconstructed phase space. Rather than tallying the recurring locations of a single embedded time series (auto-recurrence), the number of instances for which locations are shared by the two time series is tallied in CRQ (see Figure 4.5). Measures comparable to those of RQA are available with CRQ. *Percent recurrence* (%REC) in CRQ corresponds to the ratio of

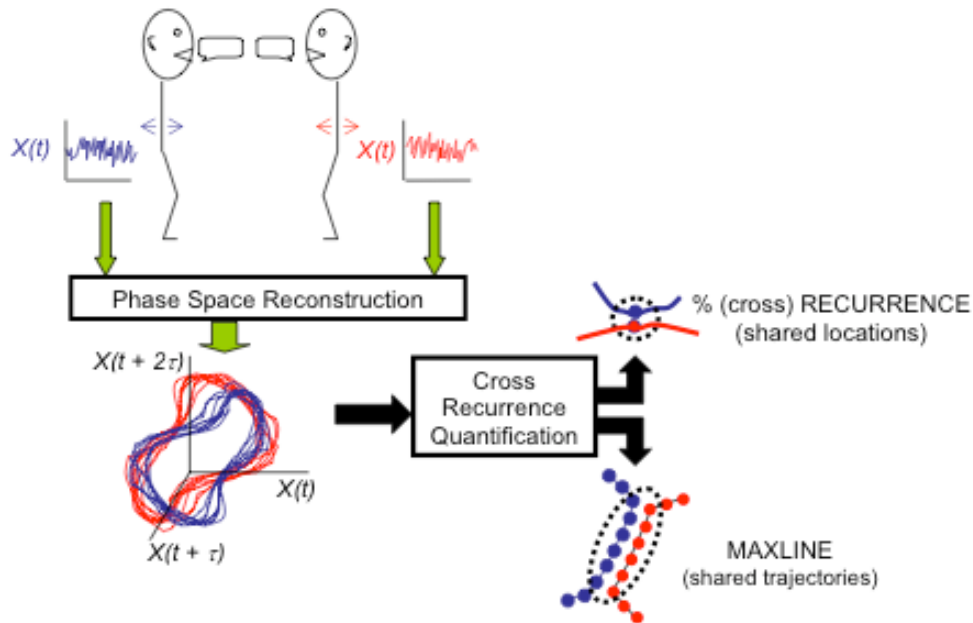


Figure 4.5. Illustration of time series collection, phase space reconstruction, and CRQ measures %REC and MAXL. Blue corresponds to data from one member of the participant pair and red corresponds to data from the other member of the participant pair. %REC quantifies shared locations in reconstructed phase space of two points from the two time series. MAXL quantifies the longest of parallel trajectory of the two time series in reconstructed phase space.

the number of shared location relative to the number of possible shared locations (see Figure 4.5). **Percent determinism** (%DET) is the ratio of the number of shared locations that are part of a sequence of shared locations relative to the total number of shared locations. **Maxline** (MAXL) is the longest shared trajectory and is a measure of the stability of the shared activity (see Figure 4.5). **Entropy** (ENT) is the Shannon entropy of the distribution of lengths of sequences of shared locations.

It was recently demonstrated that CRQ is a useful measure of the coupling of two signals by evaluating physically coupled oscillators (Shockley, Butwill, Zbilut, & Webber, 2002). An apparatus was

constructed that immersed a rotor with a paddle into a container filled with viscous fluid. The container (i.e., the driver) was then oscillated in a translational fashion at a fixed frequency while the immersed rotor was allowed to spin in the fluid at its natural frequency. The idea was to vary the strength of the coupling of the two oscillators by changing the viscosity of the fluid. In this coupled-oscillator system, the coupling strength of the signals was directly manipulated so that the efficacy of CRQ for detecting shared activity could be evaluated. Very subtle couplings between two signals were detected by CRQ measures that remained undetected by conventional, linear measures of coupling, such as cross-spectral analysis. For example, in medium and low coupling conditions, CRQ was able to detect the influence of the driver tray on the rotor oscillation to which linear spectral analysis was blind. Having CRQ as a tool for quantifying the shared activity between two signals allowed Marie-Vee Santana, Carol A. Fowler, and I to turn our attention to the problem of quantifying interpersonal coordination (Shockley et al., 2003). We endeavored to evaluate the utility of CRQ in detecting subtle postural coupling that may exist between two people engaged in conversation.

## VERBAL COORDINATION OF INTERPERSONAL POSTURAL ACTIVITY—THE EXPERIMENT

### *The Task*

The strategy of Shockley et al. (2003) was to track the postural activity of two people engaged in a conversation. In order to generate conversation, a puzzle task was used that required participants to determine the differences between two similar cartoon pictures.

Shockley

Similar types of puzzles can often be found in puzzle books or newspapers. Typically, however, the task involves a single person comparing two pictures. The innovation we introduced was to give each member of a participant pair one of the two similar cartoon pictures. We did not allow participants to visually inspect each other's picture during the course of a trial. This constraint left only verbal interaction to facilitate finding differences between the two pictures. This method was quite effective in generating normal conversation. Furthermore, the participants expressed genuine interest in the task both during and after data collection, as indicated by their reluctance to stop at the end of a trial and their unsolicited positive comments following the data collection session.

In recognition that visual interaction may influence postural sway in addition to the verbal interaction required by the task, two independent variables were factorially combined, *Task Partner* and *Body Orientation*. There were two levels of each variable (see Figure 4.6). A participant's *Task Partner* could be either the other member of the participant pair (*Participant*) or one of the experimenters (*Confederate*), who was seated out of view. The *Body Orientation* of the participant pairs involved either facing each other (*Facing*) or facing away from each other (*Away*). In all conditions, participants were instructed to discuss their pictures with their task partner and determine as many differences as possible between the two pictures over the course of two minutes. In all trials, the dependent measures were the postural sway of the two members of a given participant-pair, irrespective of the *Task Partner* on a given trial. Thus, the shared postural activity between two persons engaged in conversation with

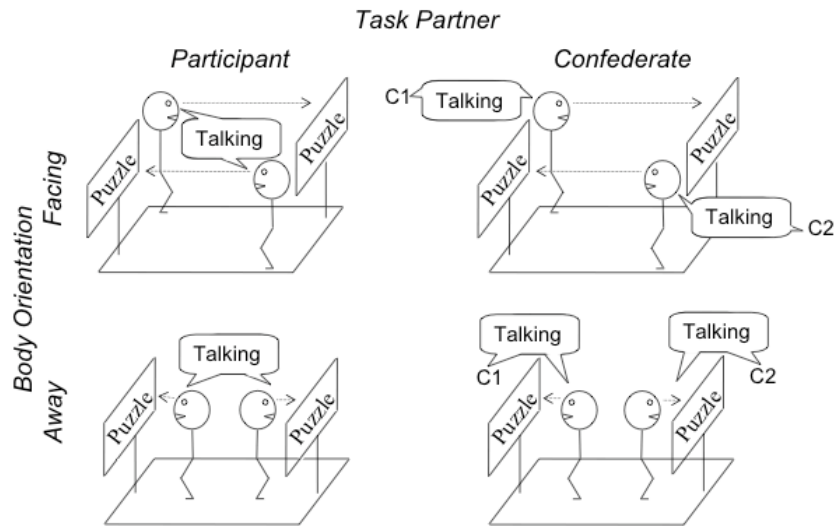


Figure 4.6. Method for evaluating interpersonal postural constraints involved in cooperative conversation. Participants faced toward or away from one another and conversed with each other or a confederate (C). Figure adapted from Shockley, Santana, and Fowler (2003).

each other could be compared to the shared postural activity of the same two persons engaged in conversation with others. Greater shared postural activity (i.e., greater %REC) was expected when participant pairs were conversing with each other than when participant pairs were conversing with confederates.

#### ***Data Collection and Reduction***

A Polhemus FasTrak magnetic motion capture system (Polhemus, Inc., Colchester, VT) was used with *6-D Research System* software (Skill Technologies, Phoenix, AZ) to track the participants' movements in the anterior-posterior direction. Sensors were placed using Velcro straps at the waist and the forehead. For the purposes of this chapter I am only reporting data measured at the waist. Participants stood on opposite sides of the magnetic field emitter and were each

Shockley

approximately 18 inches away from the emitter. Data columns of displacement in the anterior-posterior direction were extracted from the data file recorded by the motion capture software.

Unless otherwise indicated, for the subsequent analyses *Recurrence Quantification Analysis* software was used (the package is available free of charge from <http://homepages.luc.edu/~cwebber/>). Detailed instructions for how to use the recurrence analysis software can be found in the *README.TXT* file, which is provided with the software. It is assumed that the user has a working knowledge of an *MS-DOS* environment. The program *ZSCORE.EXE* was used to convert our displacement data into z-scores to ensure a common scale for all participants.

#### ***CRQ Parameters***

Prior to calculating recurrence quantities, one must select the settings for seven parameters (embedding dimension, delay, range, norm, rescaling, radius, and line length). Embedding dimension, delay, and radius are among the most challenging parameters to determine. When the system in question is of unknown dimensionality and periodicity (e.g., postural sway data), one method for estimating these parameters is to evaluate the number of recurrent points for a range of these parameter settings (Zbilut & Webber, 1992; Riley et al., 1999; see Pallecchia & Shockley, Chapter 3). For a range of parameter settings it is important that there are smooth changes in the number of recurrent points in response to small changes in parameter values (see Trulla, Giuliani, Zbilut, & Webber, 1996). A large, discontinuous change in the number of recurrent points may correspond to a change in the scale of activity in the system to which the recurrence measures

are sensitive. Selecting parameters that are near such a threshold of sensitivity could, therefore, yield changes in recurrence values due to crossing the threshold, rather than changes due to experimental manipulations. Thus, it is safer to use parameter values within a range that exhibits smooth changes in %REC.

The program *KRQS.EXE* may be used to calculate %REC for a range of the three parameters in question. For each execution of the program, one inputs the file names corresponding to the two time series to be compared as well as an output file name to which the recurrence measures are saved. In our case, the input files corresponded to the z-score time series for Person A and Person B, respectively, of a given participant pair for a given 2-minute trial. After entering the command to execute *KRQS.EXE*, one is prompted for the minimum and maximum values for delay, embedding dimension, and radius.

*Embedding Dimension.* Embedding dimension specifies how many dimensions will be used in reconstructing the phase space. As discussed previously, the goal is not to determine exactly how many dimensions the system has. The goal is to be confident there are sufficient embedding dimensions to allow the dynamics of the system to be revealed without distortions. Webber (2004) suggested, for physiological data, starting with embedding dimensions between 10 and 20 and working downward. Based on Webber's suggestion and previous investigations of postural activity using recurrence analysis (e.g., Balasubramaniam, Riley, & Turvey, 2000; Riley et al., 1999), I elected a range of 8 through 14 embedding dimensions for the present discussion.

Shockley

**Delay.** The delay parameter specifies the time lag to use for the time-delayed copies of the original time series (i.e., the surrogate dimensions in the reconstructed phase space). For illustrative purposes of this chapter and data processing economy, I selected delays ranging between 15 and 25 data points. A larger range, however, would certainly be appropriate. The sampling rate of the motion capture system used in the present study was 60 Hz. This means that delays of 15 to 25 data points would correspond to time delays of 0.25 to 0.42 s.

**Radius.** The radius parameter specifies the Euclidean distance within which points from the two time series are considered neighbors (i.e., recurrent) in the reconstructed phase space. The selected radius should yield a sparse recurrence matrix. That is, %REC should remain low (no larger than 5%), but not so small as to produce a floor effect (%REC at or near 0%). I selected radii ranging between 20 and 40, with a step size of 2. Given that mean distance rescaling will be selected (see below), the radius corresponds to the percentage of the mean distance separating points in reconstructed phase space.

**Norm.** The norm parameter specifies how distances are normalized in reconstructed phase space. I selected Euclidean normalization, which is consistent with previous studies using recurrence analysis to evaluate postural activity (see Riley, et al., 1999; Riley & Clark, 2003).

**Rescale.** The rescale parameter determines the method used to rescale the distance matrix (i.e., matrix of all distances among postural data points of person A and person B). Given that each participant pair may have had different distance magnitudes, Shockley et al. (2003) elected to rescale the distances among the points to the mean distance.

This served to intrinsically define the inclusion radius (see above) to a percentage of the average distance separating the postural trajectories of a given participant pair, rather than using an arbitrarily defined threshold (e.g., an absolute Euclidean distance). A distance corresponding to the mean distance separating postural locations in reconstructed phase space would, therefore, have a value of 100. Mean distance rescaling also serves to minimize the influence of an outlier value (e.g., large postural excursion due to laughing or sneezing)—as compared to rescaling to the maximum distance, for example.

**Range.** Each time series consisted of 7200 data points (120 seconds of data at 60 Hz). In the present study, there is no reason not to include as many data points as possible. Therefore, the first data point should be 1 and the last point should be 6875 (given a maximum embedding dimension of 14 and a maximum delay of 25). These values guarantee the use of the maximal number of data points and the same number of data points within each surrogate dimension in the phase space (see Pellecchia & Shockley, Chapter 3, for a detailed explanation of how to determine the last data point). The value for the last data point does not need to be determined, however. The software will provide a range of values, and the user can simply enter the maximum in the range presented by the software.

**Line Length.** Line length specifies the number of consecutive recurrent points required to define a line segment. This parameter should be set to two points (the minimum option) unless one has reason to believe that a more conservative estimate of a line is warranted.

The next step in determining parameters for CRQ is to randomly select a few trials from each experimental condition and execute the

Shockley

program *KRQS.EXE* to compute recurrence measures for the selected parameter ranges for the selected trials. For illustrative purposes, I selected four sets of data to submit to *KRQS.EXE*.

#### *Surface Plots for Parameter Selection in CRQ*

One method of evaluating the %REC values for the selected range of parameter values is to use surface plots, which can be generated in the *MatLab* software environment (Mathworks, Inc., Natick, MA). For each embedding dimension, one can plot the %REC values returned from *KRQS.EXE* for a given data set as a surface (see Figure 4.7). A surface corresponds to a numeric matrix (stored in a *MatLab* variable that I arbitrarily named “rec”). The number of rows of the matrix corresponds to the number of values of radius used by *KRQS.EXE* and the columns of the matrix correspond to the number of values of delay used by *KRQS.EXE*. The values in the matrix correspond to the %REC values for one set of data (generated by *KRQS.EXE*) for each radius (rows) and delay (columns) for a given embedding dimension. To review, the extents of the two sides of each surface correspond to the range of radius and delay, respectively.

To create a surface plot in *MatLab*, one needs two vectors—one of extents corresponding to the numbers of columns and rows of the %REC matrix, respectively, and the matrix that I called “rec” in *MatLab*. First, create two *MatLab* vectors—“radius” [20 22 24 26 28 30 32 34,36 38 40] and “delay” [15 16 17 18 19 20 21 22 23 24 25]—to be used for all surfaces plotted. As discussed above, the matrix should be created from the %REC values returned from *KRQS.EXE*. The values of %REC will, therefore, be different for each trial analyzed. The matrix will, accordingly, need to be re-created for each surface to be plotted. Each

## Interpersonal Postural Activity

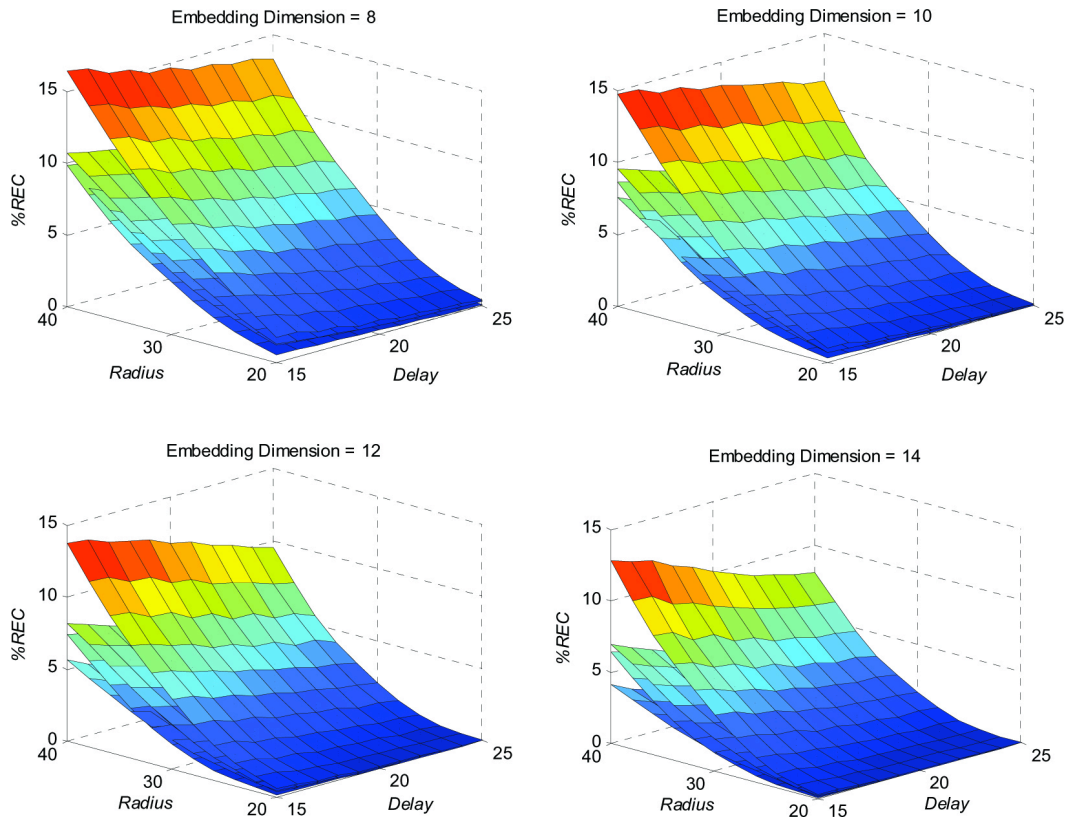


Figure 4.7. Shared postural locations (%REC) in reconstructed phase space for a randomly selected subset of data from Shockley, Santana, & Fowler (2003) for a range of values of the following parameters: Embedding dimension, delay, and radius. Each surface in a given plot corresponds to a different data set and each plot represents the same data sets for the parameter ranges.

surface plot is created by the following command: `surf(delay, radius, rec)`. To plot multiple surface plots on one graph (as seen in Figure 4.7), type 'hold' after the first surf command. I have found that it is most useful to create a different plot for each embedding dimension. To generate new plots, open a new figure window and repeat the procedure. For illustrative purposes I have plotted four of the eight embedded dimensions (see Figure 4.7).

### *Inspection of Surface Plots*

***Embedding Dimension.*** Notice in Figure 4.7 that the recurrence values for the sampled data files tend to bottom out (%REC equals 0) for higher values of the delay and low values of the radius for embedding dimensions 12 and 14. Thus, an embedding dimension of 10 allows sufficient unfolding of the time series and still yield a sparse recurrence matrix (i.e., recurrence values just above 0%).

***Delay.*** The particular delay selected is often arbitrary for postural data. What is most important is that the patterning of recurrence measures is consistent across a range of delay values. If so, one can be confident that any observed differences across experimental conditions are not artifacts of the delay. Shockley et al. (2003) selected a delay of 25 data points, which fits these criteria.

***Radius.*** As discussed above, the radius is the maximum Euclidean distance by which points can be separated in reconstructed phase space and still be considered recurrent points. One should choose a value of radius that ensures that the number of recurrent points is reasonably low (so as to avoid global recurrence, i.e., all points recurrent). Webber (personal communication, June 2000) suggested that recurrence should be approximately 1%. Given that CRQ must be performed on multiple trials of multiple participants, however, Webber's prescribed recurrence range tends to be a bit too low. This is so because data from some trials may yield %REC = 0 for the same parameter settings that yield 1% recurrence for other participants. For biological movement data, I have found that recurrence of around 3%-5% for a randomly selected subset of data

tends to yield non-zero %REC values for all subjects, but still offers sufficiently low recurrence.

In summary, Shockley, et al. (2003) selected a delay of 25 data points, an embedding dimension of 10, and a radius of 30% of the mean distance separating points in reconstructed phase space. Modest changes of each of the values of those parameters does not change the patterning of results found by Shockley et al. (2003).

### ***Full Analysis***

After the parameters to be used for the analysis have been selected, the next step is to run the CRQ with the selected parameter settings on the entire set of experimental data. Shockley et al. (2003) used ***KRQE.EXE*** to compute the recurrence variables—%REC, %DET, MAXL, and ENT—for each participant pair. The reason for using ***KRQE.EXE***, rather than ***KRQD.EXE***, for example, is that the former allows multiple analyses to be executed in batch mode, rather than waiting for each file to be analyzed and then typing the next command for the next file to be analyzed.

To review, the following parameter settings were used with ***KRQE.EXE***: delay = 25, embedding dimension = 10, range = 1-6875, norm = Euclidean, rescaling = mean distance, radius = 30, and line length = 2. The program ***KRQEP.EXE*** was used to generate a parameter file to be accessed by the commands in the batch file. This obviates the need to type in the parameters for each file to be analyzed. An ASCII (text), tab-delimited batch file (***filename.bat***) was set up such that each row corresponded to the ***MSDOS*** command for analyzing one file using ***KRQE.EXE***. The number of rows corresponded to the number of files to be analyzed (see ***README.TXT*** file for complete instructions). Program

Shockley

run time for the present data was several hours. Mean values for the recurrence measures were calculated for the four trials of each condition. Separate ANOVAs were conducted on each recurrence measure for postural time series pairs.

***Results of Shockley, Santana, & Fowler (2003)***

Among the measures derived from the tallied cross recurrence values, %REC (the ratio of the number of recurrent points to the number of possible recurrent points) and MAXL (the length of the longest trajectory of consecutive parallel recurrent points; a measure of the stability of the shared activity) were found to be significantly influenced by the experimental manipulations. Representative cross recurrence plots are provided in Figure 4.8A and 4.8B. The plots are organized such that the postural time series of one member of a participant pair (**A**) is indexed along the abscissa while the postural time series of the other member of a participant pair (**B**) is indexed along the ordinate. Points are plotted in the cross recurrence plot when the trajectories of the unfolded time series, **A** and **B**, occupy the same area of the reconstructed phase space within some radius of inclusion. That is, if a given position (*i*) in time series **A** occupies the same position in reconstructed phase space as the position (*j*) of time series **B** (i.e.,  $A[i] = B[j]$ ), then the point is considered recurrent (see Figure 4.5). Shockley et al. (2003) found greater shared postural activity among pairs of participants engaged in conversation with each other as compared to the activity shared among the same participants engaged in conversation with confederates, regardless of visual interaction.

They also found that trajectories of participant pairs stayed parallel longer when the participant pairs were engaged in

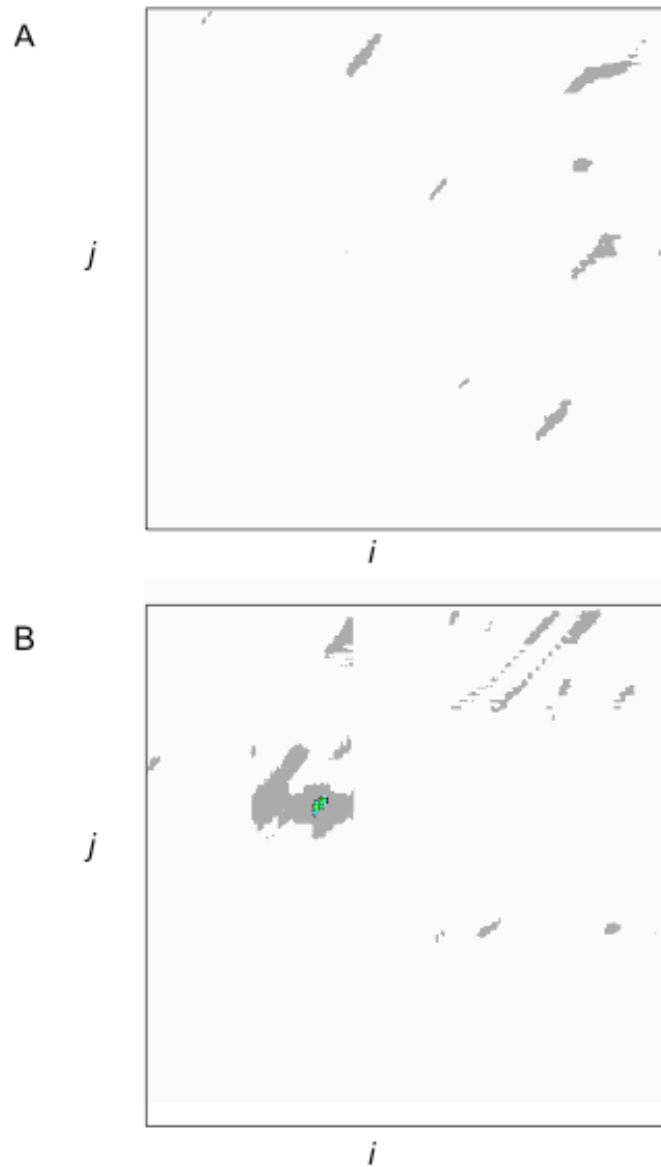


Figure 4.8. (A) Sample cross recurrence plot of the postural activity of two persons engaged in conversation with confederates. (B) Sample cross recurrence plot of the postural activity of two persons engaged in conversation with each other. Both are examples of the participant-pair facing away from each other. Indices along the abscissa ( $i$ ) and the ordinate ( $j$ ) corresponds to data points of person A and B, respectively of a participant-pair. Illuminated pixels correspond to shared postural locations in reconstructed phase space.

Shockley

conversation with each other than when participant pairs were engaged in conversation with others. As far as the authors could determine, their observations mark the first objective measures of interpersonal postural coordination. Representative examples of a linear method of shared signal activity—coherence analysis—are provided in Figure 4.9. In Figure 4.9A, the participants were speaking to each other. In Figure 4.9B, the participants were each speaking to a confederate. Coherence analysis is effectively a correlation of Fourier spectrum power estimates compared across two signals for a range of frequencies. Note that there are not distinct frequencies at which power is correlated in either plot. Furthermore, on average the coherence for the two plots is the same ( $\sim 0.085$ ). This is consistent with the Shockley et al. (2002) finding that CRQ is a more sensitive measure of coupling than linear measures. Perhaps of greater importance, however, is the fact that CRQ is a more appropriate method for quantifying shared postural activity than linear methods, given that CRQ does not require the assumptions of normal distributions and stationarity of the data required by linear methods. That is, any significant effects that may have been discovered with linear methods would be suspect due to violations of the assumptions of those methods.

It is encouraging that recurrence strategies continue to prove their usefulness for the study of postural control. It remains to be seen how sensitive of a measure CRQ may prove to be. For example, is the degree of postural coordination scaled by the degree of cooperation of a given verbal interaction? Giles (1973) recognized changes in coordination among conversers with his observation that conversers in a cooperative and friendly setting show convergence of dialects, while

## Interpersonal Postural Activity

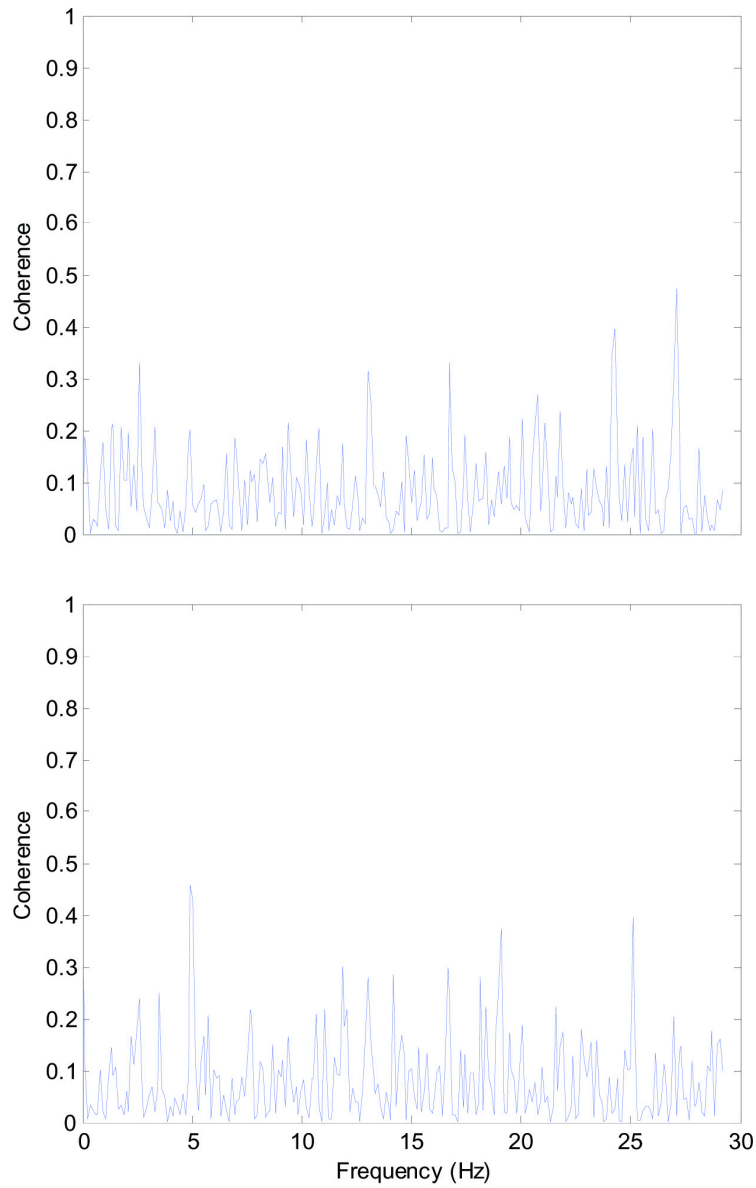


Figure 4.9. (A) Representative example of a coherence plot of the postural activity of two persons engaged in conversation with confederates. (B) Representative example of a coherence plot of the postural activity of two persons engaged in conversation with each other. Both are examples of the participant pair facing away from each other. Frequency (Hz) is plotted along the abscissa and the ordinate corresponds to the coherence between the power of the Fourier spectra of the individual time series of the participant pair.

Shockley

hostile conversations show divergence of dialects. Will %REC decrease in a less cooperative situation as compared to a more cooperative situation? Furthermore, it remains to be seen what is the mechanism of coupling that was observed by Shockley et al. (2003). Investigations are currently under way to determine what aspects of the interaction (e.g., speaking rhythms, conversational turn-taking, word similarity) facilitate the type of shared postural activity that was observed. I leave these questions to future investigations.

REFERENCES

Abarbanel, H. D. I. (1996). *Analysis of observed chaotic data*. New York, NY: Springer-Verlag New York, Inc.

Balasubramaniam, R., Riley, M. A., & Turvey, M. T. (2000). Specificity of postural sway to the demands of a precision task. *Gait and Posture, 11*, 12-24.

Belen'kii, V., Gurfinkel', V. S., & Pal'tsev, Y. (1967). Elements of control of voluntary movement. *Biophysics, 12*, 154-161.

Cappella, J., & Planalp, S. (1981). Talk and silence sequences in informal conversations: III. Interspeaker influence. *Human Communication Research, 7*, 117-132.

Carroll, J. P., & Freedman, W. (1993). Nonstationarity properties of postural sway. *Journal of Biomechanics, 26*, 409-416.

Clark, H. H. (1996). *Using language*. New York, NY: Cambridge University Press.

Collins, J. J., & De Luca, C. J. (1993). Open-loop and closed-loop control of posture: a random-walk analysis of center-of-pressure trajectories. *Experimental Brain Research, 95*, 308-318.

Collins, J. J., & De Luca, C. J. (1994). Random walking during quiet standing. *Physical Review Letters, 73*, 764-767.

Shockley

Condon, W., & Ogston, W. (1971). Speech and body motion synchrony of the speaker-hearer. In D. Horton and J. Jenkins (Eds). *The Perception of Language*. (pp. 150-184) Columbus, OH: Charles E. Merrill.

Eckmann, J. P., Kamphorst, S. O., & Ruelle, D. (1987). Recurrence plots of dynamical systems. *Europhysics Letters*, *4*, 973-977.

Fel'dman, A. (1966). Functional tuning of the nervous system during control of movement or maintenance of a steady posture: III. Mechanographic analysis of the execution by man of the simplest motor tasks. *Biophysics*, *11*, 766-775.

Giles, H. (1973). Accent mobility: A model and some data. *Anthropological Linguistics*, *15*, 87-105.

Giles, H., Coupland, N., & Coupland, J. (1991). Accommodation theory: Communication, context, and consequence. In H. Giles, J. Coupland, & N. Coupland (Eds.), *Contexts of Accommodation: Developments in Applied Sociolinguistics* (pp. 1-68). New York, NY: Cambridge University Press.

LaFrance, M. (1982). *Posture mirroring and rapport. Interaction rhythms*. New York, NY: Human Sciences Press, Inc.

Lorenz, E. N. (1963). Deterministic nonperiodic flow. *Journal of Atmospheric Science*, *20*, 130-141.

Natale, M. (1975). Social desirability as related to convergence of temporal speech patterns. *Perceptual and Motor Skills*, *40*, 827-830.

Newell, K. M., Slobounov, S. M., Slobounova, E. S., & Molenaar, P. C. M. (1997). Short-term nonstationarity and the development of postural control. *Gait and Posture*, *6*, 56-62.

Newton, D. (1994). The perception and coupling of behavior waves. In R. R. Vallacher & A. Nowak (Eds.) *Dynamical Systems in Social Psychology* (pp. 139-167). San Diego, CA: Academic Press Inc.

Newton, D., Enquist, G., & Bois, J. (1977). The objective basis of behavior units. *Journal of Personality and Social Psychology*, *35*, 847-862.

Newton, D., Hairfield, J., Bloomingdale, J., & Cutino, S. (1987). The structure of action and interaction. *Social Cognition*, *5*, 191-237.

Pal'tsev, , Y. I., & Elnor, A. M. (1967). Preparatory and compensatory period during voluntary movement in patients with involvement of the brain of different localization. *Biophysics*, *12*, 161-168.

Riccio, G. E., & Stoffregen, T. A. (1988). Affordances as constraints on the control of stance. *Human Movement Science*, *7*, 265-300.

Shockley

Riley, M. A., Balasubramaniam, R., & Turvey, M. T. (1999). Recurrence quantification analysis of postural fluctuations. *Gait and Posture*, *9*, 65-78.

Riley, M. A., & Clark, S. (2003). Recurrence analysis of human postural sway during the sensory organization test. *Neuroscience Letters*, *342*, 45-48.

Riley, M. A., Mitra, S., Stoffregen, T. A., & Turvey, M. T. (1997). Influences of body lean and vision on unperturbed postural sway. *Motor Control*, *1*, 229-246.

Shockley, K., Butwill, M., Zbilut, J. P., & Webber, C. L., Jr. (2002). Cross recurrence quantification of coupled oscillators. *Physics Letters A*, *305*, 59 – 69.

Shockley, K., Santana, M., & Fowler, C. A. (2003). Mutual interpersonal postural constraints are involved in cooperative conversation. *Journal of Experimental Psychology: Human Perception and Performance*, *29*, 326–332.

Stoffregen, T. A., Pagaulayan, R. J., Bardy, B. G., & Hettinger, L. J. (2000). Modulating postural control to facilitate visual performance. *Journal of Experimental Psychology: Human Perception and Performance*, *19*, 203-220.

Takens, F. (1981). Detecting strange attractors in turbulence. *Lecture Notes in Mathematics*, 898, 366-381.

Trulla, L. L., Giuliani, A., Zbilut, J. P., & Webber, C. L., Jr. (1996). Recurrence quantification analysis of the logistic equation with transients. *Physics Letters A*, 223, 255-260.

Webber, C. L., Jr. (1997). Introduction to recurrence quantification analysis, v. 4.1. Unpublished software documentation (available with *RQA v. 4.1* software).

Webber, C. L., Jr., & Zbilut, J. P. (1994). Dynamical assessment of physiological systems and states using recurrence plot strategies. *Journal of Applied Physiology*, 76, 965-973.

Zbilut, J.P., & Webber, C.L., Jr. (1992). Embeddings and delays as derived from quantification of recurrence plots. *Physics Letters A*, 171, 199-203.

## CHAPTER 5

# Introduction to Fractals

Larry S. Liebovitch

Center for Complex Systems and Brain Sciences, Center for Molecular  
Biology and Biotechnology, & Departments of Psychology and  
Biomedical Sciences  
Florida Atlantic University  
777 Glades Road  
Boca Raton, FL 33431  
U. S. A.  
E-mail: [liebovitch@clifford.ccs.fau.edu](mailto:liebovitch@clifford.ccs.fau.edu)  
<http://walt.ccs.fau.edu/~liebovitch/larry.html>

Lina A. Shehadeh

Center for Complex Systems and Brain Sciences  
Florida Atlantic University  
777 Glades Road  
Boca Raton, FL 33431  
U. S. A.

## INTRODUCTION

This chapter is a *Word* version of the *PowerPoint* presentation given by Dr. Larry S. Liebovitch at the NSF Nonlinear Methods in Psychology Workshop, October 24-25, 2003 at George Mason University, Fairfax, VA. The *PowerPoint* presentation itself is also available as a part of this web book. Here the notes which can be seen on the *PowerPoint* presentation by using "Normal View" are presented as text around their respective *PowerPoint* slides. The concept here is to try to reproduce the look and feel of the presentation at the workshop. Therefore, this is not, and is not meant to be, your usual "print" article. The form of the language here is more typical of spoken, rather than written, English. The form of the graphics is sparser, larger pictures captioned with larger fonts, that is more typical of PowerPoint presentations than printed illustrations. We hope that this experimental format may provide a simpler introduction to fractals than that of a more formal presentation. We also hope that the availability of the PowerPoint file will be of use in teaching these materials and may also serve as a starting point for others to customize these slides for their own applications.

This chapter is about "fractals". Objects in space can have fractal properties. Time series of values can have fractal properties. Sets of numbers can have fractal properties. Much of the statistics that you are familiar with deals with the "linear" properties of data. Fractals can help us describe some "non-linear" properties of data.

Most data are characterized by the mean and standard deviation, like  $45.3 \pm 0.3$ . You'll learn here that if the data are fractal, those means and standard deviations are meaningless! A pretty basic change in the simplest way we handle data.

**Fractals** are important because they **CHANGE** the most basic ways we analyze and understand experimental data.

Liebovitch & Shehadeh

We'll start with objects. Let's first see the difference between the non-fractal and fractal objects.

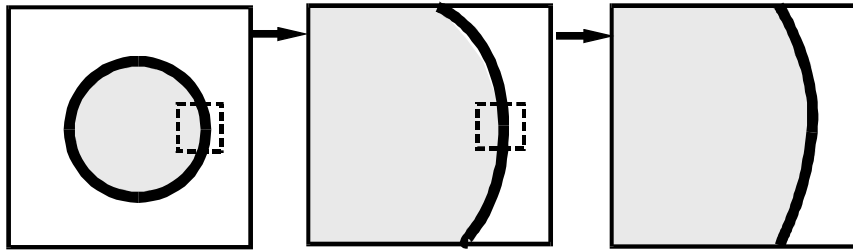
## **Properties of Objects in Space**

**Non-Fractal and Fractal Objects are different.**

As we enlarge a non-fractal object, no new details appear.

## Properties of Objects in Space

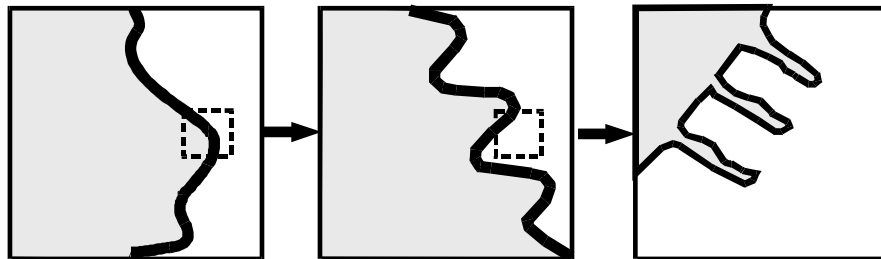
### Non-Fractal



But, as we enlarge a fractal object we keep seeing ever smaller pieces. For example, this series of pictures could show first the inside of the intestine, then the crypts between the cells, then the microvilli on each cell. The smaller pieces are copies of the larger pieces. They are not exact smaller copies, but they are smaller replicas that are kind of like the larger pieces.

## Properties of Objects in Space

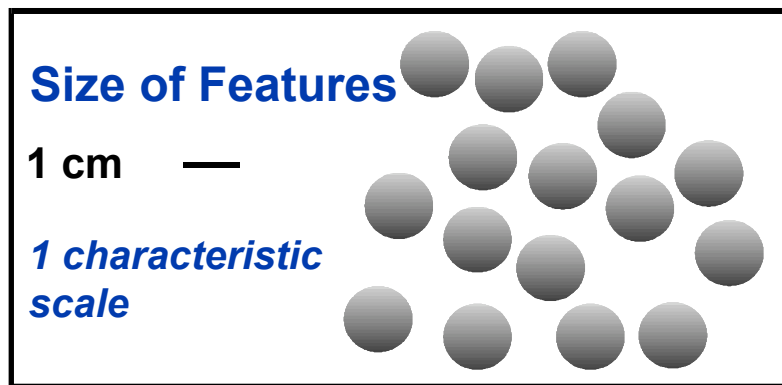
### Fractal



A non-fractal object has most pieces that are about the same size.

## Properties of Objects in Space

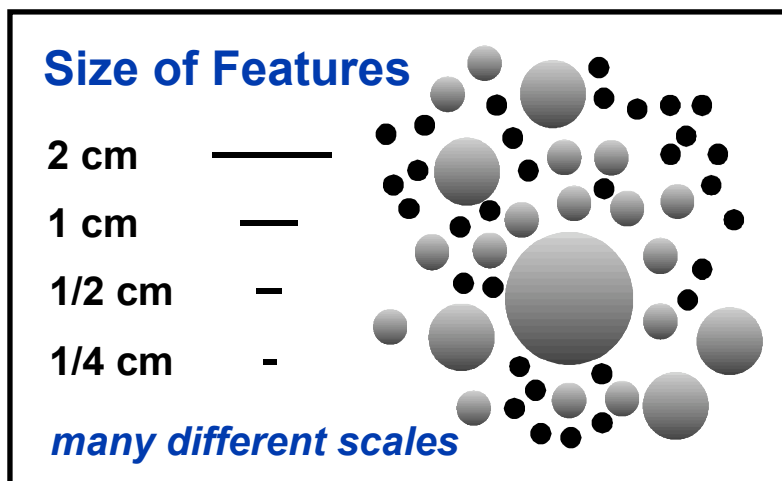
### Non - Fractal



A fractal object has pieces of all different sizes. The variation in the size of the pieces of fractal objects is much larger than the variation in the size of the pieces of non-fractal objects. Typically, there are a few big pieces, some medium-sized pieces, and very many tiny pieces.

## Properties of Objects in Space

### Fractal



Fractal objects have interesting properties. Here we describe those properties very briefly. Then later, we will describe them in more detail.

## Properties of Fractal Objects

### Self-Similarity.

The little pieces are smaller copies of the larger pieces.

### Scaling.

The values measured depend on the resolution used to make the measurement.

### Statistics.

The “average” size depends on the resolution used to make the measurement.

Liebovitch & Shehadeh

A tree is fractal. It has a few large branches, some medium-sized branches, and very many small branches. A tree is self-similar: The little branches are smaller copies of the larger branches. There is a scaling: The length and thickness of each branch depends on which branch we measure. There is no average size of a branch: The greater the number of smaller branches we include, the smaller is the "average" length and thickness.

This tree is from <http://www.febleminds-gifs.com/trees23.jpg>.

## **Example of a Fractal**

### **A tree is fractal**



from <http://www.febleminds-gifs.com/trees23.jpg>

The pattern of lightning in the sky is fractal. It has a few large branches, some medium-sized branches, and very many small branches. The lightning pattern is self-similar: The little branches are smaller copies of the larger branches. There is a scaling: The length of each branch depends on which branch we measure. There is no average size of a branch: The greater the number of smaller branches we include, the smaller is the “average” length and thickness.

## Example of a Fractal

### Lightning is fractal



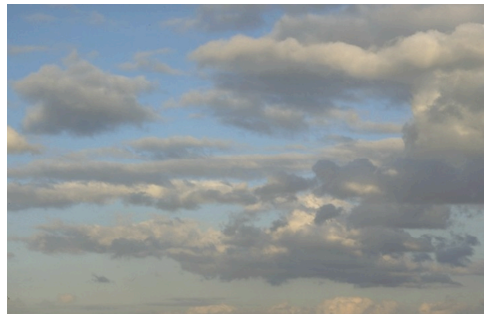
from <http://bobqat.com/Mazama/Sky/013.html>

Liebovitch & Shehadeh

The pattern of clouds in the sky is fractal. They are made up of a few big clouds, some medium-sized clouds, and very many small clouds. The cloud pattern is self-similar: The little clouds are smaller copies of the larger clouds. There is a scaling: The size of each cloud depends on which cloud we measure. There is no average size of a cloud: The greater the number of smaller clouds we include, the smaller is the "average" size of a cloud.

## **Example of a Fractal**

### **Clouds are fractal**



From <http://www.febleminds-gifs.com/cloud-13.jpg>

The pattern of paint colors in a Jackson Pollack painting is fractal. The pattern is made up of a few big swirls, some medium-sized swirls, and very many small swirls. The pattern is self-similar: The little swirls are smaller copies of the larger swirls. There is a scaling: The size of each swirl depends on which swirl we measure. There is no average size of a swirl: The greater the number of smaller swirls we include, the smaller is the “average” size of a swirl.

## Example of a Fractal

### A Pollock Painting is Fractal



Autumn Rhythm, 1950, oil on canvas, 266.7 cm by 525.8 cm

From R. P. Taylor. 2002. Order in Pollock's Chaos, Sci. Amer. Dec. 2002

# Fractals

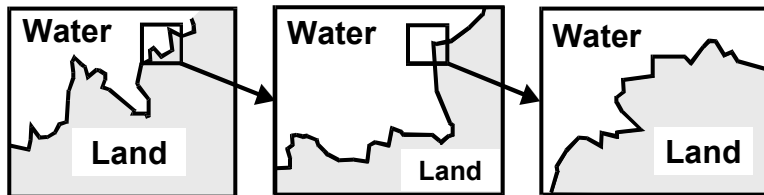
## Self-Similarity

Self-similarity: Objects or processes whose small pieces resemble the whole.

The coastline, the fractal border between the land and the sea, has many bays and peninsulas. As you magnify the coastline you see ever smaller bays and peninsulas. The structure at a large scale is similar to the structure at a small scale. It is similar to itself at different scales. This is called self-similarity.

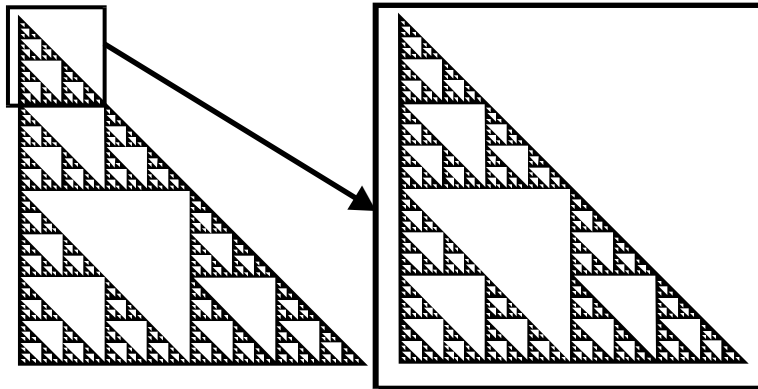
## Self-Similarity

**Pieces resemble the whole.**



This is the Sierpinski Triangle. In this mathematical object each little piece is an exact smaller copy of the whole object.

## Sierpinski Triangle

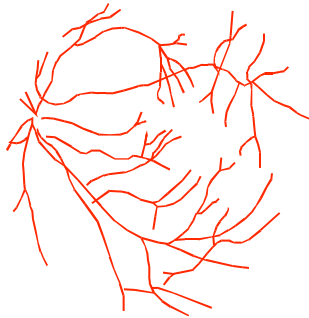


The blood vessels in the retina are self-similar. The branching of the larger vessels is like the branching of the smaller vessels. The airways in the lung are self-similar. The branching of the larger airways is like the branching of the smaller airways. In real biological objects like these, each little piece is not an exact copy of the whole object. It is kind of like the whole object which is known as *statistical self-similarity*.

## Branching Patterns

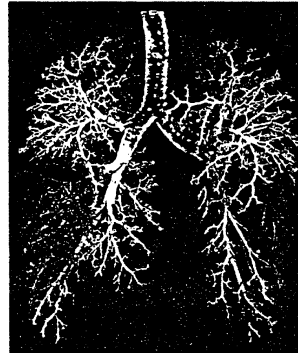
### blood vessels in the retina

*Family, Masters, and Platt 1989  
Physica D38:98-103  
Mainster 1990 Eye 4:235-241*



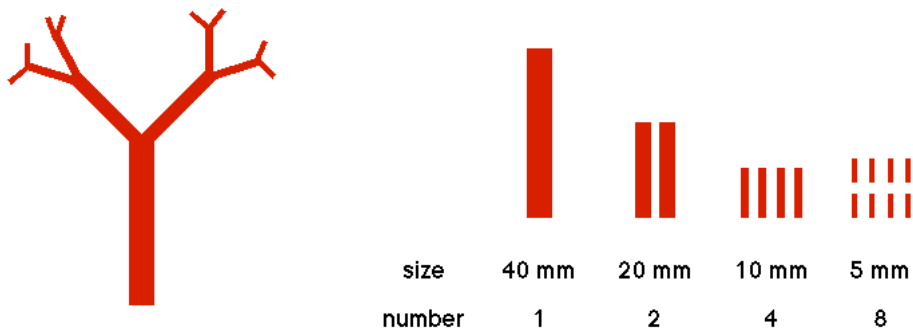
### air ways in the lungs

*West and Goldberger 1987  
Am. Sci. 75:354-365*



Let's try to understand statistical self-similarity. Here is an unrealistically simplified picture of the blood vessels in the retina. If we ask how many vessels are there of each different size we see that there is one that is 40mm long, two that are 20mm long, four that are 10mm long, and eight that are 5 mm long.

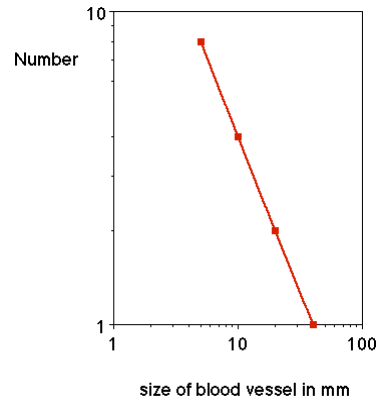
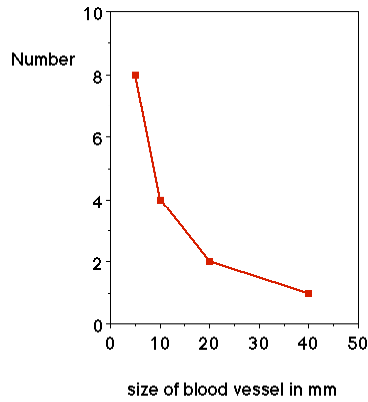
### Blood Vessels in the Retina



We can plot how many vessels there are of each size. This is called the Probability Density Function (PDF). A power law distribution is evidenced in a straight line on a plot of log (number) vs. log (size).

## PDF - Probability Density Function

### HOW OFTEN there is THIS SIZE



**Straight line on log-log plot  
= Power Law**

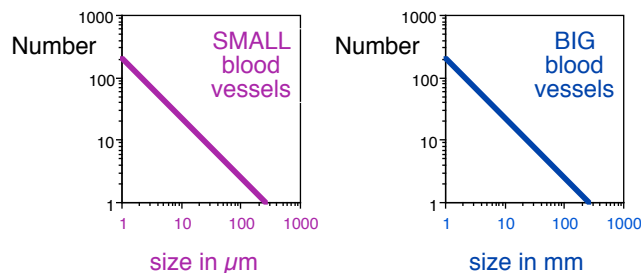
The PDF of the large vessels is a straight line on a plot of  $\log(\text{number})$  vs.  $\log(\text{size})$ . There are a few big-big vessels, many medium-big vessels, and a huge number of small-big vessels.

The PDF of the small vessels is also a straight line on a plot of  $\log(\text{Number})$  vs.  $\log(\text{size})$ . There are a few big-small vessels, many medium-small vessels, and a huge number of small-small vessels.

The PDF of the big vessels has the same shape (i.e., is similar to) the PDF of the small vessels. The PDF is a measure of the statistics of the vessels. So, the PDF (the statistics) of the large vessels is similar to the PDF (the statistics) of the small vessels. This is statistical self-similarity. The small pieces are not exact copies of the large pieces, but the statistics of the small pieces are similar to the statistics of the large pieces.

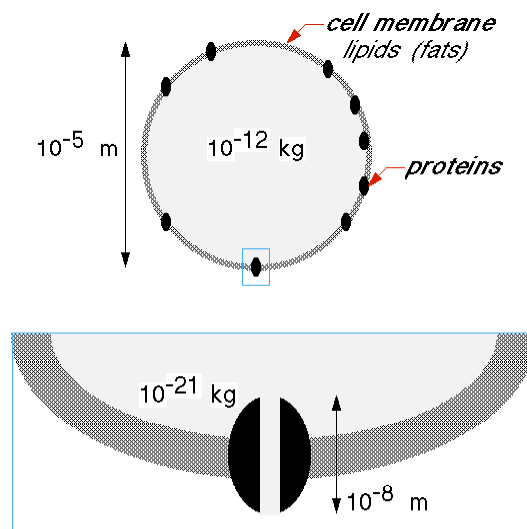
## Statistical Self-Similarity

The statistics of the big pieces is the same as the statistics of the small pieces.



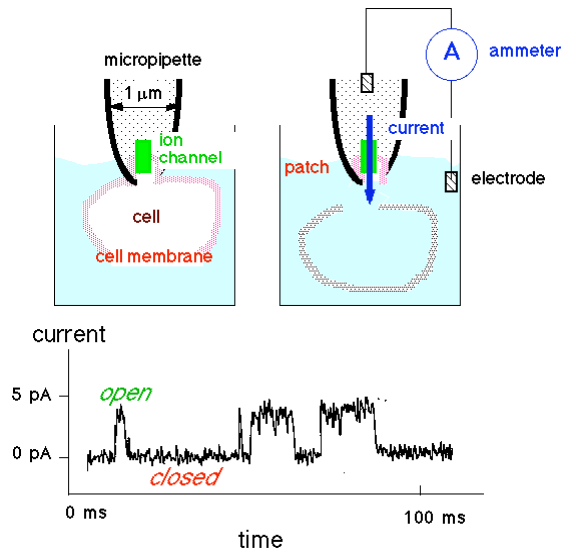
Fractals are not only objects in space, but can also be processes in time. There are proteins, called "ion channels," in the fatty membranes of living cells that let ions, like sodium and potassium, enter or exit the cell.

### Fractal Properties in Time: Currents Through Ion Channels



A small pipette can suck up a small piece of cell membrane with only one ion channel in it, and even it tear it off and away from the cell. The movement of sodium or potassium through the ion channel produces an electrical current that can be measured. It's a pretty small current, a picoAmp, which is about one billionth ( $1/1,000,000,000$ ) of the current from a "D" battery. This is called the "Patch Clamp." What's really interesting is that these ion channel proteins act like little electrical switches. Either they are either fully open or fully closed to the movement of sodium or potassium. They switch, all the time, between these fully open and fully closed states. It's impressive to watch this technology measure the changes in a single molecule at a time.

## Fractal Properties in Time: Currents Through Ion Channels

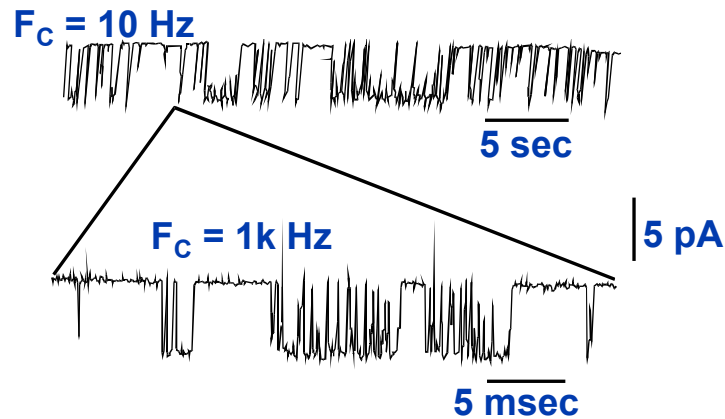


These open and closed times are fractal! If you record them and play them back slowly you see a sequences of open and closed times. But if you take one segment of time, and play it back at higher resolution, you see that it actually consists of many briefer open and closed times. It is self-similar in time.

## Currents Through Ion Channels

### ATP sensitive potassium channel in $\beta$ cell from the pancreas

*Gilles, Falke, and Mislner (Liebovitch 1990 Ann. N.Y. Acad. Sci. 591:375-391)*

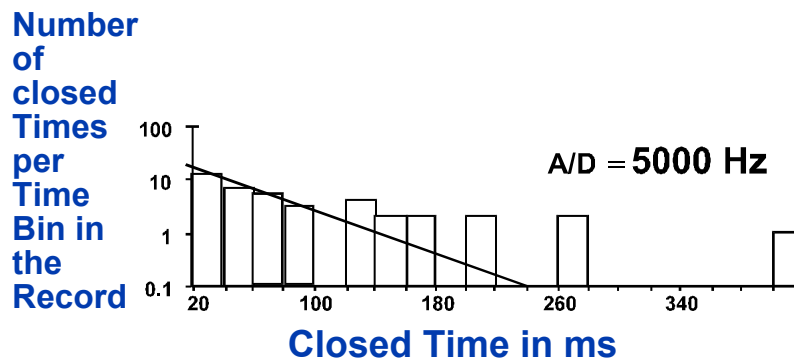


Here is a histogram of the times (in ms) that one channel was closed. The recording was made at the fastest time resolution, allowing the briefest closed times to be recorded. The PDF is mostly a straight line on this log (number) versus time (t) plot, but with an occasional longer closed time. Data with fractal properties often have unusual events that occur more often than expected from the usual "Bell Curve." Those occasional longer closed times are a hint that these data might be fractal.

## Closed Time Histograms

### potassium channel in the corneal endothelium

*Liebovitch et al. 1987 Math. Biosci. 84:37-68*

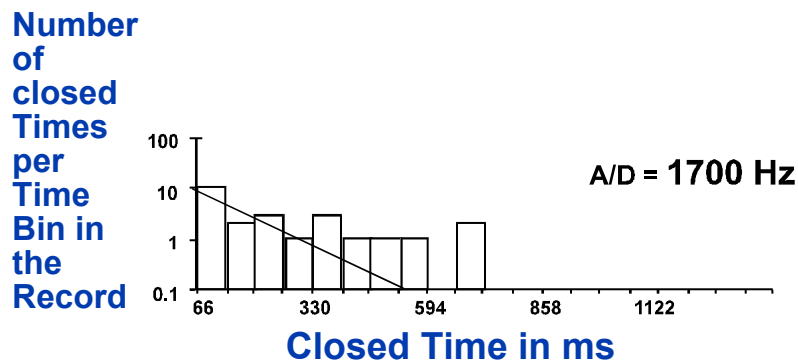


Here is another histogram of the closed times (in ms) of that same ion channel. This recording was made at a little slower time resolution and so longer closed times were recorded. The PDF is mostly a straight line on this log (number) versus time (t) plot, but with an occasional longer closed time.

## Closed Time Histograms

potassium channel in the  
corneal endothelium

*Liebovitch et al. 1987 Math. Biosci. 84:37-68*



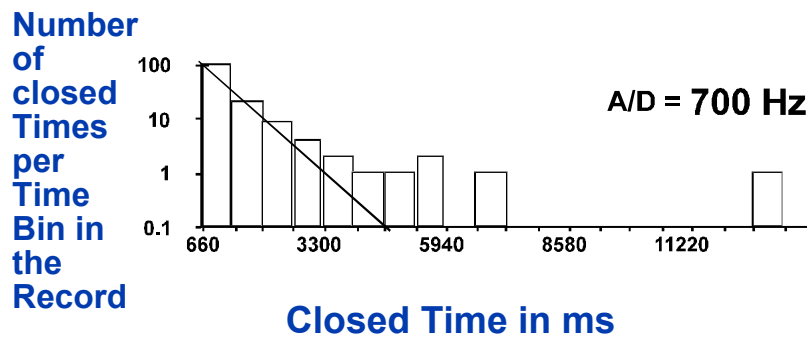
Liebovitch & Shehadeh

Here is another histogram of the closed times (in ms) of that same ion channel. This recording was made at an even slower time resolution and so even longer closed times were recorded. The PDF is mostly a straight line on this log (number) versus time (t) plot, but with an occasional longer closed time.

## Closed Time Histograms

potassium channel in the  
corneal endothelium

*Liebovitch et al. 1987 Math. Biosci. 84:37-68*

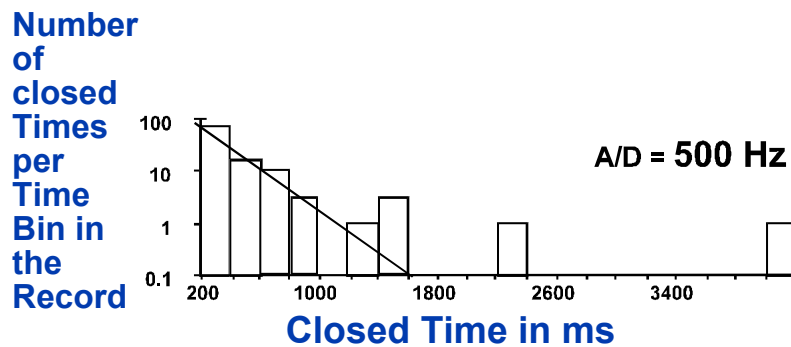


Here is another histogram of the closed times (in ms) of that same ion channel. This recording was made at a much lower time resolution and so only the longest closed times were recorded. The PDF is mostly a straight line on this log (number) versus time (t) plot, but with an occasional longer closed time. The PDF looks similar at different time resolutions. The PDF is a measure of the statistics. So, the statistics is similar to itself at different time resolutions. This is statistical self-similarity in time.

## Closed Time Histograms

**potassium channel in the  
corneal endothelium**

*Liebovitch et al. 1987 Math. Biosci. 84:37-68*

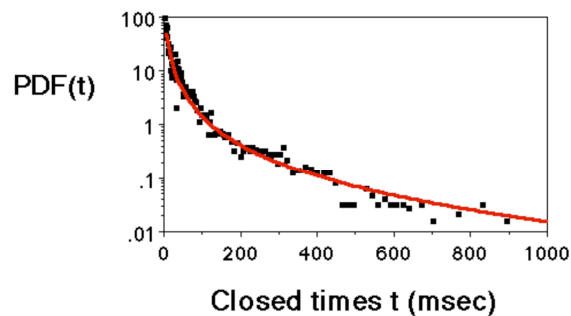


Each of those histograms of the closed times is measured at its own time resolution, the time width of each bin. Wouldn't it be nice to see all those different time scales at once? We can't do that with a histogram, but we can convert each histogram into its PDF and then combine those PDFs. Here is the PDF of all those histograms combined. Now we can see that there is a simple relationship (red line) between all the different closed times. Thus, there is a relationship between the closed times as short as a millisecond and those as long as a second. This relationship is called a scaling relationship.

## Closed Time PDF

### potassium channel in the corneal endothelium

*Liebovitch et al. 1987 Math. Biosci. 84:37-68*



# Fractals

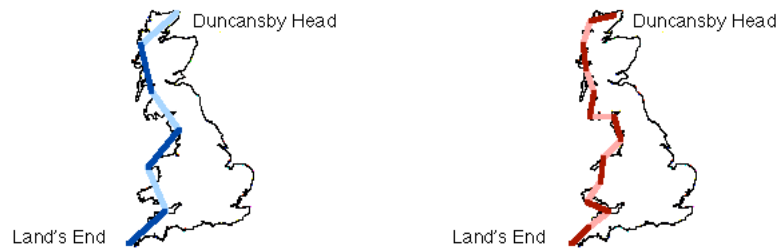
## Scaling

Scaling: The value measured depends upon the resolution used to make the measurement.

If we measure the length of the west coast of Britain with a large ruler, we get a certain value for the length of the coastline. If we now measure it again with a smaller ruler, we catch more of the smaller bays and peninsulas that we missed before, and so the coastline measurement is longer. The value we measure for the coastline depends on the size of the ruler that we use to measure it.

## Scaling

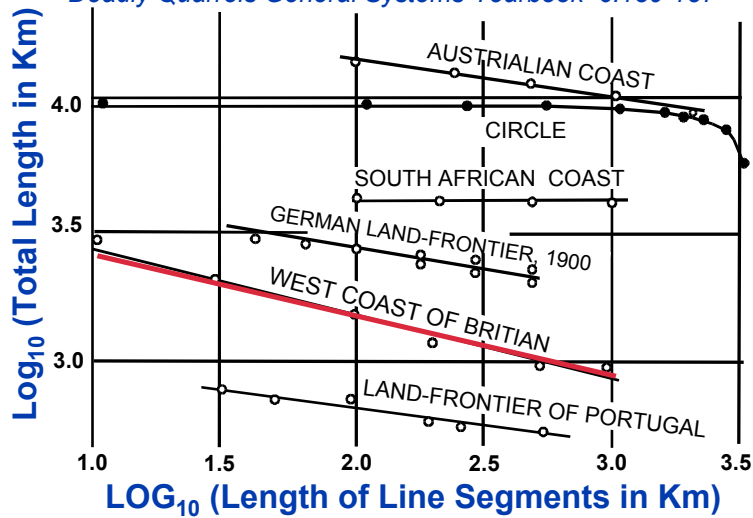
**The value measured depends on the resolution used to do the measurement.**



Here is a plot of how the length of the west coast of Britain depends upon the resolution that we use to measure it. There is no one value that best describes the length of the west coast of Britain. It depends upon the scale (resolution) at which we measure it. As we measure it at a finer scale, we include the segments of the smaller bays and peninsulas, and the coastline is longer. This is one of the surprising way in which fractals change the most basic way that we analyze and understand our data. There is no one number that best describes the length of the west coast of Britain. Instead, what is important is how the length depends upon the resolution that we use to measure it. The more smaller bays and peninsulas, the more the length of the coast increases when it is measured at a finer resolution, and the steeper the slope on this plot. This plot therefore shows that the coast of Britain is rougher than that of Australia, which is rougher than that of South Africa, which is rougher than that of a plain circle.

### How Long is the Coastline of Britain?

*Richardson 1961 The problem of contiguity: An Appendix to Statistics of Deadly Quarrels General Systems Yearbook 6:139-187*



Iannaccone and his colleagues study how organisms develop in order to understand and cure cancer in kids. They mix cells from another animal into an embryo so that the fate of these marker cells can be traced out as the animal develops. The cells that are added have a different enzyme, which attaches to a radioactive marker that blackens a photographic film to make a picture. On the following page are some of those pictures of the liver. Look, the added cells are not in one clump. They are in islands of all different sizes.

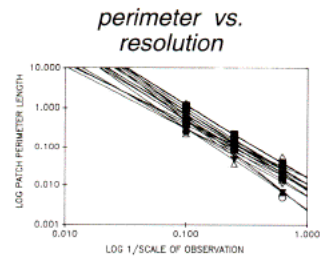
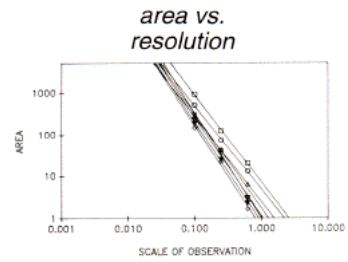
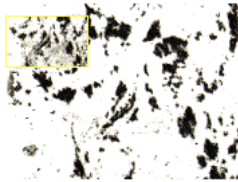
There is no one area that best describes the size of these islands. The area measured depends on the resolution used. This scaling relationship is a straight line on a plot of  $\log(\text{area})$  versus  $\log(\text{resolution})$ .

There is no one perimeter that best describes the size of these islands. The perimeter measured depends on the resolution used. This scaling relationship is also a straight line on a plot of  $\log(\text{perimeter})$  versus  $\log(\text{resolution})$ .

This is one of the surprising ways in which fractals change the most basic way that we analyze and understand our data. There is no one number that best describes the area or perimeter of these islands. Instead, what is important is how the area or perimeter depends upon the resolution that we use to measure it.

## Genetic Mosaics in the Liver

*P. M. Iannaccone. 1990. FASEB J. 4:1508-1512.*  
*Y.-K. Ng and P. M. Iannaccone. 1992. Devel. Biol. 151:419-430.*



So far, we've seen fractal scaling in space. There are also fractal scaling in time. The usual way to measure the switching of an ion channel is the "kinetic rate constant." That tells us the probability that the ion channel switches between open and closed states. But the ion channel must be closed (or open) long enough for us to see it as closed (or open). A more appropriate measure is the probability that the ion channel switches between open and closed states, given that it has already remained in a state for a certain amount of time. That certain amount of time defines the time resolution at which we measure the switching probability. We called that probability the "effective kinetic rate constant" ( $k_{\text{eff}}$ ),

$$k_{\text{eff}} = \text{Pr} (T=t, t+\Delta t \mid T > t_{\text{eff}}) / \Delta t, \quad [5.1]$$

which is the probability (Pr) for the ion channel to open (or close) during the time interval  $T = (t, t+\Delta t)$ , given that it has already remained closed (or open) for a time  $T > t_{\text{eff}}$ . In the branch of statistics called renewal theory,  $k_{\text{eff}}$  is called the "age specific failure rate," for example, the probability that a light bulb fails in the next second given it has already burned for  $t_{\text{eff}}$  hours. In the branch of statistics used in epidemiology and insurance,  $k_{\text{eff}}$  is called the "survival rate," for example, the probability that a patient dies of cancer this year, if they have already had cancer for  $t_{\text{eff}}$  years.

## Fractal Kinetics

Liebovitch et al. 1987 *Math. Biosci.* 84:37-68.

### Kinetic Rate Constant:

$k$  = Prob. to change states in the next  $dt$ .

### Effective Kinetic Rate Constant:

$k_{\text{eff}}$  = Prob. to change states in the next  $dt$ ,  
given that we have already remained  
in the state for a time  $k_{\text{eff}}$ .

*age-specific failure rate*

$$\begin{aligned} k_{\text{eff}} &= \Pr ( T=t, t+dt \mid T > t_{\text{eff}} ) / dt \\ &= - \frac{d \ln P(t)}{dt} \end{aligned}$$

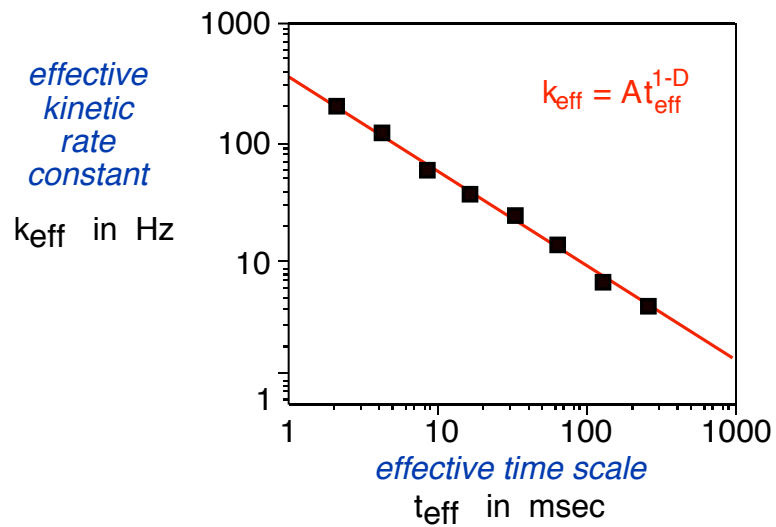
$P(t)$  = cumulative dwell time distribution

Liebovitch & Shehadeh

We measured the open and closed times for an ion channel in the cells in the cornea, the clear part in the front of the eye that you look through to see these words. The effective kinetic rate constant is a straight line on a plot of log (effective kinetic rate constant) versus log (effective time used to measure it). This is a fractal scaling relationship in time. The faster we could look, the briefer open and closed times we would see.

## 70 pS K<sup>+</sup> Channel Corneal Endothelium

*Liebovitch et al. 1987 Math. Biosci. 84:37-68.*



Fractals have given us a new way to analyze data from the patch clamp measurements of the open and closed times of ion channels. Instead of measuring a property (the kinetic rate constant) at one time scale, we measure how a property (the effective kinetic rate constant) changes when we measure it at different time scales. We have been using the information in this fractal scaling relationship to give us clues about the structure and motions in ion channel protein. Specifically, we have been using the scaling relationship to calculate the energy difference between the open and closed states of the ion channel protein and how that energy difference varies in time. The picture of ion channels before fractals analysis was that they are firm, sharp, upright things that go click, click, click, between a few, very different static states. The picture of ion channels after fractal analysis is that they are complex dynamic things, with many pieces of different size that move over different time scales, whose new shapes and movements determine what it's going to do next.

### Fractal Approach

*Liebovitch 1989 Math. Biosci. 93:97-115.*

*Liebovitch and Tóth 1991 Bull. Math. Biol. 53:443-455.*

*Liebovitch et al. 2001 Methods 24:359-375.*

#### New viewpoint:

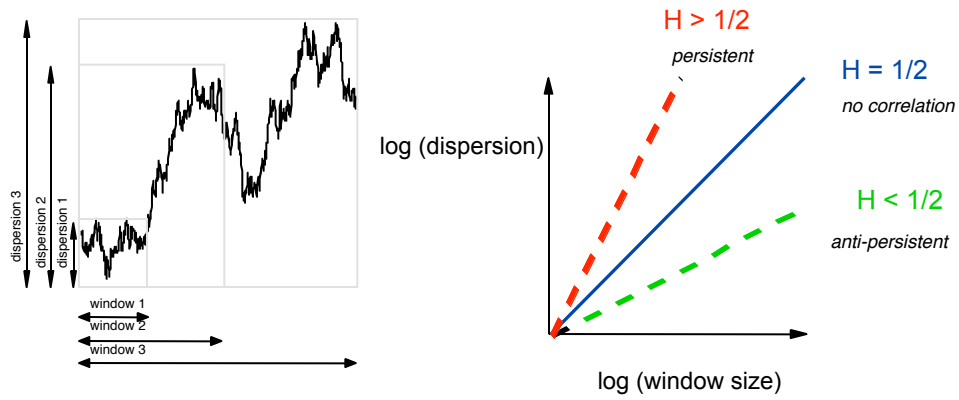
Analyze how a property, the effective kinetic rate constant,  $k_{\text{eff}}$ , depends on the effective time scale,  $t_{\text{eff}}$ , at which it is measured.

#### This Scaling Relationship:

We are using this to learn about the structure and motions in the ion channel protein.

We have seen examples of scaling relationships for measurements in space and time. There can also be scaling relationships for the correlations between measurements. Like the scaling relationships for measurements, the scaling relationship for the correlations between the measurements is often a power law, that is, a straight line on a logarithmic-logarithmic plot. For example, at the left in the figure on the following page is a measurement in time. It is self-similar—there are ever larger fluctuations over ever longer times. We can measure the dispersion, the variation in the value, over different windows of time. The dispersion is ever larger over ever longer time windows. The slope of this scaling relationship on a plot of  $\log(\text{dispersion})$  versus  $\log(\text{window size})$  is called the Hurst Exponent,  $H$ . When  $H = 0.5$ , the measurements are not correlated. When  $H > 0.5$ , the measurements are positively correlated. This is called persistence. An increase now is more likely followed by an increase at all time scales later. When  $H < 0.5$ , the measurements are negatively correlated. This is called anti-persistence. An increase now is more likely followed by a decrease at all time scales later. There are many different ways to find the correlational scaling relationship. One method is the Hurst Rescaled Range Analysis. Another method is Detrended Fluctuation Analysis.

## Correlations



### Measures of dispersion:

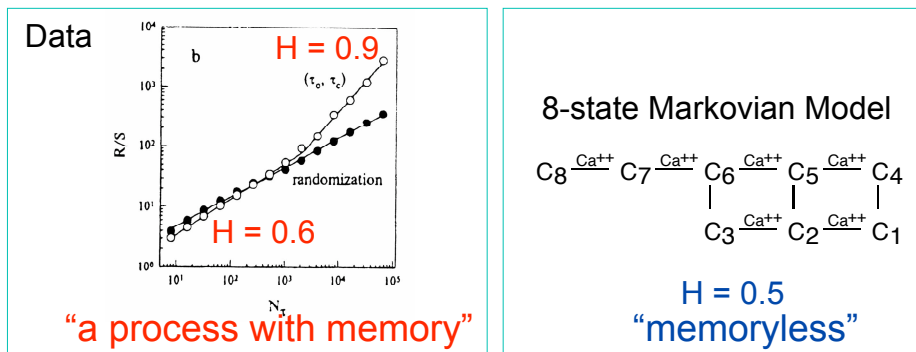
Hurst Rescaled Range Analysis: R/S

Detrended Fluctuation Analysis: DFA

On the left, the Hurst rescaled range analysis was used to measure the correlations in the open and closed times of an ion channel protein (open circles). At short times,  $H = 0.6$ , and at along times  $H = 0.9$ . These are very persistent correlations. The correlations disappear (black circles) when the order of the open and closed times was randomly shuffled. This means that there is a long term “memory,” which gets stronger with time, in how the shape of the ion channel protein changes in time. Previous models of ion channels, as shown on the right, assumed that the channel switched between a few, discrete shapes, without any memory. This fractal analysis tells us that ion channels do not behave that way. Instead, the fractal analysis has enabled us to see that there are important, continuous dynamical processes, with memory, going on inside the ion channel protein.

## Fractal Kinetics

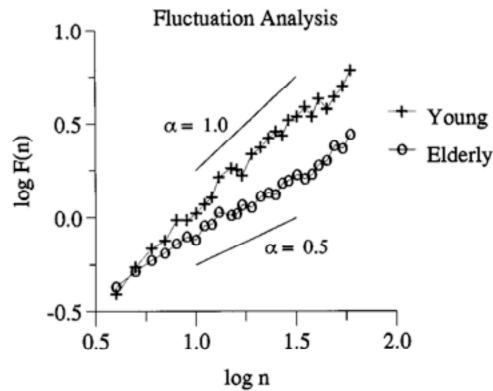
*Kochetkov, et al. 1999. J. Biol. Phys. 25:211-222.*



Here, the detrended fluctuation analysis was used to measure the correlations in the time between footsteps. This scaling relationship is also a power law, a straight line on a logarithmic-logarithmic plot. The scaling exponent of that power law is different for the young and the elderly person. These studies have given us insight into how the brain controls coordination and walking, and how that control depends on age and is changed by disease.

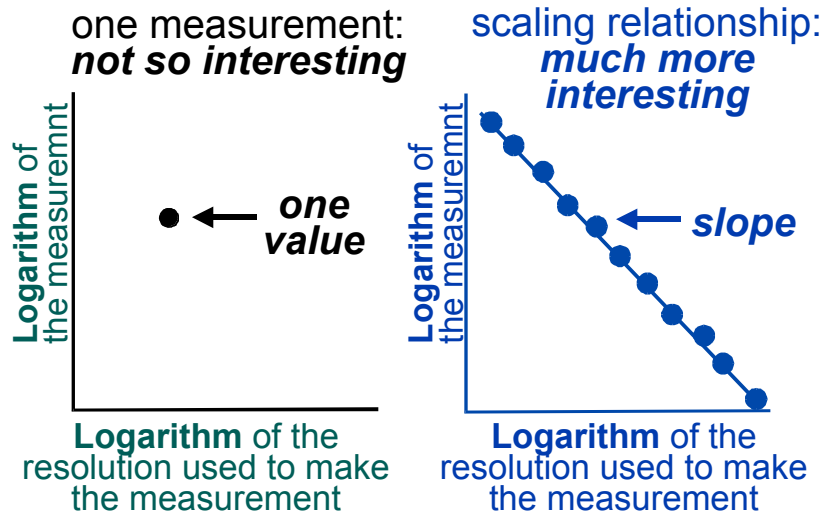
## Fractal Walking

*Hausdorff et al. 1997. J. Appl. Physiol. 82:262-269.*



This is the take-home lesson: We are used to thinking that there is one measurement that best describes a property of an object. For a fractal object that extends over many scales, in space or time, a property depends on the scale at which it is measured. There is no one measurement that best describes the object. The object is best described by how the property measured depends upon the resolution at which it is measured. This relationship is characterized by a parameter called the fractal dimension. The fractal dimension can be calculated from the slope of this logarithmic-logarithmic graph.

## Scaling



# Fractals

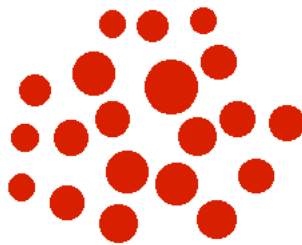
## Statistics

Fractals have some unique statistical properties. The “average” size depends on the resolution used to make the measurement. What is important is not the average, but how the average depends on the resolution used to make the measurement.

Liebovitch & Shehadeh

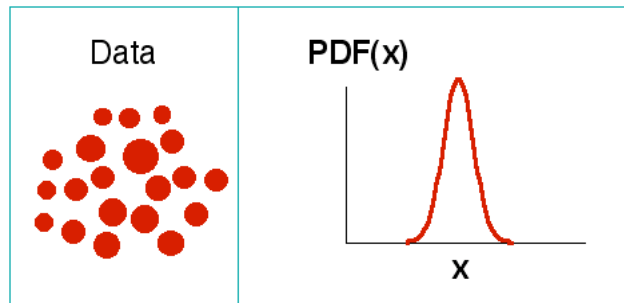
Here is a set of numbers; maybe they are the values measured from an experiment. I have drawn a circle to represent each number. The diameter of the circle is proportional to the magnitude of the number. Here is a non-fractal set of numbers. Most of them are about the size of an average number. A few are a bit smaller than the average. A few are bit larger than the average.

## Not Fractal



Here is the PDF of these non-fractal numbers. The PDF is how many numbers there are of each size. The PDF here is called a “Bell Curve,” a “Gaussian Distribution,” or a “Normal Distribution.” It’s strange that someone chose to call this a “normal” distribution. We are about to see that much of the world is definitely not like this kind of “normal.”

## Not Fractal



Liebovitch & Shehadeh

Here is a picture of Gauss on the old 10 Deutsche Mark German bill. He has now been replaced by the 5 Euro. You can see his curve and even the equation for it on this bill! There are no equations on American money. (There is a scientist on American money. Do you know who it is?)

## Gaussian Bell Curve “Normal Distribution”



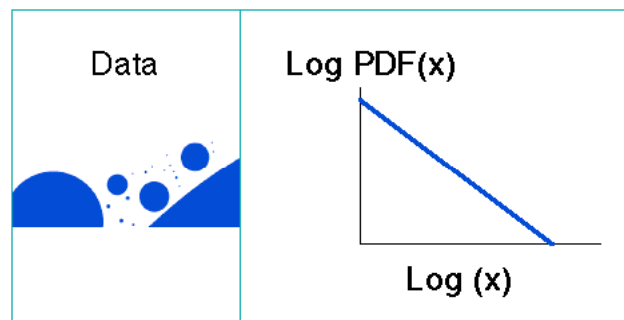
Here is a set of numbers from a fractal distribution. The diameter of each circle is proportional to the size of the number. These numbers could be from the room around you. Look around your room. There are few big things (people and chairs), many medium-sized things (pens and coins), and a huge number of tiny things (dust and bacteria). It is not at all like that “Normal” distribution. Sets of data from many things in the real world are just like this. We call this a fractal distribution of numbers because it has the same statistical properties as the sizes of the pieces in fractal objects.

## Fractal



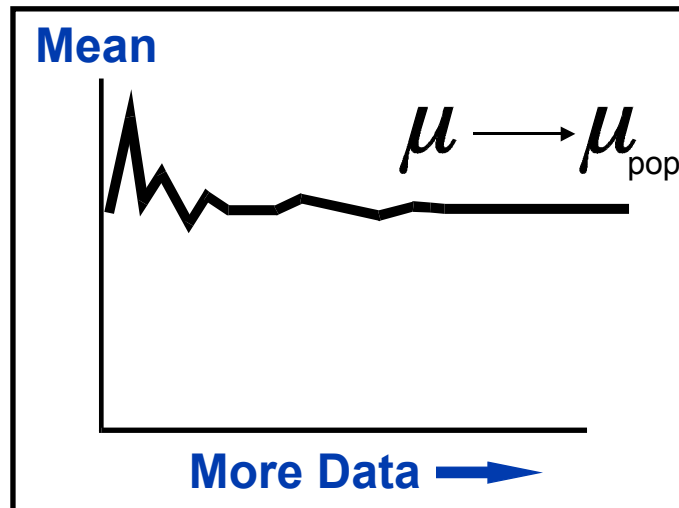
Here is the PDF of these fractal numbers. The PDF is how many numbers there are of each size. There are a few big numbers, many medium sized numbers, and a huge amount of tiny numbers. The PDF is a straight line on a plot of  $\log(\text{How Many Numbers; the PDF})$  versus  $\log(\text{value of the numbers})$ .

## Fractal



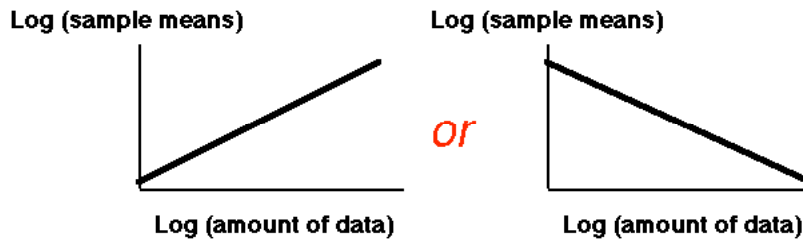
The statistics of a fractal set of numbers is very different from the statistics of "normal" numbers that they taught you about in Statistics 101. The statistics you learned in Statistics 101 is only about non-fractal numbers. Take the average of a sample of non-fractal numbers. This is called the Sample Mean. As you include ever more data, the sample means, shown here as  $\mu$ , get ever closer to one value. We call that value the Population Mean, shown here as  $\mu_{\text{pop}}$ . We think that the population mean is the "real" value of the mean.

### Non - Fractal



The statistics of fractal numbers is very different. Take the average of a sample of fractal numbers. This is called the Sample Mean. As you include ever more data, the sample means do NOT get ever closer to one value. Either the sample means keep increasing OR the sample means keep decreasing as you include more data. THERE IS NO Population Mean. There is NO one value that best describes the data. The data extend over a range of many different values.

## The Average Depends on the Amount of Data Analyzed

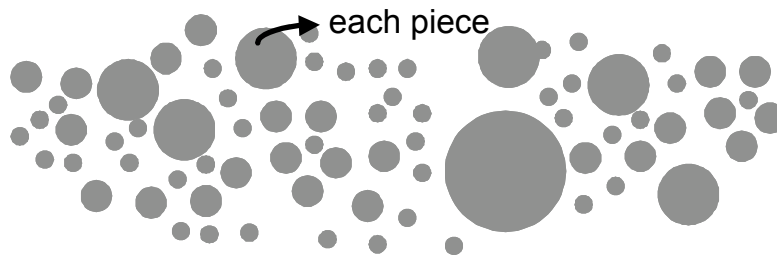


Here is why that happens. Again, here is a set of fractal numbers. The diameter of the circles are proportional to the size of the numbers. As you include ever more numbers one of two things will happen:

1. If there is an excess of many small values, the sample means get smaller and smaller.
2. If there is an excess of a few big values, the sample means get larger and larger

Whether 1 or 2 happens depends on the ratio of the amount of small numbers to the amount of big numbers. That ratio is characterized by a parameter called the Fractal Dimension.

## The Average Depends on the Amount of Data Analyzed



Let's play a non-fractal game of chance. Toss a coin, if it comes up tails we win nothing, if it comes up heads we win \$1. The average winnings are the probability of each outcome times how much we win on that outcome. The average winnings are  $(1/2) \times (\$0) + (1/2) \times (\$1) = 50\text{¢}$ . Let's go to a fair casino to play this game. Fair casinos exist only in math textbooks; "fair" means the bank is willing only to break even and not make a profit. We and the casino think it's fair for us to be charged 50¢ to play one game. That seems reasonable; half the time we win nothing, half the time we win \$1, so if it costs 50¢ to play each time, on average, we and the casino will break even.

### Ordinary Coin Toss

**Toss a coin. If it is tails win \$0, If it is heads win \$1.**

**The average winnings are:**

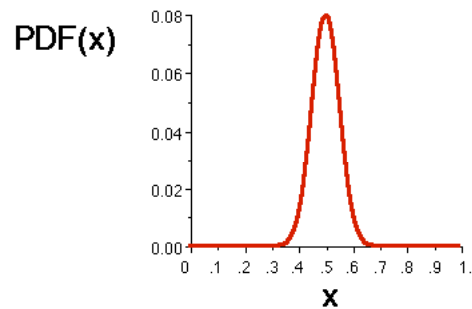
$$2^{-1.1} = 0.5$$

$$\mu \rightarrow 1/2$$

*Non-Fractal*

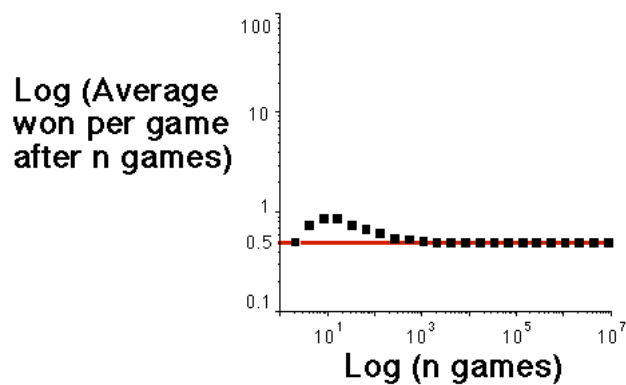
Here is the PDF of that non-fractal game of chance. It shows how often (the PDF on the vertical axis) you will win how much money (the  $x$  value on the horizontal axis) if you play 100 times. It's a Bell Curve—a Gaussian, Normal distribution—just the kind of distribution they taught you about in Statistics 101.

## Ordinary Coin Toss



Here's what happens when I played that non-fractal game, over and over again. A computer (actually a Macintosh Plus running Microsoft BASIC!) picked a random number to simulate flipping the coin. Here, the average winnings per game is shown after  $n$  games. For a while I (the Mac) was lucky. I was winning more than an average 50¢ in each game. But, as you might suspect (this is called the Law of Large Numbers), after a while my luck ran out. In the long run, I was winning exactly an average of 50¢ in each game.

## Ordinary Coin Toss



Now, let's play a fractal game of chance. This game was invented by Niklaus Bernoulli who lived in St. Petersburg, Russia, and was published by his uncle Daniel Bernoulli who lived in Germany, about 350 years ago. Here, we toss a coin UNTIL it comes up heads. If it comes up heads on the first toss, we win \$2. If it comes up tails first, and then heads on the second toss, we win \$4. If it comes up tails twice, and then heads on the third toss, we win \$8. And so on.

The average winnings are the probability of each outcome times how much we win on that outcome. The average winnings are  $(1/2) \times (\$2) + (1/4) \times (\$4) + (1/8) \times (\$8) + (1/16) \times (\$16) + \dots = 1 + 1 + 1 + 1 \dots = \infty$ . We say to the casino, "Half the time we'll win \$2; the median winnings of this game is \$2" because half the time the coin comes up heads on the first toss and we win \$2. "So, we think it is very fair to put up twice the median winnings, \$4, to play each game". To our surprise, the now angry casino owner says, "No!" He adds, "The average winnings of this game are infinite, you must put up more than all the money in the universe to play this game, even once!"

This game became known as the St. Petersburg Paradox, because we and the casino cannot agree on the fee to play this game. It was called a "paradox" because it was so surprising, and difficult for many people to believe, that the player and the casino owner could disagree on what is fair for such a simple game. This game is well known amongst mathematicians, which means it's well known amongst the people who know it well. But, because of its unusually mathematical character, it was not one of the threads of probability theory that was woven into the

fabric of statistics that became popular in the natural sciences and that is taught in Statistics 101. Now, with the popularity of fractals, it is being rediscovered and its importance in analyzing and understanding real data increasingly appreciated.

### St. Petersburg Game (Niklaus Bernoulli)

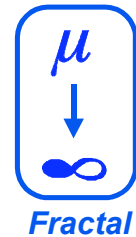
**Toss a coin. If it is heads win \$2, if not, keep tossing it until it falls heads.**

**If this occurs on the N-th toss we win  $\$2^N$ .**

**With probability  $2^{-N}$  we win  $\$2^N$ .**

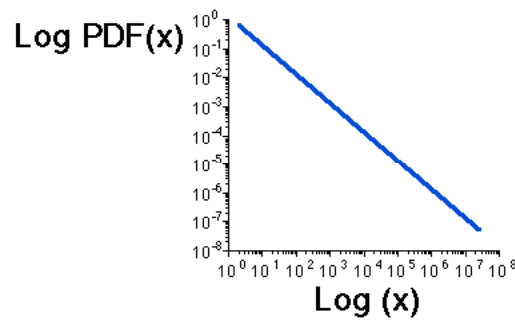
H	\$2
TH	\$4
TTH	\$8
TTTH	\$16

The average winnings are:									
$2^{-1}2^1$	+	$2^{-2}2^2$	+	$2^{-3}2^3$	+	...	=		
1	+	1	+	1	+	...	=	$\infty$	



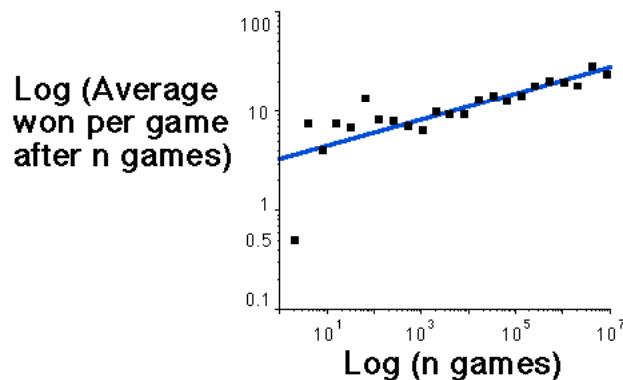
Here is the PDF of that fractal game of chance. It shows how often (the PDF on the vertical axis) you will win how much money (the x value on the horizontal axis). It's NOT a Bell Curve, Gaussian, or Normal distribution. Most often you win only a small amount, more often you win a bigger amount, very rarely you win a huge amount. It is just like the fractal PDF of the blood vessels in the retina, or any fractal object! It is a straight line on a plot of log (How Often) versus log(How Much).

## St. Petersburg Game (Niklaus Bernoulli)

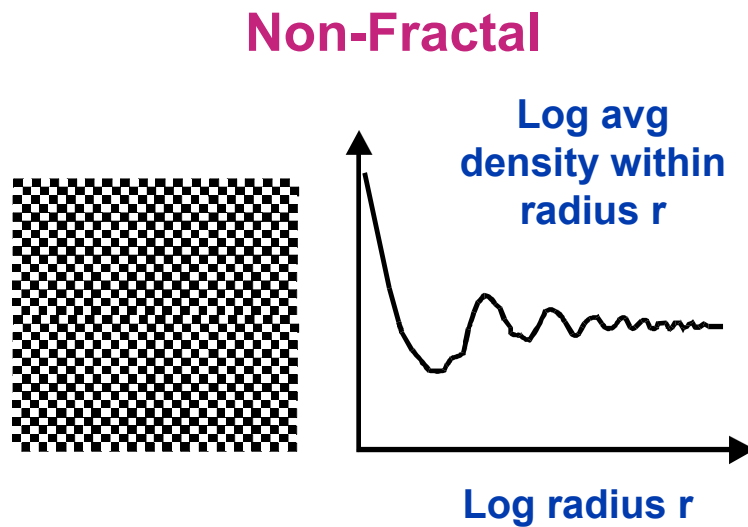


Here's what happens when I played that fractal game over and over again. Here, the average winnings per game is shown after  $n$  games. The more I played, the more often there was sometimes a lot of tails before that first head. When there are a lot of those tails, I won a huge jackpot. As more and more of those jackpots happened, the average winnings per game kept increasing. There is no average (population mean) for this game. The more I played, the more the average kept changing. They told you in Statistics 101 that the more data you have, the closer the sample means are to the population mean. Not here! There is no population mean. The more data we have (the more games I played) the more the sample means keep changing. The few exponentially large wins keep pushing the sample mean up, which is very different than what you learned in Statistics 101. Welcome to fractals.

## St. Petersburg Game (Niklaus Bernoulli)



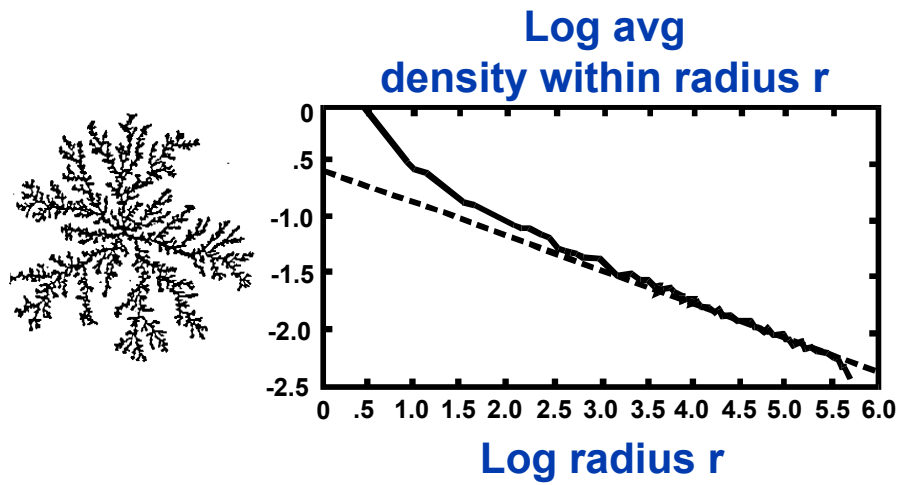
Here is a non-fractal object. It is a checkerboard. Actually, I'm only showing you a piece of it; it should really extend forever in each direction. Place a circle on it. Count all the black pixels in that circle, and divide by the total number of pixels. That is the average density within that circle. The graph shows how that density changes as the circles get bigger and bigger. The average density fluctuates a bit; after all, we are putting a round circle over a square grid. But, as the circles get bigger and bigger, the average density gets closer and closer to  $1/2$ . This seems reasonable because the checkerboard is  $1/2$  black and  $1/2$  white.



The figure on the next page is a fractal object. It is called a Diffusion Limited Aggregation (DLA). It is statistically self-similar. It has little spaces between its little arms, medium spaces between its medium-sized arms, and large spaces between its large arms. We're only showing you a piece of it, but it should also really extend forever in each direction. Place a circle on it. Count all the black pixels in that circle, and divide by the total number of pixels. That gives the average density within that circle. The graph shows how that density changes as the circles get bigger and bigger. As the circles get bigger we catch more of the ever larger spaces between the arms, and so the density gets smaller. As the circles get ever bigger, the density gets ever smaller. There is no one density that describes this object. What's more, the local density on a big arm is very high. The local density between big arms is very low. Yet, the same mechanism makes the arms and the spaces between them. Based upon our Statistics 101 training, we are used to thinking that when the local average changes, when there is a difference in the mean value between an experiment and a control, or between now and then, that the system must have changed. Here, fractals, with infinite variance, have moments, such as the mean, that can be very different in space and time or between experiments and controls, even though the basic process has not changed at all!

## Fractal

*Meakin 1986 In On Growth and Form: Fractal and Non-Fractal Patterns in Physics Ed. Stanley & Ostrowsky, Martinus Nijhoff Pub., pp. 111-135*

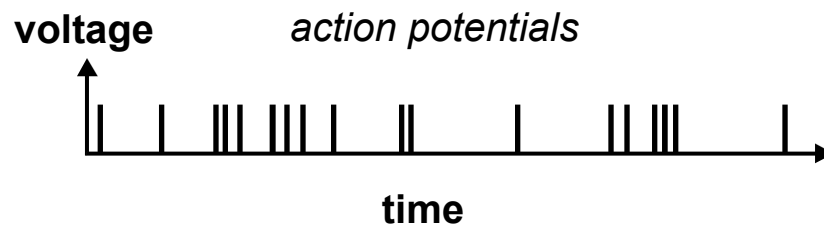


Liebovitch & Shehadeh

Here is yet another example of fractal data. Data from many experiments have fractal properties. Here are the action potentials, the little electrical sparks, that encode information sent down the nerves in your body. Teich et al. measured them in the auditory nerve, which brings information about sounds from your ear to your brain.

## Electrical Activity of Auditory Nerve Cells

*Teich, Jonson, Kumar, and Turcott 1990 Hearing Res. 46:41-52*



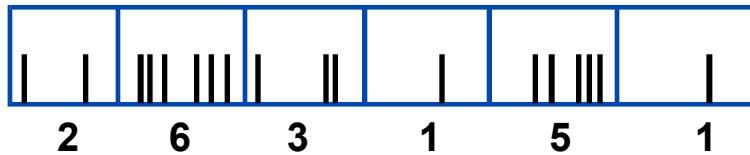
They divided the time record into windows and counted the number of action potentials in each window. Here, two in the first window, six in the second, and so on. The "firing rate" is the number of action potentials in each window, divided by the time duration of that window.

## Electrical Activity of Auditory Nerve Cells

*Teich, Jonson, Kumar, and Turcott 1990 Hearing Res. 46:41-52*

### ***Divide the record into time windows:***

Count the number of action potentials in each window:



**Firing Rate = 2, 6, 3, 1, 5,1**

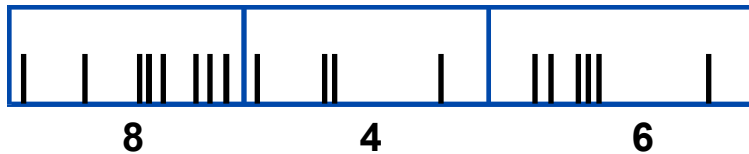
Liebovitch & Shehadeh

Here they made the windows twice as long in time, and counted the number of action potentials in each window. Again, the "firing rate" is the number of action potentials in each window, divided by the time duration of that window.

## Electrical Activity of Auditory Nerve Cells

*Teich, Johnson, Kumar, and Turcott 1990 Hearing Res. 46:41-52*

**Repeat for different lengths of time windows:**

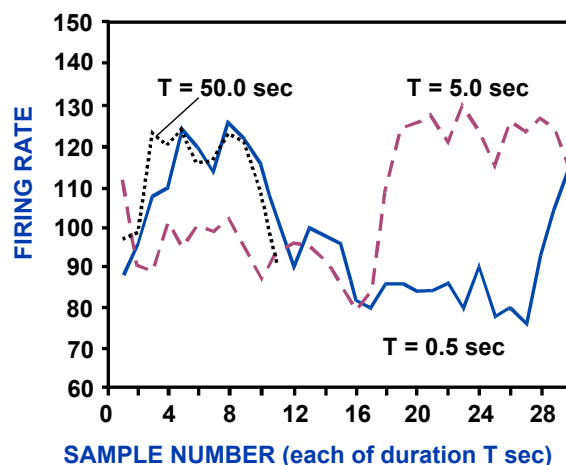


**Firing Rate = 8, 4, 6**

In Statistics 101 they taught you that as you collect more data, the fluctuations average out. You were taught to expect that the fluctuations in the firing rate should be less as the time windows get longer. But look here—the variations don't change much as the time windows go from 0.5 s to 5.0 s to 50.0 s! [Actually, the real deal here is that the variance of the fluctuations falls much slower than  $1/\sqrt{n}$ ]. You include more data, but you don't get any closer to the real firing rate. There is no one single value, like a population mean, that best describes the firing rate. The increase in variation at longer time windows is real. It represents correlations in the action potentials which may tell how information is encoded in the timing of the action potentials.

## Electrical Activity of Auditory Nerve Cells

*Teich, Jonson, Kumar, and Turcott 1990 Hearing Res. 46:41-52*



**The variation in the firing rate does not decrease at longer time windows.**

# Fractals

## Power Law PDFs

PDFs: Fractal data have a characteristic PDF form called a Power Law.

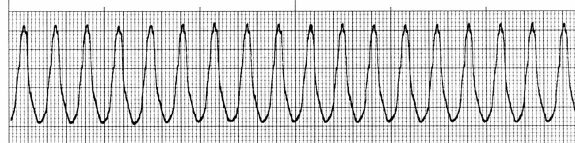
These are electrocardiograms (EKGs) that record the voltage from the heart. The first chart strip shows a normal heart. The second chart strip shows a heart that is beating dangerously fast (ventricular tachycardia). This is dangerous because it can lead to ventricular fibrillation, where the heart no longer contracts in a regular way and can result in death in 3 minutes.

## Heart Rhythms

Normal



Ventricular Tachycardia: TOO FAST



Ventricular Fibrillation = DEATH



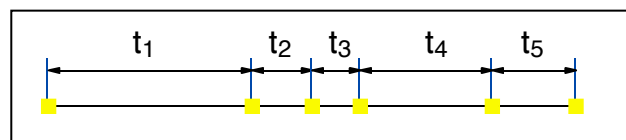
To prevent ventricular tachycardia from leading to fibrillation and death, a small device called a “cardioverter defibrillator” can be placed just under the skin in the chest. Small wires are snaked around through the blood vessels into the heart. It listens, electronically, carefully to the heartbeat. When the heart beats 3 times its normal rate for 5 beats, it sends an electrical shock strong enough to kick the heart back into a normal rhythm. But, it’s also a computer, with a small memory. It can remember when it is triggered. Back in the hospital, a small coil is placed on the patient’s chest. Over this radio link, the cardioverter defibrillator can play back when it was triggered. We have been analyzing the times between when the device was triggered. Just to be clear, we are not analyzing the time between heartbeats. We are analyzing the durations between consecutive triggerings of the cardioverter defibrillator.

## Inter-event Times

*Liebovitch et al. 1999 Phys. Rev. E59:3312-3319.*

### Cardioverter Defibrillator

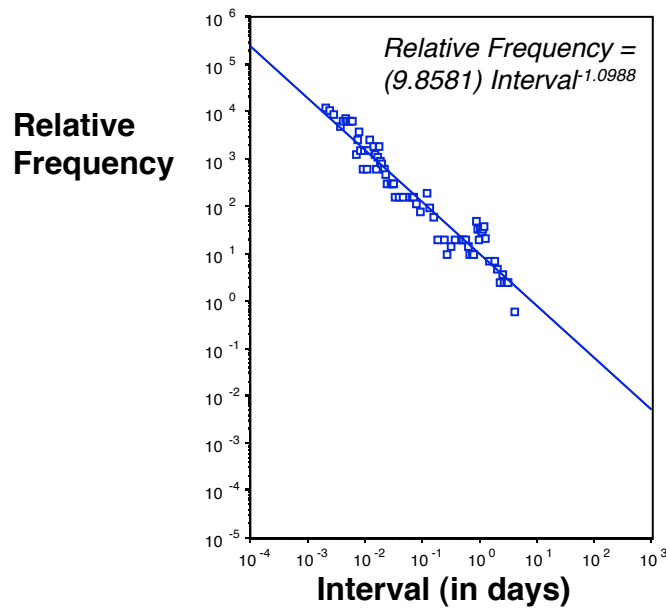
- Episodes of Ventricular Tachycardia (v-tach)



time ->

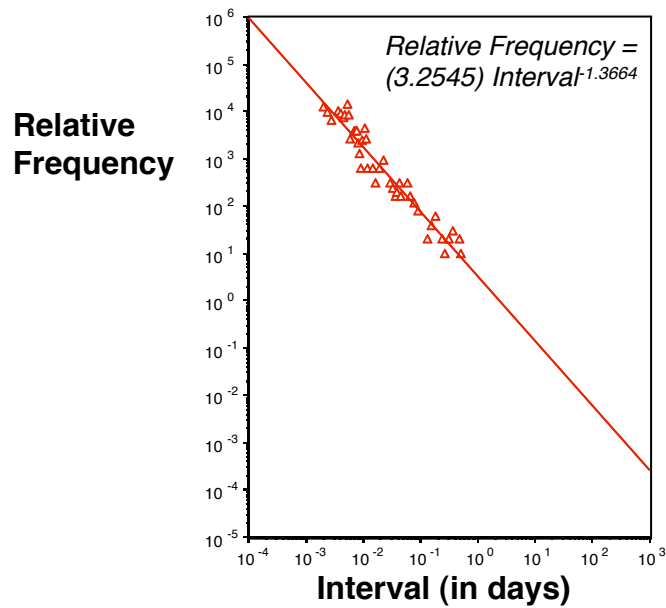
Here, from one patient, is the relative frequency, the number of occurrences of a given duration between the defibrillator events. The PDF is proportional to the relative frequency. The plot is a straight line on a log (how often) versus log (time between events) scale. This is fractal scaling. The events of rapid heart rate happen with a fractal timing.

### Patient #33



Here again, from another patient, is the relative frequency. The PDF is proportional to the relative frequency. The plot is also a straight line on a log (how often) versus log(time between events) scale. This is also fractal scaling. The events of rapid heart rate for this patient also happen with a fractal timing.

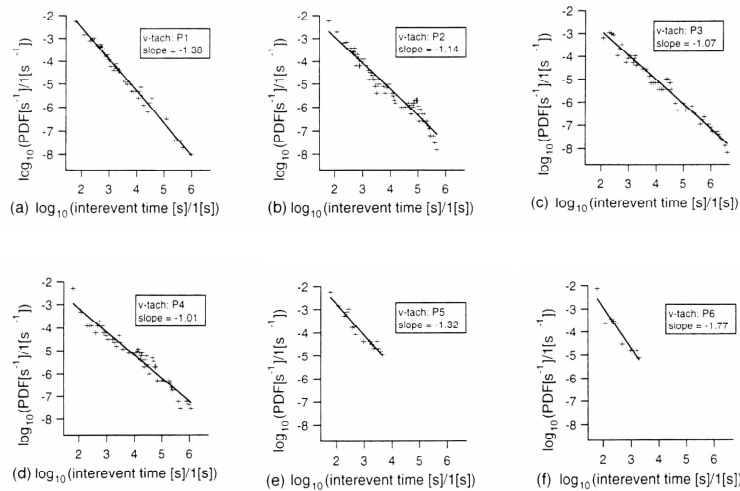
### Patient #53



In fact, for many patients events of ventricular tachycardia happen with a fractal pattern. Most of the times between events are short, sometimes they are longer, and very rarely they are very long, which is typical of fractals. There is no average time between events. If you measured the “average rate” of events you would get a different answer if you measured them over a day or a week or a year. There is no one number that best describes the time between these events. The time between events happens over many different time scales. We are working on other ways, fractal ways, of characterizing these times to assess the status of patients and the effectiveness of medical therapies. For example, we are seeing whether the slope or intercept of these PDFs is a good indicator of diagnosis or treatment outcome.

## 6 Patients

*Liebovitch et al. 1999 Phys. Rev. E59:3312-3319.*



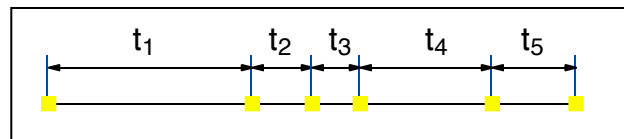
We are also analyzing the times at which different e-mail viruses arrive at the gateway into an internet service provider. On the picture on the following page are the events—the arrival times of e-mail viruses. We are looking at the duration of times between the arrival of each virus. We have studied 4 viruses:

1. *AnnaKournikova* doesn't have a picture of her, it's a file that you wouldn't want to open.
2. *Magistr* can erase sectors on your hard disk or your cmos/bios. If you don't know what the cmos/bios is, you don't want us to tell you what happens if it gets erased.
3. *Klez* puts together messages by joining fragments of phrases that it contains.
4. *Sircam* tempts you to open and execute its attached file.

Much is known about the structure of the Internet. Less is known about the dynamics of the Internet. The arrival times of these viruses depend on both the structure and dynamics of the Internet. We are hoping that our study of these arrival times will tell us how the structure interacts with the dynamics if the Internet.

## Inter-arrival Times of E-mail Viruses

*Liebovitch and Schwartz 2003 Phys. Rev. E68:017101.*



time ->

### AnnaKournikova

"Hi: Check This!" AnnaKournikova.jpg vbs.

### Magistr

Subject, body, attachment from other files: erase disk, cmos/bios.

### Klez

E-mail from its own phrases: infect by just viewing in Outlook Express.

### Sircam

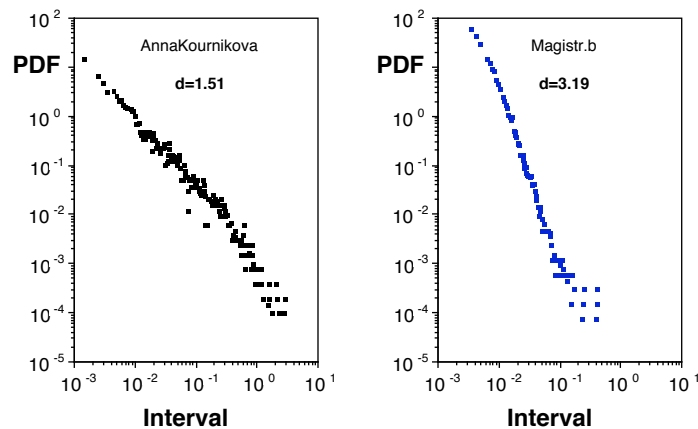
"I send you this file in order to have your advice."

Liebovitch & Shehadeh

We have data, unfortunately, from many, many virus events. Here are the PDFs from *AnnaKournikova* and *Magistr*, how often the different times between the arrivals occurred. These plots are straight lines on a log (how often) versus log(time between arrivals) scale. These are fractal scalings. The arrival of these viruses happens with a fractal timing.

## E-mail Viruses

*Liebovitch and Schwartz 2003 Phys. Rev. E68:017101.*



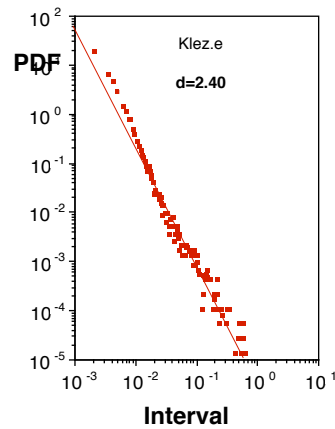
20,884 viruses

153,519 viruses

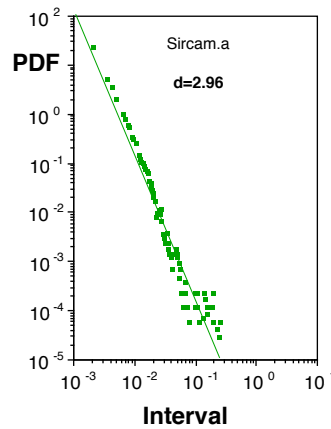
Here are the PDFs from *Klez* and *Sircam*, how often the different times between the arrivals occurred. These plots are also straight lines on a log (How Often) versus log(time between arrivals) scale. These are also fractal scalings. The arrival of these viruses also happens with a fractal timing.

### E-mail Viruses

*Liebovitch and Schwartz 2003 Phys. Rev. E68:017101.*



413,183 viruses



781,626 viruses

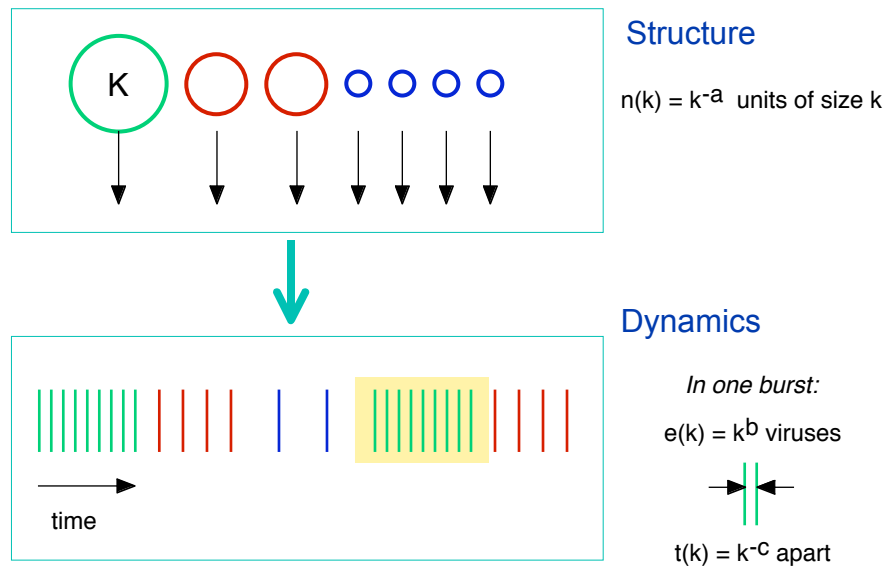
We made a simple model to study how the structure and the dynamics of the Internet are interrelated.

Structure: There are networks of computers of different sizes.

Dynamics: When each network sends out viruses, the number and time between them depend on the size of the network.

### Model: Structure + Dynamics

*Liebovitch and Schwartz 2003 Phys. Rev. E68:017101.*



There were some interesting results from these models. First, the model predicts a power law distribution in the PDF of the times between the arrival of the viruses. Second, the exponent of that power law tells us whether relatively more viruses are sent from the small number of larger networks or the larger number of small networks.

### Model: Results

$$\text{PDF}(t) = t^{-d}$$

$$\text{where } d = 1 - a/c + b/c$$

The relative number of viruses from all units of size  $k \sim k^{b-a}$

$$d = 1 - a/c + b/c \longrightarrow (b-a) = c(d-1)$$

When  $d > 1$ :  $(b-a) > 0$ ,  
relatively more viruses come from the **larger** units,  
as seen in the **data**.

When  $d < 1$ :  $(b-a) < 0$ ,  
relatively more viruses come from the **smaller** units.

# Fractals

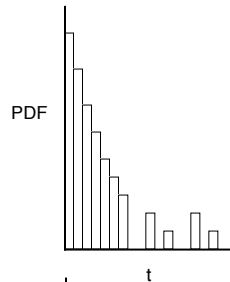
## Methods for Determining the PDFs

The PDF is an important tool in determining if experimental data have fractal properties. A power law PDF is characteristic of fractal behavior. The standard method for evaluating the PDF is to make a histogram of the data. That method is very good at determining the PDF when the data are not fractal. It is less good at determining the PDF when the data are fractal. Next, we'll see other ways of determining the PDF, and how they compare to the histogram method.

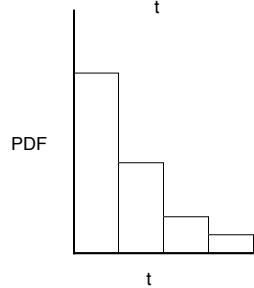
It's not so easy to make a good PDF from the histogram of How Many events there are in each time bin. If we choose the bins narrow, we get good resolution for the small events. But, at long times, because the bins are so narrow, we may see only 1 or 2 events, or even 0 events, in some of those bins. If we try to fix this by making the bins wider, we do get more events in the bins at longer times. But, at short times, we now have poor resolution.

### Determining the PDF from a Histogram

Bins  $dt$  Small  
Good at small  $t$ .  
**BAD** at large  $t$ .



Bins  $dt$  Large  
**BAD** at small  $t$ .  
Good at large  $t$ .



We figured out a nice algorithm to get a better PDF. Narrow bins are good at short times. Wide bins are good at long times. So, we make histograms of different bin sizes. But, we cannot combine histograms of different bin sizes. However, we can compute the PDF from each histogram and then combine the PDFs. For each histogram, the PDF(t) is  $N(t)$ , the number of values in the bin that covers  $(t, t+dt)$ , divided by  $N_t$ , the total number of values in that histogram, divided by  $dt$ , the width of the bins in that histogram. The histograms with narrow bins give us good resolution in the PDF at short times. The histograms with wide bins give us good values in the PDF at long times. We've found that this method yields accurate and reliable PDFs for tails of many different kinds of distributions. See Liebovitch et al. 1999 for details.

## Determining the PDF

*Liebovitch et al. 1999 Phys. Rev. E59:3312-3319.*

**Solution:**  
Make ONE PDF  
From SEVERAL Histograms of DIFFERENT Bin Size

$$\text{PDF} = \frac{N(t)}{N_{\text{tot}}dt}$$

$N(t)$  = number in  $[t, t+dt]$

$N_{\text{tot}}$  = total number in each histogram

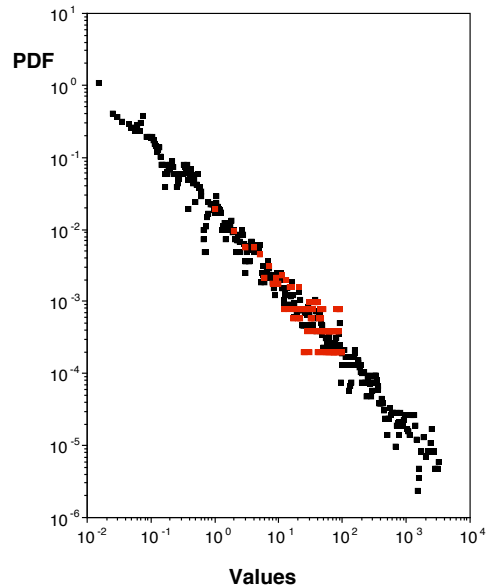
$dt$  = bin size

Choose  $dt = 1, 2, 4, 8, 16 \dots$  seconds

Here, PDFs were measured from a set of fractal data. The red boxes indicate the PDF made in the usual way from one histogram. You can see where there are only 1 or 2 events in the largest bins. The black boxes indicate the PDF generated from the same data using the new multi-histogram method to make the PDF. Pretty impressive difference.

## Determining the PDF

- New multi-histogram
- Standard fixed dt



# Fractals

## Summary

## SELF-SIMILARITY

*Definition:* Pieces of an object in space, or parts of a process in time, are smaller versions of the whole object or process.

*Examples:* The Sierpinski Triangle in space and the times between the arrival of e-mail viruses.

*Methods:* A power law distribution of the PDF of the pieces of an object in space or the parts of a process in time is indicative of fractal behavior.

*Importance for data analysis:* There is no single scale, in space or time, that characterizes such data that extends over many scales.

## Summary of Fractal Properties

### Self-Similarity

**Pieces resemble the whole.**

## SCALING

*Definition:* The value measured for a property depends on the scale, in space or time, over which it is measured.

*Examples:* The length of the west coast of Britain and the closed times of ion channel proteins in the cell membrane.

*Methods:* A power law scaling of the measured values or the correlation between the measured values is indicative of fractal scaling behavior.

*Importance for data analysis:* Since no one value properly characterizes the data, what is important is how the value measured depends on the resolution used to make the measurement.

## Summary of Fractal Properties

### Scaling

**The value measured depends on the resolution.**

## STATISTICS

*Definition:* The PDF is a power law. The population mean and population standard deviation don't exist.

*Examples:* The winnings in the St. Petersburg game and the variation in the times between action potentials recorded from auditory nerve cells in the ear.

*Methods:* A power law distribution of the PDF or a power law scaling relationship for the moments is indicative of fractal behavior.

*Importance for data analysis:* When the mean depends on the spatial scale, the temporal scale, or how much data we analyze, then the mean is meaningless. What is meaningful is how the sample means, or another scaling property, depend on the spatial scale, the temporal scale, or how much data we analyze, which is described by the fractal dimension.

## Summary of Fractal Properties

### Statistical Properties

**Moments may be zero  
or infinite.**

Probability theory started from solving gambling problems about 400 years ago. About 200 years ago, those results were used to develop basic statistics. Most of the statistical tests we use were developed less than 100 years ago. We show you this to emphasize that statistics is NOT a dead science, although it's often presented like that in Statistics 101. It has changed a lot. It is still changing. It will change even more in the future. The statistical properties of fractals are examples of new ideas that are now being incorporated into and are changing statistics.

## Statistics is NOT a dead science.

*400 years ago:*

Gambling Problems → Probability Theory

*200 years ago:*

Statistics → How we do experiments.

*100 years ago:*

Student's t-test, F-test, ANOVA

*Now:*

Still changing

The take-home lesson here is not that fractals some arcane super-sophisticated mathematical tool that only needs to be used in some strange circumstance. Fractals change the most basic way we look at experimental data. They allow us to analyze and make sense out of the huge amount of real data that “just ain’t a bell curve.” The most common use of mathematics and statistics in all science is *means ± s.e.m.* Fractals tell us that if the data are fractal, those means are meaningless! That’s a pretty basic change in the simplest way we handle data. That’s what revolutions in science are about—not about changing the complex stuff, but about changing the simplest stuff. The stuff that we were taught so firmly that we never thought it would change.

Fractals CHANGE the most basic ways we analyze and understand experimental data.

**Fractals**

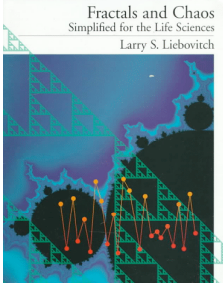
No Bell Curves  
No Moments  
No mean  $\pm$  s.e.m.

Measurements over many scales.

What is real is not one number, but how the measured values change with the scale at which they are measured (fractal dimension).

## TO LEARN MORE ABOUT FRACTALS

1. A book called *Fractals and Chaos Simplified for the Life Sciences* (Liebovitch, 1998). This book consists of facing pages, where the left page is text and the right page is a picture. It leads you, one concept at a time, through the material.
2. A CD-ROM of curricula materials for a mathematics course for college students who never liked and never did well in math (funded, in part, by the National Science Foundation, Division of Undergraduate Education). The materials emphasize what mathematics is, how mathematicians do mathematics, and how mathematics is used in science. We're almost finished with it and would be happy to send you a free demo (contact information is on the first page of this chapter).

 <p>Fractals and Chaos Simplified for the Life Sciences Larry S. Liebovitch</p>	<p><b><i>Fractals and Chaos and Simplified for the Life Sciences</i></b> <b>Larry S. Liebovitch</b> <b>Oxford Univ. Press, 1998</b></p>
 <p>CD ROM NSF DUE-9752226 DUE-9980715</p>	<p><b><i>The Mathematics and Science of Fractals</i></b> <b>Larry S. Liebovitch and Lina Shehadeh</b> <b><a href="http://www.ccs.fau.edu/~liebovitch/larry.html">www.ccs.fau.edu/~liebovitch/ larry.html</a></b></p>

We have concentrated here (and in the references noted on the previous page) on providing an introduction to fractal concepts, their importance, and what can be learned from them. Here are some books that describe the mathematical details of these methods and give examples of how scientists have used them.

## Technical Details

J. Feder. 1988. *Fractals*. Plenum Press.

J. B. Bassingthwaite, L. S. Liebovitch and B. J. West. 1994. *Fractal Physiology*. Oxford University Press.

P. M. Iannaccone and M. Khokha. 1996. *Fractal Geometry in Biological Systems*. CRC Press.

A. Bunde and S. Havlin, eds. 1994. *Fractals in Science*. Springer-Verlag.

## ACKNOWLEDGEMENTS

The development of some of these materials was supported, in part, by NSF grants DUE-9752226 and DUE-9980715.

## CHAPTER 6

# Gauging the Fractal Dimension of Response Times from Cognitive Tasks

John G. Holden

Department of Psychology  
California State University, Northridge  
Northridge, CA 91330-8255  
U. S. A.  
E-mail: [jay.holden@csun.edu](mailto:jay.holden@csun.edu)

Holden

An unexpected and exotic brand of variability resides in the trial-by-trial fluctuations of human judgments of passing time. The pattern, called  $1/f$  or pink noise, is a construct from fractal geometry. Pink noise is associated with complex systems whose components interact on multiple time scales to self-organize their behavior (Bassingthwaite, Liebovitch, & West, 1994; Jensen, 1998; Van Orden, Holden, & Turvey, 2003; see also Aks, Chapter 7). This chapter describes the phenomenon of pink noise, and explains how to conduct statistical analyses that identify it in response time data from elementary cognitive tasks.

It was Gilden, Thornton, and Mallon (1995) who first reported pink noise in response time variability during the fundamentally cognitive task of estimating fixed intervals of time. Gilden et al.'s temporal estimation task required participants to repeatedly estimate fixed intervals of time—in essence to “become a clock”—by pressing a button at each instant they believed a specific time interval had elapsed. Separate laboratory sessions were administered for each of several fixed target time-interval conditions. In each session 1000 time-interval judgments were collected in succession. The time-interval conditions ranged from  $1/3$  s up to 10 s. Of course, no participant's succession of time-interval judgments was exactly the same on every trial. Instead they varied from trial to trial. Lining up the series of successive time estimates in the strict order in which they were collected (i.e., trial 1, 2, ... 1000) yielded a *trial series* of response times, which was treated very much like a standard *time series* in Gilden et al.'s statistical analyses. Pink noise was revealed in the intrinsic residual variability that remained after the average time

interval that each participant produced, for each target interval, was removed from each trial series. Thus, pink noise emerged in the structure of the “background noise” of cognitive performance—the intrinsic variability of a person’s judgments of passing time.

To begin to understand the phenomenon of pink noise it is perhaps easiest to simply examine it visually. Figure 6.1A displays an example of an individual participant’s trial series from a temporal estimation task that used a method similar to that of Gildea et al. (1995). The x-axis depicts the successive trials in the experiment and the y-axis records the participant’s time estimate on each trial, in terms of standard deviations from their average time interval, taken across all trials (i.e., the time estimates are normalized and graphed as z-scores).

The overall pattern of trial-to-trial fluctuation is consistent with pink noise. Notice the undulating “waves” of relatively longer and then shorter time estimates that travel across the series. One shorthand way to describe the overall rising and falling trends is to say that the first 500 or so trials follow a giant inverted-U shape or an arc. It is fair to say that a similar large arc begins around the 500th trial and continues to the end of the series of observations. Now, look within each large arc, and similarly shaped arcs which run across fewer trials, perhaps only 50 to 100 trials at a time, can be discerned. Inside the smaller arcs are even smaller ones, and so on. Loosely speaking, the trial series is comprised of a progression of nested, similarly shaped arcs or patterns of fluctuation. Of course, there is nothing special about the arcing inverted-U shape; you could imagine M or W shapes, or even right-side up Us, for example. What is important in this example is the concept of a shape or pattern that is comprised of smaller copies of essentially the

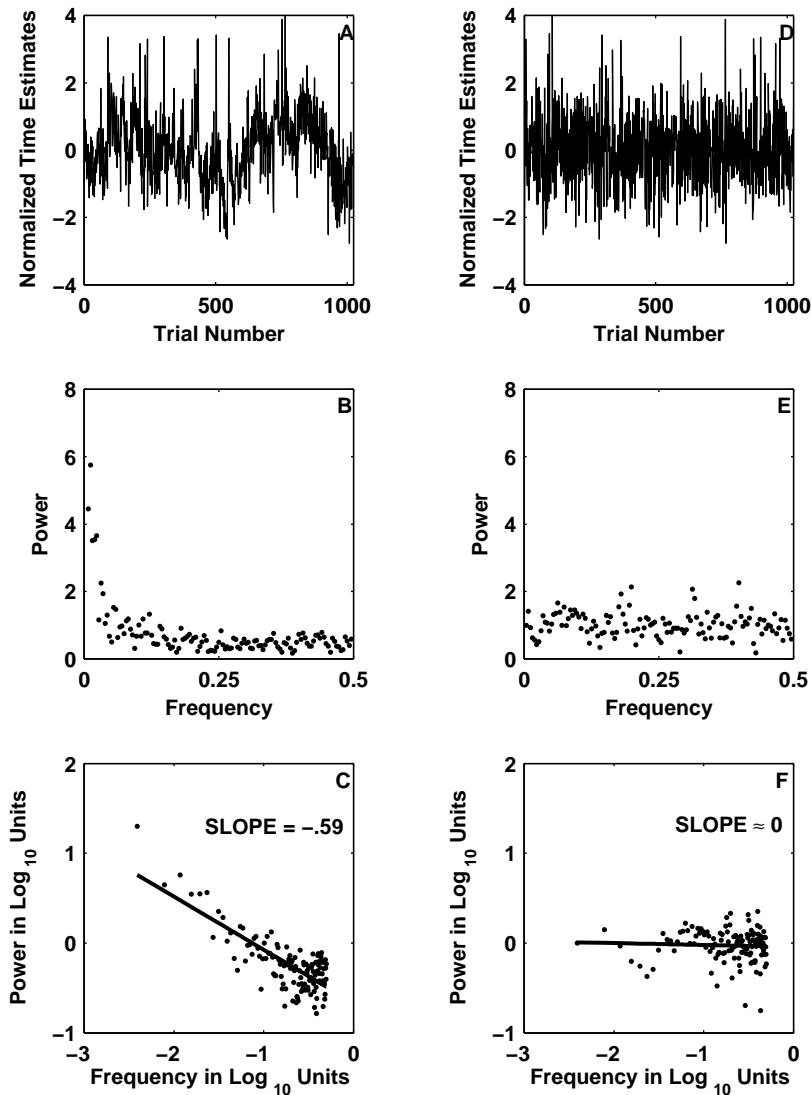


Figure 6.1. (A) A trimmed, detrended and normalized trial-series of 690 ms time interval estimates for a single participant. The x-axis indexes the successive trials in the experiment, the y-axis indexes the time interval judgments, relative to the overall mean and standard deviation of the trial series. (B) Results of a power spectral analysis, in linear units. Frequency is plotted on the x-axis, from lowest (near the origin) to highest. The y-axis indexes the power or relative energy of each frequency. Larger values indicate more power. (C) Results of the same spectral analysis plotted in (B), on double-logarithmic axes. The negatively accelerated linear relation, with a slope less than 0 but greater than  $-1$ , is consistent with pink noise. (D)-(F) The same succession of plots as (A) through (C) for a randomly reshuffled “surrogate” version of the data depicted in (A). Random reshuffling destroys the natural trial ordering and yields white noise. (E) depicts the spectral analysis of the white noise on a linear scale. There is no systematic variation in power as a function of frequency. This power spectrum is characteristic of white noise; all frequencies have roughly equal power. (F) depicts the same power spectrum on double-logarithmic coordinates. The slope of the regression line is approximately zero, which is consistent with white noise.

same shape—the notion of a nested structure of similar-shaped fluctuations.

If you are not sure you see this structure, simply compare Figure 6.1A with Figure 6.1D, which represents exactly the same data set depicted in Figure 6.1A, but where the order of the successive data points was randomly shuffled. The shuffling procedure destroyed the nested, statistically self-similar pattern of trial-to-trial fluctuations characteristic of pink noise. The random rearrangement of the series yields a pattern called *white noise*. Notice that just about any portion of the shuffled data series depicted in Figure 6.1D could be used as relatively good “stand-in” for any other portion of the series. This is not true for the trial-ordered data plotted in Figure 6.1A, for which most of the observations between trials 500-600 fall below the overall mean, while the majority of the observations between trials 800-900 fall above the overall mean.

The two different arrangements of the same data set are quite distinct, illustrating the difference between pink noise and white noise. For pink noise, the local means and standard deviations depend on where in the series the sample was taken. White noise indicates statistical independence from observation to observation, and local sample means and standard deviations do a good job of describing other local samples, and an overall population mean. This fact about white noise forms the cornerstone of inferential statistics, such as t-tests, analysis of variance (ANOVA), and regression.

In the context of response time research *pink noise* refers to a statistically self-similar (see Liebovitch, Chapter 5) pattern of trial-to-

Holden

trial variability. The pattern is structured such that persistent, long-term fluctuations across several hundred trials nest within themselves progressively smaller, proportionately scaled fluctuations across a few decades of trials. Nested within those fluctuations, one finds even smaller patterns of fluctuation, and so on. Pink noise is unexpected from the perspective of conventional statistical intuitions inherited from the standard linear statistical tools of behavioral science research. Those intuitions lead to an expectation that successive individual time judgments, decisions, or other elementary cognitive performances should vary unsystematically or randomly from trial to trial. That is, individual observations are assumed to be statistically independent. After all, it is properties of the presented stimulus that are conventionally assumed to be driving a participant's response, not aspects of the previous response.

Since Gildea et al.'s (1995) report, pink noise was uncovered in the trial-by-trial variability, or trial-series, of a wide range of standard cognitive psychology laboratory tasks that collect response times. Examples include simple reaction time, speeded word naming, choice reaction time, lexical decision, and mental rotation, among many others (e.g., Gildea, 1997; Kelly, Heathcote, Heath, & Longstaff, 2001; Van Orden et al., 2003). The pattern is not limited to cognitive activities; pink noise appears in measurements of human performance that use dependent measures other than response time, such as patterns of eye movements (Aks, Zelinsky, & Spratt, 2002), postural sway (Riley, Wong, Mitra, & Turvey, 1997), and self-reports of changes in mood over time (Delignières, Fortes, & Ninot, in press; see Gildea, 2001, and Van Orden et al., 2003, for reviews).

The goal of this chapter is to provide a primer to the geometric concepts and statistical techniques that are necessary to characterize pink noise in trial series of response time measurements derived from cognitive performances. The first step is to introduce three interrelated concepts from fractal geometry: *Self-similarity*, *scaling*, and *fractal dimension*. Those ideas motivate statistical analyses that are aimed at the identification of fractal patterns in data from empirical phenomena. A description of a simple temporal estimation task, modeled in large part after the method used by Gildea et al. (1995), follows the introductory sections. A trial-series resulting from the illustrative temporal estimation task is used to provide a practical context for a tutorial presentation of the statistical procedures involved in a fractal analysis of response time data, including spectral density estimation and fractal dimension estimation. Potential theoretical implications of pink noise are briefly discussed in the final section of the chapter.

## FRACTAL PATTERNS

### *Self-Similarity and Scaling*

Two key constructs in fractal geometry are pattern and self-similarity of pattern. The parts of fractal objects are composed, in some way, of copies of the whole object (Feder, 1988; Mandelbrot, 1982; see Liebovitch, Chapter 5). Ideal geometric fractals may be composed of exact replicas of the whole object—they are strictly self-similar. By contrast, statistical fractals are *self-affine*, or *statistically self-similar*; they are composed of statistically equivalent replicas of the whole object. Naturally occurring fractals usually exhibit statistical self-similarity.

Holden

A contrast between the left and right sides of Figure 6.2 illustrates this distinction. The left side of the figure depicts a Sieripinski Gasket, a classic mathematical fractal. It was generated by removing a white, smaller triangle, with vertices that fall at the midpoints of the sides of the largest, gray outer “initiator” triangle. Next, smaller similar white triangles were removed from the three new triangles that were formed, and their centers were, in turn, removed. The construction process can be continued indefinitely (see Peitgen, Jürgens, & Saupe, 1992, for details). The Sieripinski Gasket is comprised of smaller, exact copies of itself—it is strictly self-similar. The top panel on the right side of Figure 6.2 depicts 8192 observations of idealized pink noise, a statistical fractal. The middle panel “zooms in” on the center 4096 observations of the same series depicted in the top panel, and the bottom panel depicts the center 2048 observations that appeared in both the middle and top panels. When the x- and y-axes are appropriately scaled, the pieces of the series are visually and statistically indistinguishable from the overall series—pink noise is statistically self-similar, or *self-affine*.

Fractal patterns in nature are composed of nested forms that cannot be measured on a single scale of measurement. The result of a measurement depends on the scale, or *size* of the increment used to take the measurement (Bassingthwaight et al., 1994; Mandelbrot, 1982; Schroeder, 1991; see also Liebovitch, Chapter 5). For example, the measured length of the British coastline increases proportionally as the scale of the “yardstick” used for measurement is shortened from kilometers to meters. An even shorter, centimeter scale of measurement would result in a further proportional increase in the

## Fractal Variability in Cognitive Performance

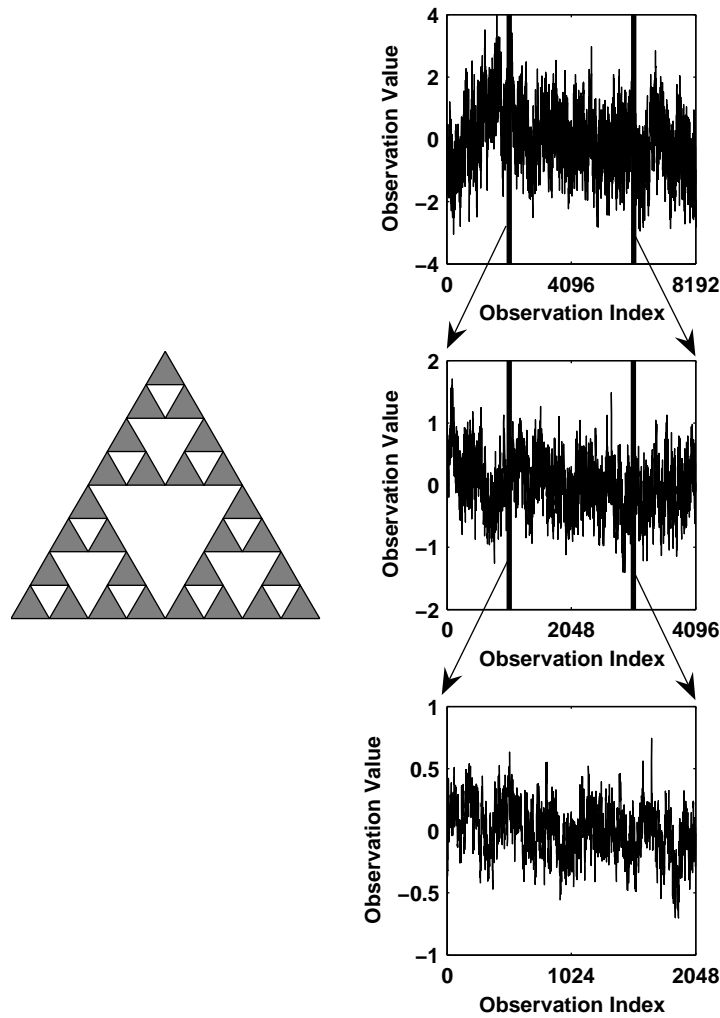


Figure 6.2. The object depicted on the left side of the figure is a classic self-similar mathematical fractal called a Sierpinski Gasket. It is generated by removing successive generations of triangles (white) from the centers of the gray triangles. The three panels on the right side of the figure illustrate how idealized pink noise is *statistically* self-similar. The middle panel zooms in on a piece of the series depicted in the top panel, and the lower panel zooms in on a piece of the series depicted in the middle panel. Each magnification of the pieces of the series results in a new series that looks essentially the same as the original series.

measured length of the coastline. The changing measurements arise as a consequence of using regular line segments, the yardstick, to approximate the irregular, nested, self-similar structure of coastal bays

Holden

and peninsulas. The length measurement increases when a bay or peninsula that was not captured at a lower resolution adds length at a higher resolution. Thus, as smaller and smaller sub-bays and sub-peninsulas are resolved, they add to the length of the coastline.

When measurements change as a function of measurement scale, there is no "true" or *characteristic* value for the measurement. The length of the British coastline grows in proportion to the precision of the yardstick used to measure length. This proportional power-law scaling relation between the size of the yardstick and the costal length implies that results of a measurement procedure depend on the measurement scale or sampling unit used to take the measurement (over a finite range of scales). A *power-law scaling relation*, a linear relation between the logarithm of the scale and the logarithm of the measurement result, is commonly observed in natural fractal phenomena, and is symptomatic of self-similar patterns (Bassingthwaight et al., 1994, Peitgen, Jürgens, & Saupe, 1992). It is the functional form of the scaling relation that, in turn, is used to describe and even model subtly different aspects of coastlines (e.g., Mandelbrot, 1982).

### ***Scaling in Statistics***

What is measured with a statistical sample depends on what statistic is computed on the sample of observations. A sample mean is a measure of location—the center or balance point of a distribution of observations. If the variability in the sample is unsystematically but symmetrically dispersed about the mean, and the observations are statistically independent of one another, then a sample mean identifies

a location on the number line of the dependent measure that best characterizes the level or amount of the measurement in the context of sampling error. For instance, mean response time is used to estimate the duration of time that passes between the presentation of a stimulus and the collection of a response in a response time task. However, response time distributions are typically positively skewed, and the pattern of pink noise implies that successive observations are not statistically independent.

Thus, patterns of variability constrain the utility of a sample mean as a point estimate of a location or amount. Dispersion measurements, like the standard deviation, are intimately linked to location measurements. They impart information about disagreement among the individual measurements, and indicate how much a measure of location, such as the mean, can be trusted.

Scale magnification makes intuitive sense for an object such as the coastline of Great Britain. The statistical counterpart to a measurement scale is sample size. Obtaining fewer statistical samples corresponds to using measurements at a lower resolution; larger or more numerous statistical samples correspond to measurements at a higher resolution.

At first, the relation between sample size and scale may not be obvious, but remember the example of Great Britain's coastline. The example helps to develop an intuitive analogy about what it means that no characteristic amount of variability may exist in response time data. The coastline scaling relation indicates that smaller spatial features are nested within larger spatial features. The key point to keep in mind

Holden

about the coastline is the measurement result (the length) depends on the scale used to take the measurement.

Statistically self-similar patterns of fluctuation affect statistical estimates of location and dispersion, like the mean and standard deviation or variance (see also Bassingthwaite et al., 1994, pp. 33-41). The answer to the question “how long” for a coastline is supplied in terms of a length measurement. The answer to the same question for a response time task is supplied by a parameter estimate, such as mean response time. In contrast to length scales, where the smallest units yield the most accurate measurements, larger sample-sizes—a larger  $N$ —corresponds to a more precise measurement scale in statistics. This may seem counterintuitive, but it is conventional to assume that certainty in estimates of a population parameter—parameter *resolution*—increases as sample sizes increase (i.e., the central limit theorem).

As mentioned, the ability of a statistic such as the mean to act as a gauge of location depends crucially on the inherent patterns of variability in the data. If the measurements emerge from a process with outputs that conform to standard statistical assumptions, those of the central limit theorem, for example, a sample mean can be trusted to reliably penetrate the variability and reveal increasingly reliable estimates of characteristic values—population parameters—as sample size is increased.

Nevertheless, another possibility exists. Suppose trial-by-trial response time measurements are comprised of a statistically-self similar pattern of positive correlation, where local patterns of

correlation, across just a few successive trials, are nested within increasingly more global and proportionally scaled (enlarged) patterns of positively correlated fluctuations, as broader and broader runs of consecutive trials are spanned. This is essentially a description of pink noise, and just as for the coastline, a change to a more detailed or inclusive scale yields essentially the same pattern that was observed at the less inclusive, lower-resolution scale.

Keeping in mind the analogy to the coastline, it is easier to begin to understand how nested patterns of fluctuation lead to counterintuitive statistical properties. The value of any given lower-resolution *locally* computed mean or standard deviation, that includes just a few adjacent samples, depends crucially on *where* in the trial-by-trial series it was taken—did it come from a waning “bay” or a waxing “peninsula,” for instance. Increasing the resolution of the sample by including more and more adjacent observations results in the inclusion of more and larger bays and peninsulas. The implication of each increase in sample resolution is the existence and inclusion of even larger scale fluctuations that reach well beyond the scope of each new, larger scale of resolution. Larger samples simply admit a broader range of variability. The resulting increase in variability created by widening the window of observation may *outpace* a sample statistic’s ability to stabilize about a particular *characteristic* value, in the normal way, through the process of aggregating larger and larger samples.

As such, the utility of the mean and standard deviation as simple measures of location and dispersion may be foiled because of the proportional, nested patterns of fluctuation. Different sample means and standard deviations, taken at different locations or times, would

Holden

tend to disagree in their location and dispersion estimates (up to the limits of the system or sample), resulting in a persistent heterogeneity, or disagreement among the sample statistics themselves. In this way, patterns of variability that are comprised of nested, interdependent, statistically self-similar fluctuations hamper the ability of these statistics to provide a uniform summary or gauge of certain kinds of data sets. Simply put, the concept of a *summary* statistic is not neatly applicable to a heterogeneous process.

All this is *not* to say that descriptive statistics such as the mean and standard deviation are not useful or applicable to fractal or nonlinear science—in many cases they are essential analytical tools. It is really only the semantics of those descriptive measures that is altered in the analysis of a fractal process. Additional and crucial statistical information resides at a higher level, in the manner in which the values of descriptive statistics change as sample size (i.e., measurement resolution) is systematically changed, rather than at the level of any particular summary value that uses a particular sample size. That is, the manner of disagreement across different sample sizes becomes a primary statistical gauge for a fractal analysis.

In the context of response time research, a *fractal dimension* analysis describes how response-time variability scales with sample size. Essentially, it is a statistical analysis that is analogous to taking measurements of a coastline's length using different ruler sizes and reporting how the length changes as the ruler size changes—the fractal dimension analysis determines a scaling relation between sample size and sample variability. The goal of the fractal dimension analysis is to describe the changes in the variability of a measurement across a

range of sample sizes (measurement resolutions) in terms of a power-law scaling relation.

### ***Fractal Dimension***

Self-similarity and self-affinity across multiple scales of resolution often gives rise to objects or patterns that occupy noninteger or *fractal* dimensions. Essentially, a *fractal dimension* refers to the spatial dimension of an object whose dimension falls between the standard Euclidean integer dimensions of one, two or three (see Bassingthwaite et al., 1994). Mandelbrot (1982) explained how the dimension of an object is partly determined by the perspective of the observer (the entry level of the analysis). A tautly stretched piece of thread closely resembles a *line*, an ideal one-dimensional Euclidean object. Tightly weaving the thread, back and forth, results in a piece of fabric, an ideal two-dimensional object. Thus, a *line* can be rearranged so that it occupies *area*. Rolling the thread onto a spool yields an object that occupies *volume* in *3-D space*. Of course, if the spool of thread is viewed from a great distance, its dimension appears to collapse to zero, a *point*.

One way to understand the link between Euclidean geometry and fractal geometry conceptually is to think of fractal geometry as a generalization or elaboration of the standard Euclidean geometry of lines, squares, cubes, and so on. Euclidean objects only occupy integer dimensions, 1 for a line, 2 for a square, and so on. Fractals, however, may occupy *noninteger* dimensions, dimensions that fall in between 1 and 2 or between 2 and 3. How can this be? Refer again to Figure 6.1A, the normalized series of temporal estimates graphed in the

Holden

order in which they were collected. They are points connected by a line. Clearly, if every successive time estimate was identical, connecting the points would form a line, and the series would have a Euclidean dimension of one. But any departure from the ideal form of a line begins to occupy or “leak into” the next higher (second, in this case) Euclidean dimension. It is in this spirit that fluctuations in trial-by-trial response times may be said to partly occupy or leak into the next higher Euclidean dimension. In a sense, the variability of time estimates results in the series occupying area, and it will have a dimension between an ideal one-dimensional line and an ideal two-dimensional area. The more jagged and irregular the graph of response times, the more area it occupies. It turns out that this intuitive continuum of relative jaggedness can be characterized formally with the help of a statistical procedure called dispersion analysis. Dispersion analysis results in an estimate of the *fractal dimension* of the trial series. The fractal dimension characterizes the structure of the intrinsic variability in the trial series.

Conventional statistical analyses presuppose that intrinsic variability is *white noise*. White noise yields a jagged and irregular line with a fractal dimension of 1.5, because successive observations are statistically independent of each other. Its fractal dimension indicates the extent to which white noise occupies 2-D space. White noise is uncorrelated noise. By contrast, the successive observations of pink noise tend to be positively correlated. This results in a less jagged trial series, and lower fractal dimensions that fall in the interval between 1 and 1.5.

## A SIMPLE TIMING EXPERIMENT

Data from a timing experiment is now used to demonstrate how to conduct statistical analyses that may uncover fractal patterns in trial series of response times. Except for the setting of trimming criteria, the required statistical techniques are the same for a host of standard cognitive tasks that record response time as a dependent measure. The laboratory protocol was modeled after Gilden et al.'s (1995) temporal judgment task. At the beginning of the experimental session each participant was presented with about one minute's worth of examples of a particular time interval. The time interval was illustrated by repeatedly flashing a simple visual stimulus on a standard PC monitor for the specified period of time. Each participant was then asked to attempt to replicate the example time interval as best as they could, 1100 times, in succession. Participants never received feedback about how accurate they were in their time estimates.

The method section that follows describes a study that replicated Gilden et al.'s (1995) essential finding of pink noise in trial series of temporal estimates. Since the purpose of this chapter is not to disseminate empirical results, but to supply a detailed "how to" tutorial on methods of fractal analysis, just a single participant's trial series is described in the results section (the series that appears in Figure 6.1A was used). The particular series was explicitly selected because it is a very clean and clear example of empirical pink noise; it lacks artifacts that sometimes appear in real-world data and that threaten to further complicate this introductory discussion.

Holden

### ***Method***

***Participants.*** One undergraduate psychology student participated in exchange for course credit.

***Procedure.*** The participant was given a one-minute sample of a target temporal interval. The sample intervals were constructed by presenting a visual stimulus (#####) at the center of a standard CRT monitor controlled by a PC running DMASTR software (Forster & Forster, 1996). The target interval duration was 690 ms or 50 monitor raster refresh cycles. The samples of the 690 ms time interval were generated by displaying the visual stimulus on the monitor for exactly 690 ms, then the monitor went blank for 690 ms, at which point the visual signal again appeared for 690 ms, and so on. The visual stimulus flashed on and off for about one minute. (There is nothing special about the 690 ms duration; the monitor's vertical raster-refresh rate was 72 Hz, or once every 13.8 ms, and 13.8 times 50 equals 690).

On each temporal estimation trial, the visual stimulus (#####) was displayed until the participant responded by saying "/ta/" into a microphone, or for a maximum of 10 s. The experimental task was paced by a computer. Each response was followed by a 690 ms inter-trial interval in which the computer monitor was blank. The participant was told to pace her responses so that the visual signal was displayed for the same time interval she saw during the one minute sample time interval session. The participant completed 25 practice trials immediately prior to completing 1100 experimental temporal estimation trials. The entire task took about 30 minutes to complete.

**Results**

Standard statistical analyses such as regression and ANOVA are typically used in a manner that either ignores the temporal order of the trials in an experiment, or that treats order as a nuisance factor. By contrast, the patterns of fluctuation that unfold across the successive experimental trials are the main focus of the fractal techniques introduced here. Thus, the analysis begins with the participant's trial series of temporal interval estimates *arranged in the order in which they were collected* (Trial 1, Trial 2 ... Trial 1099, Trial 1100).

As a practical matter, it is best to present enough trials in an experiment to be left with at least 1024 observations after any timed-out trials, extreme times, and outliers are removed. Presenting 1100 time-estimation trials left a healthy 76 trial "buffer." While it is possible, and potentially informative, to apply fractal techniques to data sets shorter than 1024 observations, the results of the analysis become less reliable as fewer and fewer data points are used. For example, the spectral slopes and the fractal dimension estimates, explained shortly, tend to become more variable as progressively shorter data sets are used (Cannon et al., 1997; Eke, Hermán, Kocsis, & Kozak, 2002). Additionally, the measurements should be collected as regularly in time as possible. A "lined up" series of measurements that were actually collected across different experimental sessions distorts the time scale, and the fractal analysis may not accurately characterize the temporal structure of the series.

**Trimming and Detrending.** Data trimming procedures are often required to bring the series of time estimates (a finite, irregular natural

Holden

object) more in line with the assumptions of spectral and dispersion analyses. The mathematics of spectral analysis assume an ideal, stationary, strictly periodic process of infinite duration. Dispersion techniques are less assumptive and more robust than spectral techniques but nevertheless ultimately assume that the measured process is at least *weakly stationary*—that its mean and standard deviation remain essentially the same over time (Caccia et al., 1997; Chatfield, 1996). If the trial series in hand happens to be a good example of pink noise, then its mean and standard deviation probably do fluctuate as a function of time, or trial.

In general, response time distributions are notorious for the fact that they often contain extreme observations, and the trial series of temporal estimates are essentially response time trial series. No matter their origin, a few extreme measurements or simple long-term trends will likely distort the outcome of a fractal analysis. It is important to note that the main issue surrounding the decision to remove extreme valued data points is not so much whether or not they represent legitimate measurements, as they certainly may. The issue is whether their inclusion will dominate and thus distort the outcome of the analysis.

Response time trial series typically require two censorship passes. The first pass eliminates times that exceed fixed extreme truncation values; different cognitive tasks require the use of different fixed truncation values. Reasonable truncation points can be identified by consulting the relevant literature for typical censorship values. Adopt conservative truncation values from that range as a starting point (err on the side of including more data). When truncating an

observation, just delete it and “close up” the series so that the deleted observation’s two immediate neighbors themselves become neighbors. While this procedure slightly disrupts the time-ordering of the series, its overall impact on the analysis is usually minimal. To best preserve the trial order, response times on trials that produced an error in, for example, a choice response time task, should be included in the trial series (see Gilden, 1997).

The main purpose of fixed-value censorship is to facilitate a second pass through the data, which uses the series mean and standard deviation as a censorship origin. For temporal interval estimates, nine observations were less than 100 ms or greater than 3500 ms and were removed. Then the series mean and standard deviation were computed. On the second censorship pass, 13 observations that fell beyond  $\pm 3$  standard deviations from the series’ mean were eliminated.

The dispersion analysis, as described below, *requires* the number of observations to be an integer power of 2 (e.g.,  $2^{10} = 1024$ ). While spectral techniques do not always strictly require a series to be an integer power of 2 in length, the algorithms work faster when the data series is an integer power of 2, and some computer implementations of spectral routines do require the series to be an integer power of 2 in length. The two censorship passes eliminated 22 observations, for a total of 1078 remaining observations. The first 54 observations were then eliminated to yield a series that was 1024 observations in length.

Trial series that display self-similar patterns of fluctuation are expected to display nonstationary drift (i.e., trends) at all scales. It can,

Holden

however, be difficult to distinguish simple long term trends, or a very-low frequency periodic oscillation from a nested, fractal pattern of long range fluctuations in empirical data sets (Hausdorff et al., 1996). This difficulty again arises from the fact that real data sets have a finite length. A linear trend at the scale of the whole data set could be either a simple linear trend, or a small piece of a fractal pattern of fluctuation that expresses itself across scales that run far beyond the duration of the particular sample of the process at hand. What appears as a linear trend across 1024 observations could be just that, or it could be part of a proportionately scaled fractal fluctuation that runs across 2000-3000 observations. Without the extra data, it is impossible to tell which option is a better description of reality. Only fluctuations that live on scales somewhat smaller than the full length of the series can be resolved clearly enough (i.e. statistically) to determine whether they are consistent with a nested fractal pattern of fluctuation.

Most importantly, simple long-term trends not only have the potential to bias estimates of spectral slopes and fractal dimension, they may also overwhelm the analyses, and yield spurious spectral slopes and fractal dimension statistics (Caccia et al., 1997; Hausdorff et al., 1996). As such, it is prudent to remove at least linear and quadratic trends before conducting the analysis. As a general rule, if the trial series has fractal structure, progressively more liberal detrending procedures will not result in dramatic changes in the overall fractal dimension estimates (Hausdorff et al., 1996). Nevertheless, detrending does eliminate variability at the larger scales, in the neighborhood of the size of the entire series, and any fractal dimension estimation procedure, like those presented later, must be tuned to accommodate

this fact. Otherwise, the detrending introduces its own bias. For the timing trial series trends up to a quadratic were removed. The basic detrending procedure involves generating a least squares linear and quadratic fit to the series, using the index of observation as the  $x$  variable and the temporal estimate as the  $y$  variable. One way to do this is to use the method of Powered Vectors, in conjunction with Hierarchical Regression (Keppel & Zedeck, 1989), which can be coded on a spreadsheet or accomplished with standard statistical software.

The final preparatory step is to normalize the series to have a mean of zero and a variance of one. That is, transform the data points into  $z$ -scores by subtracting the series mean from each observation, and dividing each observation by the series standard deviation (SD). Use the *population* formula for the SD and divide by  $N$ , the number of data points in the series, rather than the usual bias-corrected  $N - 1$ . The descriptions of the spectral analysis and the dispersion analysis that follow assume the data sets are already in this format.

*Spectral Analysis.* Spectral analysis techniques provide a general way of characterizing the correlational structure of fluctuations in a series of successive response time measurements (Gilden et al., 1995; Gilden, 1997). There are several kinds of spectral techniques; what is referred to here as a spectral analysis is a particular method called power spectral density estimation, which yields a power spectrum of a trial series.

Successful applications of spectral methods require a certain amount of care, sophistication, and background knowledge. Accessible introductions to spectral techniques are provided by

Holden

Gottman (1981) and Chattfield (1996). Press, Teukolsky, Vetterling, and Flannery (1992) describe "how to" information as well as provide source computer code for the analyses. The information presented in Press et al. is rather technical but nevertheless very helpful. In fact, much of the information presented below is adapted from more formal treatments of the same topics in Press et al.

With the exception of the censored observations, each participant's trial series of time estimates is now ordered according to the trial on which the observation was collected—the order of the successive trials in the experiment. Connecting the points that represent the successive time estimates forms a complex waveform, as in Figure 6.1A. In a sense, a power spectral density analysis decomposes a trial series much as a prism breaks white light into its basic wavelengths, or colors. Spectral analyses decompose a trial series into a set of regular oscillations, component waves with particular frequencies and amplitudes. Taken together, the component waves mimic the overall pattern of oscillation in the observed trial series. An intuitive grasp of spectral analysis may be gleaned by thinking of it as a multiple regression analysis that fits a large set of simple sine (and/or cosine) waves to the complex response time waveform. The period of oscillation (the inverse of frequency) and the amplitude (relative height) of each component wave can vary. Oscillations corresponding to quickly changing trial-to-trial "jitter" map to a high frequency wave. Persistent excursions in one direction or the other from the mean of the trial series, over the course of, say, tens to hundreds of trials, map to lower and lower frequency oscillations. The output of a spectral analysis is a set of coefficients that characterize the

relative amplitudes of all the wave forms, ordered from lowest to highest frequency. This output is called the *power spectrum* of the signal. Loosely speaking, the spectral density coefficients correspond to a relative sum of squares for each frequency of sine wave that is used to fit the trial series. This is a bit like an  $r^2$  for each sine wave that was passed through, or fit to, the series. Frequencies with larger amplitude coefficients imply more of the total variability was attributed to that particular frequency of oscillation.

As described, this basic recipe for a spectral decomposition procedure yields estimates of the amplitude (relative strength or energy) of many sinusoidal frequencies, but there is little statistical certainty in the magnitudes of any one of them. Each amplitude estimate is derived from just a single pass or "fit" of an individual ideal sine wave. Like any other statistical sample, the coefficient resulting from that fit can be unduly influenced by idiosyncratic properties of the data set in hand. Put differently, the standard deviation of each amplitude estimate for each particular frequency is huge—100% of its value (Press et al., 1992). Increasing the number of data points by using progressively longer data series only allows more and more frequencies to be estimated. A straight spectral density analysis always yields about half as many frequencies as there are data points (the highest resolvable frequency oscillates back and forth on every other data point). Thus, analyzing the entire data sequence at once yields maximum frequency resolution (many different sized sine waves are approximated), but does not lower the variability in the estimate of the amplitude for any particular frequency (see Press et al.). In terms of statistical certainty, the output is about as trustworthy as a factorial

Holden

ANOVA that has many, many experimental cells, but each cell mean is based on just one data point.

For data sets as variable as response time trial series, the procedures for computing a power spectrum must be adapted to balance the need to identify fluctuations over a suitably wide range of frequencies while simultaneously minimizing error variance in the estimation of the magnitude of any particular frequency. This is accomplished by breaking a single long 1024-trial series into several shorter, overlapping series of response times. This procedure is called data segmenting or data blocking. The individual power spectra derived from each short sub-series are then averaged. The averaging reduces the variability in the power spectral density estimate at each frequency; the cost is a reduction in the maximum number of frequencies that may be estimated.

Finally, the mathematics that govern the translation from the *time domain* (the trial-by-trial representation of the data) into the *frequency domain* (the frequency-by-frequency representation of the data) require the use of a procedure called *data windowing*. Essentially, a difficulty emerges from the fact that real data sets have distinct beginnings and ends, but the mathematics of spectral analysis assumes a data set of infinite length that is, more or less, strictly periodic. The consequence of this mismatch is a tendency for the power or energy associated with any particular frequency to "reverberate" or be blurred into the amplitude estimates of nearby frequencies. A typical data window applies a weighting function to the segment of the trial series that is undergoing spectral analysis. Data windows are designed to smooth the transition into and out of the data, and work something like

slowly turning up “volume” of the data starting at the beginning of the series, until it is at a maximum at the center of the series, and then slowly turning it down to zero again by the end of the sample (see Press et al., 1992 for details). The data blocking, spectral density averaging, and data windowing procedures, or similar statistical fixes that address the same issues, are often available as standard options in many spectral analysis computer routines.

If you are using a spectral density routine that returns the frequencies and power (the square of the absolute value of each amplitude) in linear units, the first step is to delete the highest (Nyquist) and lowest frequency (DC) coefficients, and then to transform the remaining coefficients by taking the log, base 10, of each frequency and its corresponding power estimate. Plot log-frequency against log-amplitude in a scatter plot. Reasonable evidence for inverse power-law scaling in the form of pink noise appears as a negatively sloped linear relation between the two variables on the log-log scatterplot. The linear relation must span a range of *at least* 2 decades of frequency (i.e., 2 log units, or 100 frequencies; Eke et al., 2000, 2002). Since natural fractals exhibit self-affinity across only a finite range of scales, the inverse power-law scaling relation may break down at either the highest or lowest frequencies, or both. It is also notable that the strength of the linear relation trades off with the number of frequencies that are used in the analysis. For a given series length, estimating the amplitudes of more frequencies typically yields a wider scatter of points in the log-log scatter plot. This is a consequence of the issues relating to the statistical certainty in the spectral coefficients, as was discussed previously.

Holden

The next step is to determine the value of the scaling exponent, the  $\alpha$  in the scaling relation  $1/f^\alpha$  (where  $f$  denotes frequency). The scaling exponent describes how the amplitude of the fluctuations change or scales as a function of their frequency. The easiest way to estimate  $\alpha$  is to determine the slope of a least-squares regression of power as a function of frequency, using the logarithmically transformed values. (Technically, it is more correct to fit a least-squares power law in the linear domain but few researchers feel this extra step is critical). The slope of the regression line is the scaling exponent  $\alpha$ . Response time series usually yield negatively accelerated slopes (recall that  $1/f^\alpha = f^{-\alpha}$ ) that, within certain boundary conditions, discussed later, indicate pink noise, or slopes that are statistically equivalent to zero, which suggests white noise.

One additional difficulty with the spectral method is that the high frequency portion of the power spectrum can sometimes be “whitened,” which appears either as flattening to zero slope at the highest frequencies or as combination of linear and U-shaped quadratic trends in the log-log regression that looks a bit like a tilted and mirror-reversed J. Figure 6.1C and Gildden et al.’s (1995) plots for the shorter time estimates display evidence of this pattern. The flattening at high frequencies may simply indicate a breakdown in the scaling relation at the highest frequencies, but in response time trial series it was linked to issues related to experimental design and measurement procedures that add sources of white noise to the signal (Gildden et al., 1995; Gildden, 1997; Gildden, 2001; Van Orden et al., 2003). For instance, very high frequency oscillations that unfold on a pace *faster* than the trial-by-trial pace of measurement may be “aliased” into the power of measured

frequencies. That tends to whiten the high-frequency end of a  $1/f$  spectrum. *Aliased* frequencies refer to oscillations that live outside of the measured frequency range, and that are misinterpreted by the spectral analysis as different frequencies that fall within the measured range of frequencies (Press et al., 1992). It is similar to the way a person dancing in relative dark under a regularly flashing strobe light can be perceived as not moving, or to the apparent, but false, appearance of backward rotation of spoked wheels that one sometimes notices in old films. Excluding the highest frequencies in the log-log regression is often recommended to avoid the whitening of the high-frequency end (Eke et al., 2000, 2002).

The details of how the spectral analysis on the temporal estimates were conducted on the trial series appearing in Figure 6.1A can be summarized as follows. The spectral analyses resulted from averages of seven successive power spectra computations taken across successive sub-blocks of 256 trials. Each sub-block was multiplied by a triangular (Bartlett) window and the power spectrum was computed. The trial series was then shifted by 128 trials ( $1/2$  the sub-block length) and a new power spectrum was computed. This process was repeated until the end of the series was reached. Thus, the power spectrum resulting from each participant's trial series was based on an average of seven (semi-independent) samples of the data set. This process yielded estimates of 129 ( $n/2 + 1$ ) frequencies, but the highest and the lowest frequency were dropped, resulting in a total of 127 frequencies.

Figure 6.1B displays the results of the spectral analysis on linear scales. The x-axis depicts frequency, ranging from low to high. The y-axis depicts power, the square of the absolute value of each amplitude.

Holden

Figure 6.1C displays the results of same spectral analysis, now depicted on log-log scales. The approximately linear relation between the two variables in the log-log domain implies an inverse power-law scaling relation, consistent with pink noise. The slope of the regression line is  $-0.59$ , which corresponds to a  $1/f^{0.59}$  scaling relation. Note, however, that the highest frequencies in Figure 6.1C seem to be slightly “whitened,” which introduces a slight quadratic trend to the power spectrum and a slight bias in the slope of the regression line toward a shallower value. This pattern could justify eliminating the highest frequencies from the regression line by fitting only the lowest 25% of the frequencies, for instance. As expected, excluding the whitened higher frequencies yields a steeper spectral slope of  $-0.86$ .

As an additional check, it is important to recompute the spectral analysis using both more and fewer frequencies, and see comparable results. Analyses that use fewer frequencies should better resolve the linear nature of the scaling relation, and analyses using more frequencies should suggest that the scaling relation reaches into the lower frequencies, but it is critical to eliminate the detrending steps when examining the coefficients for lowest frequencies. The presented analysis, using 127 frequencies, reflects a compromise between the need for a satisfactory level of statistical certainty in the spectral coefficients (by examining frequencies that correspond to scales no larger than  $1/4$  the length of the series) and the need to establish the scaling range across at least 2 decades of frequencies.

Assuming a lack of evidence for white noise, the main reason for conducting a spectral analysis is to determine whether the value of the slope of the log-log regression line lies very near or less than  $-1$ , which

marks the boundary between a stationary fractional Gaussian noise and a nonstationary fractional Brownian motion. Dispersion analysis more accurately characterizes the fractal structure of a trial series than spectral analysis, but it can only be used on approximately or weakly stationary data sets. In this regard, idealized pink noise, with a spectral slope of  $-1$ , marks the boundary between mathematically stationary and nonstationary trial series. Fractional Brownian motions are nonstationary, and require other techniques, such as detrended fluctuation analysis (Peng, Havlin, Stanley, & Goldberger, 1995), which can be used on fractional Gaussian noise as well, or rescaled range analysis (Cannon et al., 1997). Those techniques are closely related to dispersion methods, but they will not be covered in this chapter. Response times often yield scaling exponents suggesting pink noise, and indicate that dispersion analysis is appropriate to determine the fractal dimension of the series. Next, the spectral slopes that define fractional Gaussian noise and fractional Brownian motions are described in detail.

***Variability Categories.*** The magnitude of the power-law scaling exponent circumscribes at least two general classes of temporal variability that are called ***fractional Gaussian noise*** (fGn) and ***fractional Brownian motion*** (fBm) (see Mandelbrot & Wallis, 1969a/2000; Eke et al., 2000, 2002). Collectively, they are often referred to as  $1/f^\alpha$  noise. The original theoretical development of these ideas used Gaussian-shaped probability density functions, but the classifications generalize to empirical data that have non-Gaussian density functions (Mandelbrot & Wallis, 1969c/2000).

Figure 6.3 illustrates how fGn and fBm can be described using the spectral slope of the power-law scaling relation. fGn exhibits log-log spectral slopes that range between 1 and  $-1$ . A slope of 0 indicates no historical dependence—-independent sources of random variation, or *white noise*. Slopes reliably greater than 0 and less than 1 indicate a tendency for positive data values to be followed by negative values, which is termed *anti-persistence*; this is sometimes called *blue noise*. Slopes less than 0 and greater than  $-1$  indicate *persistence*—positive data values tend to be followed by positive data values. This is the domain of *pink noise*, the main topic of this chapter. Assuming the log-log regression is linear across 2 or more decades (log units) of frequency, pink noise is simply a statistically reliable departure from white noise in the direction of persistence, evaluated using a combination of spectral and fractal analyses.

Spectral slopes less than  $-1$  and greater than  $-3$  describe a related but fundamentally different kind of variability called fractional Brownian motion. This is the domain of *random walks*. A spectral slope of  $-2$  indicates idealized Brownian motion. Slopes less than  $-1$  but greater than  $-2$  indicate anti-persistent fractional Brownian motion, in which successive increments tend to have opposite signs. Slopes between  $-2$  and  $-3$  indicate persistent fractional Brownian motion, in which successive increments tend to have the same sign (this is sometimes called *black noise*). Notably, a single parameter characterizes this entire family of noises.

Idealized pink noise, or  $1/f^1$  noise, is special mainly because when the x- and y-axes of a  $1/f^1$  noise are enlarged in like proportions; the enlarged portion of the series is statistically indistinguishable from

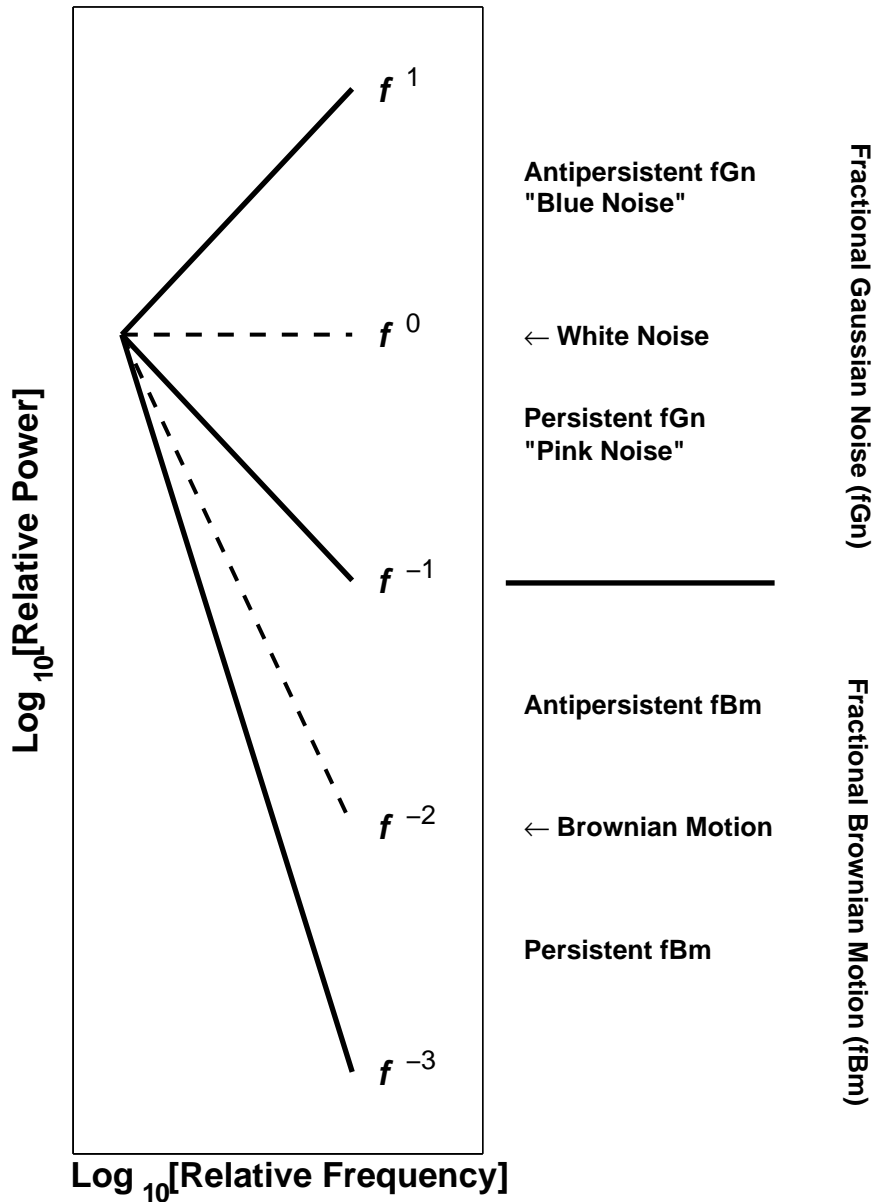


Figure 6.3. The figure adapted from Eke et al. (2000) portrays an idealization of spectral slopes that distinguish fractional Gaussian noises (fGn) and fractional Brownian motions (fBm) (see also Cannon et al., 1997). Idealized pink noise, or  $1/f^1$  noise, is special as a mathematical way-point; it marks the boundary between stationary (fGn) and nonstationary (fBm) data series, two categorically distinct kinds of variability (Eke et al., 2000, 2002).

Holden

the original series. Pink noise that has a scaling exponent that falls between 0 and 1 requires the x- and y-axes to be enlarged in *different* proportions to yield the same effect (Eke et al., 2000, 2002). Idealized pink noise is also important as a mathematical way-point, as it marks the analytic boundary between stationary and nonstationary data series. Idealized pink noise, and data series with scaling spectral slopes less than  $-1$ , have in theory, and in practice, *infinite variance*. Pink noise with nontrivial spectral slopes less than  $-1$  has infinite variance *in practice*, in the sense that the interdependence of finite statistical samples yields unreliable population parameters (Bassingthwaite et al., 1994; Mandelbrot & Wallis 1969b/2000). Thus, a spectral slope of  $-1$  marks an important boundary between two categorically distinct kinds of variability, fGn and fBm (Eke et al., 2000, 2002).

Many natural systems emit pink noise, but spectral slopes of exactly  $-1$  are not usually observed. Heart rate variability can exhibit a spectral slope very near  $-1$  (e.g., Eke et. al., 2002), but many established examples display slopes between 0 and  $-1$ . A large sample of yearly tree ring indices has average spectral slopes of  $-0.43$ . Annual precipitation statistics have average slopes of  $-0.48$ . The classic Nile River yearly minimum series yields a spectral slope of  $-0.82$  while measurements of the Nile's yearly maximum levels display a slope of about  $-0.68$  (Mandelbrot & Wallis, 1969b/2002). Natural phenomena entail sources of unsystematic external variability, in addition to sources of intrinsic  $1/f$  scaling, which results naturally in pink noise with spectral slopes greater than  $-1$ .

Typically, response times from elementary cognitive tasks, such as temporal estimation, yield scaling exponents that fall within the range of 0-1, and thus contain a nested, statistically self-similar pattern of positive correlation across successive observations. Spectral slopes that lie near  $-1$  suggest that the nested structure of positive correlation dominates the series. Spectral slopes that lie closer to zero indicate a less prominent, "whitened" structure of nested positive correlation across the series.

Next, a statistical technique called dispersion analysis is introduced. It more accurately characterizes the pattern of statistical self-similarity than spectral analysis. It yields a fractal dimension statistic (FD), which is closely related to the slope of the power spectrum. In fact,  $FD = 1 + (S + 1)/2$ , where  $S$  is the spectral slope, of the log-log regression line. This formula assumes the spectral slope of the series falls between  $-1$  and  $0$ . Note, however, that since the two analyses "break up" the trial series in mathematically different ways (e.g., Fourier analysis versus means and standard deviations) they will not typically output exactly the same fractal dimension for the exact same signal, although they should yield reasonably similar outcomes. If there is a strong disagreement between the two methods, examine the signal, and the steps in the analysis, carefully for potential artifacts.

***Dispersion Analysis.*** Dispersion analysis yields the fractal dimension of a trial series and gauges the change in variability due to changing sample sizes. Dispersion analysis determines whether the trial series variability converges fast enough, as sample size increases, to yield stable statistical estimates of population parameters. If not, then the process that produced the variability is, in practical terms,

Holden

scale free in the sense that it has no characteristic “quantity” or scale of variability.

There are several ways to compute the fractal dimension, and dispersion techniques are among the most accurate (Bassingthwaight et al., 1994; Caccia et al., 1997; Eke et al., 2000, 2002). Spectral analyses yield less reliable fractal dimension estimates than dispersion methods. A practical advantage of dispersion analysis is that familiar statistical constructs, means and standard deviations, are used for the analysis. A version of the standard technique of *relative dispersion analysis* is presented here. It allows for the use of normalized data instead of raw data—call this *standardized dispersion analysis* to avoid confusion with other methods. Note that the standardized dispersion analysis yields dispersion measurements that are in units of the standard error of the mean; the standard deviation of a sampling distribution of means, comprised of means of (adjacent) samples of specified sizes. By contrast, the original method described by Bassingthwaight et al. is based on the relative dispersion statistic that is comprised of a ratio of the standard deviation and the mean (i.e.  $RD = SD/M$ ). The outcomes of the two techniques are identical. However, the spectral technique presented earlier assumes a normalized trial-series and standardized dispersion analysis allows the same detrended and normalized data set to be submitted to both analyses.

When computing the dispersion statistics in the subsequent steps, compute the standard deviation using the population formula (i.e. use  $N$ , the number of data points, in the calculation, rather than the usual bias corrected  $N - 1$ ).

A dispersion analysis repeatedly resamples the trial series using sampling units of different sizes to estimate the fractal dimension of a trial-series. In the steps that follow, variability is gauged using the standard deviation of means of progressively larger adjacent samples. That is, the analysis tracks how variability in sample means decrease as progressively larger samples of adjacent data points are aggregated together in a sample mean. If the samples are statistically independent, then it should not matter that adjacent samples are being grouped and regrouped to form samples of different sizes.

To perform the analysis first construct a table, like Table 6.1. Begin the table by recording a 1 in the points-per-bin column and another 1 in the dispersion column. The overall standard deviation ( $SD = 1$ ) of the normalized series represents the overall dispersion of the series, given that the data points are treated individually. Essentially, the overall trial series standard deviation is treated as a population parameter, and for this initial step,  $N$  is also 1. The overall standard deviation is identical to the variability of a sampling distribution of 1024 “means,” computed across single, individual observations, which is just the raw score standard deviation.

The next step involves grouping the data points into adjacent pairs, which makes it more obvious that variability in the means of sample bins is being tracked. Compute the mean for each successive pair of points—*each bin*. This yields the new set of data points; a sampling distribution of means that contains the 512 values of each 2-point mean. Compute the standard deviation of this new distribution. Enter a 2 in the points-per-bin column of the table, because 2 point sample means were used. Then enter the standard deviation of the

Holden

sample means in the dispersion column. If the trial series were composed of statistically independent observations, then the expected standard deviation of the sampling distribution of the 512 two-point means would be  $1/\sqrt{2}$  or about 0.71. Interested readers may consult Van Orden et al. (2003) for an explanation of the relation between the standardized dispersion statistic and the equation for the standard error of the mean.

Table 6.1: Standardized dispersion as a function of sample bin size in linear and logarithmic units.

Bin Size	Standardized Dispersion	Log <sub>10</sub> (Bin Size)	Log <sub>10</sub> (Standardized Dispersion)
1	1	0	0
2	0.88	0.30	-0.06
4	0.79	0.60	-0.10
8	0.73	0.90	-0.14
16	0.68	1.20	-0.17
32	0.60	1.51	-0.22
64	0.54	1.81	-0.27
128	0.47	2.11	-0.32
256	0.15	2.41	-0.82
512	0.02	2.71	-1.68

Repeat the previous step until only two data points are left (i.e., the third iteration will use 256 bins of every four successive data points, the fourth iteration uses 128 bins of size eight, and so on, until there are two bins of size 512). At the culmination of each step, enter the number

of points that comprises each bin, and the standard deviation of the distribution of the sample means into the table. In the final repetition, the final two data points come from a bin containing the first half of the original trial series and a bin containing the last half. To summarize: Each step in constructing the table generates an  $N$  that is equal to the bin size and a standard deviation that estimates dispersion at that bin size. If the trial series was a series of statistically independent data points, then the standard deviation should diminish very nearly as a function of  $1/\sqrt{N}$ , as the size of the sample bin sizes are progressively increased.

Finally, plot the logarithm of the numbers in the points-per-bin column against the logarithm of the numbers in the standard deviation column as in Figure 6.2. Base-10 logarithms were used here, but other bases also work. For instance, using base 2 represents the number of samples in the bins as integer powers of 2—just be sure to use the same base for taking the log of the dispersion values as well. The relation between the two variables should be linear on double-log scales, except perhaps for the three or four points that correspond to the largest bins. Typically, the last few relative dispersion measurements that correspond to the very largest bin sizes are excluded at this point (Cannon et al., 1997); this is a critical adjustment when detrending is used. Here, the three largest bins were excluded because the detrending procedures removed the variability at these scales. Natural fractals exhibit scaling relations across a finite range of scales, so the linear relation is expected to break down at some point, for either (or both) the smallest or largest bin sizes. (Points excluded in the log-log regression in Figure 6.2 appear as open circles.) If using a

Holden

standardized series the dispersion values at the largest bin size approach zero (and negative infinity when the log transformation is performed). As such, they bias the slope of the regression line (see Caccia et al., 1997, for additional refinements of this technique, especially for shorter data sets).

A linear relation with a negative slope in log-log coordinates establishes an inverse power-law scaling relation and indicates that the trial series is a simple fractal (Bassingwaighte et al., 1994). The fractal dimension of the series is given by subtracting the slope of the least-squares regression line from one, the Euclidean dimension of the series. The relation illustrated in Figure 6.4 is an inverse power-law scaling relation. The slope of the log-log regression line is  $-0.14$ , and the fractal dimension of this trial series is therefore  $1.14$ . Transforming the spectral slope of  $-0.59$  into a fractal dimension yields  $1.21$ ; although those values are not identical, they are in the same neighborhood. Also recall that the spectral plot revealed evidence that the high-frequencies were “whitened,” which tends to bias the spectral slope towards shallower slopes, and thus, larger fractal dimensions. For instance, returning to the spectral coefficients and fitting only the lowest 25% of the power spectrum coefficients yields a spectral slope of  $-0.86$ , which translates to a FD of  $1.07$ .

At this point, a reader might ask him or herself, which characterization is the correct one? It is important to be mindful of the fact that each method of analysis has strengths and susceptibilities. For example, the spectral methods are sensitive to a host of artifacts that affect the high-end of the frequency range, but dispersion analysis is not as susceptible to these influences since it is not based on a Fourier

## Fractal Variability in Cognitive Performance

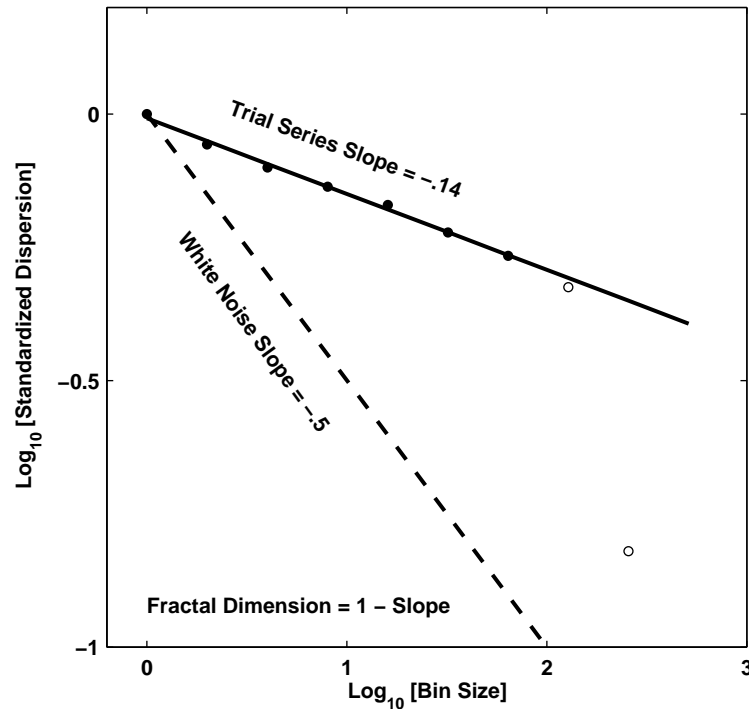


Figure 6.4. Standardized dispersion is depicted as a function of sample-bin size, on double logarithmic scales. The x-axis indexes the base-10 logarithm of the number of adjacent data points in each adjacent sample bin. The y-axis indicates the base-10 logarithm of the standard deviation of the mean standardized dispersion measures, across all the sample bins. The solid line is a least-squares regression line for the first 7 data points, represented by the solid points. The three points depicted as open circles correspond to the three largest bins and were not included in the regression analysis because the detrending procedures tends to eliminate variability at those larger scales. The open circle corresponding to the 2 largest 512 point bins is not shown because it fell below the limit of the y-axis.

transform. Moreover, the earlier discussion of spectral analysis illustrates that the raw data is subjected to a series of transformations to yield a spectral slope. Dispersion analysis, on the other hand, can be unduly influenced by simple linear trends that span the full length of the series. Dispersion analysis has been shown to lose some of its accuracy in characterizing time series that display very strong

Holden

interdependence, such as pink noise with a spectral slope near  $-1$ , (Eke et al., 2000, 2002), which are essentially nonstationary signals in the case of limited sample sizes. Dispersion analysis should not be used on fBm series, which are truly nonstationary signals.

Most importantly, both methods should yield solid, converging evidence of the presence of a power-law scaling relation. All other things being equal, the fractal dimension based on the dispersion method is more accurate, but it would not be unreasonable to report an average across these two, or perhaps additional methods in research reports. Notice the complementary nature of the two analyses; spectral methods are reliable at the intermediate and larger scales (the intermediate and lower frequencies), while dispersion methods are reliable at the intermediate and smaller scales (medium and higher frequencies).

The take-home point is that both spectral and dispersion methods decompose the raw data in different ways, and thus interact with the idiosyncrasies of a given empirical signal in slightly different ways. In addition, both analyses require the researcher to make a number of choices about a range of parameters, such as the manner of detrending, the number of spectral coefficients or bin sizes to fit with a regression line, and so on. Each choice will impact the outcome of the analysis in some way, at least compared to other choices that could have been made. As such, both methods should agree qualitatively, and yield similar, but not necessarily identical, fractal dimension estimates. Redoing the analysis using other parameter choices may change the value of the fractal dimension statistics somewhat, but it will typically do so in a systematic manner (e.g., fitting the whole spectrum

often yields shallower spectral slopes). As long as the fractal description survives trivial changes in the parameters that are used to govern the analysis (e.g., dropping the 3 or 4 largest bins in the dispersion analysis or fitting the entire spectrum versus the lowest 25%-30% of the spectrum), it is likely accurate. It is then up to the researcher to present a succinct, conservative analyses that, in his or her best judgment, accurately portrays the data at hand.

*Significance Testing.* There are two general kinds of statistical tests that one may want to conduct on the fractal dimension or spectral slopes resulting from the analyses discussed earlier. The first situation involves experimental research designs that entail contrasts between two or more conditions, and standard linear statistical methods such as a t-test or ANOVA (or nonparametric equivalents) can be used to establish differences in fractal dimension across groups. However, such comparisons must be carefully considered. Simple issues of measurement affect the fractal dimension and spectral slope of trial series arising from different tasks (e.g., Van Orden et al., 2003), so the fact of a statistically significant difference across tasks may not point to a theoretically interesting difference.

The second, and perhaps more novel, approach is to determine whether white noise or pink noise better describes an observed trial series. There are a number of ways that one or several trial series can be statistically distinguished from white noise. If a reasonably sized distribution of slope or fractal dimension estimates is available from several subjects, a single sample t-test could be used to determine if the sample mean of the spectral slopes is significantly different from 0, the expected slope of white noise (or if the fractal dimension differs

Holden

from 1.5). If only a single trial series is available, then one can easily test for a significant departure from a pattern of white noise by contrasting the observed data with surrogate data sets (e.g., the reshuffled data in Figure 6.1D.). Simply randomly reshuffle the order of the original trial-series, 10 or 20 times, each time computing the fractal dimension and/or spectral slope of each reshuffled version of the trial-series. Then calculate the fractal dimension mean and SD of the surrogate data sets and compare the mean to the observed values of the original series. If the fractal dimension and spectral slope of original series is in the pink noise range, and more than 3 SD away from the mean of the surrogates, then a null hypothesis of white noise can be rejected (Hausdorff, 1996; see Theiler et al., 1992, and Efron & Tibshirani, 1993, for more details and options).

## DISCUSSION

At first glance, Gilden et al.'s (1995) original temporal estimation task appears to be directed at understanding a person's ability to replicate a range of fixed time intervals. Thus, one might expect it to include an extensive discussion of how well or poorly people performed, but accuracy was barely mentioned in their report. The focus was instead on the structure of intrinsic patterns of trial-by-trial variability.

Conventional research methods in psychology emphasize a "cause-effect" metaphor as the only sensible route to scientific understanding. Experimental manipulations are introduced as a way of bringing empirical phenomena under experimental control. Thus,

factorial manipulations are designed to control empirical “effects.” Perhaps one experiment is designed to amplify an experimental effect, and another design may diminish the same effect. All hope of a plausible scientific explanation hinges on reducing experimental manipulations to causal factors inside the mind or brain (Van Orden, Holden, Podgornik, & Aitchison, 1999). As such, one impulse that cognitive psychologists sometimes have, especially those with solid training in conventional statistics, is to think of pink noise in terms of a statistical nuisance. If pink noise causes problems for inferential statistics (and, therefore, for the aforementioned causal logic), then perhaps pink noise can be removed, modeled, or otherwise controlled. This is a natural move for one taking a purely statistical perspective on data. However, finding pink noise can lead to fundamentally different scientific perspectives on the data. For example, one may wonder how the human mind and body might be organized to give rise to statistical interdependence, and to interact across different time scales. From a scientific perspective it seems to make sense to ask what the empirical fact of pink noise in cognitive and other human performance implies about the fundamental coupling of bodily processes.

For cognitive science, Gildea’s approach was revolutionary because it supplied the seed of an alternative format for scientific explanations of cognitive performance, and for psychology in general. That alternative began with attempts to establish the presence of pink noise *despite* a range experimental manipulations (e.g., Gildea et al., 1995), and it was subsequently expanded to include experiments in which pink noise survived changes in cognitive tasks (e.g., Cayton & Frey, 1997; Gildea, 1997, 2001; Van Orden & Holden, 2002; Van Orden

Holden

et al., 2003). Thus, the alternative approach was directed at the identification of ubiquitous performance phenomena, in the hope that those phenomena may illustrate something very general about human performance. Gildea was perhaps one of the first to suggest, on the basis of an empirical finding, that pink noise implied that complex systems theory may be relevant to cognitive psychology (Gildea et al., 1995). The link is implied, in part, because pink noise is an important (but not sufficient) footprint of self-organization and self-organizing systems in nature (see also Aks, Chapter 7, and Van Orden et al., 2003). More generally, the widespread finding of pink noise in trial series from exhaustively studied, standard cognitive tasks underscores the potential for analyses of patterns of *variability* in cognitive performance to be informative.

### AUTHOR NOTE

I gratefully acknowledge Vahe Amirian for his help in collecting the data for the timing experiment, and the helpful comments and feedback I received from three reviewers while preparing this chapter.

### REFERENCES

Aks, D. J., Zelinsky, G. J., & Sprott, J. C. (2002). Memory across eye movements: 1/f dynamic in visual search. *Nonlinear Dynamics, Psychology, and Life Sciences*, 6, 1-25.

Bassingthwaighte, J. B., Liebovitch, L. S., & West, B. J. (1994). *Fractal physiology*. New York: Oxford University Press.

Caccia, D. C., Percival, D., Cannon, M. J., Raymond, G., & Bassingthwaighte, J. B. (1997). Analyzing exact fractal time series: Evaluating dispersional analysis and rescaled range methods. *Physica A*, 246, 609-632.

Cannon, M. J., Percival, D. B., Caccia, D. C., Raymond, G. M., & Bassingthwaighte, J. B. (1997). Evaluating scaled windowed variance methods for estimating the Hurst coefficient of time series. *Physica A*, 241, 606-626.

Holden

Chatfield, C. (1996). *The analysis of time series: An introduction* (5<sup>th</sup> ed.). New York: Chapman & Hall.

Clayton, K., & Frey, B. B. (1997). Studies of mental "noise". *Nonlinear Dynamics, Psychology, and Life Sciences, 1*, 173-180.

Delingières, D. Fortes, M., & Ninot, G. (in press). The fractal dynamics of self-esteem and physical self. *Nonlinear Dynamics, Psychology, and Life Sciences*.

Efron, B., & Tibshirani, R. J. (1993). *An introduction to the bootstrap*. New York: Chapman & Hall.

Eke, A., Hermán, P., Bassingthwaite, J. B., Raymond, G. M., Percival, D. B., Cannon, M., Balla, I., & Ikrényi, C. (2000). Physiological time series: Distinguishing fractal noises from motions. *European Journal of Physiology, 439*, 403-415.

Eke, A., Hermán, P., Kocsis, L., & Kozak, L. R. (2002). Fractal characterization of complexity in temporal physiological signals. *Physiological Measurement, 23*, R1-R38.

Feder, J. (1988). *Fractals*. New York: Plenum Press.

Forster, K. I., & Forster, J. C. (1996). *DMASTR Display System for Mental Chronometry (Version 5.18)* [Computer Software]. Tucson, AZ: Authors.

Gilden, D. L. (1997). Fluctuations in the time required for elementary decisions. *Psychological Science, 8*, 296-301.

Gilden, D. L. (2001). Cognitive emissions of 1/f noise. *Psychological Review, 108*, 33-56.

Gilden, D. L., Thornton, T., & Mallon, M. W. (1995). 1/f noise in human cognition. *Science, 267*, 1837-1839.

Gottman, J. M. (1981). *Time-series analysis: A comprehensive introduction for social scientists*. Cambridge, UK: Cambridge University Press.

Hausdorff, J. M., Purdon, P. L., Peng, C.-K., Ladin, Z., Wei, J. Y., & Goldberger, A. L. (1996). Fractal dynamics of human gait: Stability of long-range correlations in stride interval fluctuations. *Journal of Applied Physiology, 80*, 1448-1457.

Jensen, H. J. (1998). *Self-organized criticality*. Cambridge, UK: Cambridge University Press.

Holden

Kelly, A., Heathcote, A., Heath, R., & Longstaff, M. (2001). Response time dynamics: Evidence for linear and low-dimensional structure in human choice sequences. *Quarterly Journal of Experimental Psychology: Human Experimental Psychology*, *54A*, 805-840.

Keppel, G., & Zedeck, S. (1986). *Data analysis for research designs: Analysis of variance and multiple regression/correlation approaches*. New York: W. H. Freeman & Co.

Mandelbrot, B. B. (1982). *The fractal geometry of nature*. San Francisco: W. H. Freeman & Co.

Mandelbrot, B. B., & Wallis, J. R. (1969a). Computer experiments with fractional Gaussian noises, Part 1, 2 & 3. *Water resources research*, *5*, 228-267. Reprinted in Mandelbrot B. B. (2000), *Gaussian Self-Affinity and Fractals: Globality, the Earth, 1/f Noise, and R/S*. New York: Springer-Verlag.

Mandelbrot, B. B., & Wallis, J. R. (1969b). Some long run properties of geophysical records. *Water resources research*, *5*, 321-340. Reprinted in Mandelbrot B. B. (2000). In *Gaussian Self-Affinity and Fractals: Globality, the Earth, 1/f Noise, and R/S*. New York: Springer-Verlag.

Mandelbrot, B. B., & Wallis, J. R. (1969c). Robustness of R/S in measuring noncyclic global statistical dependence. *Water resources research*, 5, 967-988. Reprinted in Mandelbrot B. B. (2000). In *Gaussian Self-Affinity and Fractals: Globality, the Earth, 1/f Noise, and R/S*. New York: Springer-Verlag.

Peitgen, H.-O., Jürgens, H., & Saupe, D. (1992). *Chaos and fractals: New frontiers of science*. New York: Springer-Verlag.

Peng, C.-K., Havlin, S., Stanley, H. E., & Goldberger, A. L. (1995). Quantification of scaling exponents and crossover phenomena in nonstationary heartbeat time series. *Chaos*, 5, 82-87.

Press, W. H., Teukolsky, S. A., Vetterling, W. T., & Flannery, B. P. (1992). *Numerical recipes in C* (2<sup>nd</sup> ed.). Cambridge, UK: Cambridge University Press.

Riley, M. A., Wong, S., Mitra, S. & Turvey, M. T. (1997). Common effects of touch and vision on postural parameters. *Experimental Brain Research*, 117, 165-170.

Schroeder, M. R. (1991). *Fractals, chaos, power laws: Minutes from an infinite universe*. New York : W.H. Freeman.

Holden

Theiler, J., Eubank, S., Longtin, A., Gladrikian, B., & Farmer, J. D. (1992). Testing for nonlinearity in time series: The method of surrogate data. *Physica D*, *58*, 77-94.

Van Orden, G. C., & Holden, J. G. (2002). Intentional contents and self-control. *Ecological Psychology*, *14*, 87-109.

Van Orden, G. C., Holden, J. G., Podgornik, M. N., & Aitchison, C. S. (1999). What swimming says about reading: Coordination, context, and homophone errors. *Ecological Psychology*, *11*, 45-79.

Van Orden, G. C., Holden, J. G., & Turvey, M. T. (2003). Self-organization of cognitive performance. *Journal of Experimental Psychology: General*, *132*, 331-350.

## CHAPTER 7

# 1/f Dynamic in Complex Visual Search: Evidence for Self-Organized Criticality in Human Perception

Deborah J Aks

Department of Psychology  
University of Wisconsin-Whitewater  
Whitewater, WI 53190  
U. S. A.  
E-mail: aksd@uww.edu

Consider the “search and select” problem we face each day. We constantly set goals for ourselves that require us to scan our environment until we find a target. Whether we are looking for a face in a crowd, our keys in a cluttered environment, or a tumor in an x-ray, we rely on this ability to search the environment. What type of process is involved? Most researchers argue that some form of memory serves as a guide to search. Attention also plays an important role (e.g., Kowler, Anderson, Doshier, & Blaser, 1995; McPeck, Maljkovic, & Nakayama, 1999), and is arguably what drives saccadic eye movements to be effective. For now, I will focus on the role of memory in guiding search. A popular view is that a record accumulates (e.g., Townsend, 1974) and persists across fixations to guide search (e.g., Irwin, 1992). Once items are visited they are tagged so as to inhibit unnecessary subsequent visits—a phenomenon known as inhibition-of-return (e.g., Posner & Cohen, 1984; Klein, 1988). Surely, search would be more efficient if we only needed to check each item once until the target was found. While this theory has empirical support (see Shore & Klein, 2000, for a review), views of what characterize this memory are widely varied, as are the experiments that attempt to test them (Irwin, 1992; Posner & Cohen, 1984; Klein, 1988; Treisman & Gelade, 1980; Wolfe, 1994). Moreover, and perhaps surprisingly, studies have shown that under some natural search conditions memory does not seem to play much of a role in guiding search (e.g., Ballard, Hayhoe, & Petz, 1995; Horowitz & Wolfe, 1998). Eye movements are often sloppy when scanning a natural environment with our eyes returning repeatedly to objects and locations that have already been visited (Ballard et al., 1995). Instead

Aks

of systematically retrieving information from memory, search may rely on the external world to serve as its guide (O'Regan, 1992).

## RECONSIDERING HOW WE STUDY VISUAL SEARCH

To help reconcile why such widely varying search behavior has been seen in those different experiments, let us consider the different methodological approaches that have been taken. Typically, the analytical focus is on comparing performance speed, accuracy, or amount of information recalled across conditions (e.g., experimental and control). In studies of inhibition-of-return, for example, researchers are interested in the effect of prior exposure on subsequent search performance. Once the eyes fixate and "take note" of a particular item, there should be no need to revisit this item. Similarly, in priming experiments, the critical comparison is between "new" vs. "repeated" information. Positive priming experiments show benefits accrued from repeated exposure to target and distractor information, and negative priming produces interfering effects on search performance (e.g., Maljkovic & Nakayama, 1994).

In these traditional experiments, RTs and error rates are combined across trials of the same conditions. The variability of the behavior, which inevitably emerges in all conditions, is attributed to extraneous noise. That variability is isolated and removed from the purported impact of the independent variable. By contrast, similar to Gilden (1996) and Gilden, Thornton, and Mallon (1995), we focus on the variability over time. As is commonly done in the dynamical systems approach in psychology, we start by asking how a behavior changes over time (within a single condition). We no longer assume

erratic fluctuations are noise in the system (Gilden, 1996). Rather, these fluctuations may contain important information about how search history may have an important influence on future behavior. In this chapter I assess whether a dynamic is driving visual search by analyzing the temporal properties of eye movements. This approach may help us understand whether a simple iterative process is behind visual search.

## PATTERNS OF SEARCH

Studying the pattern of search behavior is key to understanding what drives search, and it will help us understand essential characteristics of any mediating memory mechanism. An absence of memory will be signaled by random search. The opposing extreme of random search would be a highly systematic pattern of search, for example, looking sequentially from left to right and top to bottom. Such a systematic search guarantees coverage of the visual field until the target is located. Although this increases the likelihood of detecting a (fixed) target, there are costs involved. Perhaps most important is the substantial cost in time. A speedy search is imperative under many real world conditions, such as when the target is not fixed, its identity or context changes, when the perceiver is constrained by competing goals, or when an aggressive predator is pursuing the perceiver. Such time constraints need to be incorporated into any realistic model of human visual search.

Could a rapidly implemented, unsystematic, even haphazard search be better than a systematic one? Literature that documents examples of erratic yet effective search adds plausibility to this idea

Aks

(e.g., Ellis & Stark, 1986; Engle, 1977; Inditsky & Bodmann, 1980; Krendel & Wodinsky, 1960). Similarly, visual search has been found to be “nearly random” (Scinto, Pillalamarri, & Karsh 1986), outright “random” (Groner & Groner, 1982; Horowitz & Wolfe, 1998), and a “random walk” (i.e., brown noise; Scinto et al., 1986). Likewise, studies focusing on the type of memory guiding search find little relation to the recall of objects (e.g., Melcher & Kowler, 2001; Ballard et al., 1995) or their locations in the scene (Zelinsky & Loschky, 1998). Contrary to what we might expect, and to what much conventional theorizing holds, visual search often is *unsystematic* and not necessarily related to explicit memory for what and where our eyes have just visited.

Computational theory as well as empirical findings (e.g., Megaw & Richardson, 1979; Locher & Nodine, 1974) have begun to clarify these notions and illustrate how a pseudo-random search can afford better coverage and more efficient search than many systematic ones. As we will see, a long-term memory across fixations—one that does not necessarily contain explicit information about the identity or locations of objects—may be instrumental in driving behavior. Although the complicated search behavior appears inefficient, the efficiencies come in the form of significant cognitive savings. For instance, cognitive load may be reduced since complex long-memory search behavior may require minimal resources for coding, retrieval, and recall. As described later in discussion of the SOC model, the only cognitive load required involves iteration of a very simple set of rules.

## PATTERNS OF SCALING, COLORED NOISE, & SELF-ORGANIZATION

When we look at the statistical properties of many systems' behavior we often find dynamics with well-defined scaling properties (e.g., Bak, Tang, & Wiesenfeld, 1988; Jensen, 1998). Scaling behavior (see Liebovitch & Shehadeh, Chapter 5, and Holden, Chapter 6) is a sign of long-term influences on system behavior and may be the product of a simple yet flexible process. The scaling behavior itself implies that no single characteristic scale is best suited to describe the behavior of the process. There is not just one time scale that controls the evolution of these systems; the means and variances change depending on the size of the sampling resolution. If given unlimited time, these "scale-free" distributions can stretch on indefinitely without encountering a cut-off. This stretching property is key to scaling and can be quantified by power laws. We can succinctly express some quantity  $N$  as some power (an exponent,  $e$ ) of another quantity,  $s$ :  $N(s) = s^{-e}$ . Therefore, by examining the exponent of the power law we know how the distribution changes as a function of some underlying variable, which in this case is time.

Importantly, systems characterized by power laws often produce complex behavior that appears random. In a particular form of power scaling, one that emerges frequently in complicated behavior, slower (i.e., low-frequency) behavior dominates. The temporal phenomenon scales as the inverse of the frequency ( $f$ ), or as *1/f noise*. Bak et al. (1987) suggested that these systems, with a power spectral exponent  $\alpha = -1.0$  (i.e.,  $f^\alpha$ ), consist of many interacting components, are ubiquitous in nature (see Bak et al., 1987 for examples), and,

Aks

under many conditions, are dynamical systems which organize themselves into a state with a complex structure. Self-organization (see, e.g., Kelso, 1995) implies that patterns develop without a need for a controlling agent. The patterns emerge from a decentralized set of interactions that are intrinsic to the system.

Recognizing that difficult visual search tasks are often unsystematic, yet effective, has led to my belief that the oculomotor system uses subtle, self-organizing properties that produce erratic fluctuations in search behavior. Because the process involves very simple, iterated rules, only a minimal cognitive load is needed to carry out the complicated search behavior. The amount of information needed to be stored is reduced to a simple iterative function. This highly compact code may suffice to guide search. Evidence for such a self-organizing, complex system would reflect determinism inherent to the system and support the notion that a simple memory persists across fixations. It is a memory quite different from that of conventional thinking—the use of “memory” here does not imply “memory” in the everyday sense—and one that shares known properties of neurophysiology (e.g., spreading activation and inhibition).

## SELF-ORGANIZED CRITICALITY AS A MODEL OF VISUAL SEARCH

One candidate model of visual search is Self-Organized Criticality (SOC<sup>1</sup>; Bak et al., 1987). In the SOC model, dramatic change,

---

<sup>1</sup> Despite the controversy regarding Bak's original conception of SOC as a reliable model of 1/f dynamics, slight variants have proven to be reliable (Jensen, 1998). Alternative models maintain many similar properties including simple rules producing complex behaviors and self-organization. Thus, SOC or similar alternatives could account for described data trends.

or *criticality*, arises from the local interactions of the system's component parts. Such changes give rise to both the complex behavior as well as the *self-organization* within the system. The *simplicity* of the local rules according to which neighbors interact implies the cognitive load for driving eye-movements is minimal. In previous work, we have illustrated how SOC can easily be generalized to a neural network capable of evoking perceptual changes (Aks & Sprott, 2003). Here I describe how local interactions can occur through lateral inhibition and excitation across neurons. Together with simple threshold rules (as are typical in SOC models), these interactions can produce perceptual changes (i.e., Stassinopoulos & Bak, 1995). Similarly (as illustrated later in Figure 7.12 and the Discussion), we can conceive of eye movements being driven by the interaction of neurons across an underlying network of neurons.

Applications of dynamical approaches to other cognitive and perceptual phenomena (Gilden et al., 1995; Kelso, 1995; Port & Van Gelder, 1995; Pressing, 1999; Ward, 2002) show great promise for extending that approach to the visual search system. My proposal that a simple deterministic process may drive the human visual system has been tested in a challenging visual search task (Aks, Zelinsky, & Sprott, 2002). As described in the Method section in this chapter, our analysis focused on the impact of time on the resulting probability distributions and power spectra. We looked for scale-invariance in eye movements by evaluating whether the means and variances of those data distributions changed over time, and whether power laws emerged in the power spectra. Finding a scale-invariant perceptual system, characterized by a power law, would suggest that there is

Aks

determinism and compact coding of information in visual search (c.f. Voss, 1992). Furthermore, evidence of SOC or a similar such iterative mechanism in the perceptual system (as indicated by  $1/f$  power laws) would present another illustration of a complex system with a simple underlying dynamic—one that can potentially account for the flexibility of our visual system in adapting to novel environments.

## METHOD

The visual search task, illustrated in Figure 7.1, consisted of eighty-one  $0.43^\circ$  T shapes. Targets and distractors differed in orientation by  $90^\circ$ . Items were presented in a pseudo-random arrangement so that all locations had an equal probability of being searched. The participant's task was to search the array and press a hand-held button when the target was located.

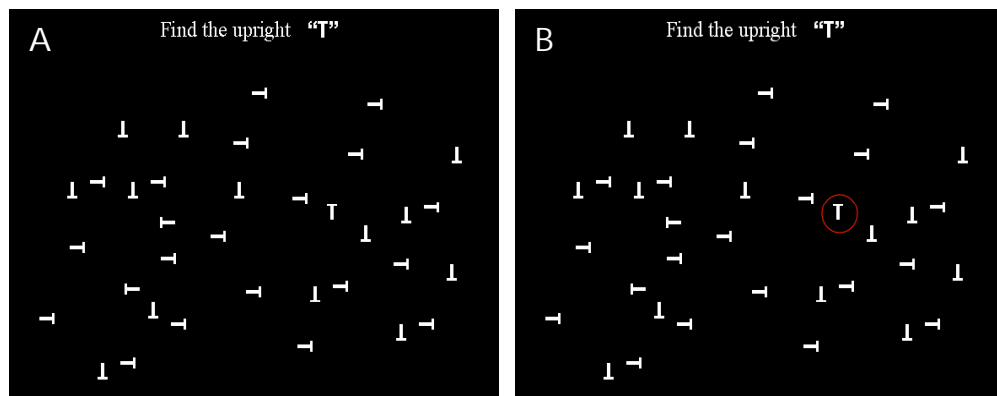


Figure 7.1. (A) Sample display from the search task. The subject searched for an upright 'T.' (B) The correct target is circled in red

The experiment consisted of 400 target-present trials and lasted approximately 2.5 hours. Every effort was made to emulate a

continuous search but factors such as fatigue and actual target detection forced brief discontinuities in the data series. The two types of discontinuities that occurred in this study were due to (1) inter-trial intervals between when the participant found the target and a new trial began, and (2) subdividing the trials into eight sessions separated by five-minute rest periods. Eye movements were sampled using a Generation V dual purkinje-image (DPI) tracker that was controlled by a computer.

The duration and x and y positions of the eyes were recorded at each fixation. Each measure was treated as a set of data points whose spatial and temporal properties were analyzed over the course of search. Additional parameters of the eye movements were used to map the trajectory of the eyes as they moved from fixation to fixation. These included differentiation of consecutive eye positions (e.g.,  $x_n - x_{n+1}$ ), eye movement distance  $(x^2 + y^2)^{1/2}$ , and eye movement direction  $[\arctan (y/x)]$ .

## ANALYSIS STRATEGY

Many of the tools of complexity theory involve formalizing (with mathematical and visual representations) the interactions that occur within a network. A typical aim is to look for a statistical pattern that might emerge in data that have been collected over time. In our analysis of the eye fixations we looked for scaling and other patterns across data points in the series. Here I will focus on three sets of analyses—spectral analysis (FFT), power laws, and the Iterated Functions System (IFS) clumpiness test.

Aks

Spectral and Fourier analyses<sup>2</sup> are well-established methods to test for correlations within a time series. Jagged data series (appearing superficially as a random series) are often produced by natural complex systems. The data series can be described as a complex waveform best estimated by the composite of simple regular (sine) waves that span a range of frequencies. A Fourier transform involves first decomposing the observed series into simple waves and then plotting the power against frequency to describe what combination of waves best describes the observed waveform. The analysis in our study used a Fast Fourier transform (FFT; Press, Flannery, Teukolsky, & Vetterling, 1986) and the resulting plot of the power (mean square amplitude) against frequency. For an introduction to Fourier analyses see one of many tutorials, such as Peak and Frame (1994) and Sprott (2003).

### ***Power Laws in Spectral Analyses***

Can the eye movement data be described by a power law, and do the data possess scale invariance associated with a self-organizing complex system? A linear function on a double-log plot produced by FFT indicates the presence of a power law. The regression slope of this function, denoted by  $\alpha$ , is the power exponent. When the exponent of the power spectrum is  $\alpha = -1.0$  (as shown in the middle

---

<sup>2</sup> Spectral analysis is a linear method that can be effectively used to characterize a nonlinear (fractal scaling) process. A linear method can be very useful in detecting correlated structure in noisy data regardless of the process that produced it. For example, the eye movement data that we have analyzed can be the output of either a linear or nonlinear process. I argue that the  $1/f$  structure—estimated by FFT spectral analysis—may suggest that a SOC-type process drives eye-movements. SOC is a simple nonlinear process (iterated many times over) which can operate in a neural network—perhaps to produce complicated eye movements. The linear Fourier analysis is an effective tool to uncover (and estimate) correlated structure regardless of whether it has emerged from a linear or nonlinear process.

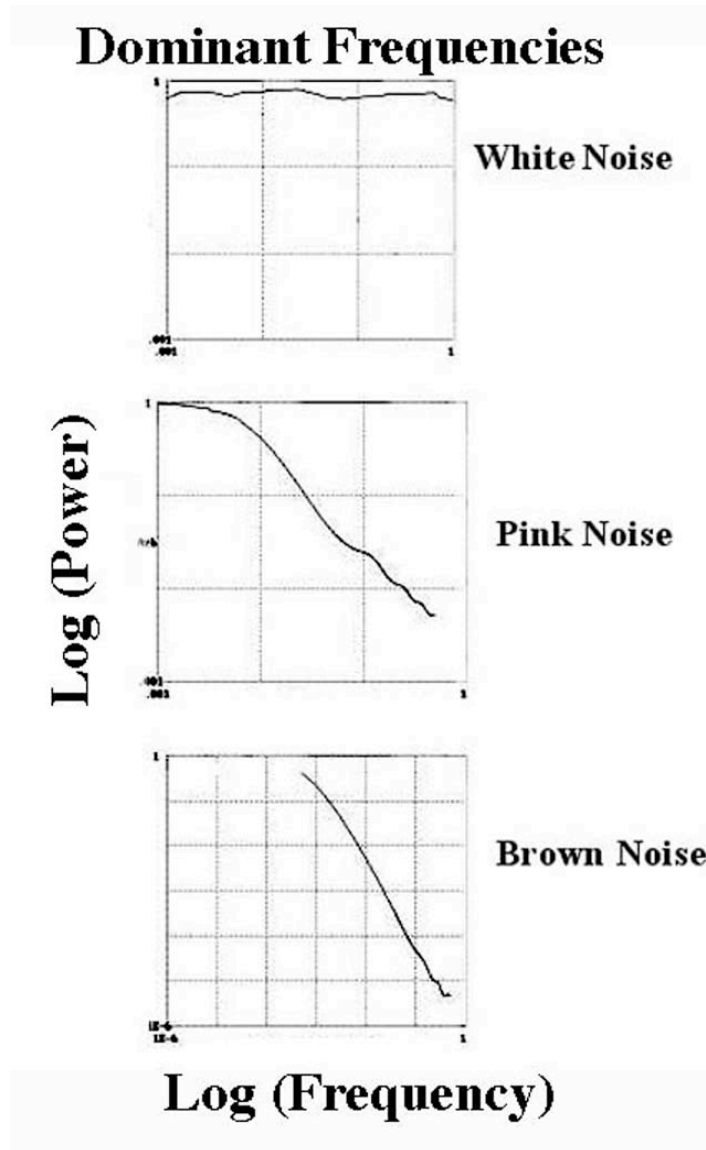


Figure 7.2. Spectral analysis of three types of colored noise. White ( $1/f^0$ ) noise with a flat spectrum indicates no correlation across data points; Brown ( $1/f^2$ ) noise has a steep slope indicating short-term correlation; and Pink ( $1/f$ ) noise has a shallow slope indicating extremely long time correlation. The white noise is a Gaussian distribution of scores with all frequencies equally represented. Sprott and Rowland (1995) included this sample data set in their *Chaos Data Analyzer* software. Brown noise is a simple integration of the white noise. To generate the pink noise I took the Fourier transform of the white noise data to isolate the frequency domain, multiplied the amplitude of the frequency components by  $1/f$ , and performed an inverse Fourier transform. See also Equations 9.35 and 9.36 in Sprott (2003).

Aks

panel of Figure 7.2), the given temporal phenomenon scales as the inverse of the frequency ( $f$ ), or as  $1/f$  noise. In this particular form of scaling, fluctuations occur in the same proportion at all scales (i.e., they are self-similar and scale invariant), and there exists a great deal of fine structure in the data.

An important aspect of spectral analysis is that it serves as a useful measure of the strength of memory across the system. Revealing temporal correlation is important not only in assessing whether memory exists across eye-movements, but the magnitude of the exponent also quantifies memory strength. The steepness of the slope (on a log-log scale) reflects the duration of memory (i.e., correlation across points). As shown in Figure 7.2, Brown ( $1/f^2$ ) noise has a steep slope, indicating short-term correlation. Pink ( $1/f^1$ ) noise has a shallow slope, indicating extremely long time correlation, and white ( $1/f^0$ ) noise, with its flat spectrum, indicates no correlation across data points. Implications for these trends are described in the Discussion section, including how pink noise hints at a process that has important self-organizing properties.

*Iterated Function Systems (IFS)* provides an interesting alternative to determine whether temporal correlations exist across fixations (Peak & Frame, 1994; Jeffrey, 1992; Sprott & Rowlands, 1995; Mata-Toledo & Willis, 1997). This technique is used to create a pattern that helps to visually characterize the color of noise. It does so by producing clumped patterns for colored noise while producing homogeneously filled spaces when the data are uncorrelated. At a minimum we learn whether our data deviates from a random pattern, but there is also the potential for learning about the degree of

correlation present in noisy data. The different degrees of temporal correlation correspond to the different forms of coloring to the noise. As can be seen in Figure 7.3, white ( $1/f^0$ ), pink ( $1/f^1$ , or  $1/f$ ), and brown ( $1/f^2$ ) noise are easily distinguishable. White noise produces a pattern that uniformly fills its representation space. At the other extreme, brown ( $1/f^2$ ) noise produces a pattern in which the dots accumulate over the diagonals and some of the sides of the square, leaving most of the representation space empty. Pink ( $1/f$ ) noise produces self-similar repeating triangular structures of different sizes, and accumulates, albeit in a dispersed way, near the diagonals. These examples illustrate how to visualize the fine structure of time series using the IFS test to help distinguish the color of noise in a system.

#### ***The IFS Procedure***

First, take either the x or y fixation series (or some derivative as shown in Figure 7.4), and sort the data from the minimum to the maximum value. Then, subdivide the series into four quartiles, in such a way that each group contains the same number of points. The original unsorted data set is then normalized and grouped into one of four values, 1 to 4, representing the quartile to which the data belong.

As shown in Figure 7.5, the representation space is a square that provides a 2-D picture of the correlation structure present in the trajectory of eye movements. The four corners are labeled 1 to 4 in a clockwise direction (starting in the lower left corner) to represent the quartile of that fixation. The first fifteen fixations from Figure 7.4 are used here to demonstrate the IFS procedure.

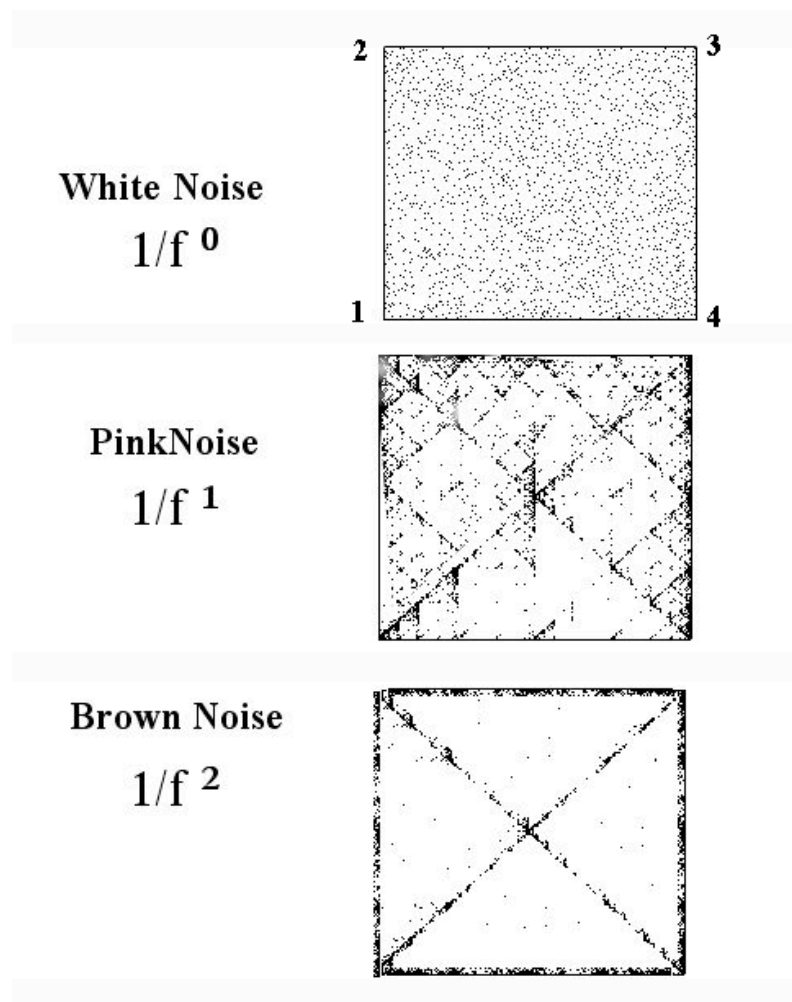


Figure 7.3. Output of the IFS test performed on white, pink, and brown noise (the same simulated data used in the analysis of Figure 7.2). Each case is easily distinguishable. White noise uniformly fills the representation space. Brown noise produces a pattern in which the dots accumulate over the diagonals and some of the sides of the square, leaving most of the representation space empty.  $1/f$  (pink) noise produces self-similar, repeating, triangular structures of different sizes, and accumulates, albeit in a dispersed way, near the diagonals.

Because previous points determine the position of each subsequent point, the plot represents a trajectory of the eye movements. Each point gives a short-term history of eye movements, since the influence of previous fixations diminishes over time. The

## Fixation Series

	Y diff	Quartile
1	-31.0	2
2	-62.0	1
3	-33.0	2
4	14.0	3
5	-12.0	2
6	20.0	3
7	-98.0	1
8	-10.0	2
9	-82.0	1
10	-34.0	2
11	-42.0	2
12	12.0	3
13	56.0	4
14	62.0	4
15	60.0	4

Figure 7.4. The first 15 data points for the difference across the y coordinate of each fixation. In the right column is the quartile to which each data point belongs.

result is a scattering of points in the plane as shown in Figure 7.3. Any departure from a uniform distribution of points is evidence for correlated structure and possibly a deterministic mechanism driving the behavior. Clustering along the diagonals in the figure reveals the short-term, highly correlated pattern associated with brown noise. The additional fractal microstructure reflects longer-term, but weaker, correlations often associated with pink noise.

## RESULTS

Visual search produced, on average, 24 fixations ( $SD = 15$ ) per trial, with each trial lasting 7.6 s ( $SD = 6.9$  s). Mean fixation duration was 212 ms ( $SD = 89$  ms) with 10,215 fixations across the complete search experiment. The number of fixations decreased from 1888 to 657 across eight sessions, with the average duration increasing from

Aks

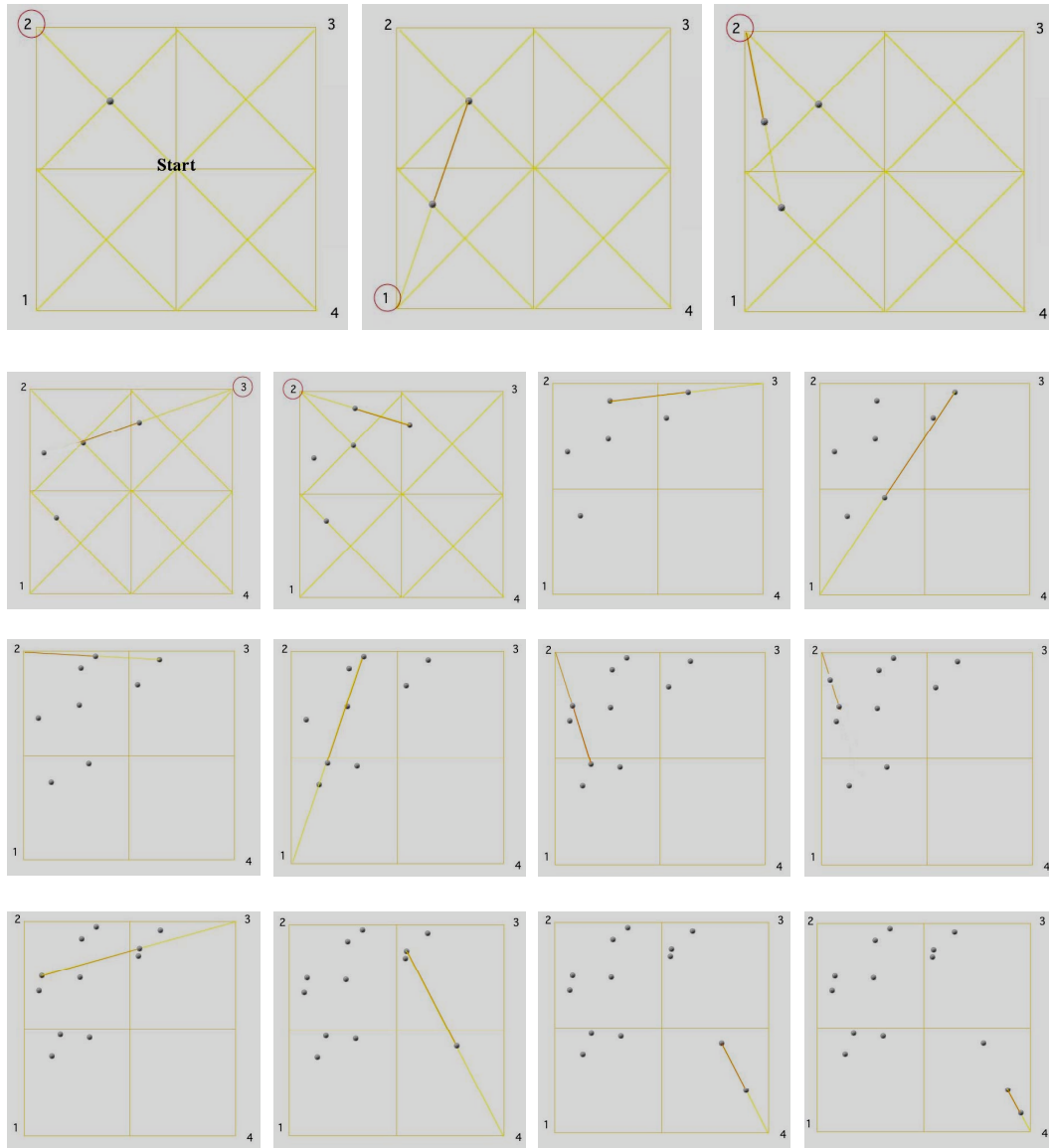


Figure 7.5. (A; top-left) A point is plotted halfway between the center of the IFS square and the quartile of the first point of the series. The first point falls into the 2<sup>nd</sup> quartile of the full data series. The quartile of the data point is circled in red. (B; top-middle) A second point (falling into the 1<sup>st</sup> quartile of the full data series) is plotted halfway between the first plotted point and the second point in the fixation series. (C; top-right) A third point (falling into the 2<sup>nd</sup> quartile) is plotted halfway between the second plotted point and the third point in the series, and so forth. (D)-(O) (smaller panels, from top-left to bottom-right) show the remaining evolution of the IFS map when applied to the first fifteen trials.

206 to 217 ms. Mean deviation from last trial fixation to new target location was  $0.4^\circ$ , indicating a high degree of accuracy in actual target detection.

Figure 7.6 shows a representative sample of the first differences across eye position ( $y_{n-1} - y_n$ ). These erratic trends were similar for x- and y-coordinate positions, except for the overall direction in which the eye position changed over time. While differences across y positions gradually increased over time, differences across x positions tended to decrease over time. The same trends occurred with relative dispersions ( $SD/M$ ), a measure which reflects system contingencies as function of sampling resolution (Liebovitch, 1998). These changes in mean and variance with fixation duration are characteristic of fractal structures and scale-invariant systems.

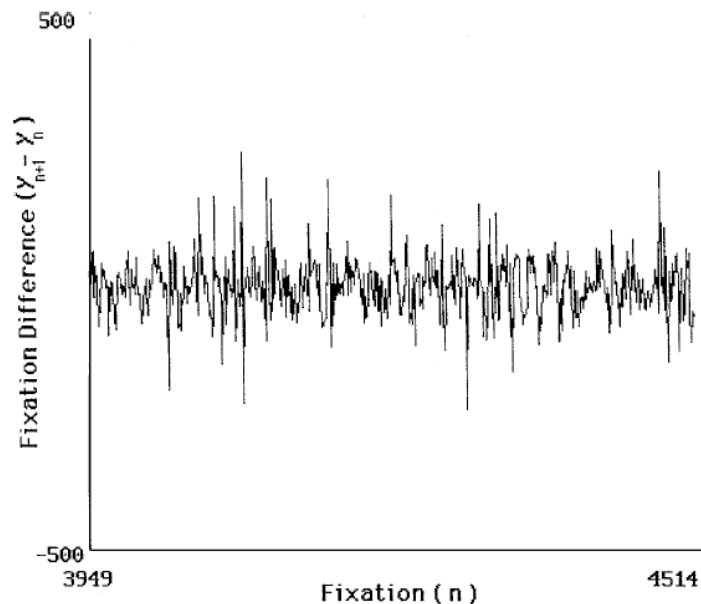


Figure 7.6. Representative fixation series for the first differences of eye position ( $y_{n+1} - y_n$ ). Only fixations along the vertical coordinate are shown. The erratic pattern in the fixation series is similar for horizontal eye positions. The spikes are typical of 1/f behavior.

Aks

The first method to assess temporal correlations (i.e., memory) in search involved FFT and power spectral analysis. The mean regression slope of the power spectra for the x and y eye-position coordinates was  $\alpha = -1.7$  (i.e., brown noise). Differentiated (x and y) data showed reduced regression slopes,  $\alpha = -0.23$ . The spurious low-frequency regions of the spectra flattened the slope. In the high-frequency region of the curve  $\alpha = -0.7$  (for y,  $\alpha = -0.7$ ; for x,  $\alpha = -0.6$ ). An example of the  $1/f$  trends is illustrated in Figure 7.7.

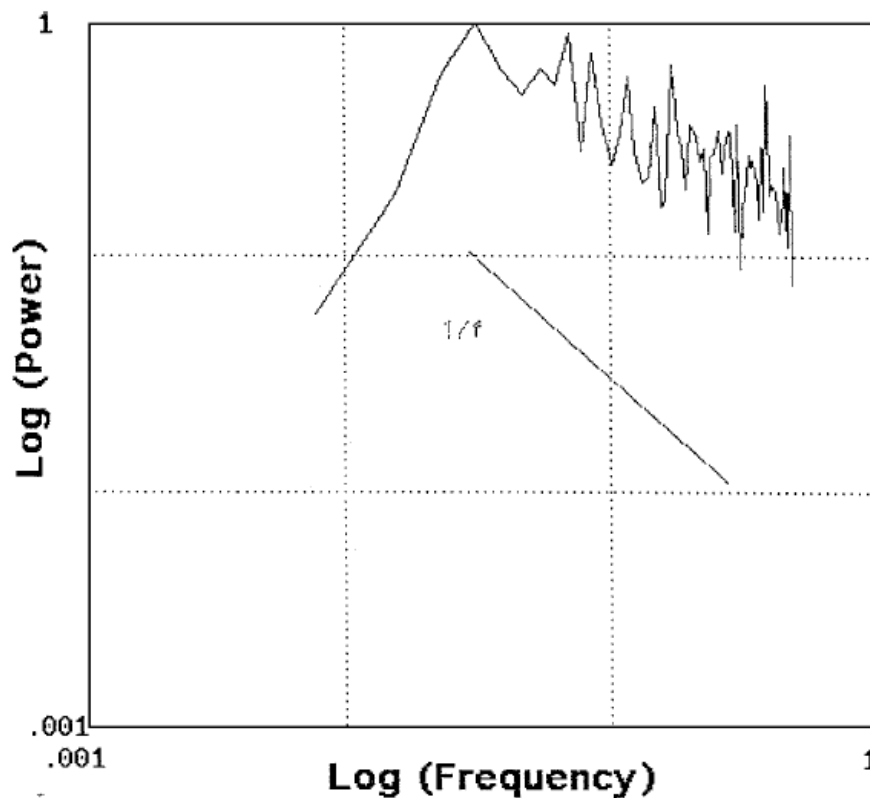


Figure 7.7. Power spectra of first differences of x and y fixation series produced pink ( $1/f$ ) noise. Spectra of differences across y fixations are shown here. Mean regression slope of the y-difference power spectrum is  $\alpha = -0.7$  in the high frequency region. Also shown is a line depicting an exact  $1/f$  power spectrum.

The second method, the IFS clumpiness test (Jeffrey, 1992), evaluates memory in complex search (i.e., temporal correlations and deviations from randomness). Clustering along the diagonals reveals short-term, highly correlated consecutive data points typically found in brown noise. Such a pattern was observed in the analysis of raw eye fixations for the x and y coordinates. Additional fractal microstructure appeared in the IFS test when fixation differences were analyzed. This trend, shown in Figure 7.8, reflects long-term, but weaker, correlations often associated with pink noise.

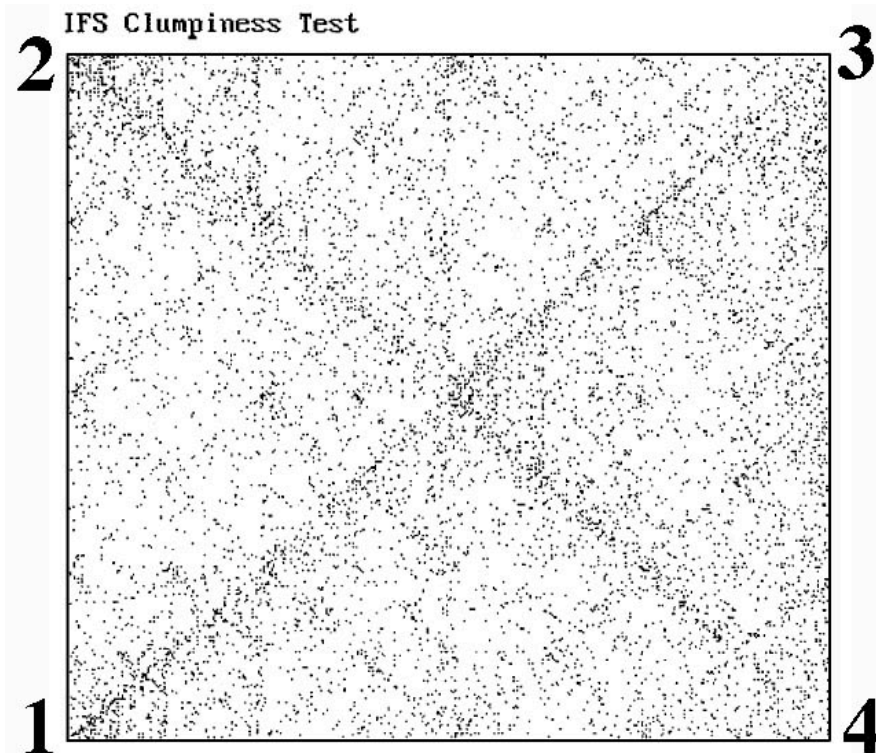


Figure 7.8. Results of the IFS clumpiness test of differentiated vertical (y) fixations. A similar pattern emerged for horizontal (x) fixations. The diffuse fractal microstructure reflects longer-term correlations appearing weaker than those in the raw data. Both cases resemble patterns associated with pink noise.

Aks

A combined measure of distance across eye fixations ( $\Delta x^2 + \Delta y^2$ )<sup>1/2</sup> produced power spectra with 1/f trends dominating the lower frequency range and 1/f<sup>2</sup> trends dominating the high frequency range (Mean  $\alpha = -0.47$ ; see Figure 7.9). The corresponding IFS test, shown in Figure 7.10, produced a clear but distinct colored noise pattern with more diffuse clustering of data points than those found in the raw and differentiated data sets. Random shuffling of x, y, and distance data sets produced white noise. Thus, differences in these fixations possessed a potentially important, long-term dynamic characterized by ~1/f pink noise.

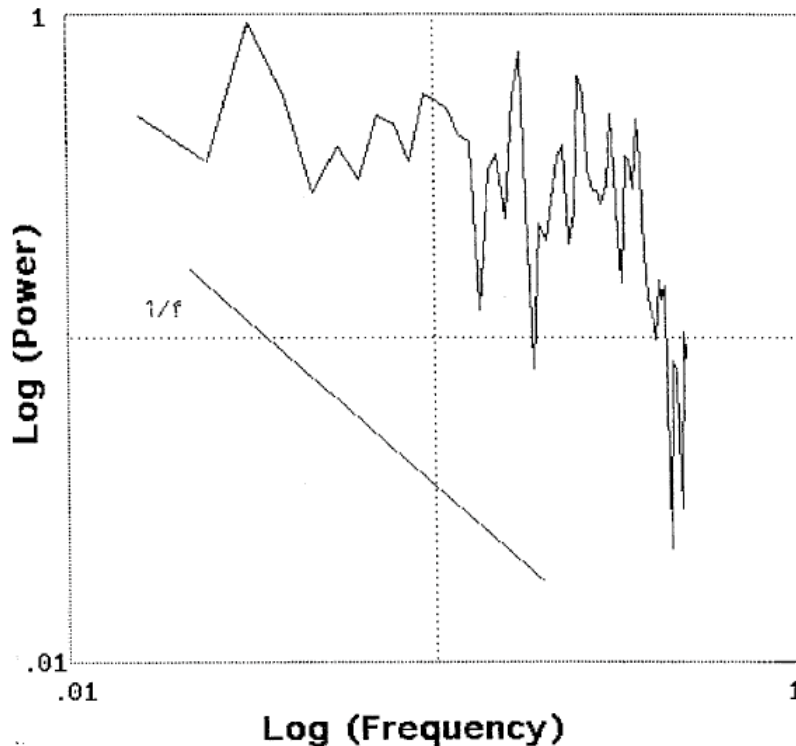


Figure 7.9. Power spectra of distance across eye fixations ( $\Delta x^2 + \Delta y^2$ )<sup>1/2</sup>. Pink (1/f) trends were dominant in the lower frequency range, and 1/f<sup>2</sup> trends were dominant in the high frequency range (mean  $\alpha = -0.47$ ). Also shown is a line depicting an exact 1/f power spectrum.

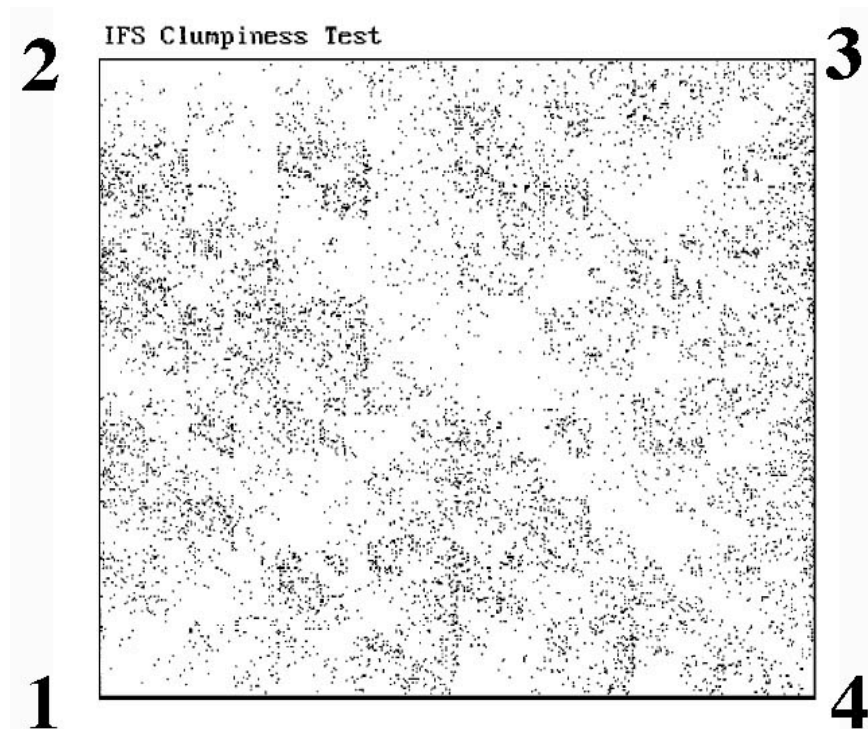


Figure 7.10. Results of the IFS clumpiness test on the time series of distances between fixations  $(\Delta x^2 + \Delta y^2)^{1/2}$ . A unique colored noise pattern emerged with more diffuse clustering of data points than those found in the raw and differentiated data sets.

## DISCUSSION

I examined complicated eye movements to gain insight into the underlying mechanism guiding visual search. Using a challenging conjunction search task, we generated and then analyzed the resulting eye movements (Aks et al., 2002). My focus on the dynamic of the fixation series offers a unique perspective to the broader study of eye movement behavior. It contributes new insights to the debate in the visual-cognitive literature on whether memory plays a role in guiding visual search (e.g., Horowitz & Wolfe, 1998; Kristjansson, 2000; Melcher & Kowler, 2001; Ballard et al., 1995; Shore & Klein, 2003).

Aks

According to conventional theory and common sense, visual search utilizes information from previous fixations to guide subsequent search. Memory models of visual search incorporate mechanisms such as inhibitory tagging (Klein, 1988) or identification of previously searched items (e.g., Irwin, 1992; Jonides, Irwin, & Yantis, 1981). Horowitz and Wolfe (1998) is a recent example of research that challenges the assumption that search is guided by memory from previous fixations. Doubts about a memory-based guidance emerge from their findings of RTs being unaffected by randomly repositioned items, together with recent research showing that visual memory is often surprisingly poor (Melcher & Kowler, 2001; Rensink, O'Regan, & Clark, 1997; Simons & Levins, 1997) and that the visual system retains little information about the locations (or identity) of objects over time. Instead, the visual system seems to act on fleeting neural representations that are overwritten by a change in the visual scene. Horowitz and Wolfe's (1998) claim that visual search does not keep track of previously searched locations comes from their examination of overall RTs to complete visual search. However, relying on such a coarse measure of behavior means that subtle contingencies in scanning behavior can be overlooked. Direct analyses of the eye movements revealed a less obvious form of memory.

The key finding that a sequence of fixations can be represented by a power law function confirmed our prediction that search might be guided by a memory of previous fixations. Contrary to Horowitz and Wolfe (1998), we found that search behavior was *not* random and that contingencies did in fact exist across fixations. While much cognitive theory implicates search mechanisms such as tagging and inhibition of

return (to previously visited items), the form of memory we have found involves general contingencies across fixations. The 1/f power law is a signature of these contingencies. The power law further indicates that the system has scale-invariant properties typically associated with a system optimized to adapt to a changing environment. Since systems characterized by power functions are known to be flexible, this suggests that the contingencies guiding search may play an important role in selection of appropriate information in an array of constantly changing environmental information. The IFS clumpiness tests confirmed the results of the power spectral analyses, showing that differences across fixations revealed pink (1/f) noise. These results suggest a long-term memory is maintained across complicated search in a manner that may involve the use of a simple set of rules with self-organizing properties (i.e., variants of Bak et al., 1988; Jensen, 1998).

### IMPLICATIONS OF 1/f NOISE

Simple neuronal interactions can produce complex, self-organizing behavior. To understand how simple rules can produce complex eye movements let us consider Bak's SOC model in the context of a neural network. Figure 7.11 depicts such a network that could be used by the human visual system to represent a scene. Activation of different neural sites on the network can serve both as a means to represent the scene and a means to guide eye movements.

Figure 7.12 shows how the network is represented as a two-dimensional grid of interacting cells. Each cell possesses a certain degree of activation represented by a numerical value,  $Z(x,y)$ . Activity

Aks

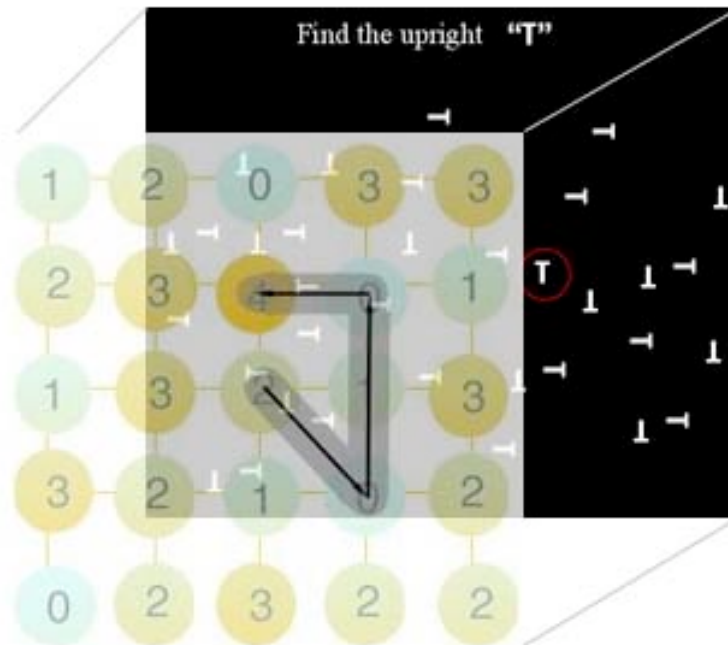


Figure 7.11. Representation of a visual search scene mapped onto a neural network. The scene is depicted in the top-right portion of the figure and shows one search display used in the experiment. Shifting attention to a particular stimulus produces an increase in the activation at the corresponding site on the neural net. Each node's numbers and colors represent the level of neural activation at that site. Nodes with the highest activation pull the eyes to that location. The resulting path of the eye movements is shown as a shifting black line superimposed on the network.

can be induced by any of a number of factors such as a salient visual feature, shifting attention to a feature of interest, or random activity that is produced even at rest. Neural activity can also be triggered by movement of the eyes to different locations. As individual neurons are activated beyond a threshold of, say, 4 arbitrary units, the activity in the original site is dispersed to surrounding cells, incrementing the activity in these regions by 1,  $\{Z(x,y) \rightarrow Z(x,y) + 1\}$ , thus depleting the activity in the original site to zero,  $Z(x,y) \rightarrow Z(x,y) - 4$ . In the

## Visual Search and 1/f Dynamics

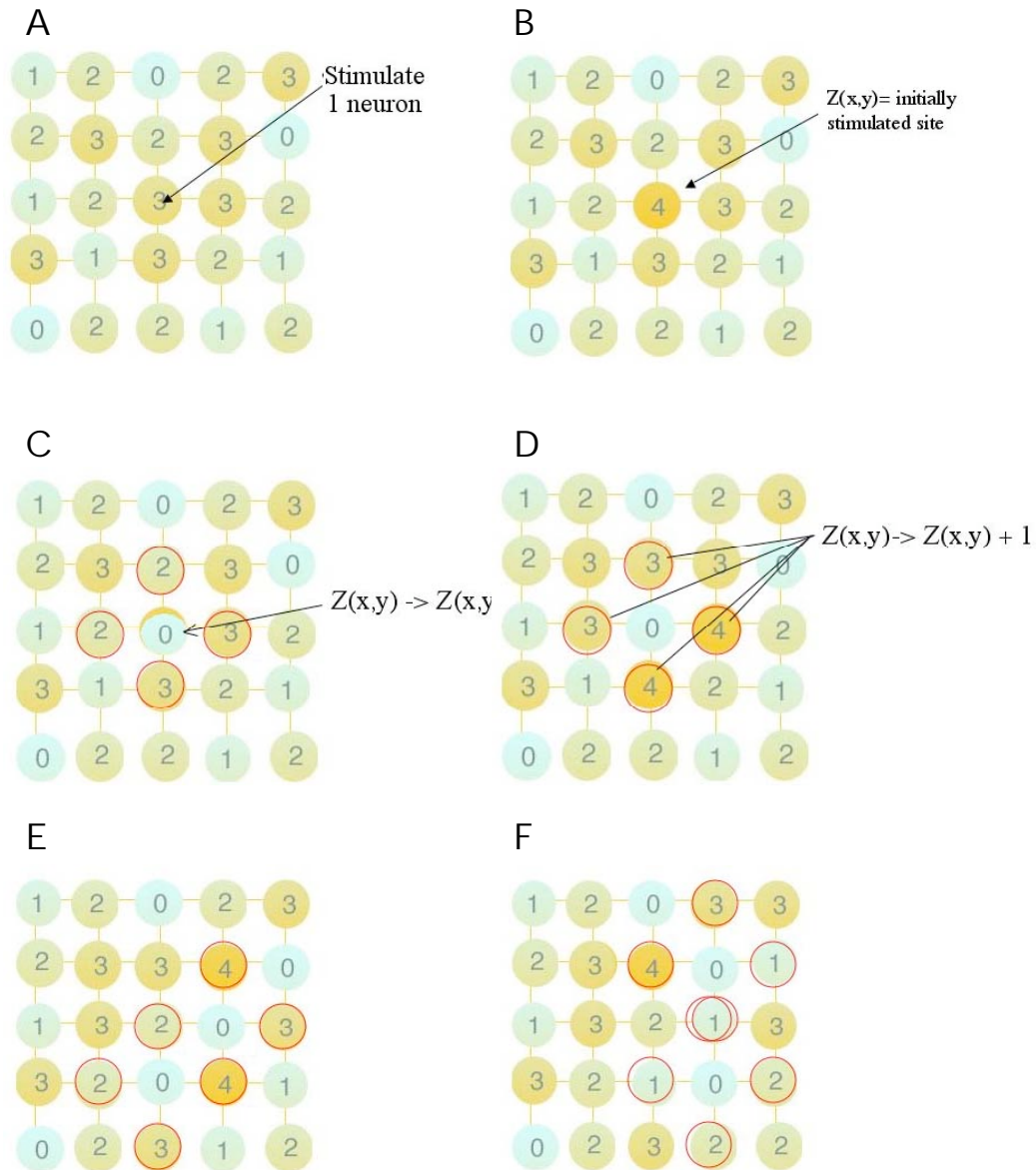


Figure 7.12. (A) A neural network. Numbers and colors indicate the relative activation of neurons. High numbers and orange colors indicate a high level of activity. Low numbers and blue colors indicate low levels of activity. (B) A one-unit increment in neural activity at the central site. This increase in neural activity can be due to any one of a number of factors, including the appearance of a salient feature, shifting attention to a feature of interest, or random activity that is produced at rest. (C) Neural activity in the original central site is depleted to zero after the threshold of 4 activation units is reached. (D) Neural activity in the immediately surrounding sites is increased by one unit. (E)-(F) Neural activity in subsequent surrounding sites is increased by one unit.

Aks

absence of useful environmental information during visual search, the eyes may be guided to sites that contain the highest level of activity among immediately surrounding cells, and evade local sites depleted of neuronal activity. The global result can be a complicated search pattern that could easily be mistaken for a random search (see Figure 7.13).

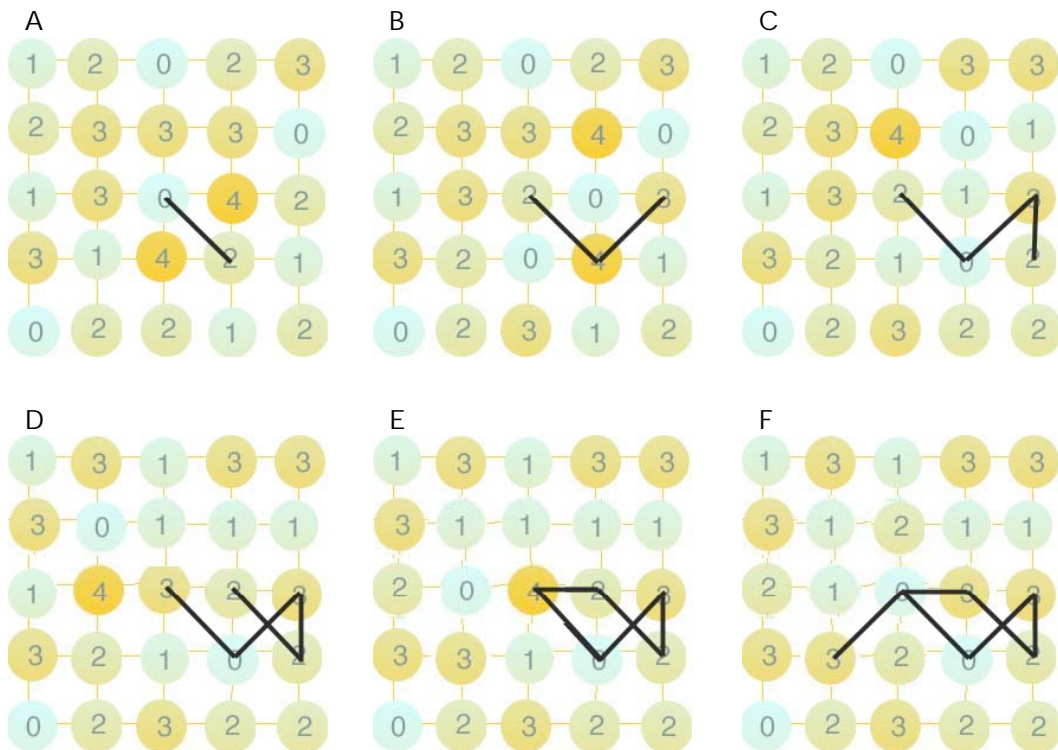


Figure 7.13. Eye-movements being pulled to sites of greatest neural activity, following the same progression of neural activity in Figure 7.12. When two sites have an equal level of activity (a tie), as in (A), the eyes traverse an intermediate path. (B) and (F) show another example of tied activity, but here the tie is on opposing sites. Rather than remaining fixed, the eyes are pulled to the site where the prevailing activity surrounding the recipient site is greater. Aside from these cases of equal activity, the general rule is that eyes are pulled to a single adjacent site of greatest activity.

The key finding of 1/f noise in eye movements has some important implications. First, we know that search is not random. Instead the eyes are guided by their history. A simple form of temporal memory exists across the sequence of eye movements. It is possible that the 1/f search pattern is produced from guidance of eye movements by changes in the intensity of neuronal activity across a network of neurons. These changes may be best described as the output of iterating a simple set of threshold-based rules such as those associated with SOC models.

The 1/f eye movements may also involve a cognitive mechanism such as attention-based sampling and selection of useful information from a complicated environment. It is an open question whether neuronal interactions and their spread of activation drives this selection process. Could this process produce the rapid and effective search known to occur in humans? The answer may relate to the general finding that 1/f systems offer an optimal compromise between efficient recovery of information and the tendency to err (Voss, 1992). The significance of these complex yet adaptive behaviors remains open to future scientific inquiry.

Aks

## REFERENCES

Aks, D. J., Zelinsky, G., & Sprott, J. C. (2002). Memory across eye movements: 1/f dynamic in visual search. *Journal of Nonlinear Dynamics in Psychology & the Life Sciences*, *6*, 1-25.

Aks, D. J., & Sprott, J. C. (2003). Resolving perceptual ambiguity in the Necker cube: A dynamical systems approach. *Journal of Nonlinear Dynamics in Psychology & the Life Sciences*, *7*, 159-178.

Bak, P., Tang, C., & Wiesenfeld, K. (1987). Self-organized criticality: An explanation of 1/f noise. *Physical Review Letters*, *59*, 381-384.

Bak, P., Tang, C., & Wiesenfeld, K. (1988). Self-organized criticality. *Physical Review A*, *38*, 364-374.

Ballard, D. H., Hayhoe, M. M., & Petz, I. B. (1995). Memory use during hand-eye coordination. *Journal of Cognitive Neuroscience*, *7*, 66-80.

Ellis, S. R., & Stark, L. (1986). Statistical dependency in visual scanning. *Human Factors*, *28*, 421-438.

Engel, F. L. (1977). Visual conspicuity, visual search, and fixation tendencies of the eye. *Vision Research*, *17*, 95-108.

Gilden, D. L. (1996). Fluctuations in the time required for elementary decisions. *Psychological Science*, *8*, 296-302.

Gilden, D. L., Thornton, T., & Mallon, M. (1995). 1/f noise in human cognition. *Science*, *267*, 1837-1839.

Groner, R., & Groner, M. (1984). A stochastic hypothesis testing model for multi-term series problems, based on eye fixations. In R. Groner, C. Menz, D.F. Fisher, & R.A. Monty (Eds.), *Eye Movements and Psychological Functions: International Views* (pp. 257-274). Hillsdale, NJ: Erlbaum.

Horowitz, T. S., & Wolfe, J. M. (1998). Visual search has no memory. *Nature*, *357*, 575-577.

Inditsky, B., & Bodmann, H. W. (1980). Quantitative models of visual search. In *Proceedings of the 19<sup>th</sup> symposium of CIE* (pp. 197-201). Paris: Commission Internationale de l'Éclairage.

Irwin, D. E. (1992). Memory for position and identity across eye movements. *Journal of Experimental Psychology: Learning, Memory, & Cognition*, *18*, 307-317.

Jeffrey, H. J. (1992). Chaos game visualization of sequences. *Computers & Graphics*, *16*, 25-33.

Jensen, H. J. (1998). *Self-organized criticality: Emergent complex behavior in physical and biological systems. Cambridge lecture notes in physics*. Cambridge, UK: Cambridge University Press.

Aks

Jonides, J., Irwin, D. E., & Yantis, S. (1981). Integrating visual information from successive fixations. *Science*, *215*, 192-194.

Kelso, J. A. S. (1995). *Dynamic patterns*. Cambridge: Cambridge, MA: MIT Press.

Klein, R. (1988). Inhibitory tagging system facilitates visual search. *Nature*, *334*, 430-431.

Kowler, E., Anderson, E., Doshier, B., & Blaser, E. (1995). The role of attention in the programming of saccades. *Vision Research*, *35*, 1897-1916.

Krendel, E. S., & Wodinsky, J. (1960). Search in an unstructured visual field. *Journal of the Optical Society of America*, *50*, 562-568.

Kristjansson, A. (2000). In search of remembrance: Evidence for memory in visual search. *Psychological Science*, *11*, 328-332.

Liebovitch, L. S. (1998). *Fractals and chaos: Simplified for the life sciences*. Oxford: Oxford University Press.

Locher, P. J., & Nodine, C. E. (1974). The role of scan paths in the recognition of random shapes. *Perception & Psychophysics*, *15*, 308-314.

McPeck, R. M., Maljkovic, V., & Nakayama, K. (1999). Saccades require focal attention and are facilitated by a short-term memory system. *Vision Research*, *39*, 1555-1566.

Maljkovic, V., & Nakayama, K. (1994). Priming of popout: I. Role of features. *Memory and Cognition*, *22*, 657-672.

Mata-Toledo, R. A., & Willis, M. A. (1997). Visualization of random sequences using the Chaos Game algorithm. *The Journal of Systems and Software*, *39*, 3-6.

Megaw, E.D., & Richardson, J. (1979). Target uncertainty and visual scanning strategies. *Human Factors*, *21*, 303-315.

Melcher, D., & Kowler, E. (2001). Visual scene memory and the guidance of saccadic eye movements. *Vision Research*, *41*, 3597-3611.

O'Regan, J. K. (1992). Solving the "real" mysteries of visual perception: The world as an outside memory. *Canadian Journal of Psychology*, *46*, 461-488.

Peak, D., & Frame, M. (1994). *Chaos under control: The art and science of complexity*. New York: Freeman & Co.

Posner, M., & Cohen, Y. (1984). Components of visual orienting. In H. Bauma & D. G. Bouwhuis (Eds.), *Attention and Performance X* (pp. 531-556). Hillsdale, NJ: Erlbaum.

Aks

Press, W. H., Flannery, S. A., Teukolsky, S. A., & Vetterling, W. T. (1986). *Numerical recipes*. New York: Cambridge University Press.

Pressing, J. (1999) The referential dynamics of cognition and action. *Psychological Review*, *106*, 714-747.

Rensink, R., O'Regan, J. K., & Clark, J. J. (1997). To see or not to see: The need for attention to perceive changes in scenes. *Psychological Science*, *8*, 368-373.

Scinto, L., Pillalamarri, R., & Karsh, R. (1986). Cognitive strategies for visual search. *Acta Psychologica*, *62*, 263-292.

Shore, D. I. & Klein, R. M. (2000). On the manifestations of memory in visual search. *Spatial Vision*, *14*, 59-75.

Simons, D. J., & Levins, D. (1997). Change blindness. *Trends in Cognitive Science*, *1*, 261-267.

Sprott, J. C. (2003). *Chaos and time-series analysis*. Oxford: Oxford University Press.

Sprott, J. C. & Rowland, G. (1995). *Chaos data analyzer*. Raleigh, NC: Physics Academic software (American Institute of Physics).

Stassinopoulos, D., & Bak, P. (1995). Democratic reinforcement: A principle for brain function. *Physical Review E*, *51*, 5033.

Townsend, J. T. (1974). Issues and models concerning the processing of a finite number of inputs. In B. H. Kantowitz (Ed.), *Human Information Processing: Tutorials in Performance and Cognition* (pp. 133-168). Hillsdale, NJ: Lawrence Erlbaum Associates.

Treisman, A., & Gelade, G. (1988). A feature integration theory of attention. *Cognitive Psychology*, *12*, 97-136.

Voss, R. F. (1992). Evolution of long-range fractal correlations and 1/f noise in DNA base sequences. *Physics Review Letters*, *68*, 3805-3808.

Ward, L. (2002). *Dynamical cognitive science*. Cambridge, MA: MIT Press.

Wolfe, J. M. (1994). Guided search 2.0: A revised model of visual search. *Psychonomic Bulletin & Review*, *1*, 202-238.

Zelinsky, G., & Loschky, L. (1998). Towards a more realistic assessment of visual short-term memory. *Investigative Ophthalmology & Visual Science*, *39*, S224.

## CHAPTER 8

# Categorization and Learning in Speech Perception as Dynamical Processes

Betty Tuller

Center for Complex Systems and Brain Sciences  
Florida Atlantic University  
Boca Raton, FL 33431  
U. S. A.  
E-mail: [tuller@ccs.fau.edu](mailto:tuller@ccs.fau.edu)

Tuller

The perception and production of speech unfolds in time. Although this seems like an obvious and perhaps trivial statement, this defining quality is not well captured by linguistic descriptions of speech, most of which are fundamentally static. Over the past few decades, both the theoretical and mathematical foundations for understanding organized behavior that emerges in time have been more fully developed and have infiltrated the study of many different human behaviors. In general, nonlinearity is a hallmark characteristic of these behaviors. That is, small changes in context or constituents can produce large behavioral effects and large changes in context or constituents might, in other conditions, produce little or no behavioral effect. The conditions that reveal the nonlinearities are often exactly those conditions that are excluded from experiments since they are more difficult to analyze and understand.

One nonlinear aspect of speech perception that has been the subject of a large number of studies is the phenomenon known as categorical perception. Within certain ranges of an acoustic parameter it is extremely difficult to discriminate between different stimuli that are labeled as the same speech segment. At the same time, stimuli with the same-size acoustic difference but in a different part of the parameter range are easily discriminated (e.g. Liberman, Cooper, Shankweiler, & Studdert-Kennedy, 1967; Liberman, Harris, Hoffman, & Griffith, 1957). As an example, consider the words "say" and "stay". When a short silent gap is introduced between the "s" noise and the vowel in "say" (e.g., from 0-20 ms), listeners continue to perceive the word "say." Similarly, listeners perceive the word "stay" when the silent gap after the "s" in the original stimulus is as long as 60 ms to 80 ms. But when

the gap ranges from 30-50 ms, the same absolute difference in gap duration as in the previous two examples (i.e., 20 ms), listeners perceive an abrupt shift in the stimulus from "say" to "stay" (Best, Morongiello, & Robson, 1981). Importantly, when listeners identify two stimuli as belonging to the same phonetic category, they often have great difficulty discriminating between them. As the "category boundary" nears, stimuli are more easily discriminated from each other. Obviously, stimuli that are identified as different words or syllables are also easily discriminated. This means that there is acoustic variability but phonetic/perceptual stability in some ranges of the acoustic parameter (here gap duration) but perceptual change accompanies the same degree of acoustic change for other values of the acoustic parameter. In other words, the relationship between acoustics and phonetic perception does not change in a linear fashion.

The perceptual boundaries between categories, or "critical points," are not hard-wired by neurophysiology, or set indelibly by one's native language, but adjust flexibly with factors such as phonetic context, the acoustic information available, speaking rate, speaker, and linguistic experience (see Repp & Liberman, 1987, for review). This is not simply a laboratory demonstration: Listeners recognize the same word produced by different speakers (males, females, speakers of different ages) and by the same speaker in markedly different linguistic and intentional contexts, even when the listener has had no prior experience with the other individual's speech patterns. Thus, perceptual stability coexists with perceptual flexibility.

About a decade ago, Pam Case, Mingzhou Ding, Scott Kelso and I considered seriously the ideas that speech categorization is inherently

Tuller

nonlinear, and that the nonlinearity can serve as a window into the dynamics of speech perception (i.e., the equations of motion that characterize the intrinsic organization of speech perception). My charge by the organizers of the NSF workshop “Nonlinear Methods in Psychology” was to re-cap that work as an example of how these ideas can help guide empirical studies to allow a deeper understanding of the phenomenon under study. In exploring the process of speech perception in a non-traditional way, two things are extremely important. First, it is important not to ignore the decades of previous research on how people perceive speech. Any alternative theoretical views should be compatible with that body of work. Second, theory and experiment are related in a mutually informative fashion. The investigator’s theoretical viewpoint guides not only *what* she or he chooses to examine, but also *how* it is examined. In turn, experimental results guide theory development, which then suggests the next empirical step. In the present case, since the focus is on evaluating whether the identification of speech sounds is itself characterized by what has been termed *perceptual dynamics* (characterized by multistability, loss of stability, flexibility, etc.; cf. Kelso, 1994a, 1995), the methodology chosen for the experiment must be one that allows for the possibility to see those signature characteristics. In what follows, I give a brief description of the main features of nonlinear dynamical systems relevant to this enterprise and describe how these features offered strategic guidance for the specific experiments and the theoretical model developed.

The first step was to conceive of perceptual space as a dynamical system with context, experience, and learning (among other things) as

processes that can modify this dynamical system. Briefly, a dynamical system is one that evolves over time such that its present state always depends in some rule-governed way on previous states. Differential equations or maps (equations that dictate how a system evolves in discrete time steps) of relevant variables offer a mathematical description of the system's behavior as time passes and parameters change. Typically, one observes the stable behaviors of a system, referred to as its *attractors*. The attractor layout, or set of possible behaviors of a system, may change over time in such a way that observed behaviors change gradually or abruptly. Abrupt, or qualitative, changes (called *phase transitions* or *bifurcations*) may be thought of as the spontaneous emergence of new forms of organization (a self-organized pattern formation process) under specific boundary constraints (e.g., Haken, 1977; Nicolis & Prigogine, 1977). In a speech perception experiment, qualitative change in categorization of the stimuli allows a clear differentiation between patterns; there is no ambiguity as to what are the stable patterns for a given listener. Note that the qualitative change (here the shift in categorization) is informationally meaningful (Kelso, 1994). Although in any experimental situation there are many variables likely to be changing, the key is to discover the ones that bring about this qualitative categorical change. As Kelso (1995) has pointed out, situations where qualitative change occurs are also regions of dynamic instability and dynamic instability is the generic mechanism underlying self-organized pattern formation (Haken, 1977; Nicolis & Prigogine, 1977). Without the dynamic instability, no change in pattern would occur. In turn, if one can see evidence of growing dynamic instability, then one can study the

Tuller

emergence of the new pattern. We will return to the idea of dynamic instability when we describe the experiments evaluating speech categorization as a dynamical phenomenon.

Although this description of qualitative pattern change as some parameter varies bears a strong similarity to the results of speech categorization tasks, the similarity may be only superficial. Empirical work on speech categorization, in order to maintain the independence of treatment levels required by most parametric statistical techniques, typically presents the stimuli to listeners in random order. Such experiments thus describe the location of a statistically defined phoneme boundary (most often, the point corresponding to the 50% crossover of the response function for a two-category set; see Ganong & Zatorre, 1980, for a comparison of different methods for defining boundary location). Unfortunately, this traditional methodology is far from optimal for revealing the dynamical characteristics being evaluated, because the randomization of stimuli destroys the footprints of any underlying dynamical process that may govern the transition between speech sounds. So one's theoretical viewpoint *must* influence experimentation from the initial design stage.

The strategy in our experiments was to use a stimulus continuum for which categorical perception has often been demonstrated but to vary the acoustic parameter sequentially, i.e., as a *control parameter*. A control parameter is one that, when the appropriate range of values is used, takes the subject from one perceived categorization to another. For some behaviors, finding control parameters is non-trivial. However, the literature on categorical perception gives us many plausible control parameters for different speech categorizations. In what follows, I will

review the observed dynamical effects and delineate some of the factors responsible. A model of the results was proposed and is discussed, and unique predictions of the model tested. Lastly, I will describe how viewing the speech perception process as a nonlinear dynamical system forces, as a natural extension, a re-examination of the process that occurs when learning to hear non-native phonemic distinctions. Our experiments demonstrate the fruitfulness of the approach and reveal that speech perception and perceptual learning in speech are characterized by rich underlying dynamics.

In 1994, Tuller, Case, Ding, and Kelso examined speech categorization when an acoustic parameter—the length of the silent gap between a natural “s” and a synthetic “ay”—was varied in a stepwise fashion. We used this particular stimulus continuum because it had already been shown that listeners perceive “say” at short silent gaps but they perceive “stay” at long silent gaps (e.g., Best et al., 1981). Thus, the gap duration after the “s” was a possible control parameter by which we could explore the mechanism of switching between categorizations. However, a major difference between our experiment and those of others was that we presented the stimuli *in order*. That is, gap duration either increased systematically from 0-76 ms, then back to 0 ms, in 4-ms steps, or decreased from 76 ms to no gap, then back to 76 ms in 4 ms steps. There were 5 trials of each of these two sequences. We also randomized the stimuli and presented 10 randomizations to the listeners. The subject’s task was to indicate whether they perceived the word “say” or the word “stay” by pressing appropriately labeled keys on a computer keyboard. First, we determined that the randomized stimuli resulted in the same perceptual identification function as

Tuller

reported previously in the literature. This ensured that our stimuli (and listeners) were equivalent to those used by others. Because the point at which categorization shifts as a function of the direction of changes in gap duration is considered a theoretically important juncture, the next analysis focused on that point.

Logically, there are only three possible patterns of switching: (1) A subject will switch between “say” and “stay” at the same gap duration regardless of direction of gap change (a critical boundary); (2) A subject’s percept will change at a larger gap duration as gap increases than when gap decreases (an effect known as *hysteresis* or *assimilation*); or (3) A subject’s percept will change at a larger gap duration when gap decreases than when gap increases (a contrastive effect). All three patterns were observed, with critical boundary being much less frequent than hysteresis or contrast, which occurred equally often. Thus, the perceptual changes in this speech identification task show quite complicated dynamics when a relevant acoustic parameter is sequentially varied. Closer analysis revealed that the incidence of hysteresis and contrast was not simply random fluctuation around a critical boundary, because their relative frequency changed in predicted ways over the course of the experiment. These patterns of change reveal that dynamic instability is playing a role in perceptual switching, thereby linking phonemic categorization to self-organized pattern formation.

How do you begin to connect experimental data to a generic dynamical model? Quite simplistically, since we have two reproducibly observed states—here the two categorizations “say” and “stay”—we identify the categorizations with attractors, or stable states in

perception. We use differential equations to define systems with attractor properties that fit the observed experimental data. Differential equations allow us to model quantities that change continuously in time. We can find stable solutions of the differential equations by finding equilibrium points, values of  $x$  for which the derivative  $dx/dt=0$  (see Equation 8.1; by definition, if the derivative of some variable is zero, that means the variable is unchanging, which is what it means for that value to correspond to a stable state). Trajectories (solutions to the differential equation) may be "attracted" to an equilibrium point or "repelled." We call the first case a *stable attractor* (also called a *sink*) and we call the second case an *unstable attractor* (also called a *source* or *repeller*).

If listeners perceived only a single perceptual category, a theoretical model of a single attractor, a fixed-point, would be adequate. A situation in which two states, or categories, occur requires that the model contain at least two stable attractors that change with the control parameter. In our case, the model must be able to account for the fact that at some gap durations a listener perceives only "say" and for other gap durations the listener perceives only "stay." The presence of hysteresis and contrast is also informative, indicating that more than one stable percept can coexist for a given acoustic stimulus—either "say" or "stay" might be perceived. In this case the stimulus is *bistable*—the two attractors must coexist for some range of the control parameter.

These results were modeled concisely by the following dynamical system (Tuller et al., 1994), written as a differential equation:

Tuller

$$dx/dt = -dV(x)/dx = -k + x - x^3 \quad [8.1]$$

Differential equations may be rewritten in the form of a potential function (Equation 8.2), in which the attractors are geometrically obvious when the potential is plotted. Here  $x$  is a variable characterizing the perceptual form and  $k$  is a parameter specifying the direction and degree of tilt for the potential. This allows visualization of the behavior of the system as the parameter  $k$  is manipulated.

$$V(x) = kx - x^2/2 + x^4/4 \quad [8.2]$$

Think of Equation 8.2 as describing the motion of a viscous point mass (a "sticky" ball) moving in the potential landscape  $V(x)$  (such as one of those shown in Figure 8.1). The minima of the potential, the valleys in the landscape, are the attractors corresponding to the two perceptual categories.

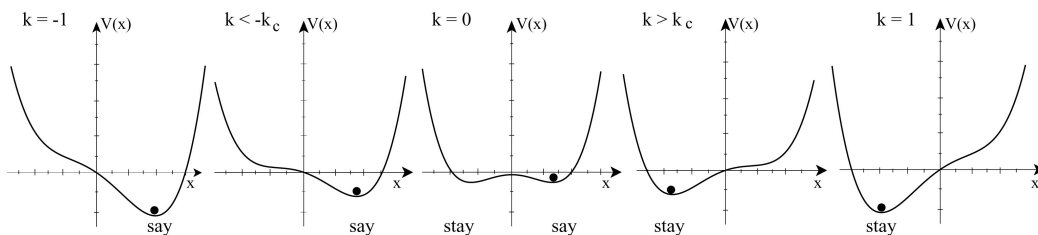


Figure 8.1. Potential landscape defined by Equation 8.2 for five values of  $k$  (adapted from Case et al., 1995).

Figure 8.1 shows how the landscape changes for several values of  $k$ . With  $k = \text{minimum}$  only one stable point exists corresponding to a

single category (e.g., “say”). As  $k$  increases, the potential landscape tilts but otherwise remains unchanged. However, when  $k$  reaches a critical point  $k = -k_c$ , a qualitative change in the attractor layout takes place. In other words, a bifurcation occurs. The particular change at  $k = -k_c$  is a saddle-node bifurcation in which a “saddle” (the point repeller, or maximum, at  $x = 0$ ) and a “node” (the point attractor at  $x < 0$ ) are simultaneously created. Thus, where there was once only a single perceptual category there are now two possible categories. This bistability, the co-existence of both categories, continues until  $k = k_c$  where the attractor corresponding to “say” ceases to exist via a reverse saddle-node bifurcation (where the qualitative change is from two available categories to one), leaving only the stable fixed point corresponding to “stay.” Further increases in  $k$  only serve to deepen the potential minimum corresponding to “stay.” Thus, the model captures the three observed states of the system: At the smallest values of the acoustic parameter only “say” is reported, for an intermediate range of parameter values either “say” or “stay” are reported, and for the largest values of gap duration only “stay” is reported.

An accurate portrait of any real-world problem must take into account the influence of random disturbances. In the present work, we considered factors such as fatigue, attention, and boredom to correspond to random disturbances because we could not measure the changes in those factors over time. Further experimental work may elaborate whether these factors are indeed random or predictable modifiers of perceptual space. Mathematically, spontaneous switches among attractive states occur as a result of these fluctuations, modeled as random noise. For a given point attractor, the degree of resistance to

Tuller

the influence of random noise is related to its stability, which, in general, depends on the depth and width of the attractor (i.e., its basin of attraction). As  $k$  is increased successively in Figure 8.1, the stability of the attractor corresponding to the initial percept decreases (the minimum becomes shallower and flatter), leading to an increase in the likelihood of switching to the alternative percept. This implies that perceptual switching is more likely with repeated presentations of a stimulus near the transition point than with repetition of a stimulus far away from the transition point, a prediction confirmed in Tuller et al. (1994).

In order to account for the three response patterns observed (critical boundary, hysteresis, and contrast), the behavior of  $k$  must have multiple determinants. One influential factor suggested by earlier research is the number of repetitions perceived from each category. Repetitive presentation of a speech stimulus has long been known to shift the location of adjacent phoneme boundaries in a predictable direction (see Darwin, 1976, and Eimas & Miller, 1978, for early reviews). Taking this factor explicitly into account we proposed the following equation describing the behavior of  $k$  as a function of the gap duration:

$$k(\lambda) = k_0 + \lambda + \varepsilon/2 + \varepsilon\theta(n-n_c)(\lambda-\lambda_f), \quad [8.3]$$

where the value of  $k_0$  specifies the percept at the beginning of a run,  $\lambda$  is linearly proportional to the gap duration,  $\lambda_f$  denotes the final value of  $\lambda$  (i.e., at the other extreme from its initial value), and  $n$  is the number of perceived stimulus repetitions in a run. The influence of the last term

depends on a step function,  $\theta(n-n_c)$ . Before a critical number of accumulated repetitions  $n_c$  is reached,  $\theta(n-n_c) = 0$ . That is, in the first half of each run, the tilt of the potential is only dependent on gap duration and the initial configuration. When  $n \geq n_c$  (during the second half of each run)  $\theta(n-n_c) = 1$ . This means that each step change in gap duration  $\lambda$  will produce a larger change in tilt  $k$  than it did in the first half of the run. An additional parameter,  $\varepsilon$ , represents cognitive factors such as learning, linguistic experience, and attention. Note that the importance of cognitive processes is well-established, for example, attention and previous experience play a large role in synergetic modeling of perception of ambiguous visual figures (Haken, 1990; Ditzinger & Haken, 1989, 1990) and contribute to factors that determine adaptation level in Helson's work (Helson, 1964).

Although the additional term was needed to incorporate contrast effects into the same model that described hysteresis and a critical boundary, it gave rise to unexpected predictions. For example, if the subject is presented with a run with gap duration first systematically increasing (from 0-76 ms) then systematically decreasing (from 76 ms back to 0 ms), the percept is predicted to be more stable—the potential would have a locally steeper slope—when the same stimulus appeared as the last item in the run than as the first item in the run. This is because the rate of change of tilt of the potential is faster in the second half of the run for the same amount of acoustic change. This prediction is unexpected given the literature on selective adaptation effects in speech. In selective adaptation, a standard identification task is first used to locate the “category boundary,” or point of subjective equality, for the test continuum. Next, the subjects listen to the stimulus from one

Tuller

end of the continuum presented many times over. After a second identification test with the original stimulus continuum, the position of the perceived category boundary moves towards the repeated stimulus. For example, in a [ba]-[pa] continuum varying in the lag of voicing onset after the initial consonant release burst, if the stimulus with the longest voicing lag is repeatedly presented after the first identification test, listeners then require a longer voicing lag for a stimulus to be perceived as a [pa] (Eimas & Corbit, 1973)—in our terms, perception of [pa] has destabilized. Somewhat counterintuitively, our model predicts that when a word is perceived many times over, its stability will increase.

This prediction was confirmed by experiment (Case, Tuller, Ding, & Kelso, 1995). In that work, we used the same “say”-“stay” stimulus continuum but asked listeners not only to categorize the stimulus as either “say” or “stay” but also to rate how good an exemplar of the category the stimulus was. The goodness rating was used as an index of the stability of the percept (the local steepness of the potential function). As predicted, regardless of whether the stimuli were presented with gap duration between the “s” and the “ay” first increasing from 0-76 ms and then decreasing back to 0 ms, or in the opposite direction, the same physical stimulus presented at the end of a sequence was judged a better exemplar of the category than was the identical stimulus presented at the beginning of the sequence (Figure 8.2). One crucial difference between the work of Case et al. (1995) and the earlier work on selective adaptation concerns the repeated stimulus. In the former, the stimuli were changing systematically, albeit at a subcategory level; in the latter, the identical stimulus (typically an

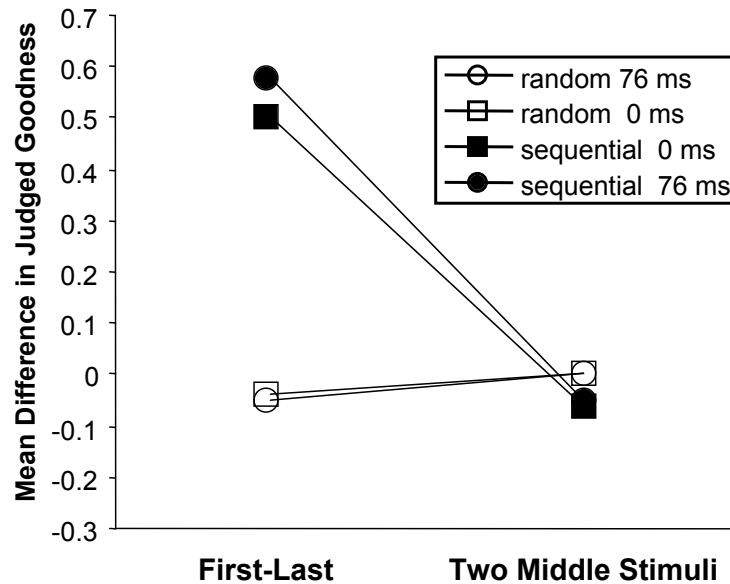


Figure 8.2. Mean differences in judged goodness versus position in sequence as a function of sequential vs. random stimulus order. When stimuli are presented sequentially (solid symbols), the last stimulus presented is judged as a better exemplar than the same stimulus when presented first in the sequence. This occurs for both 0 ms (square) and 76 ms (circle) gap stimuli and does not occur with random stimulus orders intervening (open symbols) or when the same stimuli are the “turnaround” stimuli in the middle of the trial (adapted from Case et al., 1995).

end-point stimulus) was repeated. In fact, when Case and colleagues presented stimuli with an intervening set of stimuli with randomly changing gap durations, no differences in judged goodness were observed. This result confirmed one prediction of speech categorization as a context-sensitive, pattern-forming system.

Another difference between this empirical confirmation of the model’s predictions and the literature on selective adaptation motivated additional research. The model implies that the temporal evolution of the alternative forms, and hence switching between them,

Tuller

depends on how the stimuli move through perceptual space. This was supported by Case et al. (1995), described above, at least for the judged goodness of the stimuli as members of the identified category. Thus, systematic change in an acoustic control parameter, and not solely the number of stimulus repetitions, is crucial. This was tested directly by presenting subjects with a single "say"-"stay" trial with gap duration either increasing or decreasing (again, in 4-ms steps between 0-76 ms silent gap). The second trial was adjusted for individual subject responses to the first trial. If, for example, a subject heard a switch from "say" to "stay" on the 6th stimulus in the first trial, then in the second trial stimulus #1 was presented 5 times, then stimulus #6 was presented, then the trial continued to the end, with each successive stimulus presented once. Selective adaptation leads one to expect that repeating the initial stimulus in trial 2 should cause listeners to switch earlier, or at the same stimulus, as in trial 1 (*contrast* or *critical boundary* should increase in observed frequency). Similarly, if the preponderance of hysteresis observed previously reflects only a response perseveration, then the incidence of *critical boundary* should increase markedly because both trials present the same number of instances of the initial category. Identical predictions are made by Helson's (1964) Adaptation Level Theory, which holds that all stimulus inputs in a given domain are pooled and their running average determines the level of stimulation to which the person is adapted. Alternatively, if the underlying nonlinear dynamic model has validity, then subcategorical sequential acoustic change, not simply perceived repetition, enhances hysteresis. Results confirmed overwhelmingly that only sequential acoustic change increases the frequency of hysteresis

(Figure 8.3), a result that was later shown to generalize to the perception of directional pitch (Giangrande, Tuller, & Kelso, 2003).

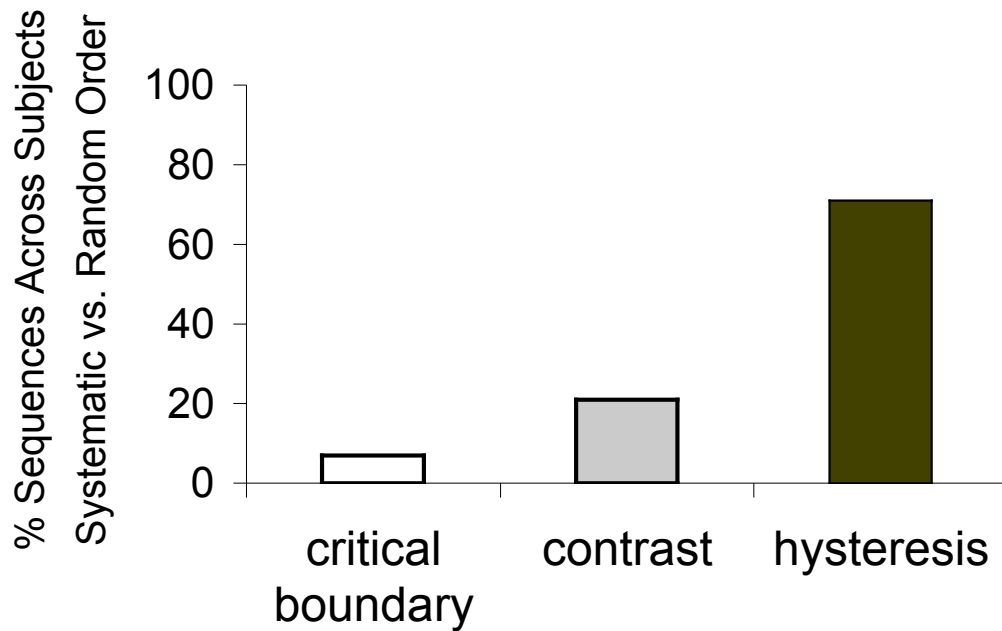


Figure 8.3. Comparison of switching behavior in sequences that contain systematic acoustic change with matched sequences that instead repeat the end-point category (see text). Percent of sequence pairs perceived as switching at the same stimulus (critical boundary; white bar), systematic stimulus change switching earlier than random change (contrast; gray bar), and systematic stimulus change switching later than random change (hysteresis; black bar).

Yet another test of the model's predictions began to address the role of learning and experience. Recall that enhanced experience (of which stimulus repetition is one example) causes the potential to change more rapidly. Minimizing learning and experience should lead to a majority of hysteresis response patterns; contrast should occur much less often. To evaluate this prediction, we presented subjects with

Tuller

a single run of the "say"-"stay" continuum with gap duration first increasing from 0-76 ms then decreasing back to 0 ms. Another group of subjects was presented with a single run of stimuli that began at 76 ms gap duration, decreased in 4-ms steps to no gap, then increased back to 76 ms gap duration. The task was to identify each stimulus as "say" or "stay." A subject's pattern of responding (hysteresis, critical boundary, or contrast) was determined by comparing the gap duration at which the perceptual switch occurred in the increasing vs. decreasing portion of a run. Results confirm that when experience with the stimuli is minimized, the proportion of hysteretic responses is far greater than either contrast or critical boundary. In fact, hysteresis is over 3 times more prevalent than any other response pattern and is independent of the direction of change in gap duration. When the first trial for each subject from Tuller et al. (1994) and Case et al. (1995) is examined, results are statistically identical to those obtained when subjects were presented with only a single trial (Figure 8.4).

Obviously, these experiments consider only a very restricted definition of "phonological learning" in adults. Typically, when adults attempt to learn new speech sounds, they do so in the context of the phonology of their native language. From the perspective we have been taking, it makes sense to think of perceptual space as a dynamical system that is modified by learning. In other words, learning a new phonological category (when a range of acoustic objects acquires a common meaning) is viewed as the creation of an attractor that modifies the existing dynamics. This allows us to predict how learning will proceed, depending on how the stimuli are initially perceived by the individual. In non-speech perceptuomotor tasks, evidence that

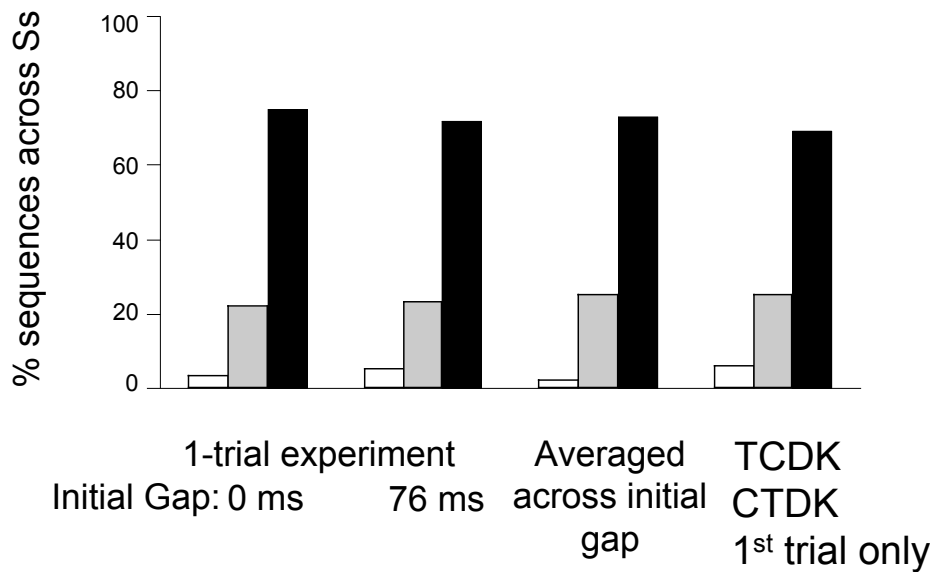


Figure 8.4. Percent of sequences perceived as having a critical boundary (white bar), contrast (gray bar), and hysteresis (black bar) when for only one trial per subject, or the first trial per subject. TCDK: Tuller et al. (1994). CTDK: Case et al. (1995).

learning consists of the interaction between pre-existing constraints that the subject brings into the learning situation and the behavior to be learned has been provided by Schöner and Kelso (1988; see also Schöner, Zanone, & Kelso, 1992). In their model, behavioral information (such as the task to be learned) acts as a parameter of the attractor dynamics, attracting behavior toward the required behavior. When the former does not correspond to a stable attractor of the existing, intrinsic dynamics, learning is predicted to take the form of a phase transition: A new behavioral attractor is found that alters the entire dynamics. When the required task is close to, or coincides with, an existing stable pattern, cooperative mechanisms ensure that learning

Tuller

will proceed rapidly and smoothly (Zanone & Kelso, 1992; 1994; 1997; see also Kelso, 1990).

How might these ideas impact upon the acquisition of new phonological categories that a person has never used? If a listener initially can perceive a non-native sound as "different" from a native one, although perhaps still acceptable as an exemplar of the native category, the existing perceptual landscape cooperates with the sound to be learned. Operationally, the rate of change of the landscape to include the sound to be learned, the progressive stabilization of the new sound, should be relatively smooth and fast. In contrast, if a listener initially perceives the non-native sound as indistinguishable from a native one, then learning to recognize the non-native sound competes with the existing perceptual organization. In this case, the strength of the attraction of the to-be-learned sound increases until a qualitative change (a bifurcation, or phase transition) reflects the emergence of a new attractor. The rate of change of the perceptual space to the new sound should be slower than when the initial perceptual landscape cooperates with the new sound. In addition, because this competition entails destabilization of the existing attractor, the bifurcation should be marked by high variability.

In order to test these ideas, it is necessary to modify the standard experimental techniques used in phonological learning tasks in two ways. First, it is not sufficiently informative simply to note whether learning occurs with a particular stimulus set and training régime. Observations of the changes in each listener's behavior as learning proceeds must supplement measures of whether the trained distinction was finally learned to some criterion. Second, the focus of analysis must

be the individual, not the language. As an example, consider Iverson and Kuhl's (1996) investigation of native English speakers' perception of English /r/ and /l/ in which multidimensional scaling analyses of individual listener's similarity ratings of stimulus pairs revealed that the warping of perceptual space corresponded best to the listener's own identification patterns. Similarly, Aaltonen, Eerola, Hellström, Uusipaikka, and Lang (1997) showed individual differences in mismatch negativity EEG patterns depending on how the subject categorized the stimulus sequence. In other words, perceptual learning as a result of language training must be assessed relative to the individual's perceptual space as it exists before training begins. To do this, appropriate probes, or maps, of the latter should be conducted prior to, and during, the learning process.

In a doctoral thesis that embodied these attributes, Case (1996) used the voiced Hindi dental stop consonant /d/, which is acoustically similar to the American English alveolar stop consonant /d/, as the category to be learned. The major articulatory distinction between these two sounds is in place of articulation—in /d/ the tongue tip is placed against the upper front teeth, and in /d/, the tongue tip is against the alveolar ridge. There is no phonemic contrast between the dental and alveolar place of articulation in either Hindi or American English, although it is contrastive in at least a half dozen languages (including Malayalam and several Australian and African languages; Jongman, Blumstein, & Lahiri, 1985).

Here I will concentrate on the following questions: What are the dynamics of the learning process itself? Does the form that learning takes depend on the relationship between the sounds to be learned and

Tuller

how the individual initially perceives them? What are the effects of learning a new speech sound on an acoustically/articulatorily close native speech sound? That is, does an individual's phonetic system reorganize during learning by modifying native categories (e.g., Flege, 1995)?

To answer these questions, we used a “perceptual mapping” procedure that included three different tasks (identification, judged goodness, and difference ratings). These tasks together allow a more complete assessment of each listener's perceptual space than use of any of the tasks alone. Each of the tasks taps somewhat different aspects of speech perception. Identification tasks encourage phonetic coding, and a variable stimulus context that includes different speakers, utterances, and phonetic contexts facilitates robust category formation with training (Lively, Logan, & Pisoni, 1993; Pisoni & Lively, 1995). The judged goodness task examines the internal structure of a category in a way that an identification task obscures, allowing the listener to determine how good an exemplar of a category a given stimulus is and focusing attention on differences among stimuli. Data from the difference-rating task allow one to investigate the internal structure of one or more categories simultaneously. Incorporating the results of all three tasks gives a fuller picture of how a given listener perceives the stimuli.

A group of monolingual American English listeners first completed the three-task perceptual mapping procedure and then participated in a 15-session training program distributed over a three-week period. Their progress was monitored throughout training. Following training, the perceptual mapping procedure was repeated.

Pre-training/post-training comparisons as well as daily assessments during the training process were performed to assess whether learning occurred and, if so, to reveal its dynamics. Persistence of learning was evaluated by follow-up testing administered a few weeks after the training was completed. This methodology stems from the scanning probes of the dynamics employed during the learning process by Zanone and Kelso (1992, 1997) in order to understand how, in their case, pre-existing coordination tendencies were modified by practicing a new skill.

The training stimuli, a list of /CV/ syllables and / $\alpha$ CV/ disyllables, were produced by four native speakers of Hindi (H) and two native speakers of American English (AE). The consonant was either / $\underline{d}$ / or /d/ and the vowels were those in "hot," "heat," "hoot," and "hut." Hindi speakers were instructed in the production of the alveolar stop, and AE speakers were instructed in the production of the dental stop. Three native speakers of AE rated all intended alveolar productions and three native speakers of H rated all intended dental productions. Only productions judged to be acceptable by all native listeners were used in training. The final training set was acoustically diverse in that it included 3 tokens each of the 16 different syllables (8 dental, 8 alveolar) from four H speakers and two AE speakers.

The test stimuli were a synthetic continuum of eleven syllables with an initial stop consonant followed by the vowel / $\alpha$ /. The consonant spanned a range from the Hindi dental / $\underline{d}$ / to the American English alveolar /d/ by manipulating the second (F2) and third (F3) formant onset frequencies. Hindi listeners judged stimuli from the dental end of

Tuller

the continuum to be better exemplars of their native category than stimuli from the alveolar end of the continuum.

Monolingual speakers of American English (AE) participated in two pre-training sessions of about one hour each. In the first session, they performed the judged goodness and identification tasks. In the second session, they performed the difference-rating task. For the judged goodness procedure, subjects were presented with a randomized set of ten tokens each of the eleven unique synthetic stimuli. The task was to rate from 1 to 7 (poorest to best) how good an exemplar of /d/ the stimulus was.

For the identification task, subjects were presented with a differently randomized set of ten tokens each of the eleven stimuli. Subjects were told that stimuli would be either a synthesized version of an American English alveolar /d/ or a Hindi dental /d̪/. Differences in how the two sounds are produced were described and examples of the endpoint stimuli from the continuum representing the two sounds were presented. The two-alternative forced-choice task was to identify the stimulus as either alveolar or dental.

In the difference rating task subjects heard all possible pairs of stimuli from a 6-stimulus subset of the continuum (stimuli 1, 3, 5, 7, 9, and 11). Pairs were rated on a scale from 1 to 7, with 1 being "exactly the same" and 7 being "most different."

After the initial perceptual mapping subjects participated in 15 training sessions within a 3-week period, a second perceptual mapping just after training, and another mapping at least two weeks later. Each daily training session consisted of (in order) an initial free exploration period, a two-alternative forced-choice identification task (with

feedback) for a training set of 48 natural speech stimuli randomly chosen from the full set of 288 natural speech stimuli, the difference rating test, an identification task with feedback for a different 48-item subset of the natural speech stimuli, and a second difference rating test with a new randomization of stimulus pairs. If subjects had not been paid for participating I doubt anyone would have completed the experiment!

Although every subject showed some improvement in differentiating dental from alveolar stop consonants in natural speech, in what follows, I will discuss two subjects' learning patterns in order to address the questions posed above.

In the pre-training identification task with voiced stimuli, our first learner showed some ability to identify the four extreme dental-end stimuli as dental (Figure 8.5). Nevertheless, he still rated all stimuli as relatively good members of the alveolar category (Figure 8.6). These results are intriguing in that stimuli consistently identified as dental were still judged as relatively good alveolars. This underscores not only the poverty of using only a single measure of an individual's phonetic perception but also the flexibility of perception.

In both the post-training and follow-up identification tasks, the identification functions partition the stimuli into two clear categories with more stimuli now being identified as dental (Figure 8.5). In contrast to the pre-training mapping, however, stimuli on the dental end of the continuum are now judged to be poor exemplars of the alveolar category and the stimulus judged as the "best" alveolar moves toward the alveolar end of the continuum (Figure 8.6).

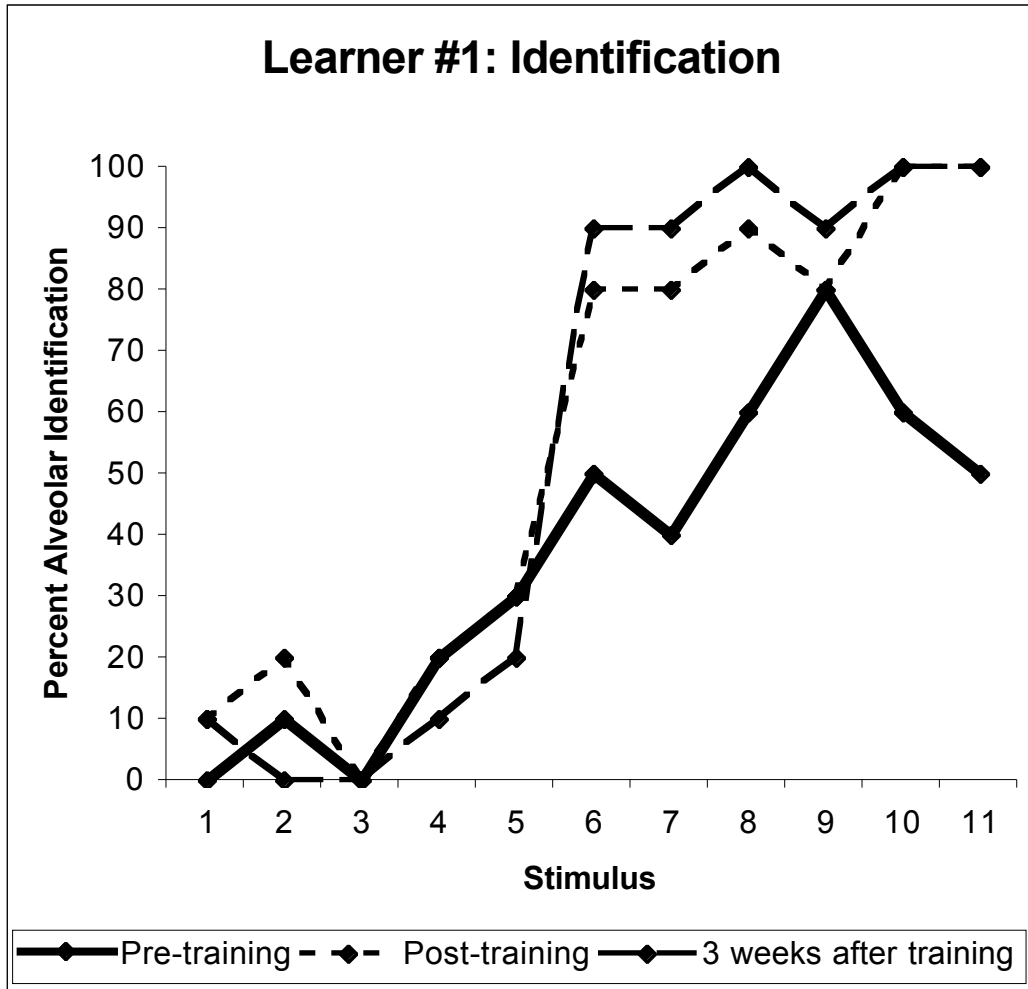


Figure 8.5. Identification functions pre-training (solid line), post-training (dotted line), and three weeks after training (dashed line) for learner #1.

Multidimensional scaling (MDS) analyses based on the difference ratings were also calculated. MDS is a technique used to uncover and visualize proximities in a low dimensional space and is strongly related to methods such as principal component analysis and cluster analysis. Although in many perceptual studies order of presentation of stimuli in a pair is presumed to have no effect

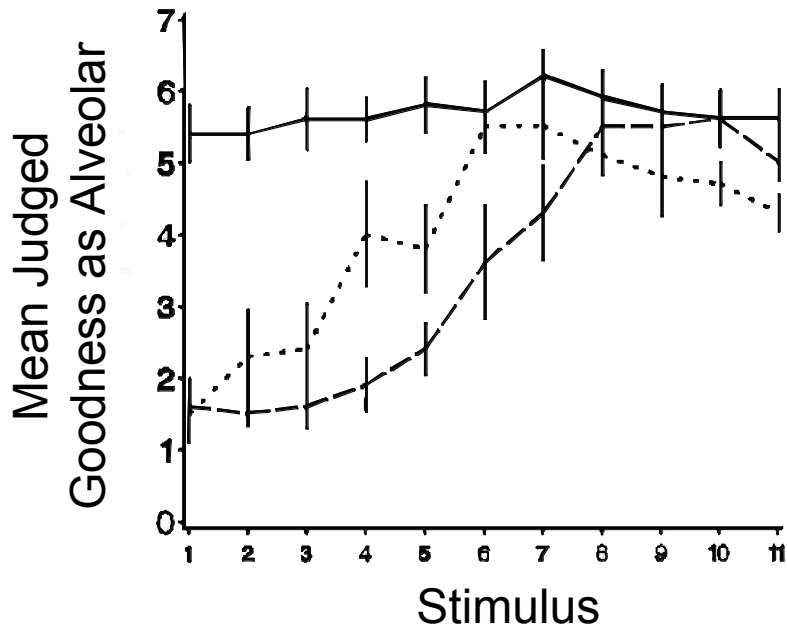


Figure 8.6. Mean judged goodness (error bars indicate one standard deviation) as an exemplar of the alveolar /d/. Pre-training (solid line), post-training (dotted line), and three weeks after training (dashed line) for Learner #1.

(Schiffman, Reynolds, & Young, 1981), our earlier data suggested that order of pair elements might indeed influence difference ratings (in other words, the initial condition, or initial categorization, matters). In the pre-training data, when the first stimulus in a pair is identified as the subject's native category, stimuli that are acoustically closest to the best exemplar are attracted or pulled in; dental-end stimuli cluster separately from the alveolar-end stimuli. When the acoustically more dental stimulus is presented first, there is little if any evidence of stimulus grouping before training. In the post-training and follow-up testing, the dental-first pairs also show an attractive effect, although the effect is still weaker than that observed for the pairs in which the native sound, the alveolar, is presented first. When the day-to-day variability

Tuller

of the MDS solutions is calculated, total variability is relatively low from the beginning of training and quickly decreases over the first six days, remaining low thereafter. The initially higher variability in the total is exclusively due to the degree of clustering across the alveolar-first pairs (Figure 8.7).

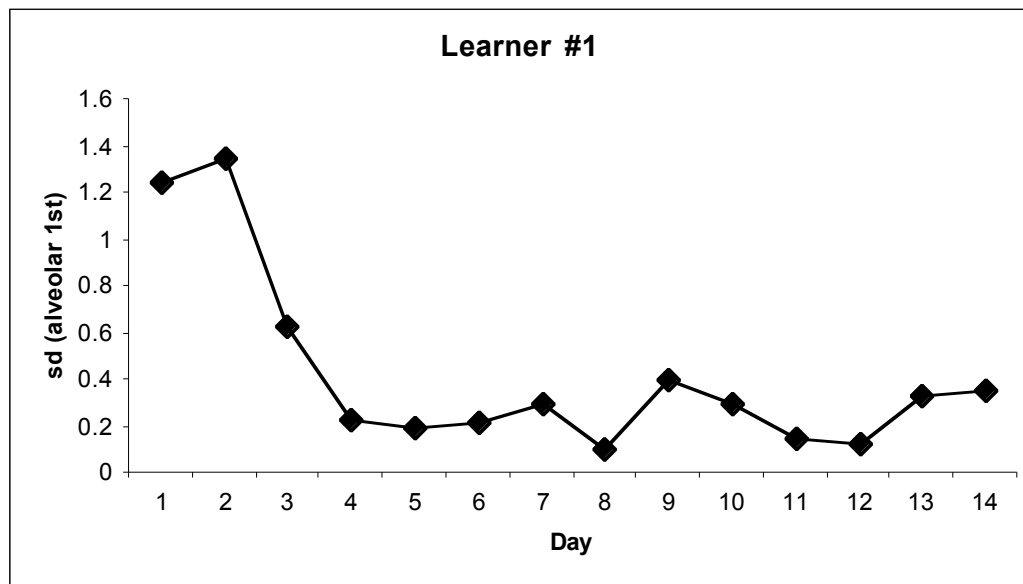


Figure 8.7. Total variability in the MDS analysis, as a function of day of training.

Our second learner showed a very different initial perceptual mapping from learner #1, and a markedly different pattern of learning over time. Pre-training, only stimuli 7 and 8 are identified at levels different from chance (both as alveolar; Figure 8.8) and stimulus 8 is judged as the "best" alveolar (although all stimuli were judged as acceptable members of the alveolar category; Figure 8.9). After training and in follow-up testing, this subject's identification functions showed clear categorization of the stimuli into alveolar and dental, with

stimuli on the alveolar end of the continuum now judged to be better exemplars of the alveolar category than stimuli from the dental end. Stimulus 11, judged the best alveolar after training, was also judged a better alveolar than before training (Figures 8.8 and 8.9).

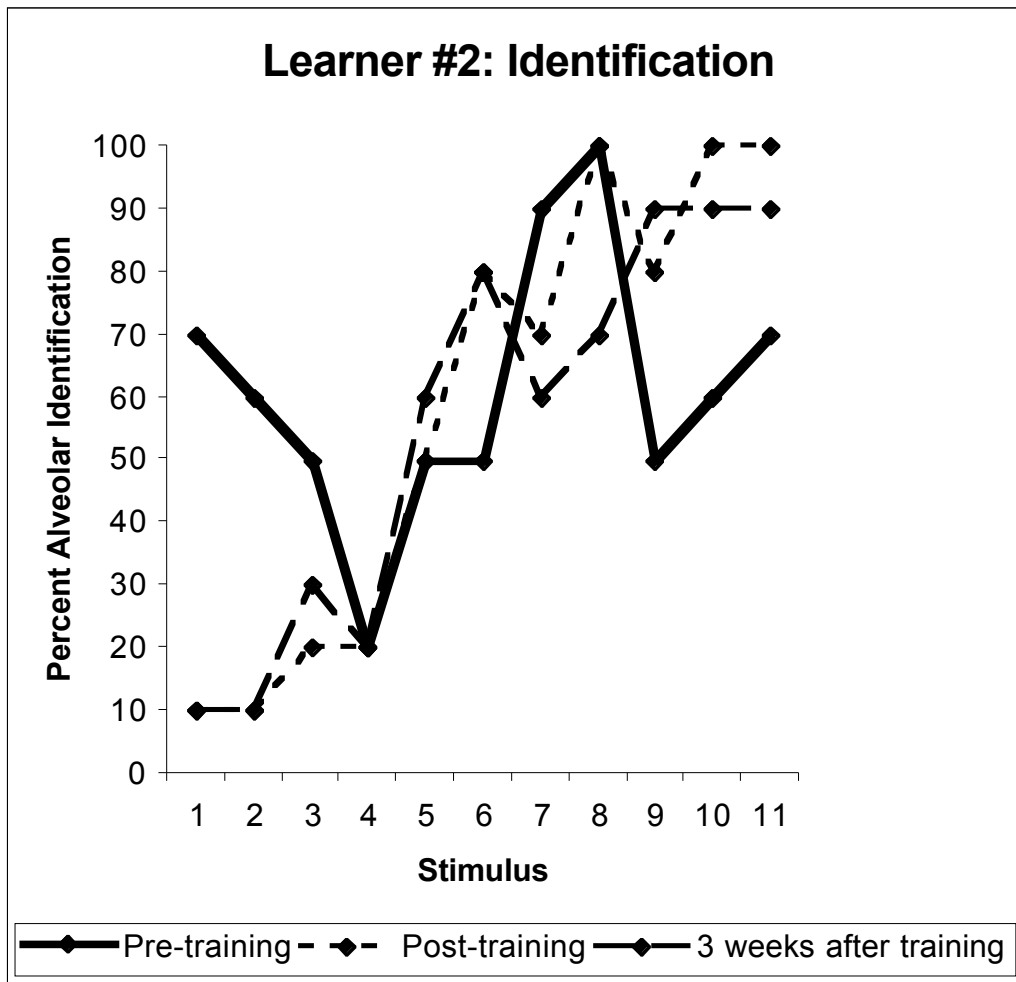


Figure 8.8. Identification functions pre-training (solid line), post-training (dotted line), and three weeks after training (dashed line) for Learner #2.

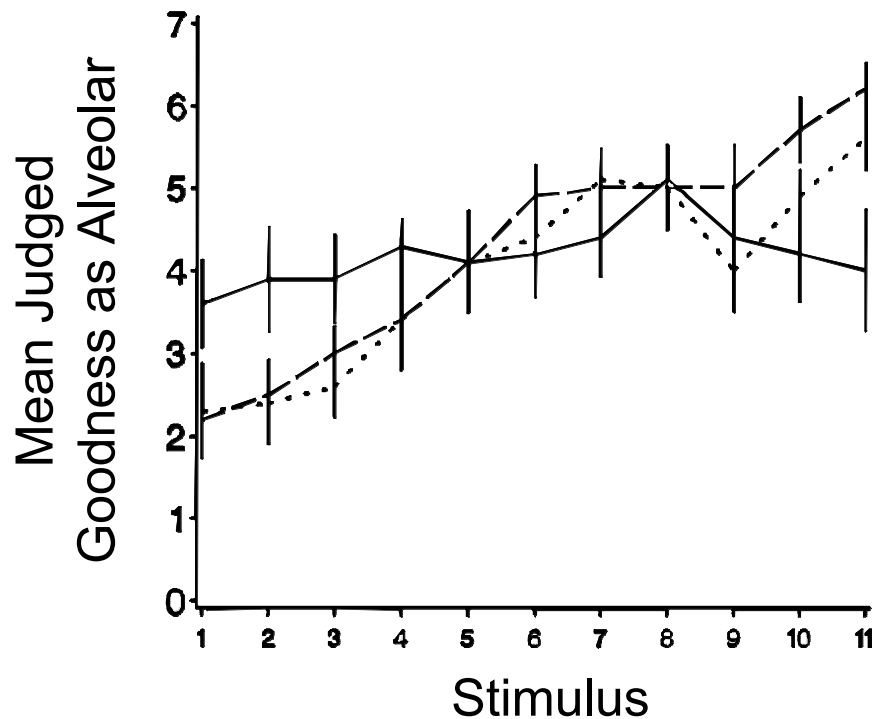


Figure 8.9. Mean judged goodness (error bars indicate one standard deviation) as an exemplar of the alveolar /d/. Pre-training (solid line), post-training (dotted line), and three weeks after training (dashed line) for Learner #2.

The MDS analyses based on difference ratings (taking order into account) revealed that the pre-training solution does not respect acoustic ordering, consistent with the initial identification results. By the time of the post-training evaluation, difference ratings of the alveolar-first pairs showed a tight clustering of stimuli into two groups corresponding to alveolars and dentals; dental-first pairs also grouped, although somewhat more weakly. Grouping of stimuli was tighter in the follow-up as well, with less of an order effect. The total variability in the MDS solutions is shown in Figure 8.10. Total variability was initially much higher than for learner #1 and showed a steady decline until,

around Day 5, an increase in variability occurred through Day 9. This increase preceded a sharp drop in total variability at Day 10 to levels equivalent to those observed for learner #1. Note that the peak in variability in judging the alveolar-first pairs may be interpreted as a *destabilization* of the attractor corresponding to the alveolar category.

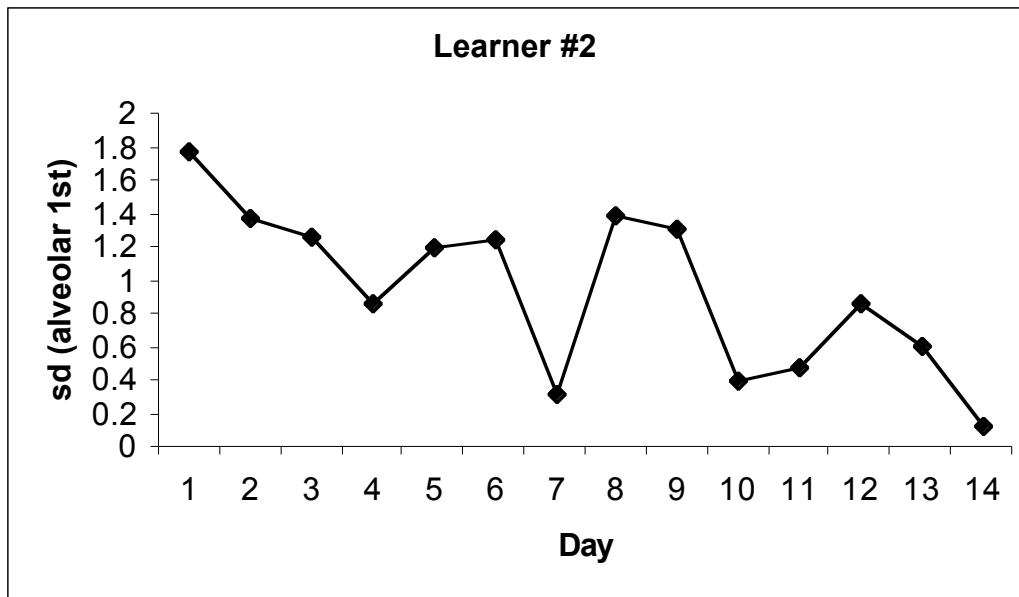


Figure 8.10. Total variability in the MDS analysis, as a function of day of training.

To summarize, learner #1 showed an initial ability to distinguish some of the dental-end stimuli from the alveolar, even though they were still acceptable as alveolars. The pre-, post-, and follow-up test results all indicate a smooth and rapid learning process occurring over the first six days of training and the decrease in variability in his MDS profile was smooth and fast. This is congruent with the initial prediction: If a listener initially can perceive a non-native sound as "different" from

Tuller

a native one, the existing perceptual landscape cooperates with the sound-to-be-learned and learning should be relatively smooth and fast. This pattern is consistent with the idea of progressively stabilizing an already existing stable pattern.

Learner #2 showed little evidence for an initial ability to hear dental-end stimuli as different from alveolar-end stimuli. Variability of the MDS solutions also began at a level nearly three times greater than initial variability for learner #1, and the rate of contraction of the stimuli into groups was slower than for learner #1. After the variability began to decrease, it reversed direction and peaked again just prior to reliable clustering of the MDS solutions. This local increase in variability occurred almost exclusively in alveolar-first pairs and can be considered analogous to critical fluctuations that often precede bifurcations (Schöner, Haken, & Kelso, 1986). Again, these results were congruent with predictions: If a listener initially perceives the non-native sound as indistinguishable from a native one, then learning to recognize the non-native sound competes with the existing perceptual organization. This process is slower than when the initial perceptual landscape cooperates with the new sound, and because this competition entails destabilization of the existing attractor, the bifurcation is marked by high variability.

One aspect of the data that has not yet been highlighted is that learning the non-native category modified perception of the native one (cf. Flege, 1992, 1995), especially for listeners who did not initially parse the stimulus continuum. After learning, not only did the stimulus judged as the best alveolar exemplar shift away from the dental group, but the best exemplar was also a better exemplar post-training than

pre-training. Thus the pre-existing phonological organization is malleable. Learning does not entail simply an addition of a new category but in fact changes the existing attractor layout (see also Sancier & Fowler, 1997).

In the cognitive, behavioral, and brain sciences, large strides have been made in understanding pattern formation using the concepts of self-organization and the mathematical tools of nonlinear dynamical systems (e.g., see Haken & Stadler, 1990, for a variety of different contributions in this context; Kelso, 1995). Explicitly dynamical investigations of speech include attempts to identify phonological units with dynamically specified gestures (Browman & Goldstein, 1986, 1989, 1992; Kelso, Saltzman, & Tuller, 1986; Kelso, Tuller, & Harris, 1983), to construct a topology of vowels (Wildgen, 1990) and consonants (Petitot-Cocorda, 1985) in terms of a landscape of attractors and repellers within an articulatory or acoustic space, and to model the phonological system of artificial languages as a self-organized solution of talker-based and listener-based constraints (Lindblom, MacNeilage, & Studdert-Kennedy, 1983). In our own work (Tuller et al., 1994; Case et al., 1995; Tuller, 2003), we demonstrated that changes in perception that occur as the acoustic signal is altered are indicative of a pattern-formation process in perception. A model of the results was proposed and unique predictions of the model were tested and confirmed.

The approach also provides a theoretically motivated way to understand the process of learning to perceive non-native speech sounds (and perhaps the emergence of categories in development). Fundamental to this approach is a methodological stance: Instead of studying features of objectively existing prototypes (either as abstract

Tuller

linguistic entities or as stored multiple exemplars) in a group of listeners, focus on the interaction of an individual perceiver with speech stimuli in context. In this way, we have observed changing patterns of categorization that parallel those observed in perceptuo-motor learning (Kelso, 1990; Kelso & Zanone, in press; Schöner, Zanone, & Kelso, 1992; Zanone & Kelso, 1992, 1994, 1997) and are consistent with the notion that reliably categorizing a new speech sound depends on whether the new category cooperates or competes with an individual's initial perceptual capabilities and that learning serves to reorganize the perceptual space.

In summary, I have described a program of research in which the tenets of dynamical systems and empirical research on speech are mutually informative and directive. In this, I have followed the basic strategy identified by Kelso (in press), but applied to the study of speech perception. This strategy entails (1) Choosing a level of analysis and description that captures the behavior you are studying. (So if I'm interested in how people learn to change their perceptual categorization of speech, it would not be fruitful to choose to describe the behavior in terms of the phasing of harmonics in the signal.); (2) Prune away complications so that the essence of your question remains foremost in the experimental design; (3) Focus on finding the conditions that yield qualitative changes in behavior. Qualitative change allows one to define the perceptual categories clearly as well as to exploit the *patterns* of change as a key to the mechanisms underlying pattern formation (e.g., dynamic instability); and (4) Explore both the coordinative and the component levels as well as the relation between them. How one defines the coordinative level and

“one level down” depends on the experimenter’s insights into step (1)—choosing the level of description. This last step, deriving the coordinative level dynamics from the usually nonlinear coupling among individual components, is as yet the weakest link in understanding the self-organizing nature of speech dynamics.

Finally, the empirical and modeling strategy described here is both speech-specific and generalizable. The approach has also been fruitfully applied to the verbal transformation effect (Ditzinger, Tuller, Haken, & Kelso, 1997; Ditzinger, Tuller, & Kelso, 1997) and more recently, auditory streaming (Almonte, Jirsa, Large, & Tuller, submitted). It also shares much with studies of the effects of attention on behavioral patterns (e.g., Temprado, Zanone, Monno, & Laurent, 1999), and with studies of learning from behavioral, theoretical, and neurophysiological perspectives (Jantzen, Fuchs, Mayville, & Kelso, 2001; Kelso & Zanone, in press; Kelso, 1995; Schöner, Zanone, & Kelso, 1992; Sporns & Edelman, 1993; Zanone & Kelso, 1992, 1994, 1997). More recently, neural correlates of the stability and change of behavioral coordination have been uncovered using several methods that reveal brain function, such as high density SQuID, multichannel EEG, and functional MRI and PET (Daffertshofer, Peper, & Beek, 2000; Frank, Daffertshofer, Peper, Beek, & Haken, 2000; Fuchs, Jirsa, & Kelso, 2000; Fuchs, Kelso, & Haken, 1992; Fuchs, Mayville, Cheyne, Weinberg, Deecke, & Kelso, 2000; Kelso, Bressler, Buchanan, DeGuzman, Ding, Fuchs, & Holroyd, 1992; Kelso, Fuchs, Holroyd, Lancaster, Cheyne, & Weinberg, 1998; Mayville, Bressler, Fuchs, & Kelso, 1999; Mayville, Fuchs, Ding, Cheyne, Deecke, & Kelso, 2001; Meyer-Lindenberg, Ziemann, Hajak, Cohen, & Berman, 2002; Ullen, Ehrsson, & Forssberg,

Tuller

2000; Wallenstein, Kelso, & Bressler, 1995). Behavioral investigations have been spurred by, and have spawned, theoretical work at the neural level (Fuchs & Jirsa, 2000; Haken, Kelso, & Bunz, 1985; Jirsa, Fink, Foo, & Kelso, 2000; Jirsa, Friedrich, Haken, & Kelso, 1994; Jirsa & Haken, 1996, 1997; Schöner, Haken, & Kelso, 1986; Schöner, Jiang, & Kelso, 1990; Treffner & Turvey, 1996) that is rapidly becoming more neurobiologically grounded (Frank et al., 2000; Fuchs et al., 2000; Jirsa, Fuchs, & Kelso, 1998; Jirsa & Haken, 1997).

Despite this wealth of information concerning the dynamics of behavior, the specific boundary conditions and control parameters that establish the context for speech phenomena, the coordinative and component levels that makes sense in speech, are specific to speech and must be identified within the speech context. “Dynamics” in and of itself will not give us the answers—it must be fleshed out for each system under study with conceptual content and implementation via experiment, simulation, modeling, and theory development.

REFERENCES

Aaltonen, O., Eerola, O., Hellstrom, A., Uusipaikka, E., & Lang, A. H. (1997). Perceptual magnet effect in the light of behavioral and psychophysiological data. *Journal of the Acoustical Society of America*, *101*, 1090-1105.

Almonte, F., Jirsa, V. K., Large, E., & Tuller, B. (submitted). Neural model of streaming in rhythm perception.

Best, C. T., Morongello, B., & Robson, R. (1981). Perceptual equivalence of acoustic cues in speech and nonspeech perception. *Perception and Psychophysics*, *29*, 191-211.

Browman, C., & Goldstein, L. (1986). Towards an articulatory phonology. *Phonology Yearbook*, *3*, 219-252.

Browman, C., & Goldstein, L. (1989). Articulatory gestures as phonological units. *Phonology*, *62*, 210-251.

Browman, C., & Goldstein, L. (1992). Articulatory phonology: An overview. *Phonetica*, *49*, 155-180.

Case, P. (1996). *Learning to hear new speech sounds: A dynamical approach*. Unpublished doctoral dissertation, Florida Atlantic University, Boca Raton, FL.

Tuller

Case, P., Tuller, B., Ding, M., & Kelso, J. A. S. (1995). Evaluation of a dynamical model of speech perception. *Perception and Psychophysics*, *57*, 977-988.

Daffertshofer, A., Peper, C. E., & Beek, P. J. (2000) Power analysis of event-related encephalographic signals. *Physics Letters A*, *266*, 290-302.

Darwin, C. (1976). The perception of speech. In E.C.M. Friedman (Ed.), *Handbook of Perception, Vol 1* (pp 175-226). New York: Academic Press.

Ditzinger, T., & Haken, H. (1989). Oscillations in the perception of ambiguous patterns: A model based on synergetics. *Biological Cybernetics*, *61*, 279-287.

Ditzinger, T., & Haken, H. (1990). The impact of fluctuations on the recognition of ambiguous patterns. *Biological Cybernetics*, *63*, 453-456.

Ditzinger, T., Tuller, B., & Kelso, J. A. S. (1997). Temporal patterning in an auditory illusion: The verbal transformation effect. *Biological Cybernetics*, *77*, 23-30.

Ditzinger, T., Tuller, B., Kelso, J. A. S., & Haken, H. (1997). A synergetic model for the verbal transformation effect. *Biological Cybernetics*, *77*, 31-40.

Eimas, P. D., & Corbit, J. D. (1973). Selective adaptation of linguistic feature detectors. *Cognitive Psychology*, *4*, 99-109.

Eimas, P., & Miller, J. (1978). Effects of selective adaptation on the perception of speech and visual patterns: Evidence for feature detectors. In R. Walk & H. Pick (Eds.), *Perception and Experience* (pp. 307-345). New York: Plenum.

Flege, J. E. (1992). Speech learning in a second language. In C. A. Ferguson, L. Menn, & C. Stoel-Gammon (Eds.), *Phonological development: Models, Research, Implications* (pp. 565-604). Timonium, MD: York Press.

Flege, J. E. (1995). Second language speech learning: Theory, findings, and problems. In W. Strange (Ed.), *Speech Perception and Linguistic Experience: Issues in Cross-Language Research* (pp. 233-277). Baltimore, MD: York Press.

Frank, T. D., Daffertshofer, A., Peper, C. E., Beek, P. J., & Haken, H. (2000). Towards a comprehensive theory of brain activity: Coupled oscillator systems under external forces. *Physica D*, *144*, 62-86.

Fuchs, A., & Jirsa, V. K. (2000). The HKB model revisited: How varying the degree of symmetry controls dynamics. *Human Movement Science*, *19*, 425-449.

Fuchs, A., & Kelso, J. A. S. (1994). A theoretical note on models of interlimb coordination. *Journal of Experimental Psychology: Human Perception and Performance*, *20*, 1088-1097.

Tuller

Fuchs, A., Jirsa, V. K., & Kelso, J. A. S. (2000). Theory of the relation between human brain activity (MEG) and hand movements. *NeuroImage*, *11*, 359-369.

Fuchs, A., Kelso, J. A. S., & Haken, H. (1992). Phase transitions in the human brain: Spatial mode dynamics. *International Journal of Bifurcation and Chaos*, *2*, 917-939.

Fuchs, A., Mayville, J., Cheyne, D., Weinberg, H., Deecke, L., & Kelso, J. A. S. (2000). Spatiotemporal analysis of neuromagnetic events underlying the emergence of coordinative instabilities. *NeuroImage*, *12*, 71-84.

Ganong, W. F., & Zatorre, R. J. (1980). Measuring phoneme boundaries in four ways. *Journal of the Acoustical Society of America*, *68*, 431-439.

Giangrande, J., Tuller, B., & Kelso, J. A. S. (2003) Perceptual dynamics of circular pitch. *Music Perception*, *20*, 241-262.

Haken, H., & Stadler, M. (1990). *Synergetics of cognition*. Berlin: Springer-Verlag.

Haken, H. (1977). *Synergetics, an introduction: Non-equilibrium phase transitions and self-organization in physics, chemistry, and biology*. Berlin: Springer.

Haken, H. (1990). Synergetics as a tool for the conceptualization and mathematization of cognition and behavior—How far can we go? In H. Haken & M. Stadler (Eds.), *Synergetics of Cognition* (pp. 2-31). Berlin: Springer-Verlag.

Haken, H., Kelso, J. A. S., & Bunz, H. (1985). A theoretical model of phase transitions in human hand movements. *Biological Cybernetics*, *51*, 347-356.

Helson, H. (1964). *Adaptation-level theory: An experimental and systematic approach to behavior*. New York: Harper and Row.

Iverson, P., & Kuhl, P. K. (1996). Influences of phonetic identification and category goodness on American listeners' perception of /r/ and /l/. *Journal of the Acoustical Society of America*, *99*, 1130-1140.

Jantzen, K. J., Fuchs, A. Mayville, J. M., & Kelso, J. A. S. (2001). Neuromagnetic activity in alpha and beta bands reflects learning-induced increases in coordinative stability. *Clinical Neurophysiology*, *112*, 1685-1697.

Jirsa, V. K., Fink, P. W., Foo, P., & Kelso, J. A. S. (2000). Parametric stabilization of biological coordination: A theoretical model. *Journal of Biological Physics*, *26*, 85-112.

Tuller

Jirsa, V. K., Friedrich, R., Haken, H. & Kelso, J. A. S. (1994). A theoretical model of phase transitions in the human brain. *Biological Cybernetics*, *71*, 27-35.

Jirsa, V. K., Fuchs, A., & Kelso, J. A. S. (1998). Neural field theory connecting cortical and behavioral dynamics: Bimanual coordination. *Neural Computation*, *10*, 2019-2045.

Jirsa, V. K., & Haken, H. (1996). Field theory of electromagnetic brain activity. *Physical Review Letters*, *77*, 960-963.

Jirsa V. K., & Haken, H. (1997). A derivation of a macroscopic field theory of the brain from the quasi-microscopic neural dynamics. *Physica D*, *99*, 503-526.

Jongman, A. Blumstein, S. E., & Lahiri, A. (1985). Acoustic properties for dental and alveolar stop consonants: A cross-language study. *Journal of Phonetics*, *13*, 235-251.

Kelso, J. A. S. (1990). Phase transitions: Foundations of behavior. In H. Haken & M. Stadler (Eds.), *Synergetics of Cognition* (pp. 249-268). Berlin: Springer.

Kelso, J. A. S. (1994a). Elementary coordination dynamics. In S. Swinnen, H. Heuer, J. Massion, & P. Casaer (Eds.), *Interlimb Coordination: Neural, Dynamical, and Cognitive Constraints* (pp.301-318). San Diego: Academic Press.

Kelso, J. A. S. (1994b). The informational character of self-organized coordination dynamics. *Human Movement Science, 13*, 393-413.

Kelso, J. A. S. (1995). *Dynamic patterns: The self-organization of brain and behavior*. Cambridge: MIT Press. [Paperback edition, 1997].

Kelso, J. A. S., Bressler, S. L., Buchanan, S., DeGuzman, G. C., Ding, M., Fuchs, A., & Holroyd, T. (1992). A phase transition in human brain and behavior. *Physics Letters A, 169*, 134-144.

Kelso, J. A. S., Ding, M., & Schöner, G. (1992). Dynamic pattern formation: A primer. In A. Baskin & J. Mittenthal (Eds.), *Principles of Organization in Organisms* (pp. 397-439). Santa Fe, NM: Addison-Wesley Publishing Co.

Kelso, J. A. S., Fuchs, A., Holroyd, T., Lancaster, R., Cheyne, D., & Weinberg, H. (1998). Dynamic cortical activity in the human brain reveals motor equivalence. *Nature, 392*, 814-818.

Kelso, J. A. S., Saltzman, E., & Tuller, B. (1986). The dynamical perspective on speech production: Data and theory. *Journal of Phonetics, 14*, 29-60.

Kelso, J. A. S., Tuller, B., & Harris, K. (1983). Converging evidence for the role of relative timing in speech. *Journal of Experimental Psychology: Human Perception and Performance, 9*, 829-835.

Tuller

Kelso, J. A. S., & Zanone, P. G. (in press). Coordination dynamics of learning and generalization across different effector systems. *Journal of Experimental Psychology: Human Perception & Performance*.

Lieberman, A. M., Cooper, F. S., Shankweiler, D. P., & Studdert-Kennedy, M. (1967). Perception of the speech code. *Psychological Review*, *74*, 431-461.

Lieberman, A. M., Harris, K. S., Hoffman, H., & Griffith, B. (1957). The discrimination of speech sounds within and across phoneme boundaries. *Journal of Experimental Psychology*, *54*, 358-368.

Lindblom, B., MacNeilage, P., & Studdert-Kennedy, M. (1983). Self-organization processes and the explanation of phonological universals. In B. Butterworth, B. Comrie, & O. Dahl (Eds.) *Explanations of Linguistic Universals* (pp. 181-203). Berlin: Molton.

Lively, S. E., Logan, J. S., & Pisoni, D. B. (1993). Training Japanese listeners to identify English /r/ and /l/: II. Their role of phonetic environment and talker variability in learning new perceptual categories. *Journal of the Acoustical Society of America*, *94*, 1242-1255.

Mayville, J. M., Bressler, S. L., Fuchs, A., & Kelso, J. A. S. (1999). Spatiotemporal reorganization of electrical activity in the human brain associated with a phase transition in rhythmic auditory-motor coordination. *Experimental Brain Research*, *127*, 371-381.

Mayville, J. M., Fuchs, A., Ding, M., Cheyne, D., Deecke, L., & Kelso, J. A. S. (2001) Event-related changes in neuromagnetic activity associated with syncopation and synchronization tasks. *Human Brain Mapping, 14*, 65-80.

Meyer-Lindenberg, A., Ziemann, U., Hajak, G., Cohen, L. & Berman, K.F. (2002). Transitions between dynamical states of differing stability in the human brain. *Proceedings of the National Academy of Science, 99*, 10948-10953.

Nicolis, G., & Prigogine, I. (1977). *Self-organization in nonequilibrium systems*. New York: Wiley.

Petitot-Cocorda, J. (1985) *Les catastrophes de la parole. De Roman Jakobson à René Thom*. Paris: Maloine.

Pisoni, D. B., & Lively, S. E. (1995). Variability and invariance in speech perception: A new look at some old problems in perceptual learning. In W. Strange (Ed.), *Speech Perception and Linguistic Experience: Issues in Cross-Language Research* (pp. 433-459). Baltimore, MD: York Press.

Repp, B. H., & Liberman, A. M. (1987). Phonetic categories are flexible. In S. Harnad (Ed.), *Categorical Perception* (pp. 89-112). Cambridge, UK: Cambridge University Press.

Sancier, M., & Fowler, C. A. (1997). Gestural drift in a bilingual speaker of Brazilian Portuguese and English. *Journal of Phonetics, 25*, 421-436.

Tuller

Schiffman, S. S., Reynolds, M. L., & Young, F. W. (1981). *Introduction to multidimensional scaling*. New York: Academic Press.

Schöner, G., & Kelso, J. A. S. (1988). A synergetic theory of environmentally-specified and learned patterns of movement coordination. I. Relative phase dynamics. *Biological Cybernetics*, *58*, 71-80.

Schöner, G., Haken, H. & Kelso, J. A. S. (1986). A stochastic theory of phase transitions in human hand movement. *Biological Cybernetics*, *53*, 442-452.

Schöner, G., Jiang, W.-Y., & Kelso, J. A. S. (1990). A synergetic theory of quadrupedal gaits and gait transitions. *Journal of Theoretical Biology*, *142*, 359-391.

Schöner, G., Zanone, P. G., & Kelso, J. A. S. (1992). Learning as change of coordination dynamics: Theory and experiment. *Journal of Motor Behavior*, *24*, 29-48.

Sporns, O., & Edelman, G. M. (1993). Solving Bernstein's problem: A proposal for the development of coordinated movement by selection. *Child Development*, *64*, 960-981.

Temprado, J. J., Zanone, P. G., Monno, A., & Laurent, M. (1999). Attentional load associated with performing and stabilizing preferred

bimanual patterns. *Journal of Experimental Psychology: Human Perception and Performance*, *25*, 1595-1608.

Treffner, P. J., & Turvey, M. T. (1996). Symmetry, broken symmetry, and the dynamics of bimanual coordination. *Experimental Brain Research*, *107*, 463-478.

Tuller, B. (2003). Computational models in speech perception. *Journal of Phonetics*, *31*, 503-507.

Tuller, B., Case, P., Ding, M., & Kelso, J. A. S. (1994). The nonlinear dynamics of speech categorization. *Journal of Experimental Psychology: Human Perception and Performance*, *20*, 1-14.

Ullen, F., Ehrsson, H. H., & Forssberg, H. (2000). Brain areas activated during bimanual tapping of different rhythmical patterns in humans. *Society for Neuroscience Abstracts*, *26*, 458.

Wallenstein, G. V., Kelso, J. A. S., & Bressler, S. L. (1995). Phase transitions in spatiotemporal patterns of brain activity and behavior. *Physica D*, *84*, 626-634.

Wildgen, W. (1990). Basic principles of self-organization in language. In H. Haken & M. Stadler (Eds.), *Synergetics of Cognition* (pp. 415-426). Berlin: Springer-Verlag.

Tuller

Zanone, P. G., & Kelso, J. A. S. (1992). The evolution of behavioral attractors with learning: Nonequilibrium phase transitions. *Journal of Experimental Psychology: Human Perception and Performance*, *18*, 403-421.

Zanone, P. G., & Kelso, J. A. S. (1994). The coordination dynamics of learning: Theoretical structure and experimental agenda. In S. P. Swinnen, H. Heuer, J. Massion, & P. Casaer (Eds.), *Interlimb Coordination: Neural, Dynamical, and Cognitive Constraints* (pp. 461-490). San Diego: Academic Press.

Zanone, P. G., & Kelso, J. A. S. (1997). The coordination dynamics of learning and transfer: A multilevel study. *Journal of Experimental Psychology: Human Perception and Performance*, *23*, 1454-1481.